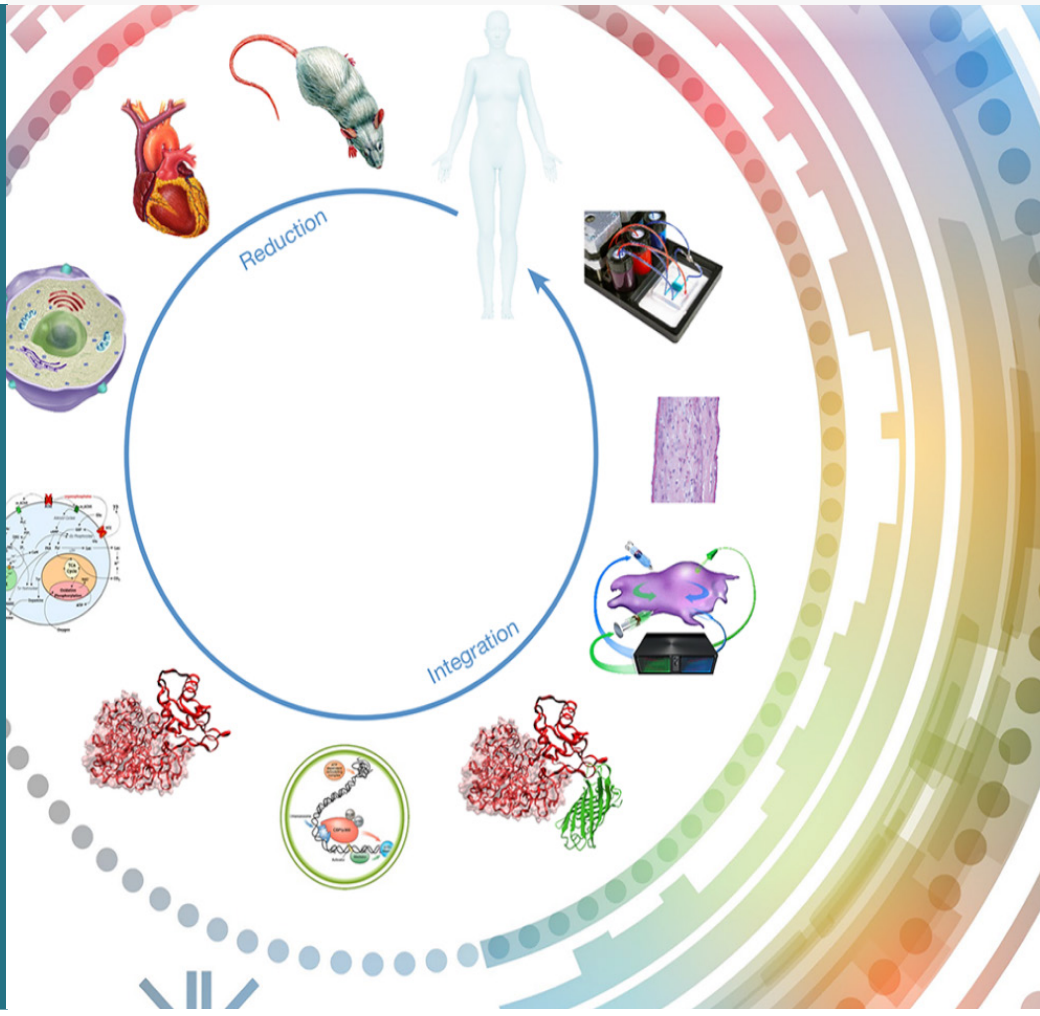
EBM Experimental Biology and Medicine

Volume 251 | Issue 6

Experimental Biology and Medicine

Editor-in-Chief

Nicola Conran
University of Campinas, Brazil



ISBN 978-2-8325-8846-8
DOI 10.3389/978-2-8325-8846-8

frontiers | Publishing Partnerships

SEBM Executive Council

PRESIDENT

Clinton Allred, PhD
University of North Carolina Greensboro

TREASURER

Louis Justement, PhD
University of Alabama at Birmingham

PAST PRESIDENT

Michael Lehman, PhD
New Mexico Tech

TREASURER ELECT

Thomas B. Thompson, PhD
University of Cincinnati

PRESIDENT ELECT

TBA

Publication Committee

Robert Mallet, PhD '26 (Chair)
Renata Sesti Costa, PhD '28,
Agnes Luo, PhD '29,
Sulev Koks, PhD '27

Society for Experimental Biology and Medicine
3220 N Street NW, #179
Washington DC 20007, USA
Executive Director – ed@sebm.org

www.sebm.org

EBM Experimental Biology and Medicine

Editorial Board

Editor-in-Chief
Nicola Conran
University of Campinas

DEPUTY EDITORS
Sulev Kõks
Murdoch University
Shaw-Jenq Tsai
National Cheng Kung University

GLOBAL EDITORS

Africa
Gordon Awandare
University of Ghana

Asia
Shaw-Jenq Tsai
National Cheng Kung University

Europe
Farzin Farzaneh
King's College London

Americas
Nicola Conran
University of Campinas

Australia/Oceana
Sulev Kõks
Murdoch University

Aging

Associate Editor

Shigemi Matsuyama
Case Western Reserve University

Ricki Colman
Aolin Allen Hsu
Akihiro Ikeda
Masaru Miyagi
Vincent Monnier

Bioimaging

Associate Editor

Shuliang Jiao
Florida International University

Kamran Avanaki
Zygmunt Gryczynski
Xinmai Yang
Xincheng Yao
Baohong Yuan
Weizhao Zhao

AI in Biology and Medicine

Associate Editor

Huixiao Hong
US Food and Drug Administration

Xiaohui Fan
Ping Gong
Ruili Huang
Jie Liu
Fred Prior
Paul Rogers
Tieliu Shi
Wei Shi
Wenming Xiao

Biomarkers in Regulatory Science

Associate Editor

William Slikker, Jr.
Retired

Gary Steven Friedman
Paul C. Howard
Donald Johann
Oh-Seung Kwon
Ann M. Marini
Igor Pogribny

Biochemistry and Molecular Biology

Associate Editor

Muriel A. Lambert
Rutgers New Jersey Medical School

Albert Alhatem
Brian D Adams
Bin Guo
J. Patrick O'connor

Biomedical Engineering

Associate Editor

F. Kurtis Kasper
University of Texas Health Science Center at Houston

Salman R. Khetani
Deok-Ho Kim
Aditya Kunjapur
Andre Levchenko
Angela Pannier

Bionanoscience

Associate Editor

Juan Melendez
University of Albany

Nathaniel Cady
Hassan A. Elfawal
Jonathan F Lovell
Ya-Ping Sun
Maria Tomassone
Siyang Zheng

Cancer Biology

Associate Editor

Michael Chan
National Chung Cheng University

Cell and Developmental Biology

Associate Editor

Lidiane Torres
Albert Einstein College of Medicine

David Dean
Leszek Kotula
Huihui Li
Alexander V. Ljubimov
Harold I Saavedra
Yigang Wang
Warren Zimmer

Clinical Trials

Giuseppe Pizzorno
Daniel Vaena

Endocrinology and Nutrition

Co Associate Editors

Clint Allred and Keith Erikson
University of North Carolina Greensboro

Demin Cai
Sam Dagogo-Jack
Weiqun Wang
Malcolm Watford
Chia-Shan Wu

Genomics, Proteomics, and Bioinformatics

Associate Editor

Sulev Kõks
Murdoch University

Mark Geraci
Paul Potter
John P Quinn
Giovanni Stracquadanio

Immunology

Associate Editor

Renata Sesti-Costa
State University of Campinas

Sandra Regina Costa Maruyama
Alexandra Ivo de Medeiros

Infectious Diseases

Co Associate Editors

Flávio Guimarães Da Fonseca
Federal University of Minas Gerais

Andrea Doria
Farzin Farzaneh
Kam Hui
Francois Villinger

Neuroscience

Associate Editor

Michael Neal Lehman
Kent State University

Lique M. Coolen
Terrence Deak
Max L Fletcher
Sandra Mooney
Gregg Stanwood
Richard M Xu

Oral Biology and Disease

Associate Editor

Poliana Mendes Duarte Reis
University of Florida

Pharmacology/Toxicology

Associate Editor

Santosh Kumar
University of Tennessee Health Science Center

Guzel Bikbova
Pawel Brzuzan
Laetitia Dou
Jianxiong Jiang
Youngmi Jung
Li-Fu Li
Jonathan Shannahan
Manish Tripathi
Chaowu Xiao
Wuxiang Xie
Qihe Xu

Physiology, Pathophysiology and Mechanisms of Disease

Associate Editor

Robert T. Mallet
University of North Texas Health Science Center

Rong Ma
Patricia J. McLaughlin
Gabor Tigyi
Shaw-Jenq Tsai
Samuel Verges
Lei Xi
Ian Zagon
Chunyu Zeng

EBM Experimental Biology and Medicine

Population Health

Associate Editor

Rebecca C. Christofferson
Louisiana State University

Structural Biology

Associate Editor

Tom Thompson
University of Cincinnati

Andrew P. Hinck
James Horn
Rhett Kovall
Vincent Luca
Rick Page

Stem Cell Biology

Associate Editor

Jian Feng
State University of New York at Buffalo

Vania Broccoli
Jose Cibelli
Guoping Fan
Antonis Hatzopoulos
Dan S. Kaufman
Chun-Li Zhang

Translational Research

Associate Editor

Chia-Ching (Josh) Wu
National Cheng Kung University

Jing An
Pan Pan Chong
Hyacinth Idu Hyacinth
Monica M. Jablonski
Chulso Moon
Esther Obeng
Athena Starland-Davenport

EBM eBook Copyright Statement

The copyright in the text of individual articles in this eBook is the property of their respective authors or their respective institutions or funders. The copyright in graphics and images within each article may be subject to copyright of other parties. In both cases this is subject to a license granted to Frontiers.

The compilation of articles constituting this eBook is the property of Frontiers.

Each article within this eBook, and the eBook itself, are published under the most recent version of the Creative Commons CC-BY licence. The version current at the date of publication of this eBook is CC-BY 4.0. If the CC-BY licence is updated, the licence granted by Frontiers is automatically updated to the new version.

When exercising any right under the CC-BY licence, Frontiers must be attributed as the original publisher of the article or eBook, as applicable.

Authors have the responsibility of ensuring that any graphics or other materials which are the property of others may be included in the CC-BY licence, but this should be checked before relying on the CC-BY licence to reproduce those materials. Any copyright notices relating to those materials must be complied with.

Copyright and source acknowledgement notices may not be removed and must be displayed in any copy, derivative work or partial copy which includes the elements in question.

All copyright, and all rights therein, are protected by national and international copyright laws. The above represents a summary only. For further information please read Frontiers' Conditions for Website Use and Copyright Statement, and the applicable CC-BY licence.

ISSN 1535-3699
ISBN 978-2-8325-8846-8
DOI 10.3389/978-2-8325-8846-8

Generative AI statement
Any alternative text (Alt text) provided alongside figures in the articles in this ebook has been generated by Frontiers with the support of artificial intelligence and reasonable efforts have been made to ensure accuracy, including review by the authors wherever possible. If you identify any issues, please contact us.

EBM Experimental Biology and Medicine

2026 | Volume 251 | Issue 6 | ISSN 1535-3699

Table of contents

Biochemistry and Molecular Biology

Review

07 The interaction between oxidative stress and Schwann cells

Sihan Yang, Zijun Zhang, Qing Liao, Qipeng Ouyang, Yongyou Ye, Wei Lu and Zhendong Jiang

Biomarkers in Regulatory Science

Original Research

38 Causal association between clonal hematopoiesis indeterminate potential and cancer: a Mendelian randomization study

Juan Jin, Qian Pu, Chengrong Wu, Yu Lei, Yaxin Hu, Xiuju Yang, Jinghui Huang, Fangfang Wu, Li Xiao and Lei Yu

Genomics, Proteomics and Bioinformatics

Highlight

Original Research

48 Genetic evidence for causal relationships between brain functional networks and domain-specific recovery after nondisabling ischemic stroke

Huan Cai, Zhenchun Huang, Jialin Liang, Hao Zhang and Zhonghua Liu

Immunology

Highlight

Review

57 The role and mechanism of neutrophils in oncolytic virus therapy

Baixian Huang, Qixin Yang, Ruixue Wang and Chaochao Zhao

Neuroscience

Review

68 Genetics of epilepsy

Kynen Piacentini, Athanasios Gaitatzis and Sulev Kõks

Stem Cell Biology

Mini Review

80 Mitochondrial transfer and mesenchymal stem cells in ophthalmology: current evidence and therapeutic implications

Xiaoli Liu, Mingqi Zhang and Zhuoshi Wang

Translational Research

Original Research

89 The value of serum exosomal miRNA signature profiles for the early diagnosis of feline infectious peritonitis

Hongxia Gu and Huisheng Wu

Pharmacology and Toxicology

Correction

98 Correction: Protective effects of berberine-loaded chitosan/solid lipid nanoparticles in streptozotocin-induced gestational diabetes mellitus rats

EBM Production Office

EBM Experimental Biology and Medicine

TYPE Review
PUBLISHED 27 August 2026
DOI 10.3389/ebm.2026.11146

Check for updates

OPEN ACCESS

*CORRESPONDENCE
Wei Lu,
luwei0613@163.com
Zhendong Jiang,
jzd1987521@163.com

‡These authors have contributed equally to this work and share first authorship

RECEIVED 15 April 2026
REVISED 19 July 2026
ACCEPTED 07 August 2026
PUBLISHED 27 August 2026

CITATION
Yang S, Zhang Z, Liao Q, Ouyang Q, Ye Y, Lu W and Jiang Z (2026) The interaction between oxidative stress and Schwann cells.
Exp. Biol. Med. 251:11146.
doi: 10.3389/ebm.2026.11146

COPYRIGHT
© 2026 Yang, Zhang, Liao, Ouyang, Ye, Lu and Jiang. This is an open-access article distributed under the terms of the Creative Commons Attribution License (CC BY). The use, distribution or reproduction in other forums is permitted, provided the original author(s) and the copyright owner(s) are credited and that the original publication in this journal is cited, in accordance with accepted academic practice. No use, distribution or reproduction is permitted which does not comply with these terms.

The interaction between oxidative stress and Schwann cells

Sihan Yang[1‡], Zijun Zhang[2‡], Qing Liao[1], Qipeng Ouyang[1], Yongyou Ye[1], Wei Lu[3*] and Zhendong Jiang[1*]

[1]Department of Basic Education, Zhuhai Campus of Zunyi Medical University, Zhuhai, China, [2]Xiaolan People's Hospital of Zhongshan, Zhongshan, China, [3]College of Basic Medicine, Guangdong Jiangmen Chinese Medical College, Jiangmen, China

Abstract

After peripheral nerve injury (PNI), a moderate increase in reactive oxygen species (ROS) levels can promote the proliferation and differentiation of Schwann cells (SCs) and participate in signal transduction. However, excessive ROS can trigger oxidative stress, and its harmful effects can overshadow the beneficial ones, such as inducing apoptosis, activating inflammation, disrupting environmental stability, and severely hindering neural processes. Therefore, if the damage caused by oxidative stress to SCs can be effectively alleviated, it will provide a new approach for the precise regeneration between peripheral nerves and target organs, thereby reducing the complications of PNI. With the advancements in materials science and neural tissue engineering, functional and precisely designed neural scaffolds and conduits have emerged as highly promising therapeutic strategies. This article focuses on revealing the interaction between SCs and oxidative stress during nerve injury, as well as the innovative tissue engineering technologies and new paradigms for damage repair that have emerged based on this interaction. It aims to provide effective new methods for addressing temporary or permanent functional impairments of PNI/peripheral neuropathies.

KEYWORDS
oxidative stress, reactive oxygen species, Schwann cells, peripheral nerve injury, nerve guidance conduit, nerve tissue engineering, antioxidation, mitophagy

Impact statement

After peripheral nerve injury (PNI), a moderate increase in reactive oxygen species (ROS) levels can promote the proliferation and differentiation of Schwann cells (SCs) and participate in signal transduction. However, excessive ROS can trigger oxidative stress, and its harmful effects can overshadow the beneficial ones, such as inducing apoptosis, activating inflammation, disrupting environmental stability, and severely hindering neural processes. Therefore, if the damage caused by oxidative stress to SCs can be effectively alleviated, it will provide a new approach for the precise regeneration between peripheral nerves and target organs, thereby reducing the complications of PNI. This review provides a comprehensive overview of the mechanisms of excessive ROS production, oxidative stress-induced SCs' damage, and endogenous antioxidant defense in PNI, as well as emerging nerve tissue engineering strategies for intervention. By constructing a discussion framework that progresses from "mechanism elucidation" to "technology integration" and ultimately to "clinical translation," this work strives to provide guidance for the future development of intelligent neural repair systems that possess both dynamic responsiveness and functional remodeling capabilities.

Introduction

Peripheral nerve injury (PNI), a highly prevalent neurological disease, is often caused by trauma, traffic accidents, mechanical tension, and other factors, and has become a heavy burden on global public health and economic development [1]. Despite the regenerative potential of peripheral nerves, their slow regeneration rate may lead to dysfunction or irreversible damage of target organs due to long-term loss of innervation, such as dyskinesia, sensory abnormalities, pain sensitization, and muscular atrophy, and some patients may even face lifelong disability risk [2]. The primary challenge for PNI repair is the disruption of the microenvironment triggered by oxidative stress (OS) [3]. Reactive oxygen species (ROS), originating from oxygen metabolism, can harm cells by interacting with biological macromolecules such as lipids, proteins, and nucleic acids. Its excessive accumulation has been confirmed to cause in-cell and tissue damage. During aging, it is the leading contributor to cell and tissue damage [4, 5]. Under physiological conditions, the endogenous intracellular antioxidant system can maintain an exquisite metabolic balance between ROS generation and scavenging through sophisticated regulation [6, 7].

However, during the repair process of PNI, combined cellular damage and inflammation exacerbate mitochondrial electron transport chain (ETC.) leakage, further stimulating ROS production. Such as NADPH oxidase (Nox), oxidative burst during ischemia-reperfusion injury (IRI), and so forth. Nox, oxidative burst during Ischemia-Reperfusion Injury (IRI), and other ROS generation pathways. Excessive ROS production overwhelms endogenous antioxidant defenses, disrupting the critical balance between oxidative stress and reduction [8, 9]. The unbalanced oxidative microenvironment can not only directly induce neuronal apoptosis but also facilitates SC senescence transition, which disrupts the regenerative microenvironment and diminishes neural repair capacity [4, 10, 11]. As crucial regulators of peripheral nerve regeneration, Schwann cells (SCs) modulate the redox microenvironment through antioxidant mechanisms and signaling pathways (e.g., Hedgehog), which may help preserve neuronal redox homeostasis and support regenerative responses [12, 13]. Of interest, ROS fluctuations serve dual regulatory functions, mediating both host immune responses and essential physiological signaling pathways: immune cells activate the inflammatory response by synergistically releasing large amounts of ROS to clear pathogens, whereas low concentrations of ROS act as redox signaling molecules that participate in the regulation of cell proliferation, differentiation, and other basic life activities [14, 15]. Moreover, the interaction between OS and SCs in neuropathies such as diabetic peripheral neuropathy (DPN) and neurofibromatosis type 1 (NF1) also plays a key role in the pathological microenvironment [16, 17]. This duality of biological properties suggests the need for an in-depth analysis of the spatiotemporal distribution of ROS, the mechanisms of SC damage, and the dynamic regulation of antioxidant pathways. Such an analysis will provide a theoretical foundation for developing smart neural scaffolds with both anti-inflammatory and antioxidant functions.

Conventional neural scaffolds are single-function designs, challenging to respond to the complex dynamic changes in the regenerative microenvironment due to their single-function design, leading to deficient nerve fiber regeneration and constrained functional recuperation [18, 19]. The convergence of cell biology and advanced materials science has propelled neural tissue engineering beyond structural imitation, ushering in an era of functionally integrated regenerative strategies. This paradigm focuses on fabricating tripartite functional constructs that combine living cells, scaffold matrices, and bioactive signaling factors in three-dimensional architectures. Based on this approach, nerve guidance conduits (NGCs) are designed to actively direct axon growth by integrating SCs, neurotrophic factors, and other key regenerative components [20]. In addition, advanced NGC iterations feature embedded biosensing modules and responsive drug release mechanisms, allowing dynamic tracking of redox status and demand-based neuroprotection [21]. This dynamic regulatory mechanism overcomes the static limitations of traditional scaffolds. By precisely maintaining redox homeostasis, it simultaneously promotes vascular regeneration and the reconstruction of the bioelectrical signaling network [22, 23].

In the future, with the development of ROS-responsive drug delivery systems, engineered exosome platforms, and advanced technologies such as 4D bioprinting, the analysis of the spatiotemporal dynamics of OS will drive breakthroughs in personalized treatment strategies. These advances are expected to support the sustained functional regeneration of complex nerve injuries. A summary timeline of significant events in SC and OS research is shown in Figure 1.

This review is built on a central framework: the dynamic interplay between OS and SCs dictates the success of peripheral nerve repair, and understanding this mechanism provides the blueprint for next-generation interventions. To strengthen the narrative flow, we organize our discussion into a structured progression: (1) Mechanism elucidation: uncovering how ROS production and endogenous antioxidant defenses govern SC fate; (2) Technology integration: highlighting how novel nerve tissue engineering, such as smart drug delivery and 4D bioprinting, actively intervenes in this OS-SC axis; (3) Clinical translation: evaluating these strategies in disease models and clinical applications. This structured approach aims to guide the evolution of neural repair from passive scaffolds to active, microenvironment-responsive systems.

Retrieval strategy

This study systematically retrieved literature from PubMed using combined keywords related to oxidative stress, reactive oxygen species, peripheral nerve injury, nerve tissue engineering, and nerve guidance conduits, covering the period from March 2021 to March 2026 without language or study type restrictions. To deeply explore the interplay between OS and PNI repair, articles focusing unidirectionally on either OS or PNI without addressing their interaction in nerve regeneration were excluded. Eligible high-quality studies underwent full-text assessment, and a snowballing approach was applied to reference lists for additional relevant publications. All searches were completed by June 2026, with the literature screening process detailed in Figure 2.

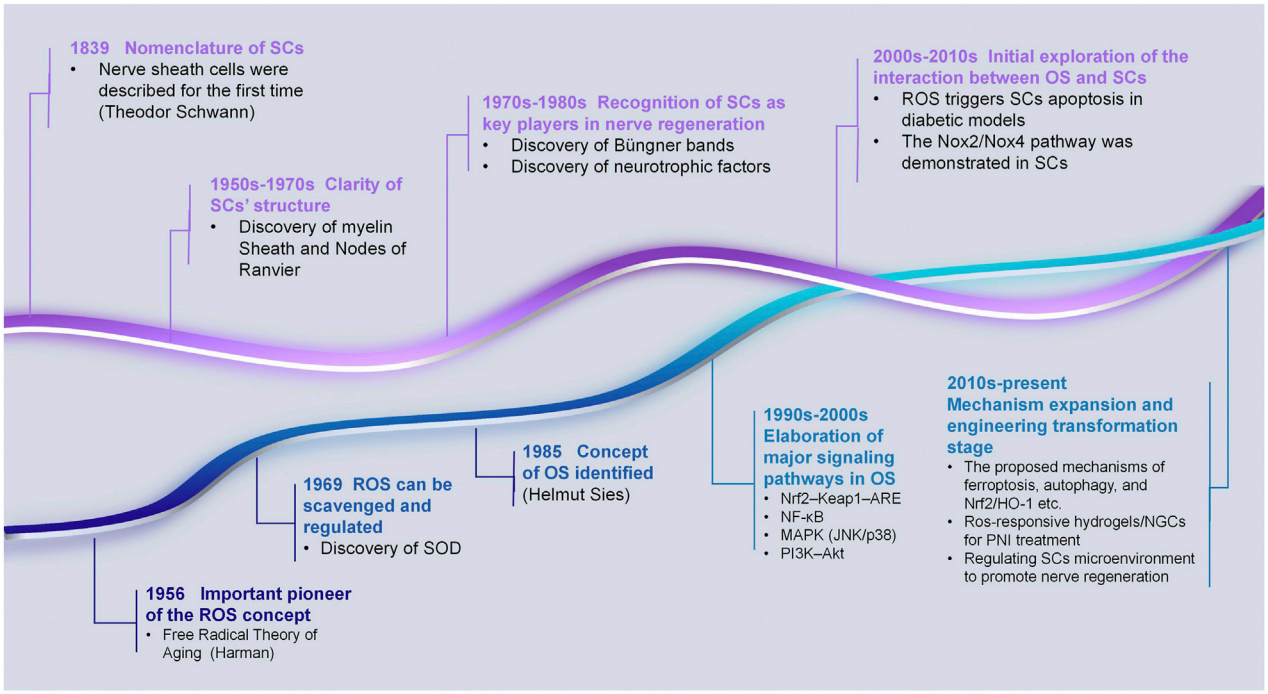


FIGURE 1
Timeline: The significant events of SC and OS research and the new paradigm of their interaction. Abbreviations: SCs, Schwann cells; OS, oxidative stress; ROS, reactive oxygen species; Nox2/Nox 4, NADPH Oxidase 2/NADPH Oxidase 4; NGCs, nerve guidance conduits; PI3K-Akt Pathway, Phosphatidylinositol 3-Kinase; p38, p38 Mitogen-Activated Protein Kinase; JNK, c-Jun N-terminal Kinase; MAPK, Mitogen-Activated Protein Kinase; Nrf2-Keap1-ARE, Nuclear Factor Kappa-Light-Chain-Enhancer of activated B cells.

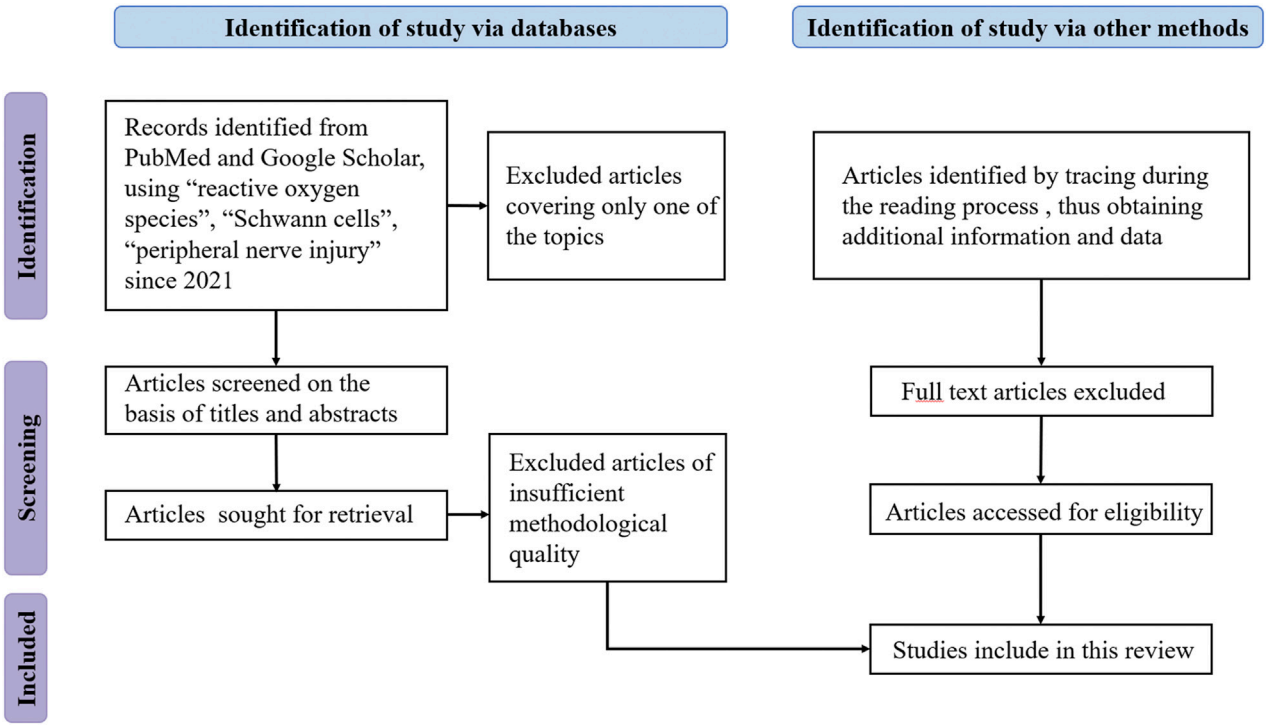


FIGURE 2
Flowchart of the retrieval process: This figure illustrates the strategy used in this review for searching the literature.

The molecular mechanism of the interaction between SCs and oxidative stress

As a key response mechanism for the body to cope with harmful stimuli in the internal and external environment, OS manifests through the pathological accumulation of ROS and reactive nitrogen species (RNS), disrupting redox homeostasis [24]. ROS include strong oxidizing substances such as superoxide anion (O^{2-}), hydroxyl radical (OH^{-}), and hydrogen peroxide (H_2O_2). Similarly, RNS encompasses highly reactive molecules like nitric oxide (NO) and peroxynitrite ($ONOO^-$) [25]. These free radicals induce DNA strand breaks, protein conformational changes, and lipid peroxidation through direct oxidative damage or cascade reactions, ultimately leading to cellular dysfunction and compromised tissue regeneration.

This pathological microenvironment not only promotes neuronal apoptosis but also exacerbates the neuroregenerative microenvironment by inducing senescence-like phenotypic switching in SCs [4, 10, 11]. What is more noteworthy is that excessive accumulation of ROS can cause neuronal cells and SCs to arrest in the G0/G1 phase and enter a quiescent, senescent, or even apoptotic state. This condition significantly impairs their core repair functions, including myelin clearance, neurotrophic factor secretion, and axon regeneration. As a result, the overall regenerative capacity of the nerves is compromised [26, 27].

Furthermore, recent studies have also indicated that ROS/RNS can modify key signaling proteins such as components of the Mitogen-Activated (MAPK), Phosphoinositide 3-Kinase/Protein kinase B (PI3K/Akt), and Nuclear Factor Erythoid 2-Related Factoe 2 (Nrf2) pathways, influencing the dedifferentiation and redifferentiation processes of SCs [28–30]. They also participate in regulating the immune system and metabolic reprogramming of the regenerative microenvironment, forming a complex network of interactions between OS and SCs.

The generation of ROS and its interaction with SCs

Mitochondrial electron leakage and calcium overload

Under physiological conditions, as the major cellular ROS producer, the ETC generates free radicals through unavoidable electron escape during adenosine triphosphate (ATP) synthesis. These leaked electrons readily react with molecular oxygen, generating ROS species, such as O^{2-}. Mitochondrial-derived ROS represent one of the primary pathogenic mediators in OS development due to their continuous production during aerobic respiration [31]. Its initial site of generation is usually considered to be the semiquinone radical ($QH^{\bullet}$) or reduced flavin (FMN and FAD). At mitochondrial respiratory Complex I (CI), O^{2-} may be generated at either the flavin or I_Q site and partitions completely into the mitochondrial matrix. In mitochondrial respiratory Complex III (CIII), O^{2-} is produced at the Qo site and released into the membrane space and matrix [32]. The vast majority of physiological ROS originates from the electron leakage at CI and CIII, and a small fraction arises from the direct electron leakage from the 3Fe-4S cluster of mitochondrial respiratory Complex II (CII) to oxygen, yielding O^{2-} [33]. At physiological concentrations, appropriate amounts of ROS are essential factors involved in SCs signaling and metabolic regulation.

Moreover, in pathological niches with intact glia-neuron units, drastic microenvironmental changes trigger significant Ca^{2+} influx through activation of SC surface channels such as TRPA1. This aberrant Ca^{2+} accumulation serves as the priming factor for subsequent mitochondrial dysfunction [34, 35]. Mechanistically, Kievit et al. observed in an *in vitro* axotomy model that mitochondrial ROS production preceded late-stage Ca^{2+} entry [36]. Owever, this sequence likely reflects a distinctive phenotype of glia-free isolated axon systems. In this highly simplified model, severed axons lack physical ensheathment and metabolic support from SCs. They undergo rapid, autonomous NAD^+ depletion, which triggers intrinsic mitochondrial collapse and places mitochondrial ROS generation upstream of channel activation. Consequently, in in vivo, *ex vivo*, or co-culture systems with preserved SC-axon communication, extrinsic glia-derived oxidative stress and localized Ca^{2+} perturbations typically dominate the induction of mitochondrial dysfunction.

Nox activation and ROS generation

The Nox family remains as enzymes that specialize in ROS generation and still play a significant role, with members including NOX1, NOX2 (gp91phox), NOX3, NOX4, NOX5, and DUOX1 and DUOX2 [37]. The distribution of members of this family varies in the peripheral nervous system: dorsal root ganglion neurons express Nox1, Nox2, and Nox4, macrophages express Nox2 and Nox4, and SCs express Nox1 and Nox4 [38]. Due to the structural homology of Nox enzymes, the core mechanism of ROS production is basically the same. This reactive species subsequently undergoes dismutation, either spontaneously or via superoxide dismutase (SOD) catalysis, yielding H_2O_2. The subsequent fate of H_2O_2 is highly dependent on the local microenvironment. H_2O_2 undergoes the Fenton reaction catalyzed by transition metal ions, involving Fe^{2+}, generating OH^-. In the absence of such ions, residual H_2O_2 serves as a substrate for myeloperoxidase (MPO) to generate hypochlorous acid (HOCl), a potent oxidant involved in innate immune responses [39].

Distinct activation modes represent a key factor underlying the functional diversity among enzymes of the Nox family [38]. Regarding Nox1 expressed in SCs, De Logu et al. demonstrated that ROS derived from macrophage Nox2 activate Transient Receptor Potential Ankyrin 1 (TRPA1) channels in SCs, leading to calcium influx and subsequent activation of Nox1. The oxidative product released by activated Nox1 is H_2O_2. Additionally, a high-glucose environment serves as a key activator of Nox4 in Schwann cells. Elevated blood glucose levels inhibit the liver X receptor (LXR) pathway in macrophages, thereby relieving its transcriptional repression on Nox4. This approach leads to upregulated Nox4 expression and subsequently results in massive ROS production [40].

IRI-induced oxidative bursts

IRI is a biphasic pathological process comprising ischemic and reperfusion phases [37, 41]. At the ischemic stage, blockage of

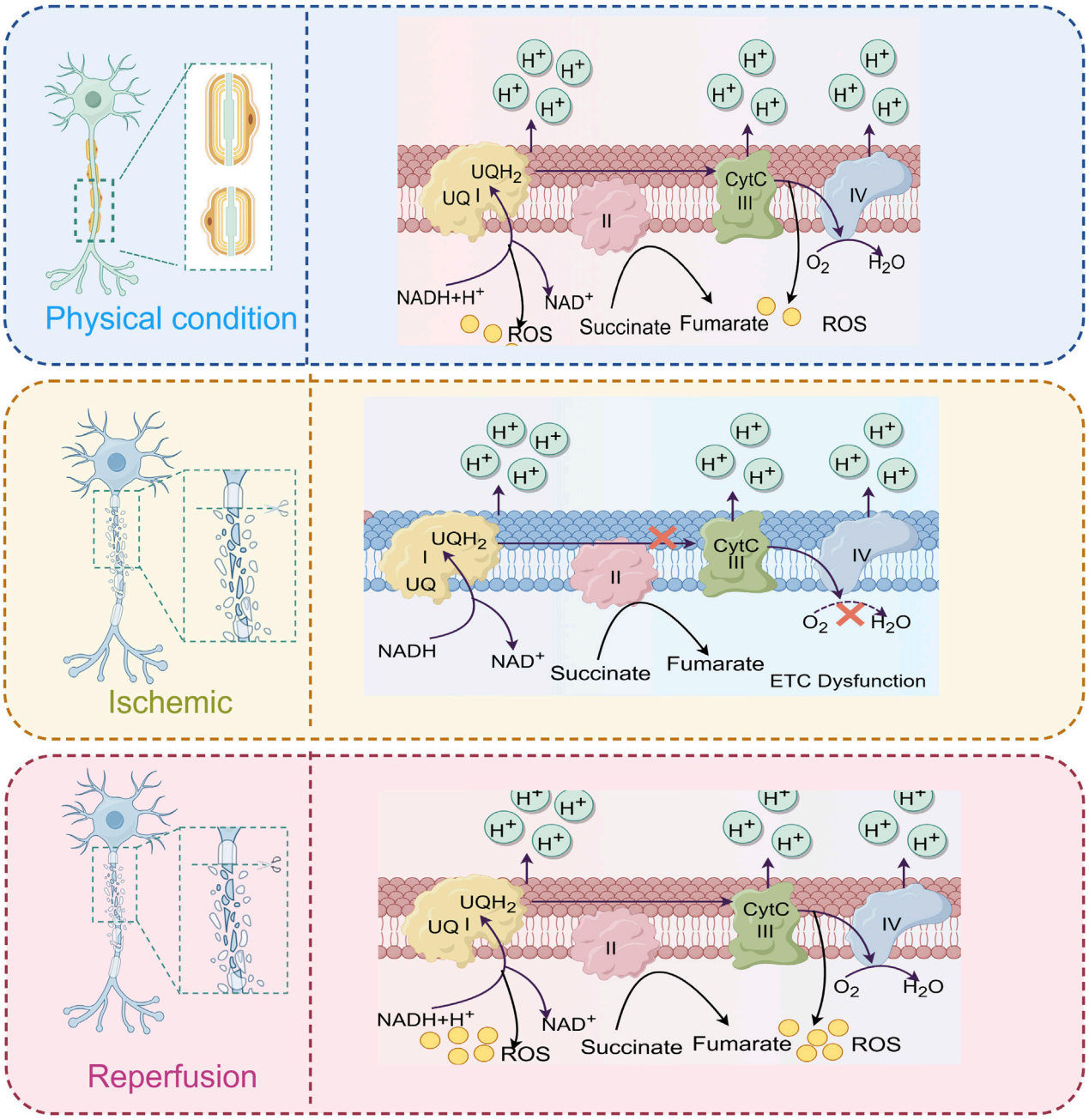


FIGURE 3
Under physiological conditions, a small amount of ROS leaks from CI and CIII during normal electron transfer in the respiratory chain. However, PNI-induced ischemia and hypoxia impair the synthesis of H_2O at CIV, leading to electron transfer blockage and the accumulation of succinate at CII. Upon reperfusion, as the respiratory chain resumes function, the rapid oxidation of accumulated succinate generates excessive electrons, which flow in reverse to CI via RET, resulting in a burst of ROS production at CI.

oxidative phosphorylation in mitochondria results in the cessation of ATP synthesis, ionic homeostasis imbalance, calcium overload, intracellular acidosis, and accumulation of succinate [42]. Among these changes, succinate is a mitochondrial metabolite, and evidence suggests that the tissue-specific retention of this molecule serves as a metabolic signature of ischemia, while also functioning as a critical mediator of reperfusion-induced oxidative damage. Under normal physiological conditions, the proton drive (Δp) is less than the redox drive (ΔEH) to maintain the membrane potential (ΔΨm) required for ATP synthesis. However, metabolic alterations during hypoxia invert the relationship (Δp > ΔEH), and this is further exacerbated during reperfusion. Then the abrupt rise in oxygen availability during reperfusion facilitates the rapid oxidation of accumulated succinate by succinate dehydrogenase. This process leads to a burst of electron flow into the mitochondrial respiratory chain, resulting in a marked depletion of the reduced coenzyme Q pool. These changes ultimately initiate Reverse Electron Transport (RET), in which electrons from ubiquinol are reversed and transferred back to

CI, and RET triggers a burst of ROS during reperfusion at CI [43, 44]. RET acts as a key amplifier of OS effects during reperfusion, perpetuating a self-reinforcing vicious cycle that exacerbates oxidative damage (Figure 3).

Despite the tissue-specificity of OS mechanisms in different tissues (e.g., neural, cardiac, hepatic, renal), the highly conserved structure of the mitochondrial ETC makes theoretical migration between tissues possible [45]. Moreover, there is evidence that ischemic reperfusion injury secondary to PNI induces an oxidative burst [46, 47]. However, the initiation sites and regulatory mechanisms of ROS generation following RET remain poorly characterized, with limited studies available. In contrast, numerous studies based on myocardial ischemia–reperfusion models have elucidated the mechanism of RET and identified complex I as the primary site of RET-induced ROS production [48]. Thus, these findings in cardiac research may serve as a valuable reference for exploring similar mechanisms in SCs models. Based on this, they can seek clues to formulate hypotheses that are applicable to the PNI model and test them experimentally. This approach could facilitate fundamental exploration at the level of OS mechanisms.

Direct and indirect damage mechanisms of OS on SCs

Oxidative damage and apoptosis in SCs

In the OS state, polyunsaturated fatty acids (PUFAs) on the SC membrane are the primary targets of ROS damage. Among these, the essential fatty acids n-6 and n-3 are required for standard membrane structure and fluidity as well as for arachidonic acid-like production. Not only do ROS directly attack PUFAs, leading to disruption of cell membrane integrity, but lipid peroxides generated by this process also cause neurological changes such as axonopathy and demyelination when accumulated over time [49]. Moreover, as PUFAs are ubiquitously present in the phospholipid bilayer of organelle membranes, ROS can also damage the subcellular structures of SCs, such as altered mitochondrial membrane permeability and endoplasmic reticulum stress.

Crucially, the progression from general oxidative damage to ferroptosis in SCs is tightly linked to the collapse of the endogenous antioxidant defense system under sustained OS [50]. Excessive ROS generation rapidly depletes intracellular glutathione (GSH), which subsequently inactivates Glutathione Peroxidase 4 (GPX4). As GPX4 is the primary enzyme responsible for reducing toxic lipid hydroperoxides to non-toxic lipid alcohols, its OS-induced inactivation removes the critical brake on lipid peroxidation [51]. Furthermore, severe OS can impair System Xc- (SLC7A11), restricting cystine uptake and exacerbating GSH depletion, thereby forming a vicious cycle that sensitizes SCs to ferroptosis [52].

In addition, the Fenton reaction triggered by excessive H_2O_2 and ferrous ions (Fe^{2+}), in SCs would induce ferroptosis [53]. Iron death is an iron-dependent form of non-apoptotic cell death, and the response is mediated by increased intracellular iron content and Acyl-CoA Synthetase Long-Chain Family Member 4 (ACSL4) expression. Divalent iron catalyzes the Fenton reaction, initiating lipid peroxidation that disrupts and ruptures the SC membrane, ultimately resulting in cell death. ACSL4 exacerbates the damage to the cell membrane by increasing the content of polyunsaturated fatty acids in the cell membrane, making the lipid peroxidation reaction more prone to occur. In contrast, knockdown of the ACSL4 gene significantly suppresses lipid peroxidation and iron-mediated cytotoxicity, while the morphology and function of the cell membrane are better maintained [54] (Figure 4). These results underscore the critical role of ROS in mediating ferroptosis in SCs and highlight the targeted inhibition of ferroptosis as a highly promising therapeutic strategy for mitigating OS-induced damage and enhancing SC survival.

In the context of peripheral neuropathy and nerve regeneration, OS-induced SC ferroptosis has profound pathological consequences. It not only directly leads to demyelination [55], but also disrupts local iron homeostasis and releases lipid peroxides into the microenvironment [56]. This toxic milieu exacerbates neuroinflammation and impedes macrophage-mediated myelin debris clearance, ultimately creating a hostile environment that severely hinders axonal regrowth and subsequent remyelination [56]. These results underscore the critical role of ROS in mediating SC ferroptosis. They also highlight targeted ferroptosis inhibition as a highly promising therapeutic strategy. This approach could mitigate OS-induced damage while enhancing SC survival and overall nerve regeneration [57].

Inhibitory effects of OS on SC function

SCs can remove myelin sheaths, guide axonal regeneration, and provide the physical structural and trophic support that will, in turn, promote Neural repair of peripheral nerves [58]. However, OS directly or indirectly impairs the repair capacity of Schwann cells through a multidimensional mechanism that impairs the following: (1) Proliferation limitation: OS significantly inhibits the proliferation and survival of SCs, and its effects are dose-dependent but do not lead to a complete arrest of SCs' proliferation in the concentration range studied [54, 59]. (2) Inhibition of neurotrophic factor secretion: Brain-derived neurotrophic factor (BDNF) and nerve growth factor (NGF) can promote the migration of SC [60]. In Ma et al.'s experiments, H2O2-induced OS significantly decreased the levels of BDNF and NGF secreted by SCs [61]. (3) Extracellular matrix alterations: the extracellular matrix (ECM) regulates SCs' proliferation, migration, and myelin formation [62]. It has been demonstrated in spinal cord injury studies that excess ROS can cause degradation of key scaffolding components, such as laminin and fibronectin, in the extracellular matrix ECM, destroying the physical support structures necessary for axonal regeneration [63]. Peripheral nerve tissue is also rich in similar ECM components, such as laminin and fibronectin [62]. Therefore, OS may similarly damage this ECM and impair nerve regeneration. In addition, the OS conditions in peripheral nerve tissues contributed to the dysfunction of mitochondrial metabolism, immunomodulation, and other functions in SCs [64, 65]. If SCs are in a high-glycemic environment, OS will synergistically exacerbate the metabolic disturbances of the cells [66]. The above interactions between the pathologic microenvironment and SCs will be further developed in subsequent sections (Figure 5).

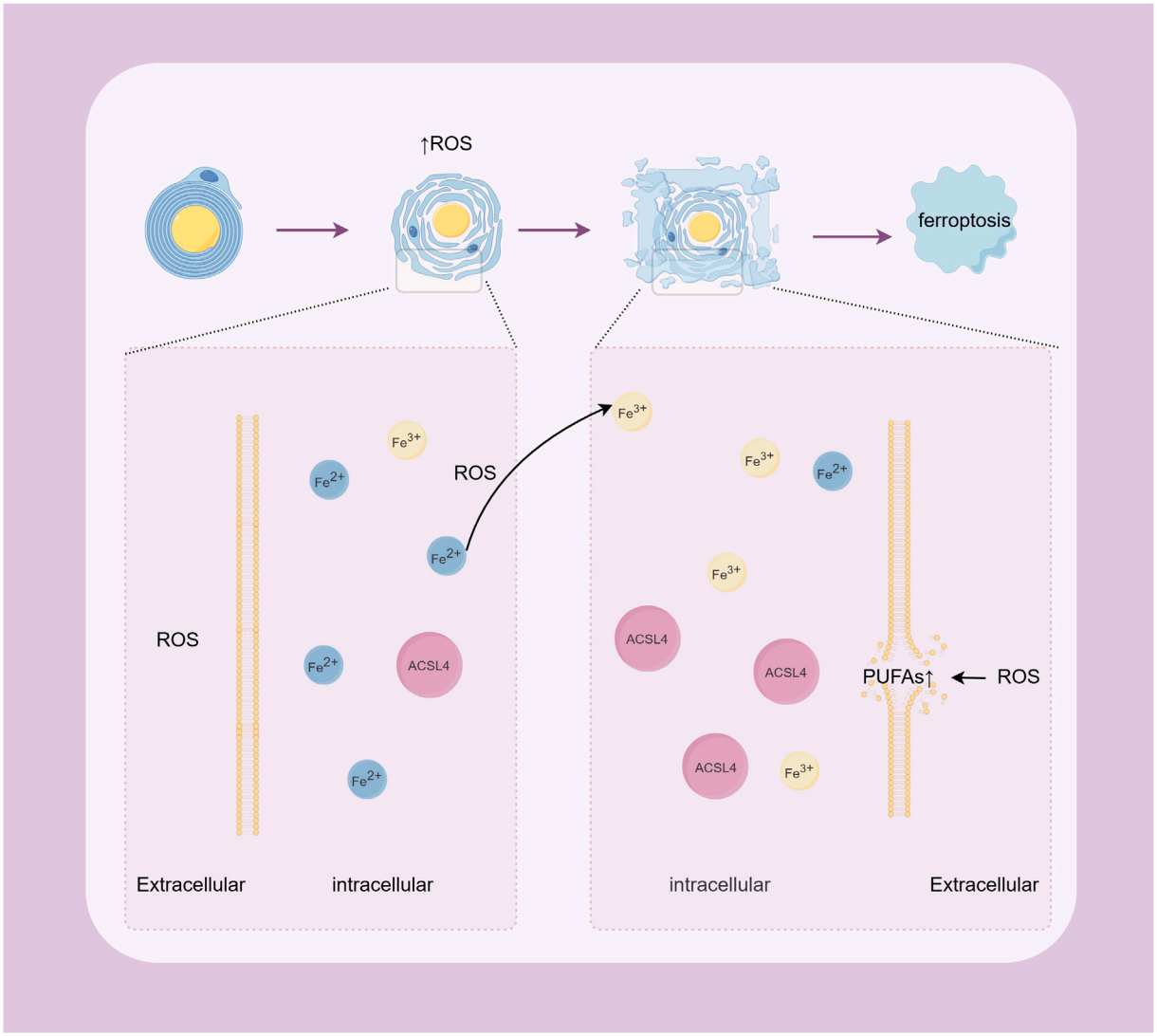


FIGURE 4
The mechanism of ferroptosis induced by oxidative stress in Schwann cells.

Dynamic balance and regulatory mechanism of ROS content

The dual role of ROS and stage-specific regulation

ROS function as pivotal signaling mediators in the context of cellular injury, orchestrating adaptive responses, damage resolution, autophagic homeostasis, and intracellular signal transduction [67]. Such regulatory roles of ROS are particularly prominent in the repair process following PNI. Upon activation of the repair program, SCs undergo a series of coordinated stages, including dedifferentiation, microenvironmental remodeling, the secretion of neurotrophic factors, and axonal regeneration. Each stage critically depends on the dynamic balance between ROS generation and elimination.

It is worth noting that ROS are not merely harmful metabolic byproducts. Recent studies have demonstrated that injury-induced H_2O_2 acts as a pro-regenerative signal. Negro et al. showed that H_2O_2 activates ERK1/2 and c-Jun to drive Schwann cell phenotype conversion. Simultaneously, it upregulates Ctgf via YAP/TEAD to remodel the ECM, which guides Schwann cell migration and oriented axonal growth [68, 69]. Moreover, ROS exhibit stage-specific regulatory effects during nerve repair, driven by a concentration window phenomenon. At certain phases, maintaining an appropriate level of ROS can positively influence SC behavior. This underscores the dose-dependent and temporally specific nature of ROS signaling in the SC-mediated repair process. For instance, during the dedifferentiation phase, SCs may increase ROS production to activate pro-proliferative signaling pathways, thereby facilitating adaptive cellular responses and promoting proliferation [70]. While moderate levels of ROS facilitate intracellular signaling and cytoskeletal remodeling during the axon guidance stage, they also contribute to growth cone navigation. Furthermore, ROS participates in bidirectional

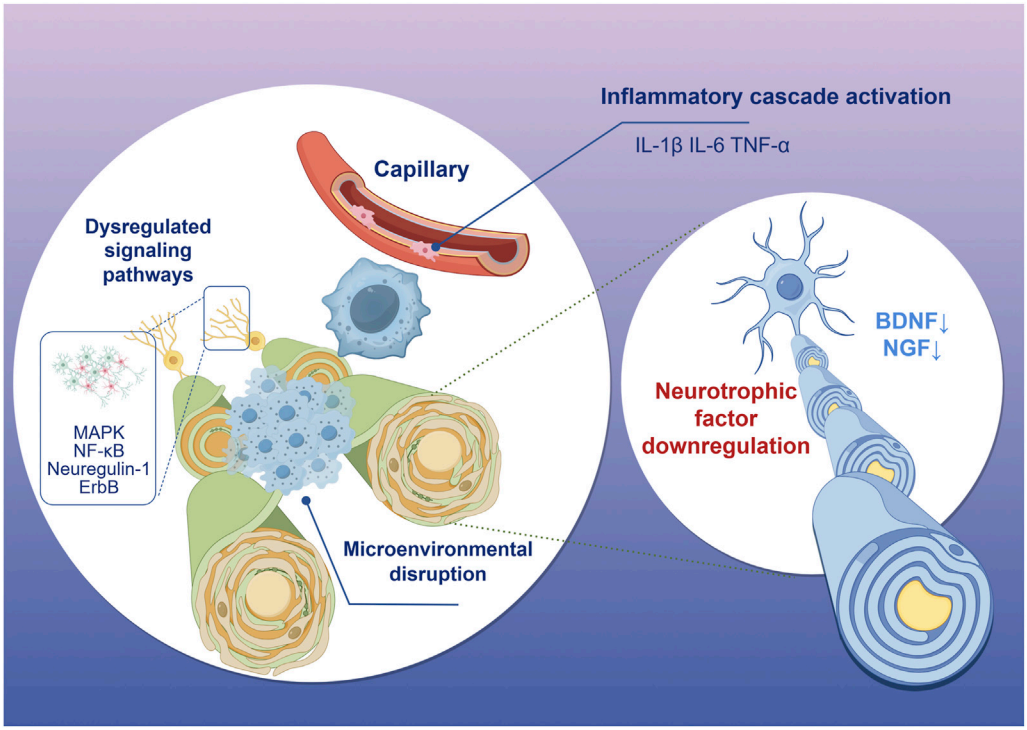


FIGURE 5
OS indirectly impairs the repair function of SCs through disrupting the neural microenvironment and the signal communication between cells, mainly in four aspects: (1) dysregulation of key signaling pathways; (2) destruction of ECM; (3) activation of inflammatory cascade reactions; (4) inhibition of neurotrophic factor secretion. These processes are interrelated and collectively form a vicious cycle that inhibits neural regeneration.

interactions with the autophagy system via the mTOR pathway. This interplay helps sustain the metabolic homeostasis of SCs [71].

In summary, the generation and elimination of intracellular ROS is a tightly regulated process, and the maintenance of redox equilibrium is essential for preserving normal cellular physiology. Consequently, dynamic and accurate regulation of intracellular ROS levels across different stages of nerve injury and repair is a crucial determinant of SCs' repair capacity and successful peripheral nerve regeneration [72–74].

Equilibrium of pro-survival and pro-apoptotic pathways

At the molecular level, this precise regulation relies heavily on the dynamic equilibrium between two core signaling networks: pro-survival and pro-apoptotic pathways [57]. Excessive *in vivo* ROS can directly or indirectly activate multiple intracellular signaling pathways, influencing cell fate by regulating gene expression. In pro-survival signaling, ROS promote cell survival by triggering pathways such as Nrf2/ARE, MAPK/ERK, PI3K/Akt, and NF-κB [29, 75–77], which upregulate the expression of molecular chaperones. Conversely, in pro-apoptotic signaling, elevated ROS activate the JAK/STAT, ATM/p53, and MAPK/JNK/p38 pathways [46], enhancing the expression of pro-apoptotic proteins such as Bax and Caspase-3, ultimately leading to cell apoptosis. Therefore, achieving a dynamic balance between these opposing pathways through the precise regulation of key signaling nodes represents a central mechanism for governing SC survival.

This molecular foundation enables the manipulation of ROS kinetics through engineering strategies. For example, mung bean-derived carbon dots (MB-CDs) activate Nrf2 and downstream Heme Oxygenase-1 (HO-1) and GPX4, converting hemoglobin into CO, Fe^{2+}, and bilirubin to halt SC ferroptosis via lipid peroxidation inhibition [30]. Similarly, porous nanocomposites effectively activate the PI3K/Akt signaling pathway through the sustained release of selenium, reducing ROS generation while suppressing apoptosis, and endowing cells with enhanced migration and nerve regeneration capabilities [75].

These mechanisms construct a systematic framework for ROS regulation: applying active substances restores intracellular anti-oxidation and anti-apoptosis homeostasis, while biocompatible slow-release materials, such as nanoplatforms or hydrogels, enhance spatiotemporal targeting during nerve regeneration. Integrating fragmented pathway research into a synergistic oxidative stress network deepens the understanding of ROS dynamics and provides a solid theoretical foundation [76, 77] for coupling molecular mechanisms with physical stimuli, such as biomimetic matrix topographies, to strategically tailor therapeutic intracellular responses.

TABLE 1 Comparison of mainstream ROS detection technologies in terms of sensitivity, dynamics, specificity, and *in vivo* applicability.

ROS detection technologies	Sensitivity	Temporal & spatial dynamics	Specificity	Applicability	References
EPR	Irreversible cumulative endpoint detection	Bulk measurements lacking subcellular resolution	Capable of targeting specific ROS species	ROS capture strictly *in vivo* (via injection/incubation) with *ex vivo* readouts	[79–81]
Fluorescent staining	Limited response to low ROS; DCFH-DA requires peroxidases or metal ions for H_2O_2; Nonspecific oxidation and redox cycling amplify signals, causing artifacts	Irreversible end-point accumulation; Conventional probes lack real-time dynamic tracking; Advanced probes enable organelle targeting but not traditional ones	Poor specificity; DCFH-DA oxidized by ·OH, $ONOO^-$, heme proteins, glutathione radicals, *etc.*,; DHE/MitoSOX products have overlapping fluorescence spectra	Suitable for cells, tissue sections, and transparent models; Deep-tissue *in vivo* imaging limited by light penetration and autofluorescence	[82–84]
Electrochemical sensors	μM to nM detection limits; Material- and probe-dependent; tunable via design	Real-time, *in situ*, dynamic; μm-scale resolution via microelectrodes implanted in brain regions; rapid response; No sub-organellar resolution	Limited intrinsic selectivity; Achieved via probe/receptor design to exclude electroactive interferents	*In vitro* cell supernatants; *in vivo* brain monitoring; Implantable long-term potential; microtrauma and stability considerations	[85, 86]
GEFIs	Nanomolar sensitivity; Ratiometric normalization via fusion with constitutive RFP to correct expression-level fluctuations	Real-time dynamic imaging; Genetic targeting to specific cell types and subcellular organelles; Suitable for chronic process monitoring; Limited by tissue autofluorescence	High specificity for H_2O_2via OxyR-based sensing domain; C121S mutant as H_2O_2-insensitive control to confirm signal specificity	Live cells, primary neurons, brain slices, and living animals; AAV-mediated delivery for stable expression in specific brain regions; Long-term monitoring in transgenic models	[87, 88]

Abbreviations: EPR, Electron Paramagnetic Resonance; DCFH-DA, 2',7'-Dichlorodihydrofluorescein Diacetate; DHE, Dihydroethidium; MitoSOX, Mitochondrial Superoxide Indicator; RFP, Red Fluorescent Protein; AAV, Adeno-Associated Virus; GEFIs, Genetically Encoded Fluorescent Indicators.

Methodologies and challenges in ROS detection

Understanding and precise monitoring of this dynamic balance is a prerequisite for intervening in the ROS-SC interaction. Nevertheless, molecular characteristics such as millisecond half-life and complex diffusion kinetics pose a significant challenge for its accurate detection. Currently, commonly employed methods for ROS detection include electron paramagnetic resonance (EPR), fluorescent staining, chemiluminescence, chromatographic techniques, spectrophotometry, electrochemical biosensors, and fluorescent protein-based approaches. However, these mainstream detection techniques still exhibit various limitations [78]. To facilitate a critical assessment of these methods, we have synthesized their key advantages and limitations in Table 1, providing a comprehensive perspective on their utility for monitoring ROS dynamics in nerve regeneration research.

In conclusion, excessive OS disrupts SC function via ferroptosis and signaling impairments. However, SCs counteract this redox imbalance through intrinsic antioxidant defenses, a self-rescue mechanism that forms the biological basis for the biomaterial designs discussed in the next section.

Activation of intracellular antioxidant pathways

Activation and regulation of the autophagy pathway

Molecular mechanisms of the mitophagy pathway

Following recognition by autophagy receptors, damaged mitochondria are sequestered into autophagosomes characterized by a double-membrane structure. These autophagosomes then fuse with lysosomes, where lysosomal hydrolases ultimately degrade the enclosed mitochondria [89]. This process helps alleviate oxidative damage by clearing dysfunctional organelles and degrading protein aggregates, thus limiting further ROS production. It is involved in preserving cellular homeostasis while actively facilitating tissue repair processes within the injury microenvironment [90].

The specific mechanisms are as follows: (1) PTEN-induced putative kinase 1/Parkin (PINK1/Parkin)pathway: OS-induced mitochondrial dysfunction or structural damage reduces $\Delta\Psi_m$, thereby preventing PINK1 translocation into the inner mitochondrial membrane for degradation. Instead,

PINK1 accumulates on the outer mitochondrial membrane, where it recruits and activates the E3 ubiquitin ligase Parkin. Parkin, in turn, tags damaged mitochondria by ubiquitinating their outer membrane proteins. Autophagy receptors, such as p62/SQSTM1, subsequently recognize these ubiquitinated proteins and interact with autophagy-related proteins, like LC3, to initiate autophagosome formation. This process ultimately delivers the sequestered mitochondria to lysosomes for degradation [91]. (2) NIX/BCL2 Interacting Protein 3 (BNIP3) pathway: Under OS, the expression levels of BNIP3 and NIX are markedly upregulated. These proteins directly interact with LC3 via their LC3-interacting region (LIR), thereby initiating mitophagy [92]. (3) FUN14 Domain-Containing Protein 1(FUNDC1) pathway: FUNDC1 is an outer mitochondrial membrane protein that primarily initiates mitophagy by interacting with LC3 [93]. These pathways act synergistically to preserve mitochondrial functional homeostasis by eliminating damaged mitochondria and reducing ROS accumulation, thereby playing a pivotal role in maintaining cellular equilibrium and promoting repair following PNI.

Bidirectional regulation of macroautophagy in SCs

The AMPK and Mechanistic Target of Rapamycin (mTOR) signaling pathways play key roles in regulating macroautophagy in SCs. The occurrence of OS is accompanied by enhanced SC activity and increased energy consumption. The resulting low-glucose environment enables AMPK to directly activate Unc-51-Like Kinase 1(ULK1) through phosphorylation at Serine 317 and Serine 777. As the key initiator kinase of autophagy, ULK1 promotes autophagy in SCs upon activation to counteract energy stress. Concurrently, ROS elevates the AMP/ATP ratio, which activates AMPK and induces autophagosome formation. This process clears damaged cellular components, thereby reducing further ROS production and exerting an indirect antioxidant effect. However, under nutrient-sufficient conditions (a high-glucose environment), mTOR signaling phosphorylates ULK1 at Ser757 and disrupts the interaction between ULK1 and AMPK, blocking ULK1 activation and preventing excessive autophagy in SCs [94, 95]. Taken together, this mechanism is bidirectionally and precisely regulated by nutrient availability, leading to the activation or inhibition of ULK1 through the AMPK and mTOR signaling pathways, respectively. Although ULK1 regulation produces divergent effects on SCs, the net outcome is the same: maintaining cellular survival and function. Elucidating the interplay between autophagy and antioxidant mechanisms in SCs will aid the development and validation of targeted therapies.

Synergistic action of enzymatic and non-enzymatic antioxidant systems

SCs contribute to improving the microenvironment at the injury site by eliminating OS products through the activation of both enzymatic and non-enzymatic antioxidant defense systems. When the body is subjected to OS, cells respond by activating the antioxidant enzyme system to upregulate the activity of key antioxidant enzymes [96]. These enzymes neutralize ROS by converting them into non-toxic metabolites, thereby attenuating ROS-induced cellular damage. The key enzymes involved in this defense mechanism include SOD, catalase (CAT), and glutathione peroxidase (GSH-Px) [97]. In parallel, non-enzymatic antioxidants such as vitamin C, vitamin E, vitamin A, melatonin, and GSH directly neutralize ROS to protect neural cells.

The two systems cooperate to regulate the OS environment through enzymatic and non-enzymatic reactions efficiently [98]. Superoxide dismutase (SOD) can convert O_2^- to H_2O_2. The low and high levels of H_2O_2 scavenging enzymes are Peroxiredoxin (Prx) and CAT, respectively. Glutathione peroxidase (GSH-Px), which utilizes glutathione (GSH) as the electron donor, exhibits a higher affinity for organic peroxides. In addition, antioxidant enzymes such as Glutaredoxin (GRX) and Thioredoxin (Trx), along with non-enzymatic GSH, provide NADPH-driven reducing equivalents. These reducing agents restore oxidized proteins or regenerate antioxidant enzymes through distinct pathways. Through this mechanism, antioxidant enzymes are regenerated and reused, thereby establishing a sustainable cyclic process.

Different from the above macromolecules, vitamin C (Vit C), vitamin E (Vit E), and vitamin A (Vit A) can directly scavenge ROS, which is one of the keys to the antioxidant function of SCs [98–100]. This multi-layered, interwoven defense system strengthens the antioxidant capacity of anti-SCS and enables them to better cope with the OS pathological environment.

New strategies: regulation of signaling pathways and precise delivery of antioxidants

Excessive ROS *in vivo* can directly or indirectly activate multiple intracellular signaling pathways, influencing cell fate by regulating gene expression. Both pro-survival and pro-apoptotic pathways may be triggered in response to elevated ROS levels [57]. In pro-survival signaling, ROS promote cell survival by the activation of relevant pathways such as Nrf2/ARE, MAPK/Extracellular Signal-Regulatied Kinase (ERK), PI3K/Akt, and NF-κB [101–104]. These pathways upregulate the expression of molecular chaperones. Alternatively, in pro-apoptotic signaling, ROS activate the Janus Kinase (JAK)/Signal Transducer and Activator of Transcription (STAT), Ataxia Telangiectasia (ATM)/p53, and MAPK/c-Jun N-terminal Kinase (JNK)/p38 pathways [46]. This activation enhances the expression of pro-apoptotic proteins such as Bax and Caspase-3, ultimately leading to cell apoptosis. Precise regulation of key signaling nodes is essential to maintain a dynamic balance between pro-survival and pro-apoptotic pathways. This balance represents a central therapeutic target for preserving SC survival. Moreover, this concept underpins the design of antioxidant bioactive scaffolds that mitigate OS-induced damage and promote nerve regeneration.

Related studies provide insights into antioxidant strategies targeting specific signaling pathways. For instance, Zheng et al. demonstrated that MB-CDs activate Nrf2, which subsequently upregulates HO-1 and GPX4 expression. Nrf2 also converts hemoglobin into CO, Fe^{2+}, and biliverdin. Biliverdin is then reduced to bilirubin, which exerts antioxidant effects. HO-1 and GPX4 inhibit ferroptosis in SCs by reducing the production of lipid peroxides [30]. Song et al. developed a porous $Se@SiO_2$ nanocomposite that sustains selenium release. This material effectively activates the PI3K/AKT pathway, thereby reducing

TABLE 2 Mechanisms of action of relevant signaling pathways.

Categories	Pathways/ molecules	Mechanism of activation/ intervention	Effector molecules/ expression changes	Functions/Results	Related research/ applications
Pro-survival pathways	Nrf2/ARE	Activated by oxidants	Increasing expression of NQO1, HO-1, GST (antioxidant enzymes)	Promoting cell survival	[101]
	MAPK/ERK	Activated by growth factors	Upregulating p-MEK, BDNF, and GDNF mRNA expression	Inhibiting apoptosis and promoting neurotrophic factors	[102]
	PI3-K/AKT	Activated by insulin	Reducing thioredoxin-interacting protein (TXNIP) levels	Enhancing SC survival under high-glucose conditions	[104]
	NF-κB	Activated by TNF-α	Phosphorylating IKKα/β, IκBα, and p65	Facilitating SC survival and nerve regeneration	[103]
Pro-apoptotic pathway	JAK/STAT	Activated by cytokine receptors	Promoting Bax, Caspase-3 (pro-apoptotic proteins)	Inducing apoptosis	[46]
	ATM/p53	Activated by DNA damage	Activating p53 and promoting Bax expression	Triggering an apoptotic program	[46]
	MAPK/JNK/p38	Activated by stress signaling	Activating pro-apoptotic proteins	Promoting apoptosis under OS	[46]
Antioxidant treatment cases	MB-CDs	Activated the Nrf2/HO-1/ GPX4 pathway	Up-regulated HO-1 expression and restored GPX4 activity	Enhanced ROS scavenging and improved cell viability Reduced iron-dependent lipid peroxidation	
	Se@SiO_2 nanoparticles	Activated the PI3-K/AKT pathway	Upregulating Bcl-2, Nrf2, HO-1 and SOD2; inhibiting Bax	Inhibiting OS and facilitating nerve regeneration	[75]
Collaborative therapeutic strategy	Multi-target pathway activation	Joint activation of Nrf2-Keap, FOXO1 and other pathways	Dynamic balance of pro-survival/pro-apoptotic signaling	Enhances endogenous antioxidant defence	Smart neural repair material design
	Drug delivery systems	Nanotechnology, hydrogel loading technology	Improving antioxidant bioavailability and targeting	Precisely regulates ROS levels to promote nerve regeneration	Slow-release drug scaffolds, spatiotemporal specific modulation systems
	Systemic regulatory framework	Integrating OS signaling networks with multi-target therapy	Synergistic antioxidant-antiapoptotic effects	Realizes multidimensional therapeutic system from molecular mechanism to engineering	Theoretical basis for the development of next-generation intelligent nerve repair materials

Abbreviations: Nrf2, Nuclear Factor Erythroid 2-Related Factor 2; ARE, Antioxidant Response Element; MAPK, Mitogen-Activated Protein Kinase; ERK, Extracellular Signal-Regulated Kinase; PI3-K, Phosphoinositide 3-Kinase; AKT, Protein Kinase B; NF-κB, Nuclear Factor Kappa-Light-Chain-Enhancer of Activated B Cells; JAK, Janus Kinase; STAT, Signal Transducer and Activator of Transcription; ATM, Ataxia Telangiectasia Mutated; p53, Tumor Protein p53; JNK, c-Jun N-Terminal Kinase; p38, p38 Mitogen-Activated Protein Kinase; MB-CDs, Mung Bean-Derived Carbon Dots; Se@SiO_2, Selenium-Loaded Silica Nanoparticles; GPX4, Glutathione Peroxidase 4; HO-1, Heme Oxygenase-1; SOD2, Superoxide Dismutase 2; FOXO1, Forkhead Box O1.

ROS production, suppressing apoptosis, and promoting cell migration and nerve regeneration [75] (Table 2).

Notably, the strength of evidence across these pathways is not uniform. The Nrf2/ARE and PI3K/Akt axes are the most consistently supported by *in vivo* data across multiple PNI and DPN models [29, 30, 75, 105], whereas the pro-apoptotic roles of JAK/STAT and ATM/p53 are predominantly context-dependent, with activation reported primarily under specific pathological conditions rather than as a universal response to mechanical nerve injury [46].

The mechanical and topographical cues presented by biomimetic matrices, as cross-referenced in our discussion on bionic ECM scaffolds, are not merely structural; they provide the primary physical stimuli that prime downstream signaling pathways, suggesting that material engineering can be

strategically tailored to optimize therapeutic intracellular responses. In summary, SCs combat OS via coordinated autophagy alongside enzymatic and non-enzymatic defenses. Because severe PNI often overwhelms these endogenous pathways, the next section will explore how advanced neural tissue engineering provides targeted exogenous support to amplify these exact mechanisms.

A new paradigm of neural tissue engineering based on the interaction of oxidative stress in SCs

Peripheral nerve regeneration is a highly dynamic and multifactorial regulated pathophysiologic process [106, 107]. OS, as a key pathological aspect of nerve injury, can affect neuronal survival and axonal regeneration through mechanisms such as regulating intracellular ROS content and interfering with signaling pathways and enzyme activity [25]. In the field of neural tissue engineering, overcoming the limitations of the functional singularity of traditional neural scaffolds remains a major objective. Current research focuses on the development of 3D biomimetic NGCs to build composite regenerative systems with microenvironmental responsiveness by integrating functional cells (e.g., SCs, MSCs, etc.) with smart biomaterials [108].

These novel NGCs not only replicate the spatial architecture of the neural basement membrane but also facilitate axonal regeneration through the controlled release of neurotrophic factors (NGF, BDNF, etc.) alongside antioxidant molecules [109, 110]. The core mechanism lies in the construction of an SC-mediated antioxidant-promoting regeneration molecular system, thus blocking the inhibitory effect of OS on axon growth. Evidence suggests that NGCs enable to remodeling the microenvironment to support axon extension. This is achieved by promoting macrophage polarization toward a reparative phenotype to attenuate the inflammatory response [91, 111].

With the innovation of biomanufacturing technology, the focus of current research on neural tissue engineering has shifted from pure structural biomimicry to a new stage of functionalized synergistic regeneration [112]. Looking ahead, smart NGCs are expected to integrate OS sensing modules with dynamic drug delivery systems to overcome the limitations of the static function of traditional scaffolds. By enabling real-time monitoring of ROS levels in the microenvironment and adaptive regulation of antioxidant release, these advanced systems will achieve more precise and responsive therapeutic interventions. This targeted functional reconstruction strategy facilitates both vascular regeneration and the restoration of bioelectrical signaling. Simultaneously, it allows for accurate control of local redox balance. Collectively, these effects offer a novel solution that bridges anatomical repair with functional recovery in peripheral nerve regeneration. Ongoing advances in this field suggest that neural tissue engineering is shifting from passive structural support toward active microenvironmental regulation, with the ultimate goal of achieving functional regeneration in complex nerve injuries [113–115].

The design and function of NGCs

Optimization of aperture and structure of NGCs

Based on pore size, NGCs can be categorized into large-pore, small-pore, and multi-channel scaffold types. These structural features directly influence cellular behavior, mass exchange, and ultimately the efficacy of nerve regeneration [116–118]. Therefore, designing the ideal pore size of NGCs requires in-depth consideration of its decisive role in determining the fate of Schwann cells within the OS microenvironment. Studies have shown that sufficiently large channels and highly interconnected porous structures can effectively promote the ingrowth of new blood vessels and the exchange of nutrients. [119, 120]. This is critical for reversing the energy depletion of Schwann cells caused by mitochondrial dysfunction under oxidative stress. Furthermore, the open three-dimensional structure provides space for early infiltration of immune cells, particularly macrophages, facilitating their polarization toward the alternatively activated macrophage(M2) pro-regenerative phenotype. This, in turn, accelerates the clearance of myelin debris exacerbated by oxidative stress and fundamentally breaks the vicious cycle of inflammation and oxidative stress [119].

In contrast, scaffolds with excessively small pores, while physically blocking fibroblast invasion and reducing fibrotic scar formation, may simultaneously act as a physical barrier, limiting Schwann cells from obtaining sufficient oxygen and nutrients [119].Under oxidative stress, this nutrient-restricted environment renders Schwann cells more susceptible to ferroptosis, ultimately leading to regeneration failure [121].Thus, an ideal NGC should not be a single homogeneous structure, but rather should possess graded pore sizes or composite pore architectures, so as to ensure the metabolic demands and viability of Schwann cells under stressful conditions while providing topographical guidance.

Based on the above biological requirements, researchers have developed various multilevel channel structures. For example, Maeng et al. constructed a GelMA/PECDA multichannel nerve conduit with good biocompatibility. The 200-μm main channel, combined with micro/nanoporous structures on the inner wall, acted synergistically to significantly enhance nerve regeneration efficiency in animal experiments [122]. Another approach exerts its effects by regulating the cell growth environment. Wang et al. utilized radial and longitudinal foaming techniques to flexibly adjust the pore size distribution of PCL/PVP fiber scaffolds, such that the dimensional variations of the nanoscale grooves effectively guided the directional migration of Schwann cells from the periphery to the center and from the bottom to the top of the scaffold, significantly improving cell infiltration efficiency [123].

In summary, while multichannel conduits excel at providing macroscopic guidance to enhance nerve regeneration efficiency, gradient foaming scaffolds utilize nanoscale groove variations to precisely direct the migration and infiltration of SCs from the periphery to the center. Both strategies demonstrate that over-reliance on uniform pore sizes is problematic, as excessively large channels may lack topographical precision, whereas excessively small pores act as a physical barrier that induces nutrient restriction and SC ferroptosis under oxidative stress. Therefore,

the ideal NGC must adopt graded or composite pore architectures to balance vascular nutrient exchange with topographical guidance.

Material selection for NGCs

The nature of the material is one of the core elements determining the function of NGCs and is a key research direction in neural tissue engineering [124, 125]. The material system has evolved from natural to synthetic and composite materials, with progressive optimization of their respective performance merits enabling structurally and functionally synergistic integration. Natural materials have garnered significant attention due to their excellent biocompatibility. These materials can be broadly categorized into two types. One type consists of biological tissue-derived materials such asECM. The other type includes natural polymers such as chitosan (CS), collagen, hyaluronic acid (HA), and fibrin [126, 127]. A representative example is CS, whose reactive amino groups along the molecular chain enable diverse chemical modifications, endowing it with excellent biological properties. As a result, CS is considered a highly promising biomaterial for nerve repair. Other natural polymers such as collagen, alginate, and glycosaminoglycans have also shown great potential in this field [128–130]. Li et al. [131] fabricated a nerve conduit by combining biocompatible CS with biodegradable HA. This conduit effectively promoted the proliferation of SCs while inhibiting excessive fibroblast growth, thereby reducing scar formation and tissue adhesion, and ultimately facilitating peripheral nerve repair and regeneration. By comparison, synthetic materials such as polylactic acid (PLA), polyglycolic acid (PGA), and polycaprolactone (PCL) exhibit superior mechanical strength and elasticity [132, 133]. To overcome the limitations of single-material properties, composite materials are designed to integrate the advantages of multiple components, aiming to construct NGCs with enhanced functional performance and improved adaptability to the native tissue environment. Beyond their intrinsic physicochemical properties, the selection of these materials must consider their ability to modulate SC redox homeostasis—a criterion that increasingly guides the development of next-generation NGCs.

In light of the increasingly diverse range of available biomaterials, researchers must establish a comprehensive evaluation framework that explicitly links each material property to SC fate under oxidative stress: (1) Biohistocompatibility: Traditionally, the concept of biohistocompatibility referred primarily to the absence of harmful responses within the host.

Contemporary definitions, however, require more than just compliance with basic safety parameters such as non-toxicity and non-carcinogenicity. Increasingly, emphasis is being placed on the material's ability to engage in dynamic, bidirectional interactions with host tissues and to adapt to the local biological environment [134, 135]. Jin's team [136] embedded a urolithin A (UA) hydrogel, which is known for its anti-inflammatory and antioxidant properties, into the lumen of a PCL-based UA NGC. This strategy effectively reduced ROS production and inflammation by leveraging the material's adaptive response to the microenvironment. (2) Biodegradation rate: The biodegradation rate plays a critical role in determining the pace and effectiveness of nerve regeneration. Fast-degrading materials such as CS, gelatin, and PLGA typically degrade within weeks to months, making them well-suited for acute nerve repair. While slow-degrading materials like PCL may take several months or even years to degrade, they offer prolonged and stable microenvironmental support for the regeneration of long-segmental nerve defects [137–140]. (3) Mechanical properties: Mechanical properties, as fundamental attributes of material performance, play a critical role in ensuring the functional integrity of nerve conduits under complex physiological conditions [141]. Insufficient compressive strength compromises the material's ability to withstand dynamic pressure and tensile forces during peripheral nerve regeneration, whereas excessive rigidity may inflict mechanical damage on nerve stumps and regenerating microvessels [142]. Type I collagen, for instance, is widely employed as a base material for NGCs due to its excellent biocompatibility, biodegradability, and low immunogenicity. However, its inherently poor mechanical strength poses a risk of structural collapse [143, 144]. To overcome this limitation, Duan et al. [145] developed a mineralized collagen composite conduit by integrating mineralized collagen with type I collagen. This strategy significantly improves the compressive strength of the conduit while maintaining its bioactivity, thereby enhancing its potential for clinical application [146]. This multidimensional evaluation framework calls for researchers to move beyond the limitations of single-performance metrics and achieve synergistic improvements in bio-responsiveness and functional durability through strategies such as biomimetic design and composite modification (Table 3). Each material category inherently presents a distinct trade-off between bioactivity and physical robustness, prompting the field to increasingly favor composite and biomimetic designs that reconcile these competing demands while introducing new challenges in fabrication reproducibility and long-term *in vivo* stability.

Excessive rigidity disrupts the delicate mechanical microenvironment, which renders SCs increasingly vulnerable to OS [147]. Emerging evidence suggests that the ideal matrix stiffness should mimic the native neural ECM, modulating cell behavior through integrin-mediated mechanotransduction [148, 149]. Furthermore, material mechanical properties function as active regulators rather than passive supports [150]. SCs transduce physical stimuli, such as matrix stiffness or mechanical stretching, into biochemical signals through integrin-mediated mechanotransduction and mechanosensitive channels [141, 150]. This mechanochemical coupling facilitates the homeostasis of pro-survival signaling pathways and metabolic fitness, creating a synergistic framework where material engineering actively participates in biological regeneration.

Innovative functional neural stents

Scaffolds with biologically conductive properties

Electrophysiologic homeostasis of nerve cells is the basis for maintaining the physiologic function of the nervous system [13]. Neuroinjury-induced oxidative stress not only exacerbates microenvironmental deterioration by triggering a surge of proinflammatory cytokines and aberrant protease secretion but also critically disrupts the functional integrity of voltage-gated ion channels, such as Na^+/K^+-ATPase [151–153]. Specifically,

TABLE 3 Key properties and research progress of various types of nerve guidance catheter materials.

Categorical dimensions	Evaluation index	Key elements	Representative materials/ technologies	Research cases/ applications
Material type	Natural materials	Tissue-derived materials: ECM, etc.	CS	CS + HA composite catheter → promotes Schwann cell production, inhibits fibroblast proliferation, and reduces scar formation [131]
		Natural polymers: CS, collagen, HA, fibrin		
	Synthetic material	PCL,PLGA	PLGA/PCL	[132]
Rating system	Biological histocompatibility	Uniform standards: Non-toxic, non-carcinogenic	UA hydrogel	UA hydrogel embedded in the lumen of PCL catheter → reduction of ROS and inflammation [136]
		Modern criteria: Bidirectional interaction and adaptability of materials to host tissues		
	Biodegradation rate	Highly degradable material (weeks - months): Suitable for acute nerve repair	CS/gelatine /PLGA	PLGA: Acute repair; PCL: Providing a stable microenvironment for large segmental defects [137–140]
		Low degradation materials (weeks - years): Supporting long-term repair of large nerve defects	PCL	
	Mechanical properties	Insufficient compressive strength: Structure prone to collapse	Type I collagen (natural defect: Insufficient mechanical strength)	Mineralized collagen + type I collagen → increase stress resistance [145]; Bi-layer knitting technology → optimization of mechanical properties and modulation of SCs [146]
		Excessive rigidity: causes mechanical damage		
		Ideal: Balancing dynamic stress with injury avoidance		
Improvement of technology	Composite modified	Skill enhancement through composite/structural design synergy	Mineralized collagen composite catheter, CS/HA composite catheter	[131, 145]
	Bionic design	Modeling the structure and function of the natural neural microenvironment	Double braided conduit	Bilayer structure → maintains stability + promotes controlled release/proliferation/spatial distribution of SCs [146]
Key challenges and responses	Optimization of mechanical properties	Insufficient mechanical strength of natural materials (e.g., collagen) → improvement by composite mineralized collagen or structural design	Mineralized collagen complex catheter	[145]
	Functional synergy enhancement	Biological responsiveness (e.g., anti-inflammatory, antioxidant)	Degradation rate adaptive material selection	UA hydrogel/PCL composite [136]
		Functional durability (degradation-matched regeneration cycle)		

Abbreviations: CS, Chitosan; HA, Hyaluronic Acid; PCL, Polycaprolactone; PLGA, Poly(Lactic-co-Glycolic Acid); UA, Urolithin A; ECM, Extracellular Matrix.

ROS can induce thiol-oxidizing modifications that alter the conformation of ion or protein channels on the neuronal membrane, resulting in a marked prolongation of the action potential refractory period and consequently disrupting neuronal electrical signaling [154, 155]. This dual disruption of the electrochemical microenvironment initiates a vicious cycle: oxidative stress aggravates environmental deterioration and impairs the myelin regenerative capacity of SCs, and impaired action potential conduction suppresses the secretion of neurotrophic factors. Together, these effects culminate in the failure of axonal regeneration.

Based on this, the design of the new generation of conductive bioscaffolds has evolved from the traditional concept of electrical conductivity to the "electroactivity-modulated" smart materials

[156, 157]. Fundamentally, the material must integrate efficient charge transport across the cell-substrate interface with the capacity to modulate both cell-substrate and cell-cell interactions [158–162]. These materials contribute to the optimization of the nerve regeneration microenvironment through several mechanisms. They promote the adhesion of SCs and growth factors, facilitating initial cellular integration. They also modulate cell–matrix interactions to fine-tune the scaffold's molecular architecture and surface charge distribution. Moreover, they enable functional electrical coupling between the scaffold and host tissues, which is essential for neuromodulation and signal conduction [163]. For example, graphene-based composite scaffolds, owing to their unique sp^2-hybridized orbital structure, can establish a three-dimensional conductive network that promotes electrical coupling among SCs. Additionally, the abundant π-electron cloud on their surface enables efficient scavenging of oxidative species such as OH^-, thereby achieving a synergistic enhancement of both electrical conductivity and antioxidant capacity [162, 164, 165].

Biologically, this graphene-mediated microenvironment optimization facilitates the dual activation of Schwann cells in the peripheral nervous system and astroglia in the central nervous system. *In vivo* evidence confirms that this translates to robust remyelination by upregulated MBP and restored functional electrical coupling, significantly increasing nerve conducting velocity and compound motor action potentials compared to pure PCL controls [165].

Moreover, conductive scaffolds are not merely physical conductors of electrical current; more importantly, the weak electrical signals they induce can act as exogenous biophysical signals that activate endogenous calcium signalling in Schwann cells [166] and downstream FAK/AKT pro-survival pathways [167]. This, in turn, counteracts the OS microenvironment [74] and ultimately reverses the OS-induced suppression of neurotrophic factor (e.g., BDNF and NGF) secretion by Schwann cells [166, 167]. Notably, graphene-based scaffolds distinguish themselves from most conductive polymers by offering concurrent charge transfer and intrinsic ROS scavenging, whereas other conductive materials predominantly rely on exogenous biophysical stimulation to indirectly alleviate oxidative stress. This distinction underscores the growing importance of multifunctionality in scaffold design for the OS-compromised microenvironment.

Biomimetic ECM scaffolds

Compared with conventional scaffolds, biomimetic ECM scaffolds mimic physiological structures, not only restoring anatomical integrity but also enabling targeted functional reconstruction [168]. Bionic ECM scaffolds reconstruct nanofiber networks mimicking basement membrane pore size and mechanical gradients via electrospinning, 3D printing, and other techniques, thereby accelerating guided axon regeneration and reducing ROS exposure time [169–171]. Such scaffolds provide not only physical support for regenerating tissues but also act as dynamic signaling platforms. Through the multimodal integration of bioactive molecules, anti-inflammatory agents, antioxidants, and conductive components, they enable precise regulation of the regenerative microenvironment [127, 172, 173].

As discussed in earlier sections, the OS environment induces mitochondrial metabolic dysfunction and homeostatic imbalance in SCs. Jiang et al. fabricated a multilayered conduit combining PCL nanofiber topology with blend-loaded melatonin (MLT) and reduced graphene oxide (RGO). Biologically, while RGO restores bioelectrical conduction, MLT maintains a stable $\Delta\Psi_m$ as confirmed by JC-1 assay, which bioenergetically prevents the proton motive force reversal to abort the RET-induced ROS burst at Complex I and III. This metabolic rescue amplifies ATP supply for energy-demanding myelin regeneration, achieving functional and morphological recovery close to autologous nerve grafts in a 10-mm rat sciatic nerve defect model. Beyond chemical ROS-scavenging designs, the anisotropic physical topology of biomimetic ECMs (e.g., aligned nanofibers and microgrooves) independently drives directional SC migration and upregulates crucial myelination-associated genes, including *Mbp* and *Sox10*. Mechanistically, this topographic guidance running via cytoskeleton-mediated mechanotransduction specifically targets and activates three major intracellular cascades: the Wnt/β-catenin, ERK/MAPK, and TGF-β signaling pathways [174]. This biophysical regulation runs parallel and complementary to biochemical antioxidant signaling, cooperatively rescuing SC functions and accelerating re-myelination within the hostile oxidative niche.

The bionic ECM scaffold, with its multidimensional bionic advantages in structure, signal, and function, is promoting the upgrade of peripheral nerve repair from "passive support" to "intelligent guidance." Chen et al.'s composite conduit actively scavenges ROS via disulfide bonds. This suppresses NF-κB/IL-1β and restores PI3K/AKT/mTOR signaling, which promotes Schwann cell proliferation and angiogenesis. Consequently, the repair strategy shifts from passive guidance to active microenvironmental reprogramming. [175]. Through the biomimicry of the native microenvironment and the integration of multimodal regulatory strategies, this approach improves both the spatial and temporal precision of axonal regeneration. It thereby establishes a robust foundation for the construction of personalized nerve grafts capable of achieving tissue integration and functional restoration [176].

These biomimetic ECM strategies promote regeneration through distinct yet complementary mechanisms: physical anisotropic topologies directly drive SC migration and myelination gene expression via mechanotransduction signaling, whereas biochemical modifications actively scavenge ROS, prevent RET-induced oxidative bursts, and restore bioelectrical conduction. Although combining these physical and biochemical cues successfully shifts nerve repair from passive guidance to active microenvironmental reprogramming, realizing a clinically feasible solution still requires further optimization of the dynamic coupling between material degradation and factor release, as well as maintaining the long-term stability of the scaffold-cell interface.

The new concept of intelligent drug delivery system

A drug delivery system (DDS) refers to the use of specific technical means to precisely control the timing, location, and dosage of drug release, delivering drugs to target tissues or organs in a controlled, efficient, and safe manner to enhance drug efficacy and reduce side effects. Its core advantages lie in

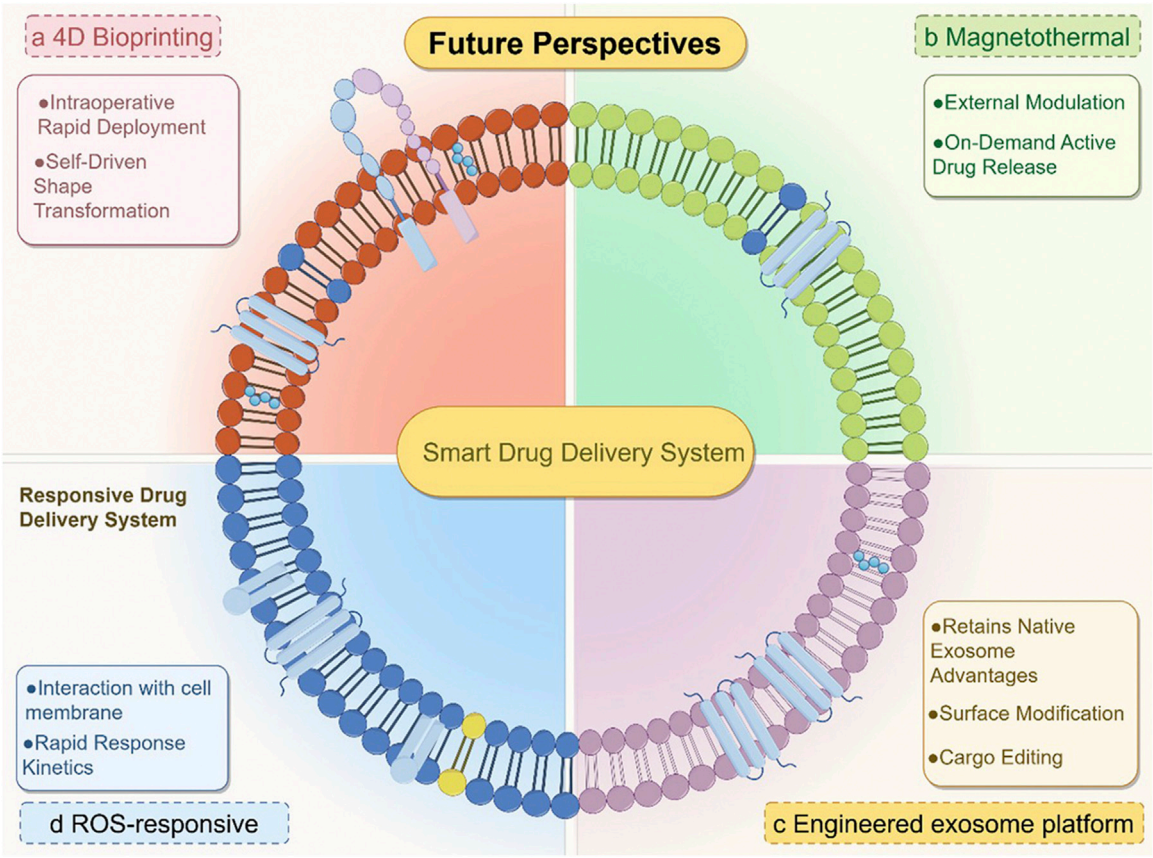


FIGURE 6
(a) The ROS-responsive drug-controlled release system offers high targeting specificity and enables rapid response to injury-induced ROS in early stages; **(b)** the magnetothermal controlled-release system permits external remote activation for on-demand drug release; **(c)** the engineered exosome platform retains the innate targeting capability, biocompatibility, and complex biomolecule-delivery functions of natural exosomes while allowing programmable surface modifications and cargo editing; and **(d)** 4D bioprinting facilitates rapid in vivo formation of NGCs with self-morphing capabilities via hydration-driven expansion or programmed design. Collectively, these approaches promote peripheral nerve regeneration through distinct mechanisms.

improving drug stability, optimizing distribution characteristics, and reducing side effects [135, 136]. Conventional drug delivery systems lack precise spatiotemporal control, which hinders their ability to achieve specific targeting and optimal biodistribution of therapeutic agents [177, 178]. In contrast, intelligent drug delivery systems are capable of dynamically recognizing the lesion microenvironment, performing subcellular targeting, and achieving programmed release in response to endogenous signals (e.g., pH, enzymes, temperature) or external stimuli (e.g., light, ultrasound, magnetic fields). These systems complete a closed-loop delivery process, from protecting drug activity to enabling precise spatiotemporal regulation [3, 113, 179]. In response to the OS microenvironment, the development of ROS-responsive drug-controlled release systems, magnetothermal-regulated release systems, and engineered exosome-based delivery platforms holds significant potential for mitigating ROS-induced damage and enhancing the proliferation of SCs (as shown in Figure 6).

ROS-responsive drug-controlled-release system

The significant increase in ROS levels at the site of nerve injury provides a theoretical basis for the construction of a ROS-responsive drug-controlled release system. Such systems are typically engineered with ROS-sensitive linkers to create stable ROS-responsive materials. They may also incorporate hydrogels or nanoparticle-based carriers loaded with functional cells, neurotrophic factors, antioxidants, and anti-inflammatory agents to enable intelligent stimulus-responsive release and precise therapeutic modulation [180, 181]. ROS-responsive drug piggyback systems vary in the drugs that researchers choose to piggyback. According to the different purposes, they can be broadly categorized into the following four types: (1) Antioxidants can effectively scavenge free radicals and reduce ROS levels, thereby reducing oxidative stress and cell damage [182, 183]. (2) NGF plays a critical role in the nervous system. It facilitates the elongation of neuronal axons and also contributes to the formation of myelin sheaths, both of which are essential for nerve repair and signal conduction [8, 171]. (3) Anti-inflammatory drugs reduce the local inflammatory response by down-regulating pro-inflammatory factors such as TNF-α, IL-6, and IL1-β. Moreover, since OS and inflammation are mutually reinforcing, controlling inflammation can in turn alleviate oxidative stress, thereby further breaking the vicious cycle [60, 133, 184]. [4] Gene therapy drugs can act directly on key pathological links after nerve injury, for example, PINK1 mRNA enters the cell and directs the synthesis of

PINK1 protein, which is closely related to mitochondrial autophagy [185].

The above strategies facilitate the diverse development of ROS-responsive systems. o precisely modulate the oxidative and senescent microenvironment, Zhao et al. developed a ROS/Ca^{2+}-responsive dynamic hydrogel composed of HA-PBA, TPA, and CS-EDTA. [185]. This hydrogel delivers engineered extracellular vesicles (EVs) loaded with PINK1 mRNA. Through dual modifications, these EVs specifically target DPP4 receptors on senescent SCs. Crucially, once internalized, the PINK1 mRNA directly activates the PINK1/Parkin-mediated mitophagy pathway, which clears damaged mitochondria and halts ROS accumulation. This targeted intervention reverses SC senescence and restores pro-regenerative capacity, thereby accelerating nerve repair. In a complementary approach, Dong et al. engineered a ROS-responsive and thermosensitive hydrogel system (PTCM@PMet nanoparticles embedded within mPEG-PA-PP) to selectively deliver the H_2S donor, peroxyTCM. Triggered by the high-ROS injury microenvironment, peroxyTCM releases H_2S. Of note, beyond acting as a direct chemical ROS scavenger, H_2S serves as a gaseous signaling molecule that is known to activate the Nrf2/HO-1 antioxidant axis and suppress NF-κB-mediated inflammation. This dual-pathway modulation is expected to protect Schwann cells from lipid peroxidation-induced injury, decisively reshaping the hostile oxidative niche into a pro-regenerative milieu [115]. Moreover, this experiment employed the fluorescent probe 7-nitro-4-methylcoumarin (AzMC) to monitor and visualize the accumulation of H_2O_2 and H_2S in the cellular environment, thereby providing a more intuitive reflection of the actual ROS response.

Overall, the ROS-responsive controlled release system offers a novel approach to precisely regulate oxidative stress and inflammation following nerve injury through the synergistic integration of material design and drug loading. Nevertheless, it is worth noting that uncertainties remain regarding the specificity of the response and the persistence of efficacy under multiple pathological stimuli. Consequently, related research needs to further focus on assessing stability and practicality under complex *in vivo* environments [186].

Engineering exosome delivery platform

Exosomes are nanoscale vesicles originating from endosomal compartments that carry various biologically active molecules, including RNA and proteins. Through non-cell-autonomous mechanisms, they regulate key cellular processes such as migration, differentiation, and responses to tissue injury, thereby promoting neurite outgrowth and axonal regeneration in the peripheral nervous system [187–189]. Recent studies have shown that exosomes derived from SCs can deliver miR-21 to specifically suppress PTEN expression, thereby relieving the inhibition of the PI3K/Akt signaling pathway. This activation subsequently upregulates anti-apoptotic proteins, promoting neuronal survival and axonal regeneration [190].

In recent years, engineering exosomes to enhance their own functions or improve their targeting has gradually become a new development trend. The engineering approaches that can be employed include direct modification of exosomes, induction of cell differentiation, and pretreatment of parent cells, among others [191]. Applying this direct modification strategy, Liu et al. loaded polyphenol-engineered Saccharina japonica exosomes (CA@Exos) onto electroconductive microneedles to achieve deep-tissue delivery [192]. Concurrently, the application of exogenous electrical stimulation via this bioelectric scaffold significantly amplifies the cellular uptake of these exosomes. Mechanistically, the released caffeic acid (CA) specifically inhibits the formation of AGEs and blocks AGE-RAGE interactions, while mitigating ROS accumulation through the upregulation of antioxidant enzymes such as Sod2 and Hmox1. Furthermore, the combined bio-electroceutical intervention facilitates Ca^{2+} influx, activating Camk2a/Camk2b-mediated Erk1/2 and cGMP-PKG signaling cascades. This targeted multi-pathway modulation fosters robust crosstalk between Schwann cells and vascular endothelial cells. Ultimately, this seamless coupling of redox homeostasis with neuroangiogenesis establishes a self-amplifying loop that significantly accelerates chronic tissue repair [192]. These examples underscore the versatility of exosome engineering: by coupling innate targeting with tailored cargo and surface modifications, exosome platforms can be precisely configured to counteract specific oxidative and inflammatory pathologies in the injured nerve microenvironment.

Magneto-thermally controlled release system

The magnetothermal controlled-release system, leveraging localized heating of magnetic nanomaterials under an alternating magnetic field, enables precise delivery of neurogenerative factors and coordinated regulation of the OS microenvironment [193–195]. This feature is conducive to loading magnetic nanoparticles, exosomes, neurotrophic factors, or antioxidants together in a thermosensitive hydrogel. By using the magnetic field-triggered thermal energy, the swelling-shrinking behavior of the hydrogel can be dynamically regulated to achieve the on-demand release of active substances [196–198]. Additionally, magnetothermal stimulation activates TRPV1 channels, leading to a calcium ion influx that promotes Schwann cell migration and axonal growth. Beyond triggering drug release, magnetothermal cues directly activate specific intracellular pathways. For instance, magnetic composite scaffolds can activate the Heat Shock Protein 70 pathway to enhance synergistic tissue regeneration [199]. Furthermore, Kuznetsova et al. engineered a magnetic fibrin hydrogel that generates localized heating upon alternating magnetic field (AMF) exposure. This remote thermal cue specifically targets thermosensitive TRPV1 ion channels, triggering a Ca^{2+} influx that promotes 3D neurite outgrowth and axonal extension [200].

Although systematic application of TRPV1-targeted magnetothermal effects to NGC design remains in its early stages, the recent demonstration of magnetic fibrin hydrogels as implantable neural interfaces [200] provides a strong proof-of-concept that this modality can be integrated into next-generation nerve scaffolds, warranting further mechanistic investigation.

4D bioprinting technology

3D bioprinting can be used to fabricate biocompatible and functionally active neural scaffolds and offers innovative solutions

to meet complex neural tissue repair needs by precisely modulating the spatial distribution of cells and biomaterials. Leveraging computer-aided design, 3D printing enables the personalized fabrication of structures with physiological shapes and microstructural features, better meeting the needs of individual patients [201, 202]. Despite its considerable potential, current 3D printing technology still faces significant limitations. One key issue lies in its inability to fully replicate and integrate the complex multimodal signals present in the physiological microenvironment of implantable nerve conduits. Moreover, effectively coordinating stem cell differentiation within these constructs remains a major challenge.

4D bioprinting builds upon 3D printing by introducing a time-dependent dynamic response. This technology enables printed structures to adapt to physiological environments in real time. It achieves this adaptability by combining smart-responsive materials such as temperature-sensitive hydrogels, light-responsive hydrogels, and shape memory polymers with preprogrammed structural designs. Examples of such designs include anisotropic shrinkage, gradient degradation, and predesigned deformation patterns. The core breakthroughs are reflected in three key aspects: (1) By studying and mimicking the dynamic changes of key structures such as the extracellular matrix during the nerve regeneration process, researchers can reconstruct a functional microenvironment at the injury site. This reconstructed microenvironment is not fixed in form. Instead, it can continuously adapt and remodel itself in coordination with the distinct stages of nerve regeneration. Such adaptability ensures sustained support for cellular activity and promotes progressive tissue repair. (2) Employ computational programming to precisely regulate the spatiotemporal release of neurotrophic factors and antioxidants. This enables the deliberate setting of parameters such as dosage, timing, and release location, facilitating alignment with the evolving demands of nerve regeneration. (3) Integrate electrically active scaffolds with conventional biological scaffolds that provide structural support and directional guidance, thereby synergistically enhancing the conduction of electrical signals between neurons [203–206].

Currently, the application of 4D bioprinting specifically targeting OS in nerve repair remains largely unexplored. However, recent dynamic designs provide a strong foundational framework. For example, Wang et al. developed a 4D-printed shape-memory conduit (PLATMC/$Ti_3C_2T_x$ MXene) that autonomously self-rolls at 37 °C within 20 s to rapidly wrap injured nerves [206]. Mechanistically, its pre-programmed microchannels offer topographical guidance for directional SC migration via cytoskeleton-mediated mechanotransduction, while the conductive $Ti_3C_2T_x$ matrix promotes SC maturation and robust angiogenesis. Although their study focused on biophysical cues, $Ti_3C_2T_x$ intrinsically possesses potent ROS-scavenging properties, attributed to its inherently reducing Ti-C skeleton and antioxidant enzyme-mimicking properties (e.g., SOD-like and CAT-like activities) [207, 208]. This reveals a promising, untapped strategy: integrating such nanomaterials into 4D-printed scaffolds can synergistically couple morphological self-adaptation with active OS neutralization to comprehensively remodel the hostile regenerative microenvironment.

To systematically summarize these cutting-edge strategies, the representative applications of smart biomaterial systems (including external physical field stimulation, magneto-thermal controlled release, and 4D bioprinting) for ROS scavenging and nerve regeneration are summarized in Table 4.

In summary, tissue engineering has evolved from passive conduits to active, intelligent delivery systems capable of precise ROS regulation. These advanced engineering milestones establish a robust foundation for the targeted translational applications discussed next.

Novel approaches and therapeutic strategies for SCs-OS interactions in PNI/peripheral neuropathy

SCs are key functional units of the peripheral nervous system and play an important role in common peripheral nerve diseases. Whether the peripheral nerves are affected by acute injury or chronic lesions, SCs are involved in the process of nerve repair [209]. Meanwhile, almost all neurological diseases are associated with inflammation, and the cascade effect of OS and inflammation is a common pathological axis running through many peripheral neurological diseases; SCs are not only a key target of this pathological process, but also participate in shaping the center of microenvironmental regulation of the disease through the dynamic interactions between SCs and the immune system [210]. Notably, although the OS-SCs-immune cells "triangle" is prevalent, its specific pattern and pathological outcome are highly dependent on the disease-specific microenvironment [211]. The subsequent discussion will use PNI, DPN, and NF1 as disease models to explore the effects of OS-SCs interactions in peripheral nerve mechanical injuries, metabolic lesions, and hereditary lesions, respectively, and then focus on the precise antioxidant therapeutic strategies developed based on these mechanisms, to provide theoretical bases and prospective perspectives for the future direction of treatment.

While the last section outlined universal tissue engineering strategies, clinical success requires tailoring them to these specific microenvironments. Therefore, before exploring the clinical landscape, we should examine how OS-SC interactions differ across mechanical, metabolic, and hereditary neuropathies, using PNI, DPN, and NF1 as specific models. This will guide the design of targeted precision therapies and provide theoretical bases for future treatments.

Pathological mechanisms of SCs and oxidative stress in PNI/peripheral neuropathy

The interaction mechanism of OS-SCs in PNI

Following mechanical injury to peripheral nerves, SCs are one of the earliest cell types to respond to injury [13]. By inducing mitochondrial dysfunction and DNA damage, oxidative stress not only directly impairs the repair phenotype of SCs, but more crucially, drives their transition from pro-regenerative "repair SCs" to inhibitory "senescent SCs," thereby deteriorating the regenerative microenvironment [4, 27]. This process is regulated by the Nrf2 antioxidant pathway; insufficient Nrf2 activity

TABLE 4 Summary of antioxidant strategies and structural.

Antioxidant strategy/Mechanism	Related biomaterial/Vehicle	Main function and effect	In-text instance/ Source
Activating endogenous antioxidant pathways to inhibit cell ferroptosis	MB-CDs	Activates Nrf2 protein, initiating downstream expression of HO^{-1} and GPX4, reducing the production of lipid peroxides, and inhibiting ferroptosis in SCs	[30]
Sustained release of active elements to activate pro-survival signaling pathways	Porous Se@SiO_2 nanocomposite	Effectively activates the PI3K/AKT signaling pathway through the sustained release of selenium, thereby reducing ROS generation, suppressing apoptosis, and promoting cell migration and nerve regeneration	[75]
Environment-responsive adaptive regulation to combine anti-inflammatory and antioxidant effects	UA hydrogel embedded into the lumen of a PCL-based NGC	Reduces ROS production and inflammation by leveraging the material's adaptive response to the microenvironment	[136]
Direct ROS scavenging via surface electron clouds combined with bioelectrical coupling	Graphene-based composite scaffolds/RGO	The abundant π-electron cloud on the surface enables efficient scavenging of oxidative species such as OH^{-}; establishes a 3D conductive network to promote electrical coupling among SCs and increase nerve conducting velocity	[162, 165]
Multimodal metabolic rescue (antioxidant release + Bioelectrical conduction)	Multilayered conduit combining PCL nanofiber topology with blend-loaded MLT and RGO	RGO restores bioelectrical conduction, while MLT maintains a stable $\Delta\Psi_m$, preventing the RET-induced ROS burst and amplifying ATP supply for myelin regeneration	
Active ROS scavenging via chemical bond cleavage to reprogram the microenvironment	Composite conduit actively scavenging ROS via disulfide bonds	Scavenges ROS via disulfide bonds, suppressing NF-κB/IL-1 and restoring PI3K/AKT/mTOR signaling to promote Schwann cell proliferation and angiogenesis	[175]
Dual-responsive stimulus release for subcellular targeted gene therapy	ROS/Ca^{2+}-responsive dynamic hydrogel formed by HA-PBA, TPA, and CS-EDTA (delivering engineered EVs loaded with PINK1 mRNA)	Specifically targets DPP4 receptors on senescent SCs; the internalized PINK1 mRNA directly activates the PINK1/Parkin-mediated mitophagy pathway to clear damaged mitochondria, halt ROS accumulation, and reverse SC senescence	[185]
Intelligent controlled-release of gaseous signaling molecules for dual-pathway modulation	ROS-responsive and thermosensitive hydrogel system (PTCM@PMet nanoparticles embedded within mPEG-PA-PP)	Triggered by the high-ROS injury microenvironment to release H_2S, which acts as a gaseous signaling molecule to activate the Nrf2/HO^{-1} antioxidant axis and suppress NF-κB-mediated inflammation, protecting SCs from lipid peroxidation	
Engineered exosome delivery platform coupled with external physical stimulation	Polyphenol-engineered Saccharina japonica exosomes (CA@Exos) integrated into electroconductive microneedles	External electrical stimulation amplifies cellular uptake of exosomes, which specifically activate Camk2a/Camk2b-mediated Erk1/2 and cGMP-PKG signaling cascades to efficiently clear ROS and AGEs	[192]

(*Continued*)

TABLE 4 Continued

Antioxidant strategy/Mechanism	Related biomaterial/Vehicle	Main function and effect	In-text instance/ Source
Magneto-thermally controlled release system: Precise delivery of neurogenerative factors and coordinated regulation of the OS microenvironment	Magnetic composite scaffolds/Magnetic fibrin hydrogel (or loading magnetic nanoparticles, exosomes, neurotrophic factors, or antioxidants together in a thermosensitive hydrogel)	Uses magnetic field-triggered thermal energy to dynamically regulate the swelling-shrinking behavior of the hydrogel for on-demand release of active substances. Magnetothermal cues activate the heat Shock Protein 70 pathway and target thermosensitive TRPV1 ion channels, triggering a Ca^{2+} influx that promotes Schwann cell migration, 3D neurite outgrowth, and axonal extension	[199, 200]
4D bioprinting self-adaptation coupled with intrinsic inorganic antioxidant framework	4D-printed shape-memory conduit (PLATMC/ Ti3C2T_X MXene)	Autonomously self-rolls at 37 °C to rapidly wrap injured nerves; the inorganic matrix ($Ti_3C_2T_X$) intrinsically possesses potent ROS-scavenging properties due to its reducing Ti-C skeleton and antioxidant enzyme-mimicking properties (SOD-like and CAT-like activities)	[206–208]

Abbreviations: MB-CDs, Mung bean-derived carbon dots; SCs, Schwann cells; UA, Urolithin A; RGO, reduced graphene oxide; MLT, melatonin; AGEs, advanced glycation end products; membrane potential, ΔΨm.

accelerates the senescent transition of SCs, whereas Nrf2 activation helps sustain the repair phenotype and resist senescence [30, 105].

Specifically, SCs upregulate the expression of pro-inflammatory factors such as tumor necrosis factor-α (TNFα) and interleukin-6 (IL-6), along with chemokines such as CCL2, through perceived destructive signals in the microenvironment [212, 213]. Subsequently, the above factors recruit monocytes/macrophages to the site of injury, and the polarization of classically activated macrophage (M1) promotes the development of inflammation [214]. At the same time, Nox in SCs, M1, and neutrophils is activated and releases large amounts of ROS. For repair Schwann cells, moderate ROS levels serve as essential second messengers that sustain c-Jun expression and maintain their dedifferentiated state, as evidenced by studies showing that H_2O_2 directly modulates c-Jun and ERK activation in injured nerves [69], and that c-Jun is the master transcriptional regulator of the Schwann cell repair program [215]. However, excessive ROS triggers axonal growth cone collapse and retraction, a positive feedback between inflammation and OS formation that is a key component of Wallerian degeneration [9, 38]. The large amount of ROS generated during this process damages the myelin debris produced by SCs, which will impede nerve regeneration. SCs, macrophages, and neutrophils are all capable of phagocytosing and removing myelin debris [216, 217]. As inflammation progresses into the chronic phase, SCs induce polarization of M1 toward M2, which secretes vascular endothelial growth factor (VEGF) with pro-angiogenic effects [210, 214]. Demyelinated SCs form “Büngner bands” along the trajectory of neovascularization, providing structural guidance for axonal regeneration [218, 219].

Studies have shown that after PNI occurs, the expression of the key antioxidant defense pathway Nrf2 in SCs is downregulated, resulting in a decrease in their antioxidant capacity [64]. This change, to some extent, helps to establish the Wallerian degeneration microenvironment, thereby supporting the process of peripheral nerve repair. In addition, SCs secrete various neurotrophic factors, which regulate the survival, migration, adhesion, and chemotaxis of cells, thereby further promoting axonal regeneration [220] (as shown in Figure 7). The above-mentioned cascade reaction composed of inflammation and OS is not only a classic pathological change after PNI, but also one of the core theoretical foundations for guiding antioxidant treatment.

Although the inflammation-OS cascade is a ubiquitous pathological mechanism following PNI [10], it must be emphasized that different experimental PNI models exhibit divergent characteristics. In the nerve crush model, the basal lamina surrounding the axons remains intact, allowing axons to regrow within their original basal lamina tubes. In contrast, in the cut injury model, the connective tissue and basal lamina tubes are disrupted, compelling regenerating axons to cross the tissue bridge formed between the severed stumps [221]. Therefore, PNI should not be treated as a homogeneous pathological condition. Clearly distinguishing the microenvironmental disparities among these injury models holds significant clinical translational value, suggesting that treatment strategies for peripheral nerve injury must shift toward precision and customized therapy [222].

The interaction mechanism of OS-SCs in DPN

DPN is a typical metabolic peripheral neuropathy, and one of the core pathologic bases of its pathologic basis lies in the metabolic disorders and OS triggered by chronic hyperglycemia [223]. Redundant glucose is shifted to the polyol pathway for metabolism due to increased hexokinase activity in the high glucose environment. At this point, SCs metabolize glucose to fructose with the vascular endothelium-expressed aldose reductase AR, which depletes nicotinamide adenine dinucleotide phosphate (NADPH). Decreased levels of NADPH impede GSH

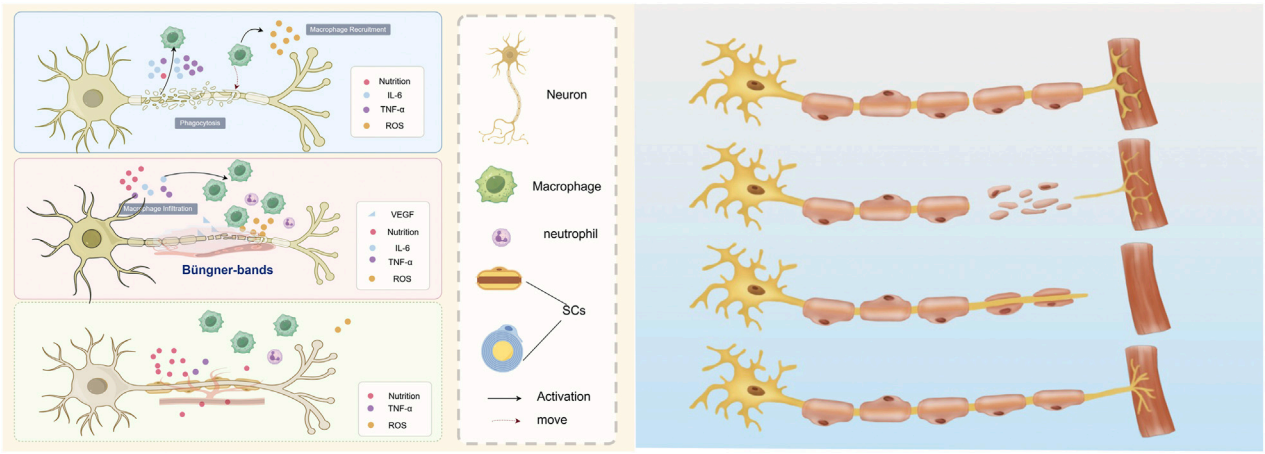


FIGURE 7
The mechanism of OS and the inflammatory cascade reaction: (1) After PNI, Schwann cells release inflammatory and trophic factors and phagocytose myelin debris. Inflammatory cues recruit macrophages and neutrophil that secrete ROS. (2) Wallerian Degeneration: Axons degenerate, Bungner bands form, and macrophages secrete VEGF to promote angiogenesis. Then SCs migrate along the newly formed vessels. (3) Nerve Regeneration (ideal situation): Axons regrow, ROS and inflammation decrease, and neurotrophic support increases.

synthesis, and cellular antioxidant capacity decreases [66]. Additionally, the Maillard reaction, polyol pathway, ketone body metabolism, and Wolff pathway produce AGEs. Hyperglycemic Glucose (HG) leads to an abnormal accumulation of AGEs [224]. Then, an abnormal accumulation of AGEs results in binding to RAGE on SCs and activating pathways such as NF-κB, JNK, and NLRP3, generating ROS and inflammatory factors that lead to SC damage and dysfunction [225, 226]. Not only that, the HG environment also activates signaling pathways such as PKC [227]. Together, the above pathways promote OS onset and further elicit an inflammatory infiltrate.

A study showed that the infiltration of M1 and resting $CD4^+$ memory T cells was increased under DPN conditions. Meanwhile, the infiltration of M2, resting mast cells, monocytes, and T follicular helper cells was decreased, which may be related to the development of DPN [132]. Moreover, *in vitro* studies have shown that high glucose conditions promote sustained M1 polarization of macrophages by downregulating IRG1 expression, suggesting a potential mechanism by which M1 macrophages may persist in diabetic complications such as DPN [228]. However, direct evidence for increased M1 infiltration and decreased M2 in DPN development remains to be established. Also, HG-induced mitochondrial dysfunction and inhibition of the Nrf2 pathway resulted in a decrease in the antioxidant capacity of SCs and a weakening of the ability to withstand stress [229, 230]. As for mast cells, HG-stimulated secretion of factors inhibits myelin formation in SCs [231]. In summary, OS-inflammation co-propels DPN progression. The major cells involved in the process are similar to those of PNI, but the pathologic changes differ in different microenvironments. In general, cells can mitigate greater damage from stressful environments through autophagy. However, HG inhibits the autophagy function of SCs, which is detrimental to the remodeling of the microenvironment [94]. Therefore, modulating the relevant signaling pathways and restoring autophagy in SCs is a promising therapeutic strategy.

The interaction mechanism of OS-SCs in NF1

SCs are the origin of NF1, and their tumorigenesis is due to mutations in the NF1 gene within SCs [232]. The mutation results in the deletion of the protein encoding the NF1 gene that inhibits Ras activity, and sustained activation of the Ras signaling pathway. Downstream signaling pathways (e.g., Raf-MEK-ERK, PI3K-Akt-mTOR, etc.) are subsequently activated, promoting the proliferation, migration, and survival of SCs [233]. At the same time, SCs secrete large amounts of Kit ligand to recruit both NF1 mast cells and CSF1 to recruit macrophages. Both NF1 mast cells and macrophages promote the migration and proliferation of SCs by inducing angiogenesis, providing nutrient support, and secreting large amounts of TGFβ to stimulate collagen production by fibroblasts and the formation of tumor strom [234–236]. In conclusion, the pathological microenvironmental regulation of NF1 by SCs-immune cells influences tumor formation to a certain extent, and the study of the mechanisms of cell-cell interactions contributes to the understanding of disease onset and progression. Additionally, activation of signaling pathways such as mTOR has been observed to upregulate ROS production in several studies [16, 237]. Moreover, ROS plays a dual role in cancer. On the one hand, ROS are carcinogenic risk factors in their own right and may also cause damage to the DNA of cells. On the other hand, the cytotoxicity of excess ROS can also act on tumor cells [16]. Therefore, modulation of OS-related signaling pathways in NF1 to intervene in NF1 may serve as a new therapeutic tool.

Precision antioxidant therapy based on OS-SCs interaction mechanism

In antioxidant treatment for PNI, traditional drugs such as vitamins, curcumin, and alpha-lipoic acid can reduce ROS to some extent [99, 238, 239]. However, these drugs generally lack selectivity for specific cell types and pathways and are considered broad-spectrum, non-targeted therapies. As research on the

molecular mechanisms of PNI progresses, antioxidant strategies are evolving toward more precise and targeted approaches.

For instance, Yadav et al. used the Histone Deacetylase (HDAC) inhibitor PBA to verify its repair efficacy in the RT4 SC inflammation model and the sciatic nerve transection model [240]. The results showed that PBA could significantly reduce the expression and secretion of TNF-α and inhibit the phosphorylation of NF-κB-p65. It effectively alleviated the inflammatory response both *in vivo* and *in vitro*. Yao et al. utilized tFNAs as carriers and loaded resveratrol by intercalation to construct a tetrahedral framework nucleic acids (tFNAs)-RSV complex. The complex significantly improved the stability, bioavailability, and cellular uptake efficiency of RSV, and ameliorated the pathological changes and symptoms of DPN by regulating redox balance and mitochondrial bioenergetic metabolism [241]. In contrast to the above strategies aimed at protecting SCs and attenuating oxidative damage, NF1, a tumor originating from SCs, was treated by combining mTOR/HDAC inhibitors with simultaneous inhibition of the two major antioxidant pathways, GSH and TRX, which resulted in dramatic accumulation of ROS and ultimately led to tumor cell death [237].

Furthermore, nerve tissue engineering also provides a new approach for targeted antioxidant therapy of PNI. Li et al. developed a multifunctional delivery system based tFNAs and microRNA-22. It enhances the communication between SCs and macrophages to reconstruct the damaged microenvironment, inhibits inflammation, and significantly reduces ROS expression. At the same time, this system can also upregulate the BDNF/Tropomyosin Receptor Kinase (TrkB) signaling pathway to promote the functional recovery of peripheral nerve injuries [242]. In another study, Wei et al. utilized a light-responsive small spherical algae hydrogel (C-Gel) to regulate local oxygen release and the immune microenvironment. This approach successfully reduced the expression of ROS, TNF-α, IL-6, and Hypoxia-Inducible Factor-1α(HIF-1α), which also promoted the polarization of macrophages from M1 to M2. Consequently, these changes enhanced the proliferation, migration, and secretion functions of SCs, ultimately improving the effect of nerve regeneration [243]. Boron ester-bonded dextran-based hydrogel patches both scavenge ROS *in vitro*, thereby protecting mitochondrial morphology and functional homeostasis in healthy RSC96 cells, and promote axonal regeneration, myelin sheath regeneration, and recovery of motor function in diabetic rats [244].

Comparing these engineered delivery platforms illustrates the diverse pathways developed to overcome the non-targeted limitations of traditional broad-spectrum antioxidants: tetrahedral framework nucleic acids (tFNAs) excel at improving drug bioavailability and enhancing SC-macrophage communication, light-responsive Chlorella hydrogels uniquely leverage biological photosynthetic oxygen generation to drive M2 macrophage polarization, and boronic ester-bonded hydrogel patches provide rapid chemical ROS scavenging to preserve SC mitochondrial homeostasis. To further enhance their therapeutic efficacy, future precision therapies must focus on integrating SC-specific targeting capabilities and developing materials that respond dynamically to both ROS and pro-inflammatory cues.

In summary, antioxidant strategies are gradually developing towards precision and targeting. The following research directions may play a positive role in the improvement of antioxidant therapeutic efficacy: (1) Design of nanoparticles with SCs targeting to achieve localized and precise delivery of therapeutic substances by combining with electrospun nerve conduits. (2) Developing ROS/pro-inflammatory factor-responsive scaffolds for precise delivery of antioxidants to damaged areas; (3) Analyzing the mechanism of interaction between SCs and the immune system at the molecular and cellular levels, and proposing ideas for targeted intervention.

Clinical transformation and application status

Research on the explicit interplay between SCs and OS in peripheral nerve injury remains an emerging field. However, therapeutic approaches targeting antioxidant strategies and SC functional modulation are actively advancing toward clinical application. We summarize the current translational landscape (Table 5) through four key aspects: (1) Recent clinical trials, focusing on highly relevant studies registered or updated within the past 5 years; (2) Major grant support, highlighting recent projects funded by agencies like the NIH, ERC, and NSFC; (3) Seminal clinical evidence demonstrating foundational safety and efficacy; and (4) FDA-approved therapeutic drugs and nerve conduits relevant to the peripheral nervous system. In conclusion, interventions such as antioxidants, biological therapies, and tissue engineering devices all share a common mechanistic theme. They rely, to varying degrees, on either modulating the oxidative stress microenvironment or supporting the functional capacity of SCs to treat peripheral nerve injury and other neurological disorders.

However, most of these strategies act indirectly on the SC-OS axis, and there are still no clinical experiments that directly target and regulate the interaction between the two. Particularly in the field of neural tissue engineering, most currently FDA-approved NGCs (such as NeuraGen®, NeuroMatrix™, Neurolac®, Neuroflex™, Reaxon®, Nerbridge®, and Avance®) are predominantly single-lumen, hollow conduits. Clinical data show that although some products perform well for short nerve defects (<3 cm), they cannot fulfill the complex biophysical and biochemical requirements for comprehensive nerve regeneration in a hostile oxidative microenvironment [245]. This suboptimal efficacy in long-gap repairs is largely attributed to the lack of an internal biomimetic ECM topographic structure, which prevents SCs from migrating and forming vital Bands of Büngner. Furthermore, the massive burst of ROS triggered by ischemia-reperfusion injury during surgical implantation often transforms these passive conduits into a "hostile zone" that accelerates SC senescence and apoptosis. Although NGCs designed for long-gap nerve defects have not yet entered clinical practice, preclinical studies have successfully achieved the regeneration of 5-cm axonal gaps and the restoration of electrophysiological functions in porcine models [246].

Translating the existing relevant designs from the preclinical stage to the clinical trial stage is currently the main challenge and opportunity. In the near-to-medium term, given their manufacturing maturity, targeted antioxidant pharmacotherapies and biomimetic/conductive nerve scaffolds are well-positioned to

TABLE 5 Summary of core advantages, limitations, and clinical translational timelines of various neural therapeutic strategies.

Therapeutic strategies and representative projects (Related sections)	Core advantages and translational prospects	Limitations and challenges	Current clinical status	References/ Project IDs
Traditional single-lumen nerve guidance conduits (NGCs) (e.G., collagen nerve conduits, mochida nerve cuff)	Provides structural support with excellent biocompatibility. Demonstrates therapeutic efficacy comparable to nerve autografts, holding tremendous potential as an alternative therapy	Lacks the capacity for active microenvironmental modulation; exhibits suboptimal repair efficacy for long-gap nerve defects (>3 cm); some products have a relatively short shelf life	FDA-approved and commercialized; clinical data indicates favorable repair outcomes for defects <3 cm	NCT01809002; 510(k): K233322
Broad-spectrum antioxidants and Systemic drugs (e.g., NAC, ALA, SKYCLARYS)	Mitigates oxidative stress (OS) and nerve injury by activating pathways such as Nrf2; effectively improves motor function and symptoms of diabetic peripheral neuropathy	Broad-spectrum in nature, lacking specific targeting to SCs or localized injured nerves; certain drugs present adverse side effects; the precise molecular mechanisms remain incompletely elucidated	Mixed stage; SKYCLARYS is FDA-approved, while NAC and others remain in the clinical trial phase	NDA: 216718; zzNCT04481035
SC Biotherapies and genetic Pathway regulation (e.g., ahSC injection, stem cell co-transplantation, PPARγ/Netrin-1 pathways)	The introduction of SCs yields superior therapeutic outcomes compared to stem cells alone; directly targets and alleviates inflammation and OS through autophagy and specific signaling pathways	Clinical trials suffer from small sample sizes and recruitment difficulties; pathway regulation mechanisms are highly complex (e.g., mismatched expression levels may induce adverse effects), leading to prolonged bench-to-bedside translational cycles	Early clinical/Basic research stage; ahSC injection is in clinical trials (progressing slowly), while pathway regulation remains in the basic research phase	NCT05541250; NIH: 1R01DE033674-01
Biomimetic and conductive smart nerve scaffolds	Restores neural bioelectrical conduction and actively scavenges microenvironmental ROS; highly mimics ECM topological structures to guide targeted axonal regeneration	The long-term *in vivo* degradability and safety of nanomaterials (e.g., graphene) require further validation; achieving perfect dynamic coupling between material degradation rates and regeneration cycles remains challenging	Preclinical research stage	Section: "Innovative functional neural Stents"
ROS-responsive targeted delivery and engineered exosomes	Achieves precise spatiotemporal control, specifically responding to high-ROS microenvironments; exosomes possess innate high biocompatibility and targeted delivery capabilities	Response specificity and therapeutic durability under complex multiple *in vivo* stimuli remain questionable; faces significant technical bottlenecks in large-scale standardized production, purification, and cargo loading efficiency	Early preclinical/Proof-of-concept stage	Sections: "The new concept of intelligent drug delivery system" and "Precision antioxidant therapy based on OS-SCs interaction mechanism"

(*Continued*)

TABLE 5 Continued

Therapeutic strategies and representative projects (Related sections)	Core advantages and translational prospects	Limitations and challenges	Current clinical status	References/ Project IDs
4D Bioprinting technology	Endows scaffolds with the capacity for time-dependent adaptive morphological changes; allows for precise programming of spatiotemporal gradient release of neurotrophic factors and antioxidants	Currently in the initial exploratory phase; involves extreme technical difficulty and struggles to perfectly integrate and respond to complex multimodal physiological signals post-implantation	Proof-of-concept/*In vitro* research stage	Section: "4D bioprinting technology"

Abbreviations: NGCs, Nerve Guidance Conduits; NAC, N-acetylcysteine; ALA, Alpha-lipoic acid; OS, Oxidative Stress; SCs, Schwann Cells; ahSC, Autologous human Schwann cell; ECM, Extracellular Matrix; ROS, Reactive Oxygen Species; PPARγ, Peroxisome proliferator-activated receptor gamma. NCT, National Clinical Trial; 510(k), Premarket Notification; NDA, New Drug Application; FDA, Food and Drug Administration; NIH, National Institutes of Health; NSFC, National Natural Science Foundation of China.

advance into clinical trials. By contrast, complex intelligent systems, including ROS-responsive hydrogels, engineered exosomes, and 4D bioprinting, face substantial barriers in long-term stability, dynamic signal integration, and scalable production, rendering their widespread clinical adoption a prolonged endeavor.

In the future, it is necessary to further deepen the understanding of the mechanism of interaction between OS and SCs from the molecular level to the cellular level and even the tissue structure, and actively develop intelligent materials, catheters and scaffolds that can respond in real time to the dynamic changes of ROS around SCs, to achieve precise regulation of the state and repair function of SCs.

Discussion

This review has provided a comprehensive overview of the mechanisms linking OS and SCs in PNI, alongside emerging tissue engineering strategies. Several limitations of this study merit consideration. Only English language literature was included, potentially omitting relevant studies in other languages, and the search cutoff of June 2026 excludes more recent findings. By concentrating on SCs, the review downplayed the contributions of other cells such as macrophages and neutrophils, which simplifies the actual microenvironmental interaction network. Furthermore, the conclusions apply primarily to OS evolution and SC stress repair in PNI and do not extensively address metabolic or genetic peripheral neuropathies; mechanistic extrapolation beyond this context requires caution.

Despite these constraints, the evidence highlights that OS driven microenvironmental disorder poses a severe challenge to nerve repair. ROS play a dual role: excessive ROS damage lipids, proteins, and DNA, triggering neuronal and SC injury and inflammatory cascades, while physiological levels support neural repair through immune defense and intracellular signaling. Importantly, even when ROS mediated effects appear similar across organs, tissue specific differences must be respected, and findings from other tissues cannot be directly transferred to peripheral nerve without proper validation. Existing research has centered on diabetic and neurodegenerative neuropathies, leaving the ROS related mechanisms in mechanical nerve trauma insufficiently explored. Future studies should therefore employ well established PNI models to systematically delineate the molecular pathways governing ROS driven degeneration and repair.

ROS imbalance drives SCs toward a senescent phenotype, which critically deteriorates the regenerative microenvironment and limits axonal regeneration. Traditional neural scaffolds, including FDA approved conduits based on collagen or polyglycolic acid, primarily offer passive structural support and lack the capacity to actively neutralize excessive ROS. Elucidating the spatiotemporal distribution of ROS, their damaging effects on SCs, and the regulation of antioxidant pathways is thus essential for creating smart responsive scaffolds with integrated anti-inflammatory and antioxidant capabilities. Recent biomanufacturing advances are shifting neural tissue engineering from structural biomimicry to functional regeneration. Next-generation nerve guidance conduits can overcome autograft limitations by combining ROS modulating mechanisms with dynamic drug delivery, enabling precise redox homeostasis control while promoting vascular regeneration and neural electrical network reconstruction.

A multi strategy integrated conduit design is highly valuable in the pro-oxidant injury environment. ROS responsive materials can trigger localized drug release or structural changes in reaction to fluctuating ROS levels. Engineered exosomes with surface or cargo modifications further enhance biological targeting, and pre programmed four dimensional structures improve adaptability to microenvironmental changes. Together, these approaches yield a tridimensional synergy of response, targeting, and adaptation centered on the ROS axis. Clinical translation remains the core challenge. Although personalized conduits improve anatomical matching, their high cost restricts large scale application; developing tiered, cost effective, and standardized solutions for short and long gap injuries is therefore necessary. Moreover, the abundance of material choices has resulted in a lack of unified evaluation standards. Even mainstream materials such as chitosan and polycaprolactone lack consensus benchmarks for degradation rate, biocompatibility, and mechanical properties, which confines most active therapies to the laboratory stage.

Future research should concentrate on the following core directions: (1) Emphasizing the timing and spatial distribution of pathogenic ROS through highly sensitive monitoring technologies with advanced spatiotemporal resolution. (2) Overcoming the limitations of traditional, single-function scaffolds (including passive FDA-approved conduits) by developing multimodal intelligent scaffolds that integrate antioxidant capacity, electrical conductivity, and immune modulation. (3) Further elucidating the bidirectional interplay between mitochondrial autophagy–mediated ROS clearance and the broader OS microenvironment. (4) Promoting the visualization of peripheral nerve regeneration status during multidimensional regulatory processes. (5) Actively advancing rigorous preclinical and clinical trials. This includes establishing cross-laboratory consensus standards for material properties (such as degradation and mechanical compliance) and utilizing large animal models for long-gap (>5 cm) nerve defects to bridge the vast gap between preclinical success and actual clinical efficacy.

Author contributions

SY and ZZ were responsible for the conceptualization and design of the review, writing and proofreading the review, ZZ and QO were responsible for the graphical tables and images of the review, QL and YY were involved in the collection of the literature and analysis of the summary, ZJ and WL was responsible for the review of the manuscript. All authors contributed to the article and approved the submitted version.

Funding

The author(s) declared that financial support was received for this work and/or its publication. The study was supported by the Fund for Less Developed Regions of the National Natural Science Foundation of China (No. 82260456), Zunyi Medical University Student Innovation Project (No. ZHCX2023013) and Guangdong Provincial Higher Education Key Areas Special Project (No. 2023ZDZX20294).

Acknowledgements

Figure created by Figdraw.

Conflict of interest

The author(s) declared no potential conflicts of interest with respect to the research, authorship, and/or publication of this article.

Generative AI statement

The author(s) declared that generative AI was used in the creation of this manuscript. During the preparation of this manuscript, the authors used Google Gemini 3.1 Pro strictly for the purpose of language polishing, grammar correction, and readability improvement. No generative AI or AI-assisted tools were used for data collection, analysis, drawing scientific conclusions, or creating any figures and illustrations. After using this service, the authors carefully reviewed and edited the content, and take full responsibility for the integrity, accuracy, and originality of the overall work.

Any alternative text (alt text) provided alongside figures in this article has been generated by Frontiers with the support of artificial intelligence and reasonable efforts have been made to ensure accuracy, including review by the authors wherever possible. If you identify any issues, please contact us.

References

1. Sundaram VK, Schutza V, Schroter NH, Backhaus A, Bilsing A, Joneck L, et al. Adipoglial signaling mediates metabolic adaptation in peripheral nerve regeneration. *Cell Metab.* (2023) 35(12):2136–52 e9. doi: 10.1016/j.cmet.2023.10.017

2. Chu XL, Song XZ, Li Q, Li YR, He F, Gu XS, et al. Basic mechanisms of peripheral nerve injury and treatment *via* electrical stimulation. *Neural Regen Res* (2022) 17(10): 2185–93. doi: 10.4103/1673-5374.335823

3. Cheng Q, Wang W, Dong X, Chai Y, Goto T, Tu R, et al. An adaptable drug delivery system facilitates peripheral nerve repair by remodeling the microenvironment. *Biomacromolecules* (2024) 25(3):1509–26. doi: 10.1021/acs.biomac.3c01094

4. Fuentes-Flores A, Geronimo-Olvera C, Girardi K, Necunir-Ibarra D, Patel SK, Bons J, et al. Senescent schwann cells induced by aging and chronic denervation impair axonal regeneration following peripheral nerve injury. *EMBO Mol Med* (2023) 15(12):e17907. doi: 10.15252/emmm.202317907

5. Pollock N, Staunton CA, Vasilaki A, McArdle A, Jackson MJ. Denervated muscle fibers induce mitochondrial peroxide generation in neighboring innervated fibers: role in muscle aging. *Free Radic Biol Med* (2017) 112:84–92. doi: 10.1016/j.freeradbiomed.2017.07.017

6. Fan H, Bai Q, Yang Y, Shi X, Du G, Yan J, et al. The key roles of reactive oxygen species in microglial inflammatory activation: regulation by endogenous antioxidant system and exogenous sulfur-containing compounds. *Eur J Pharmacol* (2023) 956:175966. doi: 10.1016/j.ejphar.2023.175966

7. Han F, Tu Z, Zhu Z, Liu D, Meng Q, Yu Q, et al. Targeting endogenous reactive oxygen species removal and regulating regenerative microenvironment at annulus fibrosus defects promote tissue repair. *ACS Nano* (2023) 17(8):7645–61. doi: 10.1021/acsnano.3c00093

8. Wei F, Yang W, Wang H, Song S, Ji Y, Chen Z, et al. Reactive oxygen species-scavenging biomaterials for neural regenerative medicine. *Biomater Sci* (2025) 13(2): 343–63. doi: 10.1039/d4bm01221f

9. Andre-Levigne D, Pignel R, Boet S, Jaquet V, Kalbermatten DF, Madduri S. Role of oxygen and its radicals in peripheral nerve regeneration: from hypoxia to physoxia to hyperoxia. *Int J Mol Sci* (2024) 25(4):2030. doi: 10.3390/ijms25042030

10. Stojanovic B, Milivojcevic BI, Dimitrijevic Stojanovic M, Stojanovic BS, Lazarevic T, Spasic M, et al. Oxidative stress, inflammation, and cellular senescence in neuropathic pain: mechanistic crosstalk. *Antioxidants (Basel)* (2025) 14(10):1166. doi: 10.3390/antiox14101166

11. Lee J, Yeo JH, Kim SS, Lee JM, Yeo SG. Production and role of free radicals and reactive oxygen species after facial nerve injury. *Antioxidants (Basel)* (2025) 14(4):436. doi: 10.3390/antiox14040436

12. Meda F, Gauron C, Rampon C, Teillon J, Volovitch M, Vriz S. Nerves control redox levels in mature tissues through schwann cells and hedgehog signaling. *Antioxid Redox Signal* (2016) 24(6):299–311. doi: 10.1089/ars.2015.6380

13. Oliveira JT, Yanick C, Wein N, Gomez Limia CE. Neuron-schwann cell interactions in peripheral nervous system homeostasis, disease, and preclinical treatment. *Front Cell Neurosci* (2023) 17:1248922. doi: 10.3389/fncel.2023.1248922

14. Dong L, Deng X, Li Y, Zhu X, Shu M, Chen J, et al. Stimuli-responsive mRNA vaccines to induce robust CD8(+) T cell response *via* ROS-mediated innate

immunity boosting. *J Am Chem Soc* (2024) 146(28):19218–28. doi: 10.1021/jacs.4c04331

15. Dent MAR, Martinez-Gomez A, Hernandez-Munoz R. Role of cell oxidant status and redox state in controlling cell proliferation and apoptosis in two models of wallerian degeneration of rat sciatic nerve. *Antioxidants (Basel)* (2025) 14(10):1236. doi: 10.3390/antiox14101236

16. Kuhn E, Natacci F, Corbo M, Pisani L, Ferrero S, Bulfamante G, et al. The contribution of oxidative stress to NF1-Altered tumors. *Antioxidants (Basel)* (2023) 12(8):1557. doi: 10.3390/antiox12081557

17. Lin Q, Li K, Chen Y, Xie J, Wu C, Cui C, et al. Oxidative stress in diabetic peripheral neuropathy: pathway and mechanism-based treatment. *Mol Neurobiol* (2023) 60(8):4574–94. doi: 10.1007/s12035-023-03342-7

18. Park J, Kim J, Choe G, Jung Y, Lee JY. Conductive hydrogel luminal filler for peripheral nerve regeneration. *Biomaterials* (2025) 317:123103. doi: 10.1016/j.biomaterials.2025.123103

19. Zhang C, Gong J, Zhang J, Zhu Z, Qian Y, Lu K, et al. Three potential elements of developing nerve guidance conduit for peripheral nerve regeneration. *Adv Funct Mater* (2023) 33(40):2302251. doi: 10.1002/adfm.202302251

20. Wu P, Tong Z, Luo L, Zhao Y, Chen F, Li Y, et al. Comprehensive strategy of conduit guidance combined with VEGF producing Schwann cells accelerates peripheral nerve repair. *Bioact Mater* (2021) 6(10):3515–27. doi: 10.1016/j.bioactmat.2021.03.020

21. Ou X, Wang Z, Yu D, Guo W, Zvyagin AV, Lin Q, et al. VEGF-loaded ROS-responsive nanodots improve the structure and function of sciatic nerve lesions in type II diabetic peripheral neuropathy. *Biomaterials* (2025) 315:122906. doi: 10.1016/j.biomaterials.2024.122906

22. Han Y, Weng W, Zhang Y, Feng Q, Ma Y, Quan A, et al. Intraoperative application of intelligent, responsive, self-assembling hydrogel rectifies oxygen and energy metabolism in traumatically injured brain. *Biomaterials* (2024) 306:122495. doi: 10.1016/j.biomaterials.2024.122495

23. Wang X, Yao X, Sun Z, Jin Y, Yan Z, Jiang H, et al. An extracellular matrix mimicking alginate hydrogel scaffold manipulates an inflammatory microenvironment and improves peripheral nerve regeneration by controlled melatonin release. *J Mater Chem B* (2023) 11(48):11552–61. doi: 10.1039/d3tb01727c

24. Chaudhuri A, Singha T, Jena BC, Shee M, Datta PK, Mandal M, et al. A two-photon responsive hydroxyphenylquinazolinone (HPQ)-based fluorescent organic nanoprodrug for H(2)S release against oxidative stress. *Chem Commun (Camb)* (2023) 59(9):1177–80. doi: 10.1039/d2cc05768a

25. Dash UC, Bhol NK, Swain SK, Samal RR, Nayak PK, Raina V, et al. Oxidative stress and inflammation in the pathogenesis of neurological disorders: mechanisms and implications. *Acta Pharm Sin B* (2025) 15(1):15–34. doi: 10.1016/j.apsb.2024.10.004

26. Chao PY, Lin JA, Ye JC, Hwang JM, Ting WJ, Huang CY, et al. Attenuation of oxidative stress-induced cell apoptosis in Schwann RSC96 cells by Ocimum gratissimum aqueous extract. *Int J Med Sci* (2017) 14(8):764–71. doi: 10.7150/ijms.19535

27. Wang P, Wang R, Huo Y, Peng Y, Fu C, Hu Y, et al. Partial reprogramming in senescent schwann cells enhances peripheral nerve regeneration *via* restoration of stress granule homeostasis. *Adv Sci (Weinh)* (2025) 12(44):e11019. doi: 10.1002/advs.202511019

28. Zhang D, Yang B, Chang SQ, Ma SS, Sun JX, Yi L, et al. Protective effect of paeoniflorin on H(2)O(2) induced Schwann cells injury based on network pharmacology and experimental validation. *Chin J Nat Med* (2021) 19(2):90–9. doi: 10.1016/S1875-5364(21)60010-9

29. Zhang X, Zhao S, Yuan Q, Zhu L, Li F, Wang H, et al. TXNIP, a novel key factor to cause Schwann cell dysfunction in diabetic peripheral neuropathy, under the regulation of PI3K/Akt pathway inhibition-induced DNMT1 and DNMT3a overexpression. *Cell Death Dis* (2021) 12(7):642. doi: 10.1038/s41419-021-03930-2

30. Zheng F, Zhang Y, Zhou H, Li J, Gao J, Qu X, et al. Mung bean-derived carbon dots suppress ferroptosis of Schwann cells *via* the Nrf2/HO-1/GPX4 pathway to promote peripheral nerve repair. *Biomater Sci* (2025) 13(10):2656–72. doi: 10.1039/d4bm01570c

31. Wu B, Woo JS, Hasiakos S, Pan C, Cokus S, Benincá C, et al. Mitochondrial reactive oxygen species regulate acetyl-CoA flux between cytokine production and fatty acid synthesis in effector T cells. *Cell Reports* (2025) 44(3):115430. doi: 10.1016/j.celrep.2025.115430

32. Fang J, Wong HS, Brand MD. Production of superoxide and hydrogen peroxide in the mitochondrial matrix is dominated by site I(Q) of complex I in diverse cell lines. *Redox Biol* (2020) 37:101722. doi: 10.1016/j.redox.2020.101722

33. Manhas N, Duong QV, Lee P, Richardson JD, Robertson JD, Moxley MA, et al. Computationally modeling mammalian succinate dehydrogenase kinetics identifies the origins and primary determinants of ROS production. *J Biol Chem* (2020) 295(45):15262–79. doi: 10.1074/jbc.RA120.014483

34. Rosenfeld D, Field H, Kim YJ, Pang KKL, Nagao K, Koehler F, et al. Magnetothermal modulation of calcium-dependent nerve growth. *Adv Funct Mater* (2022) 32(50):0224558. doi: 10.1002/adfm.202204558

35. De Logu F, Nassini R, Materazzi S, Carvalho Goncalves M, Nosi D, Rossi Degl'Innocenti D, et al. Schwann cell TRPA1 mediates neuroinflammation that sustains macrophage-dependent neuropathic pain in mice. *Nat Commun* (2017) 8(1):1887. doi: 10.1038/s41467-017-01739-2

36. Kievit B, Johnstone AD, Gibon J, Barker PA. Mitochondrial reactive oxygen species mediate activation of TRPV1 and calcium entry following peripheral sensory axotomy. *Front Mol Neurosci* (2022) 15:852181. doi: 10.3389/fnmol.2022.852181

37. Nazari B, Jaquet V, Krause KH. NOX family NADPH oxidases in mammals: evolutionary conservation and isoform-defining sequences. *Redox Biol* (2023) 66:102851. doi: 10.1016/j.redox.2023.102851

38. Eid SA, Savelieff MG, Eid AA, Feldman EL. Nox, nox, are you there? The role of NADPH oxidases in the peripheral nervous system. *Antioxid Redox Signal* (2022) 37(7-9):613–30. doi: 10.1089/ars.2021.0135

39. Sikora JP, Karawani J, Sobczak J. Neutrophils and the systemic inflammatory response syndrome (SIRS). *Int J Mol Sci* (2023) 24(17):13469. doi: 10.3390/ijms241713469

40. Eid SA, El Massry M, Hichor M, Haddad M, Grenier J, Dia B, et al. Targeting the NADPH Oxidase-4 and liver X receptor pathway preserves Schwann cell integrity in diabetic mice. *Diabetes* (2020) 69(3):448–64. doi: 10.2337/db19-0517

41. Zhang M, Liu Q, Meng H, Duan H, Liu X, Wu J, et al. Ischemia-reperfusion injury: molecular mechanisms and therapeutic targets. *Signal Transduct Target Ther* (2024) 9(1):12. doi: 10.1038/s41392-023-01688-x

42. Sorby-Adams A, Prime TA, Miljkovic JL, Prag HA, Krieg T, Murphy MP. A model of mitochondrial superoxide production during ischaemia-reperfusion injury for therapeutic development and mechanistic understanding. *Redox Biol* (2024) 72:103161. doi: 10.1016/j.redox.2024.103161

43. Chouchani ET, Pell VR, James AM, Work LM, Saeb-Parsy K, Frezza C, et al. A unifying mechanism for mitochondrial superoxide production during ischemia-reperfusion injury. *Cell Metab.* (2016) 23(2):254–63. doi: 10.1016/j.cmet.2015.12.009

44. Scialo F, Fernandez-Ayala DJ, Sanz A. Role of mitochondrial reverse electron transport in ROS signaling: potential roles in health and disease. *Front Physiol* (2017) 8:428. doi: 10.3389/fphys.2017.00428

45. Macino G, Scazzocchio C, Waring RB, Berks MM, Davies RW. Conservation and rearrangement of mitochondrial structural gene sequences. *Nature* (1980) 288(5789):404–6. doi: 10.1038/288404a0

46. Ai Y, Meng Y, Yan B, Zhou Q, Wang X. The biochemical pathways of apoptotic, necroptotic, pyroptotic, and ferroptotic cell death. *Mol Cell* (2024) 84(1):170–9. doi: 10.1016/j.molcel.2023.11.040

47. Iida H, Schmelzer JD, Schmeichel AM, Wang Y, Low PA. Peripheral nerve ischemia: reperfusion injury and fiber regeneration. *Exp Neurol* (2003) 184(2):997–1002. doi: 10.1016/S0014-4886(03)00385-6

48. Tabata Fukushima C, Dancil IS, Clary H, Shah N, Nadtochiy SM, Brookes PS. Reactive oxygen species generation by reverse electron transfer at mitochondrial complex I under simulated early reperfusion conditions. *Redox Biol* (2024) 70:103047. doi: 10.1016/j.redox.2024.103047

49. Cameron NE, Cotter MA. Effects of antioxidants on nerve and vascular dysfunction in experimental diabetes. *Diabetes Res Clin Pract* (1999) 45(2-3):137–46. doi: 10.1016/s0168-8227(99)00043-1

50. Stockwell BR, Friedmann Angeli JP, Bayir H, Bush AI, Conrad M, Dixon SJ, et al. Ferroptosis: a regulated cell death nexus linking metabolism, redox biology, and disease. *Cell* (2017) 171(2):273–85. doi: 10.1016/j.cell.2017.09.021

51. Yang WS, SriRamaratnam R, Welsch ME, Shimada K, Skouta R, Viswanathan VS, et al. Regulation of ferroptotic cancer cell death by GPX4. *Cell.* (2014) 156(1-2):317–31. doi: 10.1016/j.cell.2013.12.010

52. Dixon SJ, Lemberg KM, Lamprecht MR, Skouta R, Zaitsev EM, Gleason CE, et al. Ferroptosis: an iron-dependent form of nonapoptotic cell death. *Cell* (2012) 149(5):1060–72. doi: 10.1016/j.cell.2012.03.042

53. Huang L, Bian M, Zhang J, Jiang L. Iron metabolism and ferroptosis in peripheral nerve injury. *Oxid Med Cell Longev* (2022) 2022:5918218. doi: 10.1155/2022/5918218

54. Gwam C, Mohamed N, Ogunsola AS, Brown MG, Henry KA, Ma X. Amniotic fluid stem cell conditioned medium's role in Schwann cell proliferation, survival, and cellular antioxidant activity under normative and oxidative stress conditions. *Ann Transl Med* (2025) 13(1):1. doi: 10.21037/atm-24-107

55. Wang H, Xia L, Huang Z, Ma Y, Yao G, Hu S, et al. Suppression of Schwann cell ferroptosis mitigates demyelination and trigeminal neuropathic pain in the IoN-CCI model. *Eur J Neurosci* (2025) 62(3):e70209. doi: 10.1111/ejn.70209

56. Ruan J, He XK, Zhang SO, Teng XF, Hu Y, Chen H. Progress in research on the mechanisms and therapeutic targets of ferroptosis in peripheral nerve injury and repair. *ASN Neuro* (2026) 18(1):2678168. doi: 10.1080/17590914.2026.2678168

57. Yan Y, Ran X, Zhou Z, Gu Y, Wang R, Qiu C, et al. FGF21 inhibits ferroptosis caused by mitochondrial damage to promote the repair of peripheral nerve injury. *Front Pharmacol* (2024) 15:1358646. doi: 10.3389/fphar.2024.1358646

58. Bosch-Queralt M, Fledrich R, Stassart RM. Schwann cell functions in peripheral nerve development and repair. *Neurobiol Dis* (2023) 176(105952):105952. doi: 10.1016/j.nbd.2022.105952

59. Jain S, Webster TJ, Sharma A, Basu B. Intracellular reactive oxidative stress, cell proliferation and apoptosis of Schwann cells on carbon nanofibrous substrates. *Biomaterials* (2013) 34(21):4891–901. doi: 10.1016/j.biomaterials.2013.03.055

60. Adam MI, Lin L, Makin AM, Zhang XF, Zhou LX, Liao XY, et al. Glial cell line-derived neurotrophic factor and brain-derived neurotrophic factor regulate the interaction between astrocytes and Schwann cells at the trigeminal root entry zone. *Neural Regen Res* (2023) 18(6):1364–70. doi: 10.4103/1673-5374.354517

61. Ma J, Liu J, Wang Q, Yu H, Chen Y, Xiang L. The beneficial effect of ginsenoside Rg1 on Schwann cells subjected to hydrogen peroxide induced oxidative injury. *Int J Biol Sci* (2013) 9(6):624–36. doi: 10.7150/ijbs.5885

62. Metafune M, Muratori L, Fregnan F, Ronchi G, Raimondo S. The extracellular matrix in peripheral nerve repair and regeneration: a narrative review of its role and therapeutic potential. *Front Neuroanat* (2025) 19:1628081. doi: 10.3389/fnana.2025.1628081

63. Xia M, Zhang Y, Wu H, Zhang Q, Liu Q, Li G, et al. Forsythoside B attenuates neuroinflammation and neuronal apoptosis by inhibition of NF-kappaB and p38-MAPK signaling pathways through activating Nrf2 post spinal cord injury. *Int Immunopharmacol* (2022) 111:109120. doi: 10.1016/j.intimp.2022.109120

64. Chang W, Shah MB, Lee P, Yu X. Tissue-engineered spiral nerve guidance conduit for peripheral nerve regeneration. *Acta Biomater* (2018) 73:302–11. doi: 10.1016/j.actbio.2018.04.046

65. Tiong YL, Ng KY, Koh RY, Ponnudurai G, Chye SM. Melatonin prevents oxidative stress-induced mitochondrial dysfunction and apoptosis in high glucose-treated schwann cells *via* upregulation of Bcl2, NF-kappaB, mTOR, wnt signalling pathways. *Antioxidants (Basel)* (2019) 8(7):198. doi: 10.3390/antiox8070198

66. Lv Y, Yao X, Li X, Ouyang Y, Fan C, Qian Y. Cell metabolism pathways involved in the pathophysiological changes of diabetic peripheral neuropathy. *Neural Regen Res* (2024) 19(3):598–605. doi: 10.4103/1673-5374.380872

67. Liu S, Liu J, Wang Y, Deng F, Deng Z. Oxidative stress: signaling pathways, biological functions, and disease. *MedComm* (2020) 6(7):e70268. doi: 10.1002/mco2.70268

68. Negro S, Lauria F, Stazi M, Tebaldi T, D'Este G, Pirazzini M, et al. Hydrogen peroxide induced by nerve injury promotes axon regeneration *via* connective tissue growth factor. *Acta Neuropathol Commun* (2022) 10(1):189. doi: 10.1186/s40478-022-01495-5

69. Negro S, Baggio C, Tonellato M, Stazi M, D'Este G, Megighian A, et al. Hydrogen peroxide modulates the timely activation of Jun and erk in Schwann cells at the injury site and is required for motor axon regeneration. *Cells* (2025) 14(9):671. doi: 10.3390/cells14090671

70. Salis C, Davio C, Usach V, Urtasun N, Goitia B, Martinez-Vivot R, et al. Iron and holotransferrin induce cAMP-dependent differentiation of Schwann cells. *Neurochem Int* (2012) 61(5):798–806. doi: 10.1016/j.neuint.2012.06.023

71. Shan F, Yao X, Zhang Q, Li R, Kong L, Zheng Q, et al. NMDA receptors coordinate metabolic reprogramming and mitophagy in Schwann cells to promote peripheral nerve regeneration. *Research (Wash D C)* (2025) 8:0825. doi: 10.34133/research.0825

72. Sies H, Belousov VV, Chandel NS, Davies MJ, Jones DP, Mann GE, et al. Defining roles of specific reactive oxygen species (ROS) in cell biology and physiology. *Nat Rev Mol Cell Biol* (2022) 23(7):499–515. doi: 10.1038/s41580-022-00456-z

73. Lennicke C, Cocheme HM. Redox metabolism: ROS as specific molecular regulators of cell signaling and function. *Mol Cell* (2021) 81(18):3691–707. doi: 10.1016/j.molcel.2021.08.018

74. Murphy MP, Bayir H, Belousov V, Chang CJ, Davies KJA, Davies MJ, et al. Guidelines for measuring reactive oxygen species and oxidative damage in cells and *in vivo*. *Nat Metab* (2022) 4(6):651–62. doi: 10.1038/s42255-022-00591-z

75. Song J, Meng H, Deng G, Lin H. Sustainable release selenium laden with SiO(2) restoring peripheral nerve injury *via* modulating PI3K/AKT pathway signaling pathway. *Int J Nanomedicine* (2024) 19:7851–70. doi: 10.2147/IJN.S460397

76. Reyes RC, Brennan AM, Shen Y, Baldwin Y, Swanson RA. Activation of neuronal NMDA receptors induces superoxide-mediated oxidative stress in neighboring neurons and astrocytes. *J Neurosci* (2012) 32(37):12973–8. doi: 10.1523/JNEUROSCI.1597-12.2012

77. Yang J, Liu C, Sun H, Liu Y, Liu Z, Zhang D, et al. The progress in titanium alloys used as biomedical implants: from the view of reactive oxygen species. *Front Bioeng Biotechnol* (2022) 10:1092916. doi: 10.3389/fbioe.2022.1092916

78. Khelfi A. Other techniques for oxidative stress assessment. In: Andreescu S, Henkel R, Khelfi A, editors. *Biomarkers of Oxidative Stress*. Cham: Springer Nature Switzerland (2024). p. 525–51.

79. McDonagh B, Scullion SM, Vasilaki A, Pollock N, McArdle A, Jackson MJ. Ageing-induced changes in the redox status of peripheral motor nerves imply an effect on redox signalling rather than oxidative damage. *Free Radic Biol Med* (2016) 94:27–35. doi: 10.1016/j.freeradbiomed.2016.02.008

80. Simunkova M, Barbierikova Z, Jomova K, Hudecova L, Lauro P, Alwasel SH, et al. Antioxidant vs. prooxidant properties of the flavonoid, kaempferol, in the presence of Cu(II) ions: a ROS-scavenging activity, fenton reaction and DNA damage study. *Int J Mol Sci* (2021) 22(4):1619. doi: 10.3390/ijms22041619

81. Sabetghadam Moghadam M, Wiens E, Gauvrit S, Sammynaiken R, Collins MM. Electron paramagnetic resonance spectroscopy for analysis of free radicals in zebrafish. *PLoS One* (2025) 20(2):e0318212. doi: 10.1371/journal.pone.0318212

82. Wang X, Hurben AK, Mao Y, Ding Q, Zhang W, Li P, et al. Spatiotemporal analysis of reactive oxygen species using specific activity-based sensing fluorescent imaging probes. *Nat Rev Chem* (2026) 10(7):493–510. doi: 10.1038/s41570-026-00836-5

83. Spanolios EM, Lewis RE, Caldwell RN, Jilani SZ, Haynes CL. Progress and limitations in reactive oxygen species quantitation. *Chem Commun (Camb)* (2024) 60(86):12487–501. doi: 10.1039/d4cc03578j

84. Karges J. Reactive oxygen species detection with fluorescent probes: limitations and recommendations beyond DCFH-DA. *J Med Chem* (2026) 69(3):1970–81. doi: 10.1021/acs.jmedchem.5c03494

85. Jin Y, Liu J, Wang M, Jiang Y. Thioketal-based electrochemical sensor reveals biphasic effects of l-DOPA on neuroinflammation. *ACS Sens* (2024) 9(5):2364–71. doi: 10.1021/acssensors.3c02420

86. Chen Q, Lin R, Wang W, Zuo Y, Zhuo Y, Yu Y, et al. Efficient electrochemical microsensor for the simultaneous measurement of hydrogen peroxide and ascorbic acid in living brains. *Anal Chem* (2024) 96(17):6683–91. doi: 10.1021/acs.analchem.4c00076

87. Li X, Zhang Y, Ai HW. Ratiometric imaging of mitochondrial hydrogen peroxide in Abeta(42)-Mediated neurotoxicity. *ACS Sens* (2022) 7(3):722–9. doi: 10.1021/acssensors.1c01381

88. Pak VV, Ezerina D, Lyublinskaya OG, Pedre B, Tyurin-Kuzmin PA, Mishina NM, et al. Ultrasensitive genetically encoded indicator for hydrogen peroxide identifies roles for the oxidant in cell migration and mitochondrial function. *Cell Metab.* (2020) 31(3):642–53 e6. doi: 10.1016/j.cmet.2020.02.003

89. Li Q, Guo P, Wang S, Feng Y, Zhang H, Yu W, et al. Mitochondrial derived vesicle-carrying protein MIGA2 promotes copper-induced autophagosomes-lysosomes fusion by regulating ATG14. *J Hazard Mater* (2024) 467:133703. doi: 10.1016/j.jhazmat.2024.133703

90. Liu X, Hussain R, Mehmood K, Tang Z, Zhang H, Li Y. Mitochondrial-endoplasmic reticulum communication-mediated oxidative stress and autophagy. *Biomed Res Int* (2022) 2022:6459585. doi: 10.1155/2022/6459585

91. Kim T, Jeon J, Lee MS, Park JH, Chung Y, Yang HS. Development of electrospun nerve guidance conduits by a milk-derived protein with biodegradable polymers for peripheral nerve regeneration. *ACS Appl Bio Mater* (2025) 8(4):3498–512. doi: 10.1021/acsabm.4c02000

92. Ruhmkorf A, Harbauer AB. Role of Mitochondria-ER contact sites in mitophagy. *Biomolecules* (2023) 13(8):1198. doi: 10.3390/biom13081198

93. He W, Sun Z, Tong G, Zeng L, He W, Chen X, et al. FUNDC1 alleviates doxorubicin-induced cardiotoxicity by restoring mitochondrial-endoplasmic reticulum contacts and blocked autophagic flux. *Theranostics* (2024) 14(9):3719–38. doi: 10.7150/thno.92771

94. Xing QC, Chen J, Liu Z, Li WC, Liu X, Li W. Autophagy in Schwann cells: a potential pharmacotherapeutic target in diabetic peripheral neuropathy. *World J Diabetes* (2025) 16(6):105709. doi: 10.4239/wjd.v16.i6.105709

95. Kim J, Kundu M, Viollet B, Guan KL. AMPK and mTOR regulate autophagy through direct phosphorylation of Ulk1. *Nat Cell Biol* (2011) 13(2):132–41. doi: 10.1038/ncb2152

96. Zhu J, Zhang Y, Sun Y, Yu F, Lu Y, Hu Q, et al. Mesoporous Prussian blue nanoparticle neuroconduit for the biological therapy targeting oxidative stress reduction, inflammation inhibition, and nerve regeneration. *J Nanobiotechnology* (2025) 23(1):1. doi: 10.1186/s12951-024-02937-z

97. Schapira AH. Oxidative stress and mitochondrial dysfunction in neurodegeneration. *Curr Opin Neurol* (1996) 9(4):260–4. doi: 10.1097/00019052-199608000-00003

98. Eftekharpour E, Fernyhough P. Oxidative stress and mitochondrial dysfunction associated with peripheral neuropathy in type 1 diabetes. *Antioxid Redox Signal* (2022) 37(7-9):578–96. doi: 10.1089/ars.2021.0152

99. Huff TC, Sant DW, Camarena V, Van Booven D, Andrade NS, Mustafi S, et al. Vitamin C regulates Schwann cell myelination by promoting DNA demethylation of pro-myelinating genes. *J Neurochem* (2021) 157(6):1759–73. doi: 10.1111/jnc.15015

100. Yamamuro-Tanabe A, Kosuge Y, Ishimaru Y, Yoshioka Y. Schwann cell derived-peroxiredoxin protects motor neurons against hydrogen peroxide-induced cell death in mouse motor neuron cell line NSC-34. *J Pharmacol Sci* (2023) 153(2):73–83. doi: 10.1016/j.jphs.2023.07.006

101. Vincent AM, Kato K, McLean LL, Soules ME, Feldman EL. Sensory neurons and schwann cells respond to oxidative stress by increasing antioxidant defense mechanisms. *Antioxid Redox Signal* (2009) 11(3):425–38. doi: 10.1089/ars.2008.2235

102. Su Q, Wang J, Song Y, Zhang Z, Cai B, Xiaohalati X, et al. Bioactive silk sericin/bioceramic nerve guidance conduit for effective repair of long-gap transected peripheral nerve injury through regulating schwann cells. *Adv Sci (Weinh)* (2025) 12(38):e07241. doi: 10.1002/advs.202507241

103. Zheng X, Wang J, Zhou H, Chai Y, Li Z, Chen M, et al. Dental pulp stem cells alleviate Schwann cell pyroptosis *via* mitochondrial transfer to enhance facial nerve regeneration. *Bioact Mater* (2025) 47:313–26. doi: 10.1016/j.bioactmat.2025.01.031

104. Jiao J, Wang F, Huang J-J, Huang J-J, Li Z-A, Kong Y, et al. Microfluidic hollow fiber with improved stiffness repairs peripheral nerve injury through non-invasive electromagnetic induction and controlled release of NGF. *Chem Eng J* (2021) 426:131826. doi: 10.1016/j.cej.2021.131826

105. Lv W, Deng B, Duan W, Li Y, Liu Y, Li Z, et al. Schwann cell plasticity is regulated by a weakened intrinsic antioxidant defense system in acute peripheral nerve injury. *Neuroscience* (2018) 382:1–13. doi: 10.1016/j.neuroscience.2018.04.018

106. Sarhane KA, Qiu C, Harris TGW, Hanwright PJ, Mao HQ, Tuffaha SH. Translational bioengineering strategies for peripheral nerve regeneration: opportunities, challenges, and novel concepts. *Neural Regen Res* (2023) 18(6): 1229–34. doi: 10.4103/1673-5374.358616

107. Zhang Y, Zhao Q, Chen Q, Xu L, Yi S. Transcriptional control of peripheral nerve regeneration. *Mol Neurobiol* (2023) 60(1):329–41. doi: 10.1007/s12035-022-03090-0

108. Zhang F, Nan L, Fang J, Liu L, Xu B, Jin X, et al. Nerve guide conduits promote nerve regeneration under a combination of electrical stimulation and RSCs combined with stem cell differentiation. *J Mater Chem B* (2024) 12(45):11636–47. doi: 10.1039/d4tb01374c

109. Yang H, Li Q, Li L, Chen S, Zhao Y, Hu Y, et al. Gastrodin modified polyurethane conduit promotes nerve repair *via* optimizing Schwann cells function. *Bioact Mater* (2022) 8:355–67. doi: 10.1016/j.bioactmat.2021.06.020

110. Manoukian OS, Rudraiah S, Arul MR, Bartley JM, Baker JT, Yu X, et al. Biopolymer-nanotube nerve guidance conduit drug delivery for peripheral nerve regeneration: *in vivo* structural and functional assessment. *Bioact Mater* (2021) 6(9): 2881–93. doi: 10.1016/j.bioactmat.2021.02.016

111. Yao X, Yan Z, Liu A, Zhan L, Liu Y, Huang C, et al. Metal organic framework-modified bioadaptable implant potentiates the reconstruction of nerve microenvironment *via* immunometabolism reprogramming. *Nano Today* (2023) 49: 101814. doi: 10.1016/j.nantod.2023.101814

112. Yao X, Xue T, Chen B, Zhou X, Ji Y, Gao Z, et al. Advances in biomaterial-based tissue engineering for peripheral nerve injury repair. *Bioact Mater* (2025) 46:150–72. doi: 10.1016/j.bioactmat.2024.12.005

113. Shan Y, Xu L, Cui X, Wang E, Jiang F, Li J, et al. A responsive cascade drug delivery scaffold adapted to the therapeutic time window for peripheral nerve injury repair. *Mater Horiz* (2024) 11(4):1032–45. doi: 10.1039/d3mh01511d

114. Gao J, Zhou Y, Xu G, Wei Z, Ding L, Zhang W, et al. Hybrid hydrogels containing gradients in gold nanoparticles for localized delivery of mesenchymal stem cells and enhanced nerve tissues remodeling *in vivo*. *Mater Today Bio* (2025) 30:101411. doi: 10.1016/j.mtbio.2024.101411

115. Dong X, Zhang H, Duan P, Liu K, Yu Y, Wei W, et al. An injectable and adaptable hydrogen sulfide delivery system for modulating neuroregenerative microenvironment. *Sci Adv* (2023) 9(51):eadi1078. doi: 10.1126/sciadv.adi1078

116. Krych AJ, Rooney GE, Chen B, Schermerhorn TC, Ameenuddin S, Gross L, et al. Relationship between scaffold channel diameter and number of regenerating axons in the transected rat spinal cord. *Acta Biomater* (2009) 5(7):2551–9. doi: 10.1016/j.actbio.2009.03.021

117. Shahriari D, Loke G, Tafel I, Park S, Chiang PH, Fink Y, et al. Scalable fabrication of porous microchannel nerve guidance scaffolds with complex geometries. *Adv Mater* (2019) 31(30):e1902021. doi: 10.1002/adma.201902021

118. Stocco E, Barbon S, Emmi A, Tiengo C, Macchi V, De CR, et al. Bridging gaps in peripheral nerves: from current strategies to future perspectives in conduit design. *Int J Mol Sci* (2023) 24(11):9170. doi: 10.3390/ijms24119170

119. Wan T, Wang YL, Zhang FS, Zhang XM, Zhang YC, Jiang HR, et al. The porous structure of peripheral nerve guidance conduits: features, fabrication, and implications for peripheral nerve regeneration. *Int J Mol Sci* (2023) 24(18):14132. doi: 10.3390/ijms241814132

120. Hromada C, Heimel P, Kerbl M, Gal L, Nurnberger S, Schaedl B, et al. Silk-based nerve guidance conduits with macroscopic holes modulate the vascularization of regenerating rat sciatic nerve. *Neural Regen Res* (2025) 20(6):1789–800. doi: 10.4103/NRR.NRR-D-23-01518

121. Yang W, Chen X, Yang C, Mao Y, Zhuang W, Xiao Y, et al. Med20 regulates myelination in the peripheral nervous system by modulating ferroptosis of Schwann cells. *Cell Rep* (2025) 44(10):116448. doi: 10.1016/j.celrep.2025.116448

122. Maeng WY, Lee Y, Chen SH, Kim KS, Sung D, Tseng WL, et al. 3D printed biodegradable hydrogel-based multichannel nerve conduits mimicking peripheral nerve fascicules. *Mater Today Bio* (2025) 31:101514. doi: 10.1016/j.mtbio.2025.101514

123. Wang X, Chen S, Chen X, Wu J, Huang Z, Wang J, et al. Biomimetic multi-channel nerve conduits with micro/nanostructures for rapid nerve repair. *Bioact Mater* (2024) 41:577–96. doi: 10.1016/j.bioactmat.2024.07.018

124. Song J, Dong J, Yuan Z, Huang M, Yu X, Zhao Y, et al. Shape-persistent conductive nerve guidance conduits for peripheral nerve regeneration. *Adv Healthc Mater* (2024) 13(26):e2401160. doi: 10.1002/adhm.202401160

125. Schimelman J, Berry DB, Johnson S, Shi ZR, Brown S, Nguyen QT, et al. 3D printed nerve guidance conduit for biologics-free nerve regeneration and vascular integration. *Bioeng and Translational Med* (2025) 10:e70057. doi: 10.1002/btm2.70057

126. Harley-Troxell ME, Steiner R, Advincula RC, Anderson DE, Dhar M. Interactions of cells and biomaterials for nerve tissue engineering: polymers and fabrication. *Polymers (Basel)* (2023) 15(18):3685. doi: 10.3390/polym15183685

127. Guan Y, Ren Z, Yang B, Xu W, Wu W, Li X, et al. Dual-bionic regenerative microenvironment for peripheral nerve repair. *Bioact Mater* (2023) 26:370–86. doi: 10.1016/j.bioactmat.2023.02.002

128. Jiang H, Qian Y, Fan C, Ouyang Y. Polymeric guide conduits for peripheral nerve tissue engineering. *Front Bioeng Biotechnol* (2020) 8:582646. doi: 10.3389/fbioe.2020.582646

129. Wach RA, Adamus-Wlodarczyk A, Olejnik AK, Matusiak M, Tranquilan-Aranilla C, Ulanski P. Carboxymethylchitosan hydrogel manufactured by radiation-induced crosslinking as potential nerve regeneration guide scaffold. *Reactive Funct Polym* (2020) 152:104588. doi: 10.1016/j.reactfunctpolym.2020.104588

130. Lin R, Chen C, Zheng H, Pu C, Huang J, Duan Q, et al. Biomimetic microstructural scaffolds and their applications in tissue engineering. *Biomed Eng Commun* (2022) 1(1): 5. doi: 10.53388/bmec2022005

131. Li R, Liu H, Huang H, Bi W, Yan R, Tan X, et al. Chitosan conduit combined with hyaluronic acid prevent sciatic nerve scar in a rat model of peripheral nerve crush injury. *Mol Med Rep* (2018) 17(3):4360–8. doi: 10.3892/mmr.2018.8388

132. Li W, Guo J, Chen J, Yao H, Mao R, Li C, et al. Identification of immune infiltration and the potential biomarkers in diabetic peripheral neuropathy through bioinformatics and machine learning methods. *Biomolecules* (2022) 13(1):39. doi: 10.3390/biom13010039

133. Lee D, Tran HQ, Dudley AT, Yang K, Yan Z, Xie J. Advancing nerve regeneration: peripheral nerve injury (PNI) chip empowering high-speed biomaterial and drug screening. *Chem Eng J* (2024) 486:150210. doi: 10.1016/j.cej.2024.150210

134. Williams DF. On the mechanisms of biocompatibility. *Biomaterials* (2008) 29(20): 2941–53. doi: 10.1016/j.biomaterials.2008.04.023

135. Klimek K, Ginalska G. Proteins and peptides as important modifiers of the polymer scaffolds for tissue engineering Applications-A review. *Polymers (Basel)* (2020) 12(4): 844. doi: 10.3390/polym12040844

136. Jin XH, Fang JQ, Wang JG, Xu B, Wang X, Liu SH, et al. PCL NGCs integrated with urolithin-A-loaded hydrogels for nerve regeneration. *J Mater Chem B* (2022) 10(42): 8771–84. doi: 10.1039/d2tb01624a

137. Oleksy M, Dynarowicz K, Aebisher D. Advances in biodegradable polymers and biomaterials for medical Applications-A review. *Molecules* (2023) 28(17):6213. doi: 10.3390/molecules28176213

138. Yu L, Bennett CJ, Lin CH, Yan S, Yang J. Scaffold design considerations for peripheral nerve regeneration. *J Neural Eng* (2024) 21(4):041001. doi: 10.1088/1741-2552/ad628d

139. Cassimjee H, Kumar P, Ubanako P, Choonara YE. Genipin-crosslinked, proteosaccharide scaffolds for potential neural tissue engineering applications. *Pharmaceutics* (2022) 14(2):441. doi: 10.3390/pharmaceutics14020441

140. Zhang D, Li Z, Shi H, Yao Y, Du W, Lu P, et al. Micropatterns and peptide gradient on the inner surface of a guidance conduit synergistically promotes nerve regeneration *in vivo*. *Bioact Mater* (2022) 9:134–46. doi: 10.1016/j.bioactmat.2021.07.010

141. Kong L, Gao X, Qian Y, Sun W, You Z, Fan C. Biomechanical microenvironment in peripheral nerve regeneration: from pathophysiological understanding to tissue engineering development. *Theranostics* (2022) 12(11):4993–5014. doi: 10.7150/thno.74571

142. Ichihara S, Facca S, Liverneaux P, Inada Y, Takigawa T, Kaneko K, et al. Mechanical properties of a bioabsorbable nerve guide tube for long nerve defects. *Chir Main* (2015) 34(4):186–92. doi: 10.1016/j.main.2015.05.004

143. Cen L, Liu W, Cui L, Zhang W, Cao Y. Collagen tissue engineering: development of novel biomaterials and applications. *Pediatr Res* (2008) 63(5):492–6. doi: 10.1203/PDR.0b013e31816c5bc3

144. Meena P, Kakkar A, Kumar M, Khatri N, Nagar RK, Singh A, et al. Advances and clinical challenges for translating nerve conduit technology from bench to bed side for peripheral nerve repair. *Cell Tissue Res* (2021) 383(2):617–44. doi: 10.1007/s00441-020-03301-x

145. Duan G, Li C, Yan X, Yang S, Wang S, Sun X, et al. Construction of a mineralized collagen nerve conduit for peripheral nerve injury repair. *Regen Biomater* (2023) 10: rbac089. doi: 10.1093/rb/rbac089

146. Zhao J, Zhang S, Duan L, Yao R, Yan Y, Wang T, et al. Preparation and mechanical optimization of a two-layer silk/magnesium wires braided porous artificial nerve guidance conduit. *J Biomed Mater Res A* (2022) 110(11):1801–12. doi: 10.1002/jbm.a.37426

147. Montgomery A, Westphal J, Bryan AE, Harris GM. Dynamically changing extracellular matrix stiffness drives Schwann cell phenotype. *Matrix Biol Plus* (2025) 25:100167. doi: 10.1016/j.mbplus.2024.100167

148. Millesi F, Mero S, Semmler L, Rad A, Stadlmayr S, Borger A, et al. Systematic comparison of commercial hydrogels revealed that a synergy of laminin and strain-stiffening promotes directed migration of neural cells. *ACS Appl Mater Inter* (2023) 15(10):12678–95. doi: 10.1021/acsami.2c20040

149. Chan YM, Judge NG, Willits RK, Becker ML. Enhanced integrin-mediated adhesion and proliferation of Schwann cells using highly aligned, dual-functional

fibrous scaffolds. *NPJ Soft Matter* (2026) 2(1):14. doi: 10.1038/s44431-026-00028-7

150. Shan F, Zhang N, Yao X, Li Y, Wang Z, Zhang C, et al. Mechanosensitive channel of large conductance enhances the mechanical stretching-induced upregulation of glycolysis and oxidative metabolism in Schwann cells. *Cell Commun Signal* (2024) 22(1):93. doi: 10.1186/s12964-024-01497-x

151. Omotayo T, Akinyemi G, Omololu P, Ajayi B, Akindahunsi A, Rocha J, et al. Possible involvement of membrane lipids peroxidation and oxidation of catalytically essential thiols of the cerebral transmembrane sodium pump as component mechanisms of iron-mediated oxidative stress-linked dysfunction of the pump's activity. *Redox Biol* (2015) 4:234–41. doi: 10.1016/j.redox.2014.12.015

152. Rushendran R, Begum RF, Singh SA, Narayanan PL, Vellapandian C, Prajapati BG, et al. Navigating neurological disorders: harnessing the power of natural compounds for innovative therapeutic breakthroughs. *EXCLI J* (2024) 23:534–69. doi: 10.17179/excli2024-7051

153. Mahapatra C, Thakkar R, Kumar R. Modulatory impact of oxidative stress on action potentials in pathophysiological states: a comprehensive review. *Antioxidants (Basel)* (2024) 13(10):1172. doi: 10.3390/antiox13101172

154. Demasi M, Augusto O, Bechara EJH, Bicev RN, Cerqueira FM, da Cunha FM, et al. Oxidative modification of proteins: from damage to catalysis, signaling, and beyond. *Antioxid Redox Signal* (2021) 35(12):1016–80. doi: 10.1089/ars.2020.8176

155. Negri S, Faris P, Moccia F. Reactive oxygen species and endothelial Ca(2+) signaling: brothers in arms or partners in crime? *Int J Mol Sci* (2021) 22(18):9821. doi: 10.3390/ijms22189821

156. Rahman M, Mahady Dip T, Padhye R, Houshyar S. Review on electrically conductive smart nerve guide conduit for peripheral nerve regeneration. *J Biomed Mater Res A* (2023) 111(12):1916–50. doi: 10.1002/jbm.a.37595

157. Wang Q, Wang H, Ma Y, Cao X, Gao H. Effects of electroactive materials on nerve cell behaviors and applications in peripheral nerve repair. *Biomater Sci* (2022) 10(21):6061–76. doi: 10.1039/d2bm01216b

158. Murillo G, Blanquer A, Vargas-Estevez C, Barrios L, Ibanez E, Nogues C, et al. Electromechanical nanogenerator-cell interaction modulates cell activity. *Adv Mater* (2017) 29(24):1605048. doi: 10.1002/adma.201605048

159. Murphy WL, McDevitt TC, Engler AJ. Materials as stem cell regulators. *Nat Mater* (2014) 13(6):547–57. doi: 10.1038/nmat3937

160. Fu F, Liu D, Wu Y. Silk-based conductive materials for smart biointerfaces. *Smart Med* (2023) 2(2):e20230004. doi: 10.1002/SMMD.20230004

161. Ghosh S, Dhiman M, Gupta S, Roy P, Lahiri D. Electro-conductive chitosan/graphene bio-nanocomposite scaffold for tissue engineering of the central nervous system. *Biomater Adv* (2023) 154:213596. doi: 10.1016/j.bioadv.2023.213596

162. Jiang H, Wang X, Li X, Jin Y, Yan Z, Yao X, et al. A multifunctional ATP-generating system by reduced graphene oxide-based scaffold repairs neuronal injury by improving mitochondrial function and restoring bioelectricity conduction. *Mater Today Bio* (2022) 13:100211. doi: 10.1016/j.mtbio.2022.100211

163. Escobar A, Serafin A, Carvalho MR, Culebras M, Cantarero A, Beaucamp A, et al. Electroconductive poly (3, 4-ethylenedioxythiophene)(PEDOT) nanoparticle-loaded silk fibroin biocomposite conduits for peripheral nerve regeneration. *Adv Composites Hybrid Mater* (2023) 6(3):118. doi: 10.1007/s42114-023-00689-2

164. Qiu Y, Wang Z, Owens AC, Kulaots I, Chen Y, Kane AB, et al. Antioxidant chemistry of graphene-based materials and its role in oxidation protection technology. *Nanoscale* (2014) 6(20):11744–55. doi: 10.1039/c4nr03275f

165. Qian Y, Wang X, Song J, Chen W, Chen S, Jin Y, et al. Preclinical assessment on neuronal regeneration in the injury-related microenvironment of graphene-based scaffolds. *NPJ Regen Med* (2021) 6(1):31. doi: 10.1038/s41536-021-00142-2

166. Sun P, Guan Y, Yang C, Hou H, Liu S, Yang B, et al. A bioresorbable and conductive scaffold integrating silicon membranes for peripheral nerve regeneration. *Adv Healthc Mater* (2023) 12(32):e2301859. doi: 10.1002/adhm.202301859

167. Yi B, Zhang K, Chen X, Xu R, Zhang X, Zhang C, et al. Bioinspired aligned electroconductive hydrogel nanofiber patch enhances peripheral nerve repair through mechanosensitive calcium influx and focal adhesion kinase/protein kinase B pathway activation. *Acta Biomater* (2026) 217:243–57. doi: 10.1016/j.actbio.2026.05.011

168. Fang J, Nan L, Song K, Weng Z, Shan J, Shahin V, et al. Application and progress of bionic scaffolds in nerve repair: a narrative review. *Adv Technol Neurosci* (2024) 1(1):43–50. doi: 10.4103/atn.Atn-d-24-00004

169. Zhao Z, Xia X, Liu J, Hou M, Liu Y, Zhou Z, et al. Cartilage-inspired self-assembly glycopeptide hydrogels for cartilage regeneration *via* ROS scavenging. *Bioact Mater* (2024) 32:319–32. doi: 10.1016/j.bioactmat.2023.10.013

170. Liu Z, Liu Y, Yushan M, Yusufu A. Enhanced nerve regeneration by bionic conductive nerve scaffold under electrical stimulation. *Front Neurosci* (2022) 16:810676. doi: 10.3389/fnins.2022.810676

171. Li Y, Lv S, Yuan H, Ye G, Mu W, Fu Y, et al. Peripheral nerve regeneration with 3D printed bionic scaffolds loading neural crest stem cell derived schwann cell progenitors. *Adv Funct Mater* (2021) 31(16):2010215. doi: 10.1002/adfm.202010215

172. Chi W, Liu R, Zhou W, Li W, Yu Y. The mechanisms of interaction between biomaterials and cells/cellular microenvironment and the applications in neural injuries. *Chin Chem Lett* (2025) 36(8):110587. doi: 10.1016/j.cclet.2024.110587

173. Wu S, Shen W, Ge X, Ao F, Zheng Y, Wang Y, et al. Advances in large gap peripheral nerve injury repair and regeneration with bridging nerve guidance conduits. *Macromol Biosci* (2023) 23(10):e2300078. doi: 10.1002/mabi.202300078

174. Li G, Zheng T, Wu L, Han Q, Lei Y, Xue L, et al. Bionic microenvironment-inspired synergistic effect of anisotropic micro-nanocomposite topology and biology cues on peripheral nerve regeneration. *Sci Adv* (2021) 7(28):eabi5812. doi: 10.1126/sciadv.abi5812

175. Chen X, Gao R, Liang X, Liu K, Wei Z, Wu X, et al. ROS-scavenging lipoic acid-modified chitosan hydrogels with rapid photocrosslinked ability accelerates peripheral nerve regeneration. *Regen Biomater* (2026) 13:rbag068. doi: 10.1093/rb/rbag068

176. Liu S, Siminska-Stanny J, Yan L, Fan L, Ding X, Ma T, et al. Bioactive ECM-mimicking nerve guidance conduit for enhancing peripheral nerve repair. *Mater Today Bio* (2024) 29:101324. doi: 10.1016/j.mtbio.2024.101324

177. Delgado-Pujol EJ, Martinez G, Casado-Jurado D, Vazquez J, Leon-Barberena J, Rodriguez-Lucena D, et al. Hydrogels and nanogels: pioneering the future of advanced drug delivery systems. *Pharmaceutics* (2025) 17(2):215. doi: 10.3390/pharmaceutics17020215

178. Yuan S, Ma T, Zhang YN, Wang N, Baloch Z, Ma K. Novel drug delivery strategies for antidepressant active ingredients from natural medicinal plants: the state of the art. *J Nanobiotechnology* (2023) 21(1):391. doi: 10.1186/s12951-023-02159-9

179. Shuai C, Ding F, Shuai X, Chen Y, He P, Qi F. Near-infrared light-triggered photothermal-pyroelectric scaffold offering wireless electrical stimulation accelerates nerve repair. *ACS Appl Polym Mater* (2025) 7:1376–85. doi: 10.1021/acsapm.4c03085

180. Zhou J, Fang C, Rong C, Luo T, Liu J, Zhang K. Reactive oxygen species-sensitive materials: a promising strategy for regulating inflammation and favoring tissue regeneration. *Smart Mater Med* (2023) 4:427–46. doi: 10.1016/j.smaim.2023.01.004

181. Yao Y, Zhang H, Wang Z, Ding J, Wang S, Huang B, et al. Reactive oxygen species (ROS)-responsive biomaterials mediate tissue microenvironments and tissue regeneration. *J Mater Chem B* (2019) 7(33):5019–37. doi: 10.1039/c9tb00847k

182. Nagarajan A, Rizwana N, Abraham M, Bhat M, Vetekar A, Thakur G, et al. Polycaprolactone/graphene oxide/acellular matrix nanofibrous scaffolds with antioxidant and promyelinating features for the treatment of peripheral demyelinating diseases. *J Mater Sci Mater Med* (2023) 34(10):49. doi: 10.1007/s10856-023-06750-2

183. Fang J, Jin X, Xu B, Nan L, Liu S, Wang J, et al. Chlorogenic acid releasing microspheres enhanced electrospun conduits to promote peripheral nerve regeneration. *Biomater Sci* (2023) 11(24):7909–25. doi: 10.1039/d3bm00920c

184. Shen L, Gan Q, Yang Y, Reis C, Zhang Z, Xu S, et al. Mitophagy in cerebral ischemia and ischemia/reperfusion injury. *Front Aging Neurosci* (2021) 13:687246. doi: 10.3389/fnagi.2021.687246

185. Zhao R, Deng X, Tang Y, Yang X, Ge Z, Wang D, et al. Mitigating critical peripheral nerve deficit therapy with reactive oxygen Species/Ca2+-Responsive dynamic hydrogel-mediated mRNA delivery. *ACS Nano* (2024) 18(26):16556–76. doi: 10.1021/acsnano.3c13102

186. Xiong Y, Wu QP, Wang H, Shahbazi MA, Mi BB. ROS-responsive drug delivery systems for chronic wound healing: advances, challenges, and translational perspectives. *Mil Med Res* (2026) 13(1):100019. doi: 10.1016/j.mmr.2026.100019

187. van Niel G, D'Angelo G, Raposo G. Shedding light on the cell biology of extracellular vesicles. *Nat Rev Mol Cell Biol* (2018) 19(4):213–28. doi: 10.1038/nrm.2017.125

188. Steenbeek SC, Pham TV, de Ligt J, Zomer A, Knol JC, Piersma SR, et al. Cancer cells copy migratory behavior and exchange signaling networks *via* extracellular vesicles. *EMBO J* (2018) 37(15):e98357. doi: 10.15252/embj.201798357

189. Lopez-Verrilli MA, Picou F, Court FA. Schwann cell-derived exosomes enhance axonal regeneration in the peripheral nervous system. *Glia* (2013) 61(11):1795–806. doi: 10.1002/glia.22558

190. Lopez-Leal R, Diaz-Viraque F, Catalan RJ, Saquel C, Enright A, Iraola G, et al. Schwann cell reprogramming into repair cells increases miRNA-21 expression in exosomes promoting axonal growth. *J Cell Sci* (2020) 133(12):jcs239004. doi: 10.1242/jcs.239004

191. Li Q, Fu X, Kou Y, Han N. Engineering strategies and optimized delivery of exosomes for theranostic application in nerve tissue. *Theranostics* (2023) 13(12):4266–86. doi: 10.7150/thno.84971

192. Liu D, Gao J, Wu X, Hao X, Hu W, Han L. Conductive microneedles loaded with polyphenol-engineered exosomes reshape diabetic neurovascular niches for chronic wound healing. *Adv Sci (Weinh)* (2025) 12(43):e07974. doi: 10.1002/advs.202507974

193. Marin E, Tiwari N, Calderon M, Sarasua JR, Larranaga A. Smart layer-by-layer polymeric microreactors: ph-triggered drug release and attenuation of cellular oxidative stress as prospective combination therapy. *ACS Appl Mater Inter* (2021) 13(16):18511–24. doi: 10.1021/acsami.1c01450

194. Tommasini G, Sol-Fernández SD, Flavián-Lázaro AC, Lewinska A, Wnuk M, Tortiglione C, et al. Remote magneto–thermal modulation of reactive oxygen species balance enhances tissue regeneration *in vivo*. *Adv Funct Mater* (2024) 34(39):2405282. doi: 10.1002/adfm.202405282

195. Fan Z, Yu W, Wen X, Ding X, Li X. Aligned conductive magnetic nanofibers with directional magnetic field stimulation promotes peripheral nerve regeneration. *Adv Sci (Weinh)* (2025) 12(37):e01665. doi: 10.1002/advs.202501665

196. Huang WC, Lin CC, Chiu TW, Chen SY. 3D gradient and linearly aligned magnetic microcapsules in nerve guidance conduits with remotely spatiotemporally controlled release to enhance peripheral nerve repair. *ACS Appl Mater Inter* (2022) 14(41): 46188–200. doi: 10.1021/acsami.2c11362

197. Jalili NA, Muscarello M, Gaharwar AK. Nanoengineered thermoresponsive magnetic hydrogels for biomedical applications. *Bioeng Transl Med* (2016) 1(3): 297–305. doi: 10.1002/btm2.10034

198. Zakeri Z, Heiderzadeh M, Kocaarslan A, Metin E, Hosseini Karimi SN, Saghati S, et al. Exosomes encapsulated in hydrogels for effective central nervous system drug delivery. *Biomater Sci* (2024) 12(10):2561–78. doi: 10.1039/d3bm01055d

199. Fareed MA, Zhang B, Memon K, Hassan M, Raza Y, Zhao G. Magnetothermal nanocomposite scaffolds with dual stimulation for synergistic drug delivery and cellular modulation in wound healing. *Mater Horiz* (2026) 13(2):886–904. doi: 10.1039/d5mh01769f

200. Kuznetsova E, Shchori GS, Maierovicz T, Shalom S, Shine O, Begmatova D, et al. Magnetothermally responsive fibrin hydrogel for localized neuromodulation. *Colloids Surf B Biointerfaces* (2026) 267:115898. doi: 10.1016/j.colsurfb.2026.115898

201. Zhu W, Castro NJ, Shen Y-L, Zhang LG. Nanotechnology and 3D/4D bioprinting for neural tissue regeneration. In: Zhang LG, Fisher JP, Leong KW, editors. *3D Bioprinting and Nanotechnology in Tissue Engineering and Regenerative Medicine*. Academic Press (2022). p. 427–58.

202. Yu X, Zhang T, Li Y. 3D printing and bioprinting nerve conduits for neural tissue engineering. *Polymers (Basel)* (2020) 12(8):1637. doi: 10.3390/polym12081637

203. Sun M, You D, Zhan N, Liu C, Zhang X, Lin L, et al. 4D oriented dynamic scaffold for promoting peripheral nerve regeneration and functional recovery. *Adv Funct Mater* (2023) 34(2):2305827. doi: 10.1002/adfm.202305827

204. Cui H, Zhu W, Miao S, Sarkar K, Zhang LG. 4D printed nerve conduit with *in situ* neurogenic guidance for nerve regeneration. *Tissue Eng A* (2024) 30(11-12):293–303. doi: 10.1089/ten.TEA.2023.0194

205. Miao S, Cui H, Nowicki M, Xia L, Zhou X, Lee SJ, et al. Stereolithographic 4D bioprinting of multiresponsive architectures for neural engineering. *Adv Biosyst* (2018) 2(9):1800101. doi: 10.1002/adbi.201800101

206. Wang Z, Zheng Y, Qiao L, Ma Y, Zeng H, Liang J, et al. 4D-Printed MXene-Based artificial nerve guidance conduit for enhanced regeneration of peripheral nerve injuries. *Adv Healthc Mater* (2024) 13(23):e2401093. doi: 10.1002/adhm.202401093

207. Zoughaib M, Avdokushina S, Savina IN. MXene-Reinforced composite cryogel scaffold for neural tissue repair. *Molecules* (2025) 30(3):479. doi: 10.3390/molecules30030479

208. Qi Z, Wang S, Li Y, Wang L, Zhao L, Ge Q, et al. Scavenging activity and reaction mechanism of Ti3C2Tx MXene as a novel free radical scavenger. *Ceramics Int* (2021) 47(12):16555–61. doi: 10.1016/j.ceramint.2021.02.226

209. Wei C, Guo Y, Ci Z, Li M, Zhang Y, Zhou Y. Advances of Schwann cells in peripheral nerve regeneration: from mechanism to cell therapy. *Biomed Pharmacother* (2024) 175:116645. doi: 10.1016/j.biopha.2024.116645

210. Msheik Z, El Massry M, Rovini A, Billet F, Desmouliere A. The macrophage: a key player in the pathophysiology of peripheral neuropathies. *J Neuroinflammation* (2022) 19(1):97. doi: 10.1186/s12974-022-02454-6

211. De Logu F, Marini M, Landini L, Souza Monteiro de Araujo D, Bartalucci N, Trevisan G, et al. Peripheral nerve resident macrophages and schwann cells mediate cancer-induced pain. *Cancer Res* (2021) 81(12):3387–401. doi: 10.1158/0008-5472.CAN-20-3326

212. Wu Z, Yan W, Wang K, Xu G, Zhu D, Li X, et al. Lysosomal dysfunction in Schwann cells is involved in bortezomib-induced peripheral neurotoxicity. *Arch Toxicol* (2023) 97(5):1385–96. doi: 10.1007/s00204-023-03468-6

213. Wang F, Zhao C, Jing Z, Wang Q, Li M, Lu B, et al. The dual roles of chemokines in peripheral nerve injury and repair. *Inflamm Regen* (2025) 45(1):11. doi: 10.1186/s41232-025-00375-4

214. Sprenger-Svacina A, Svacina MKR, Otlu HG, Gao T, Sheikh KA, Zhang G. Endoneurial immune interplay in peripheral nerve repair: insights and implications for future therapeutic interventions. *Front Neurosci* (2025) 19:1602112. doi: 10.3389/fnins.2025.1602112

215. Arthur-Farraj PJ, Latouche M, Wilton DK, Quintes S, Chabrol E, Banerjee A, et al. c-Jun reprograms Schwann cells of injured nerves to generate a repair cell essential for regeneration. *Neuron* (2012) 75(4):633–47. doi: 10.1016/j.neuron.2012.06.021

216. Li R, Li D, Wu C, Ye L, Wu Y, Yuan Y, et al. Nerve growth factor activates autophagy in Schwann cells to enhance myelin debris clearance and to expedite nerve regeneration. *Theranostics* (2020) 10(4):1649–77. doi: 10.7150/thno.40919

217. Lindborg JA, Mack M, Zigmond RE. Neutrophils are critical for Myelin removal in a peripheral nerve injury model of wallerian degeneration. *J Neurosci* (2017) 37(43): 10258–77. doi: 10.1523/JNEUROSCI.2085-17.2017

218. Gold R, Archelos JJ, Hartung HP. Mechanisms of immune regulation in the peripheral nervous system. *Brain Pathol* (1999) 9(2):343–60. doi: 10.1111/j.1750-3639.1999.tb00231.x

219. Fornasari BE, Zen F, Nato G, Fogli M, Luzzati F, Ronchi G, et al. Blood vessels: the pathway used by schwann cells to colonize nerve conduits. *Int J Mol Sci* (2022) 23(4): 2254. doi: 10.3390/ijms23042254

220. Wu G, Wen X, Kuang R, Lui KW, He B, Li G, et al. Roles of macrophages and their interactions with schwann cells after peripheral nerve injury. *Cell Mol Neurobiol* (2023) 44(1):11. doi: 10.1007/s10571-023-01442-5

221. Wang BB, Guo C, Sun SQ, Zhang XN, Li Z, Li WJ, et al. Comparison of the nerve regeneration capacity and characteristics between sciatic nerve crush and transection injury models in rats. *Biomed Environ Sci* (2023) 36(2):160–73. doi: 10.3967/bes2023.001

222. Zhou P, Zhang R, Xian L, Ning L, Lu P, Liu Q, et al. Selection of sciatic nerve injury models: implications for pathogenesis and treatment. *Front Neurol* (2025) 16:1521941. doi: 10.3389/fneur.2025.1521941

223. Yang Y, Zhao B, Wang Y, Lan H, Liu X, Hu Y, et al. Diabetic neuropathy: cutting-edge research and future directions. *Signal Transduct Target Ther* (2025) 10(1):132. doi: 10.1038/s41392-025-02175-1

224. Goncalves NP, Vaegter CB, Andersen H, Ostergaard L, Calcutt NA, Jensen TS. Schwann cell interactions with axons and microvessels in diabetic neuropathy. *Nat Rev Neurol* (2017) 13(3):135–47. doi: 10.1038/nrneurol.2016.201

225. Khalid M, Petroianu G, Adem A. Advanced glycation end products and diabetes mellitus: mechanisms and perspectives. *Biomolecules* (2022) 12(4):542. doi: 10.3390/biom12040542

226. Osonoi S, Mizukami H, Takeuchi Y, Sugawa H, Ogasawara S, Takaku S, et al. RAGE activation in macrophages and development of experimental diabetic polyneuropathy. *JCI Insight* (2022) 7(23):e160555. doi: 10.1172/jci.insight.160555

227. Zuo L, Qu M, Zhang M, Cheng P, Guo M, Selvarajah D, et al. High glucose mediates diabetic peripheral neuropathy by inducing Schwann cells apoptosis through the Dgkh/PKC-alpha signaling pathway. *Acta Diabetol* (2025) 62(12):2109–19. doi: 10.1007/s00592-025-02553-9

228. Wei Luo YW, Yansong LIU, Wang Y, Lei AI. High glucose induces pro-inflammatory polarization of macrophages by inhibiting immune-responsive gene 1 expression. *J South Med Univ* (2025) 45(01):1–9. doi: 10.12122/j.issn.1673-4254.2025.01.01

229. Xu C, Hou B, He P, Ma P, Yang X, Yang X, et al. Neuroprotective effect of salvianolic acid A against diabetic peripheral neuropathy through modulation of Nrf2. *Oxid Med Cell Longev* (2020) 2020:6431459. doi: 10.1155/2020/6431459

230. Wu L, Huang F, Sun Z, Zhang J, Xia S, Zhao H, et al. Downregulation of iron-sulfur cluster biogenesis may contribute to hyperglycemia-mediated diabetic peripheral neuropathy in murine models. *Antioxidants (Basel)* (2024) 13(9):1036. doi: 10.3390/antiox13091036

231. Yao X, Wang X, Zhang R, Kong L, Fan C, Qian Y. Dysregulated mast cell activation induced by diabetic milieu exacerbates the progression of diabetic peripheral neuropathy in mice. *Nat Commun* (2025) 16(1):4170. doi: 10.1038/s41467-025-59562-z

232. Zhu Y, Ghosh P, Charnay P, Burns DK, Parada LF. Neurofibromas in NF1: Schwann cell origin and role of tumor environment. *Science* (2002) 296(5569):920–2. doi: 10.1126/science.1068452

233. Carroll SL. Molecular mechanisms promoting the pathogenesis of Schwann cell neoplasms. *Acta Neuropathol* (2012) 123(3):321–48. doi: 10.1007/s00401-011-0928-6

234. Fletcher JS, Pundavela J, Ratner N. After Nf1 loss in Schwann cells, inflammation drives neurofibroma formation. *Neurooncol Adv* (2020) 2(Suppl. 1):i23–i32. doi: 10.1093/noajnl/vdz045

235. White EE, Rhodes SD. The NF1+/- immune microenvironment: dueling roles in neurofibroma development and malignant transformation. *Cancers (Basel)* (2024) 16(5): 994. doi: 10.3390/cancers16050994

236. Yang FC, Ingram DA, Chen S, Hingtgen CM, Ratner N, Monk KR, et al. Neurofibromin-deficient Schwann cells secrete a potent migratory stimulus for Nf1+/- mast cells. *J Clin Invest* (2003) 112(12):1851–61. doi: 10.1172/JCI19195

237. Malone CF, Emerson C, Ingraham R, Barbosa W, Guerra S, Yoon H, et al. mTOR and HDAC inhibitors converge on the TXNIP/thioredoxin pathway to cause catastrophic oxidative stress and regression of RAS-driven tumors. *Cancer Discov* (2017) 7(12):1450–63. doi: 10.1158/2159-8290.CD-17-0177

238. Caillaud M, Chantemargue B, Richard L, Vignaud L, Favreau F, Faye PA, et al. Local low dose curcumin treatment improves functional recovery and remyelination in a rat model of sciatic nerve crush through inhibition of oxidative stress. *Neuropharmacology* (2018) 139:98–116. doi: 10.1016/j.neuropharm.2018.07.001

239. Viana MDM, Lauria PSS, Lima AA, Opretzka LCF, Marcelino HR, Villarreal CF. Alpha-Lipoic acid as an antioxidant strategy for managing neuropathic pain. *Antioxidants (Basel)* (2022) 11(12):2420. doi: 10.3390/antiox11122420

240. Yadav A, Huang TC, Chen SH, Ramasamy TS, Hsueh YY, Lin SP, et al. Sodium phenylbutyrate inhibits Schwann cell inflammation *via* HDAC and NFkappaB to promote axonal regeneration and remyelination. *J Neuroinflammation* (2021) 18(1): 238. doi: 10.1186/s12974-021-02273-1

241. Yao Y, Lei X, Wang Y, Zhang G, Huang H, Zhao Y, et al. A mitochondrial nanoguard modulates redox homeostasis and bioenergy metabolism in diabetic peripheral neuropathy. *ACS Nano* (2023) 17(22):22334–54. doi: 10.1021/acsnano.3c04462

242. Li J, Yao Y, Wang Y, Xu J, Zhao D, Liu M, et al. Modulation of the crosstalk between Schwann cells and macrophages for nerve regeneration: a therapeutic strategy based on a multifunctional tetrahedral framework nucleic acids system. *Adv Mater* (2022) 34(46): e2202513. doi: 10.1002/adma.202202513

243. Wei G, Li X, Huang M, Wang H, Li Z, Qu S. Light-responsive oxygen generation from chlorella hydrogels for facial nerve injury recovery: crosstalk between M1/M2 macrophages and schwann cells. *Adv Healthc Mater* (2025) 14(16):e2501123. doi: 10.1002/adhm.202501123

244. Xiao J, Ding J, Yu Z, Gao J, Zeng M, Wu X, et al. Boronic ester bonding integrated dextran-based hydrogel patch for diabetic peripheral nerve injury treatment. *Chem Eng J* (2024) 498:155336. doi: 10.1016/j.cej.2024.155336

245. Litowczenko J, Wychowaniec JK, Zaleski K, Marczak L, Edwards-Gayle CJC, Tadyszak K, et al. Micro/nano-patterns for enhancing differentiation of human neural stem cells and fabrication of nerve conduits *via* soft lithography and 3D printing. *Biomater Adv* (2023) 154:213653. doi: 10.1016/j.bioadv.2023.213653

246. Smith DH, Burrell JC, Browne KD, Katiyar KS, Ezra MI, Dutton JL, et al. Tissue-engineered grafts exploit axon-facilitated axon regeneration and pathway protection to enable recovery after 5-cm nerve defects in pigs. *Sci Adv* (2022) 8(44):eabm3291. doi: 10.1126/sciadv.abm3291

EBM Experimental Biology and Medicine

TYPE Original Research
PUBLISHED 27 July 2026
DOI 10.3389/ebm.2026.10923

Check for updates

OPEN ACCESS

*CORRESPONDENCE
Lei Yu,
myyl2024@hotmail.com

†These authors have contributed equally to this work and share first authorship

RECEIVED 04 December 2025
REVISED 10 June 2026
ACCEPTED 30 June 2026
PUBLISHED 27 July 2026

CITATION
Jin J, Pu Q, Wu C, Lei Y, Hu Y, Yang X, Huang J, Wu F, Xiao L and Yu L (2026) Causal association between clonal hematopoiesis indeterminate potential and cancer: a Mendelian randomization study.
Exp. Biol. Med. 251:10923.
doi: 10.3389/ebm.2026.10923

COPYRIGHT
© 2026 Jin, Pu, Wu, Lei, Hu, Yang, Huang, Wu, Xiao and Yu. This is an open-access article distributed under the terms of the Creative Commons Attribution License (CC BY). The use, distribution or reproduction in other forums is permitted, provided the original author(s) and the copyright owner(s) are credited and that the original publication in this journal is cited, in accordance with accepted academic practice. No use, distribution or reproduction is permitted which does not comply with these terms.

Causal association between clonal hematopoiesis indeterminate potential and cancer: a Mendelian randomization study

Juan Jin[1†], Qian Pu[2†], Chengrong Wu[3], Yu Lei[4], Yaxin Hu[4], Xiuju Yang[2], Jinghui Huang[2], Fangfang Wu[5], Li Xiao[6] and Lei Yu[2*]

[1]Department of Obstetrics, The People's Hospital of Qiannan, Duyun, Guizhou, China, [2]Central Laboratory, Guiyang Maternal and Child Health Care Hospital, Guiyang, Guizhou, China, [3]Reproductive Center, Guiyang Maternal and Child Health Care Hospital, Guiyang, Guizhou, China, [4]Prenatal Diagnosis Center, Affiliated Hospital of Guizhou Medical University, Guiyang, Guizhou, China, [5]Department of Obstetrics, The First People's Hospital of Qingzhen, Qingzhen, Guizhou, China, [6]Prenatal Diagnosis Center, Qianxinan People's Hospital, Xingyi, Guizhou, China

Abstract

Clonal hematopoiesis of indeterminate potential (CHIP) causes the expansion of mutated hematopoietic stem cells and produces immunophenotypically altered leukocytes, which induce a tumor-promoting inflammatory condition. However, the causal effect of CHIP on cancer remains unclear. We assessed the relationship of genetically predicted CHIP with the risk of 18 cancer types involving 612,576 cases using two-sample Mendelian randomization (MR). Genetic instruments for overall and sub-types of CHIP were obtained from the a large-scale genome-wide association study using independent ($r^2 < 0.001$) SNPs at genome-wide significance ($p < 5.0 \times 10^{-8}$). Summary statistics for 18 cancers were obtained from the FinnGen, MVP, PLCO study, and large consortia. Inverse-variance weighted random-effects models were used as the primary method for estimating causal effects. Findings from independent datasets were combined using the fixed-effect model and Bonferroni corrections were applied for multiple testing. We found genetic predicted overall and DNMT3A CHIP was significantly associated with an increased risk of thyroid cancer, lung cancer, kidney cancer, brain cancer, basal cell carcinoma, and malignant melanoma after corrections. In addition, we found the causal estimate of CHIP varied across histological sub-types of cancer. Sensitivity analyses confirmed that these findings were robust. Strong associations were found between genetic predicted CHIP and an increased risk of a broad range of cancers, highlighting the importance of timely screening for CHIP in cancer early detection and prevention.

KEYWORDS
cancer, clonal hematopoiesis of indeterminate potential, histological subtypes, Mendelian randomization, risk

Impact statement

Clonal hematopoiesis indeterminate potential (CHIP) defines the age-related expansion of hematopoietic clones harboring somatic mutations in the absence of overt hematologic abnormalities. Although CHIP has been associated with increased mortality in patients with solid cancer, the relationship between CHIP and solid tumor carcinogenesis remains largely unexplored. Considering the prominent role of inflammatory elements in the cancer microenvironment and emerging evidence positing the lung as a tumor of hematopoietic progenitor cells, CHIP may play a role in solid cancer pathogenesis. Indeed, CHIP is also a hot topic in cancer research recently. Using Mendelian randomization (MR) approach, this study found lifelong genetic propensity to develop overall CHIP and DNMT3A CHIP was significantly associated with increased risk of thyroid cancer, lung cancer, kidney cancer, brain cancer, basal cell carcinoma, and malignant melanoma. In addition, we found the causal estimate of CHIP vary across histological subtypes of cancer. Multiple sensitivity analyses and replication analyses also supported this observation. To our knowledge, this is the first comprehensive genetic instrumental variable study to depict the relationship between CHIP and solid cancer. Our study found significant association between genetic predicted CHIP and an increased risk of a broad range of cancers, highlighting the importance of timely screening for CHIP in cancer early detection and prevention.

Introduction

Clonal hematopoiesis of indeterminate potential (CHIP) is an age-related expansion of hematopoietic stem cells (HSCs) harboring oncogenic somatic mutations (variant allele frequency, VAF >2%) in the absence of clinical hematologic disorders. Among the list of genes identified as potential drivers of CHIP, DNMT3A, TET2, and ASXL1 are the most frequently mutated [1, 2]. In addition to its potential as a risk factor in hematological cancer [2, 3], CHIP is also linked with various non-hematological conditions, such as cardiovascular disease [4, 5], pulmonary disease [6], liver disease [7], and neurological disease [8]. Although the biological mechanisms underlying these associations are largely unknown, accumulative evidence has indicated that CHIP can induce aberrant inflammatory responses or impair the immune function, which are considered as key pathogenic features contributing towards malignant transformation [9–11].

A number of cohort studies have reported the presence of CHIP in solid tumor samples from a treatment naïve setting, further confirming infiltration of the solid tumor microenvironment by clonal hematopoiesis mutated hematopoietic cells [12–14]. Considering the prominent role of chronic inflammation in cancer development [15, 16] and the pervasive nature of circulating immune cells, CHIP may play a key role in cancer pathogenesis. Further, previous clinical studies reported certain cancers are more likely than others to be associated with CHIP [12, 13, 17], suggesting that CHIP may have distinct effects on different cancers. However, the causality of CHIP and cancer can be difficult to establish since their relationship is confounded by factors such as aging and some anti-cancer treatments. Moreover, germline causes of CHIP have been recently identified [18–20], and the potential influence of genetic susceptibility to CHIP on cancer development remains poorly understood [21]. Therefore, a comprehensive appraisal of the causal associations between CHIP and cancer is of great importance in cancer prevention.

Mendelian randomization (MR) uses germline genetic variants as proxies (or instrumental variables) for risk factors to infer a causal relation between factors on disease outcomes and thus overcome some of the conventional issues (e.g., unmeasured confounding and reverse causation bias) in observational settings [22]. In addition, MR analysis evaluates the causality for lifelong effects of risk factors on disease outcomes, which is important in the context of diseases like cancer where a long induction and latent period may be required for a particular risk factor to generate effect.

To date, no studies have comprehensively evaluated the causal effects of CHIP across cancer. Given the emerging role of CHIP in cancer etiology, we used a two-sample MR framework to examine potential causal associations between genetically predicted CHIP and the risk of 18 types of cancer.

Materials and methods

Research design

This study followed the Strengthening the Reporting of Observational Studies in Epidemiology-Mendelian Randomisation reporting guidelines (Supplementary Table S1) [23]. First, instruments to proxy CHIP exposure were generated and validated. Then, we used univariable two-sample MR to investigate the associations between genetically predicted CHIP and cancer risk. An outline of the current MR study can be found in Figure 1. All GWAS studies were approved by their respective ethical review committees and permitted the use of summary data without restriction; therefore, no further ethical approval or informed consent was required for the present study.

Genetic instrument construction and validation

Summary data for overall CHIP [inclusive CHIP (with at least one CHIP mutation) and exclusive CHIP (without CHIP mutation)] and main CHIP sub-types (DNMT3A CHIP and TET2 CHIP) were obtained from the a large-scale Genome-Wide Association Study (GWAS) performed in European cohorts, adjusting for sex, age, and population structure [20]. Single nucleotide polymorphisms (SNPs) with minor allele frequency >0.01 associated with overall, DNMT3A, and TET2 CHIP at genome-wide significance ($p < 5 \times 10^{-8}$) were considered as genetic instruments. The SNPs were further clumped

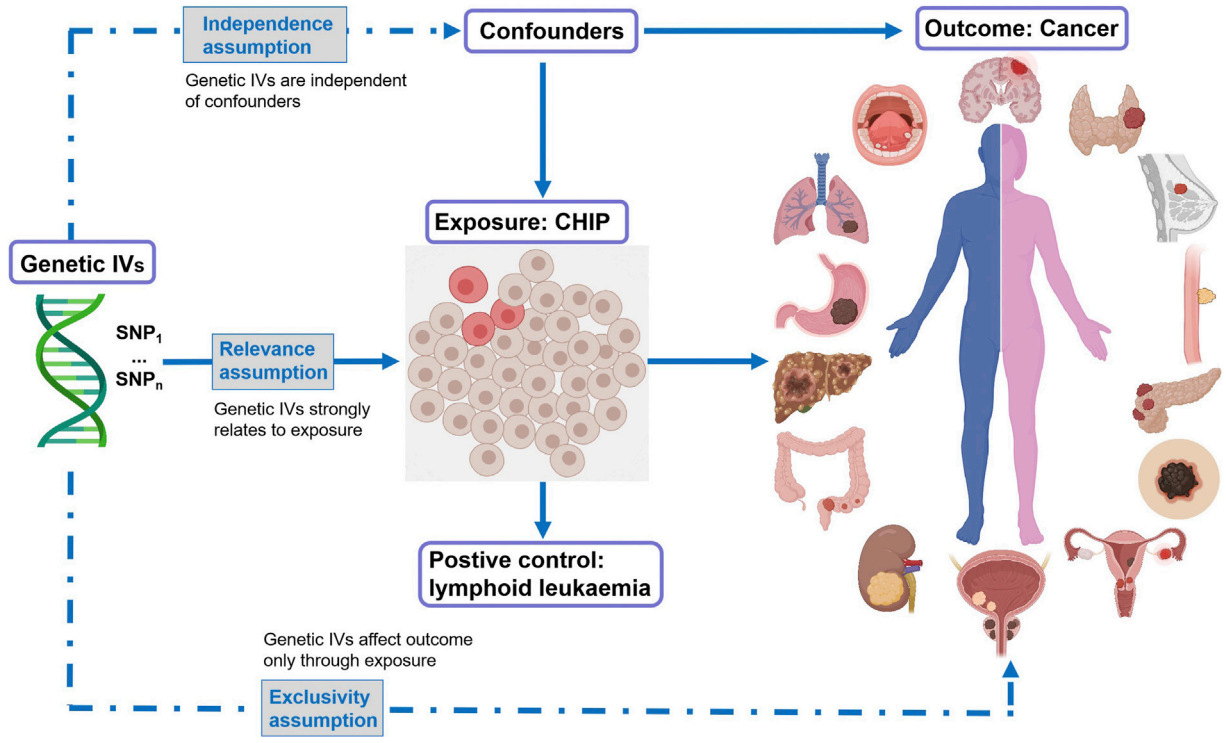


FIGURE 1
Study overview.

by the linkage disequilibrium (LD) threshold r^2 0.001 within 10,000 kilobases windows to ensure they were independent from each other. The strength of each genetic instrument was estimated using F-statistic; an F-statistic greater than 10 indicates minimally weak instrument bias [24]. As the presence of CHIP has been associated with an increased risk of hematological malignancies, we tested associations of our instrument for CHIP with lymphoid leukemia in positive control MR analysis.

Cancer GWAS data sources

This study included 18 types of cancer outcomes: brain, oral, thyroid, esophageal, lung, breast, stomach, pancreatic, liver, colorectal, bladder, prostate, kidney, ovarian, endometrial, cervical, basal cell carcinoma, and malignant melanoma. We obtained summary genetic associations with these outcomes from the FinnGen consortium [25], Million Veteran Program (MVP) [26], PLCO atlas [27], large consortia (e.g., BCAC: The Breast Cancer Association Consortium; TRICL: The Transdisciplinary Research of Cancer in Lung), and other larger GWAS meta-analysis. When sample overlapping was identified, we used the summary statistics from the study with the largest sample size. All individuals involved in each cancer GWAS analysis were of European ancestry. Detailed information on the diagnostic criteria for cancer, genotyping method, imputation, and quality control measures for these GWAS is available in the original publications. The GWAS summary for lymphoid leukemia used in the positive control MR was obtained from the FinnGen consortium.

Phenome-wide association analysis and pathway analysis

We performed SNP-level phenome-wide association studies (PheWAS) for the genetic instruments using Open Target Platform (https://genetics.opentargets.org/) [28] for secondary phenotypes associated with traditional cancer risk factors ($P < 5 \times 10^{-8}$) to further explore the impact of horizontal pleiotropy on causality estimates. Formal pathway enrichment analysis of the instrument-tagged gene set was performed using the WebGestalt online toolkit [29]. Over-representation analysis (ORA) was applied to identify significantly enriched biological pathways based on three canonical pathway databases: the Kyoto Encyclopedia of Genes and Genomes (KEGG), Reactome, and WikiPathways. All analyses were conducted for *Homo sapiens* with the gene symbol as the input identifier. Multiple testing bias was corrected for using the Benjamini-Hochberg false discovery rate (FDR) method, and pathways with an adjusted FDR value <0.05 were defined as statistically significant.

Statistical analysis

When estimating the causal effects of CHIP exposure on cancer outcome, we used the random-effects inverse-variance weighted (IVW) approach as the primary method [30]. Multiple sensitivity analyses, which each make different assumptions of validity of the genetic instruments including the weighted median, MR-Egger, weighted mode, simple mode, and MR-RAPS (Robust Adjusted Profile Score) [31], were performed to examine the robustness of

the results. The MR-PRESSO (Pleiotropy RESidual Sum and Outlier) test was also performed to detect horizontal pleiotropy (global test) and correct the effect of outliers [32]. The heterogeneity of genetic variants was examined using Cochran Q-statistic, whereas pleiotropy between genetic variants was evaluated by the MR-Egger intercept test [33]. In addition, iterative leave-one-out analysis was conducted by removing one SNP at a time from instruments to assess the influence of individual variants. The MR Steiger test was also performed to confirm the direction of causal estimation [34]. Furthermore, we examined the effects of genetic susceptibility to cancer on CHIP in reverse MR, wherein uncorrelated ($r^2 < 0.001$) SNPs associated with specific types of cancer at a genome-wide significance ($p < 5 \times 10^{-8}$) were selected as genetic instruments. The multivariable MR (MVMR) analysis was performed to identify the independent risk factors (e.g., telomere length and smoking). Moreover, the odds ratios (ORs) with a 95% confidence interval (CI) was scaled to per standard deviation (SD) increase in genetically predicted overall or sub-types of CHIP. When the associations were generated from multiple datasets for the same cancer outcome, the combined effects were obtained using the fixed-effect meta approach. The online tool mRnd was used to calculate statistical power (http://cnsgenomics.com/shiny/mRnd/). The association with a nominal p value <0.05 but a Bonferroni adjusted p value $>6.94 \times 10^{-4}$(0.05 Bonferroni-corrected for four types of CHIP with 18 cancer outcomes) was considered suggestive, and the association with a Bonferroni adjusted p value $<6.94 \times 10^{-4}$ was deemed significant. All analyses were two-sided and were conducted using the "TwoSampleMR" (V.0.5.7), "MendelianRandomization" (0.7.0), and "meta" (V.6.5-0) packages in R (version 4.3.0).

Results

Genetic variant selection

In total, 26 SNPs were used to proxy overall inclusive CHIP; 21 SNPs proxied overall exclusive CHIP; 26 SNPs proxied DNMT3A sub-type; and six SNPs proxied TET2 sub-type. For CHIP traits, the genetic instruments used explained approximately 0.52%, 0.44%, 0.56%, and 0.1% of variance in overall inclusive CHIP, overall exclusive CHIP, DNMT3A sub-type, and TET2 sub-type, respectively. Characteristics of genetic variants used to instrument CHIP are presented in Supplementary Table S2. The F-statistics of selected genetic instruments for CHIP ranged from 30.0 to 507.5, indicating minimally weak instrument bias. The positive control analyses identified associations in the expected direction between genetically predicted CHIP and lymphoid leukemia (Supplementary Table S3), further confirming the validity of the genetic instruments.

Main results

The characteristics of the cancer outcome and cancer histological sub-types GWAS data involving a total of 612,576 cancer cases are summarized in Supplementary Table S4. We had 80% power to detect an association with an OR of 1.5 or more at an α of 0.05 for most cancer outcomes (Supplementary Table S5). Among the 18 types of cancer included in analyses, we found consistent evidence for the association of CHIP in the risk of six site-specific cancers (brain cancer, thyroid cancer, kidney cancer, lung cancer, basal cell carcinoma, and malignant melanoma) (Figure 2). However, we found limited evidence that genetically predicted overall CHIP or its subtypes were causally associated with the risk of breast cancer, oral cavity cancer, esophageal cancer, stomach cancer, pancreatic cancer, liver cancer, colorectal cancer, bladder cancer, prostate cancer, endometrial cancer, ovarian cancer, and cervical cancer (Supplementary Table S6). Results from multiple MR method analyses support these associations (Supplementary Table S7).

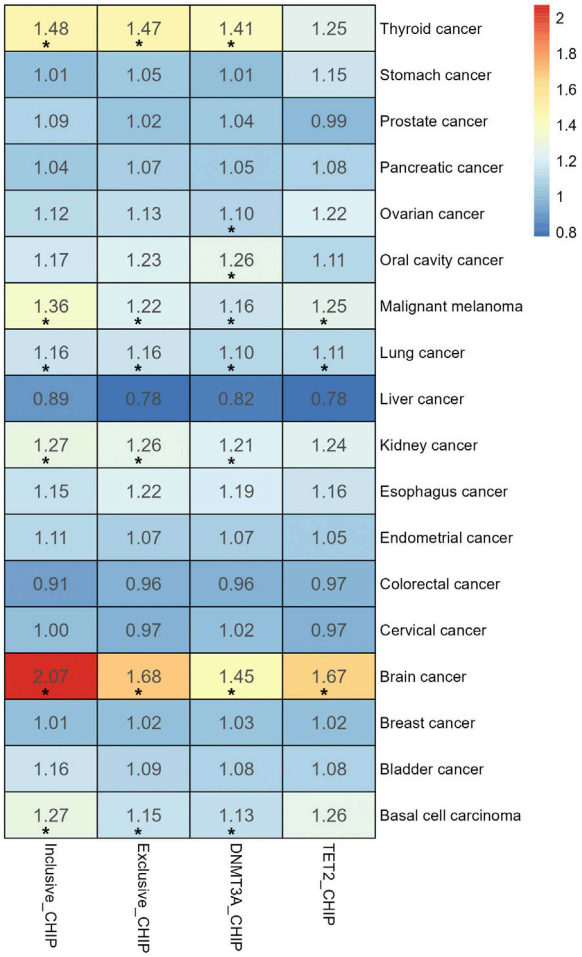


FIGURE 2
Summary of associations of genetically predicted overall and subtypes of CHIP with cancer. Numbers in the boxes are ORs for associations of exposure and each cancer outcome. The reported ORs are scaled to a 1-SD increase in log odds of genetic susceptibility to overall or subtypes of CHIP. *p < 0.05 after multiple testing correction.

Brain cancer

We observed a strong causal association between overall and sub-types of CHIP and brain cancer in both FinnGen and MVP datasets. The pooled OR of brain cancer was 1.78 (95% CI: 1.44–2.19, $p = 4.32 \times 10^{-6}$, Figure 3) for over inclusive CHIP, 1.67 (95% CI: 1.39–2.02, $p = 4.32 \times 10^{-6}$, Figure 4) for over exclusive CHIP, 1.36 (95% CI: 1.15–1.60, p = 0.02, Figure 5) for

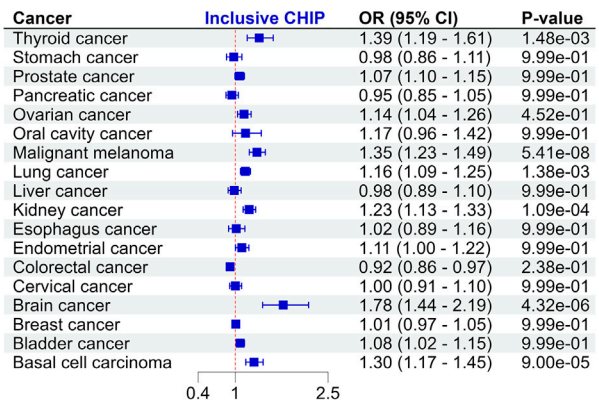


FIGURE 3
Associations of genetic susceptibility to inclusive CHIP with cancer. Mendelian randomization estimates were generated using the IVW approach. P values are for ORs (95% CIs) after multiple testing correction.

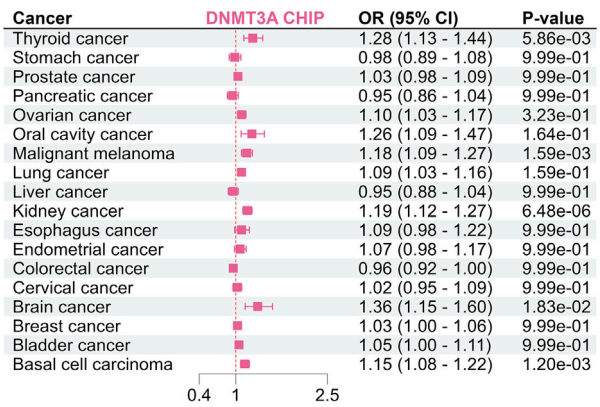


FIGURE 5
Associations of genetic susceptibility to DNMT3A CHIP with cancer. Mendelian randomization estimates were generated using the IVW approach. P values are for ORs (95% CIs) after multiple testing correction.

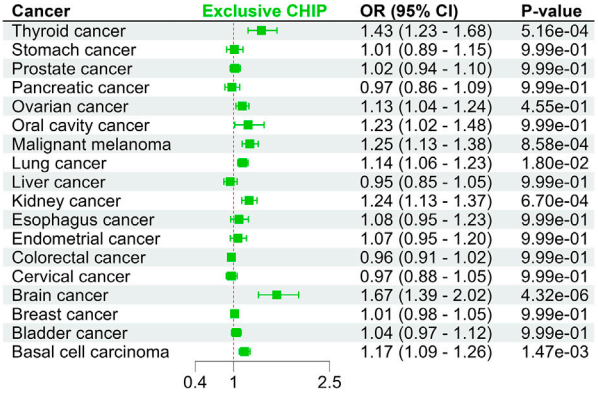


FIGURE 4
Associations of genetic susceptibility to exclusive CHIP with cancer. Mendelian randomization estimates were generated using the IVW approach. P values are for ORs (95% CIs) after multiple testing correction.

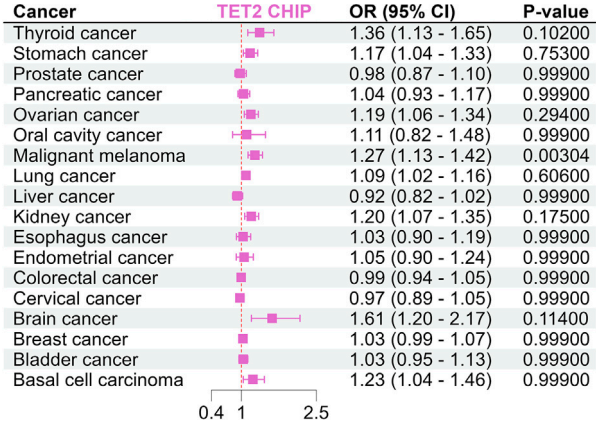


FIGURE 6
Associations of genetic susceptibility to TET2 CHIP with cancer. Mendelian randomization estimates were generated using the IVW approach. P values are for ORs (95% CIs) after multiple testing correction.

DNMT3A sub-type, and 1.61 (95% CI: 1.20–2.17, p = 0.11, Figure 6) for TET2 sub-type (Supplementary Table S6). The association for overall exclusive CHIP sustained in multivariable MR with adjustment for genetically predicted telomere length (OR = 1.35, 95% CI = 1.06–1.73, p = 0.017).

Thyroid cancer

Across three independent datasets involving 5034 cases, there was consistent evidence of an association between overall inclusive CHIP and increased risk of thyroid cancer with a pool OR of 1.39 (95% CI: 1.19–1.61, $p = 1.48 \times 10^{-3}$). Significant associations were also observed for overall exclusive CHIP (OR: 1.43, 95% CI: 1.22–1.68, $p = 5.15 \times 10^{-4}$) and DNMT3A sub-type after Bonferroni correction (OR: 1.28, 95% CI: 1.13–1.44, $p = 5.86 \times 10^{-3}$, Figure 5). The association of overall exclusive CHIP was maintained in multivariable MR with adjustment for genetically predicted telomere length (OR = 1.24, 95% CI = 1.06–1.45, $p = 7.56 \times 10^{-3}$).

Histological sub-types of thyroid cancer analysis using data obtained from the FinnGen consortium found strong evidence for an association of genetically predicted overall CHIP (inclusive CHIP, OR: 1.40, 95% CI: 1.13–1.74, p = 0.002; exclusive CHIP, OR: 1.33, 95% CI: 1.06–1.66, p = 0.01) and DNMT3A sub-type (OR: 1.23, 95% CI: 1.01–1.49, p = 0.04) with papillary adenocarcinoma risk (Supplementary Table S8).

Lung cancer

Across four independent datasets involving 44,784 cases, we identified associations in a consistent direction between CHIP and

lung cancer. Genetically predicted overall inclusive CHIP was strongly associated with an increased risk of lung cancer with a pooled OR of 1.16 (95%CI: 1.08–1.25, $p = 1.38 \times 10^{-3}$). A similar finding was also observed for overall exclusive CHIP (OR: 1.14, 95% CI: 1.06–1.23, p = 0.02). Similar results by sub-types of CHIP were also found for lung cancer (DNMT3A CHIP, OR: 1.10, 95%CI: 1.04–1.17, p = 0.009; TET2 CHIP, OR: 1.11, 95%CI: 1.04–1.17, p = 0.02). In addition, results from multivariable MR analysis confirmed that overall exclusive CHIP (OR = 1.16, 95% CI = 1.05–1.28, $p = 4.86 \times 10^{-3}$) was an independent risk factor of lung cancer after adjusting for lifetime smoking index. However, neither the genetically predicted DNMT3A subtype nor TET2 subtype showed any association with lung cancer after multiple testing corrections.

We then assessed associations between CHIP and the risk of three histological sub-types of lung cancer, namely squamous cell lung cancer, lung adenocarcinoma, and small cell lung carcinoma. The IVW estimates for having inclusive, exclusive, and DNMT3A CHIP with incident lung adenocarcinoma risk were 1.48 (95% CI: 1.15–1.90, $p = 2.09 \times 10^{-3}$), 1.44 (95% CI: 1.11–1.85, $p = 5.27 \times 10^{-3}$), and 1.25 (95% CI: 1.04–1.50, p = 0.01), respectively. However, we did not identify any genetic evidence that CHIP may increase the risk of squamous cell lung cancer or small cell lung carcinoma (Supplementary Table S9).

Kidney cancer

Significant associations between genetically predicted overall CHIP (inclusive CHIP, OR: 1.22, 95% CI: 1.13–1.33, $p = 1.09 \times 10^{-4}$; exclusive CHIP, OR: 1.24, 95% CI: 1.13–1.36, $p = 6.70 \times 10^{-4}$) and DNMT3A CHIP (OR: 1.19, 95% CI: 1.11–1.26, $p = 6.48 \times 10^{-6}$) and an increased risk of kidney cancer were identified from pooled analyses. Likewise, our multivariable MR analysis showed a robustness of associations for genetically predicted telomere length (Supplementary Table S2).

When stratified by histological sub-types, an adverse effect of CHIP appeared to be mainly associated with clear cell renal cell carcinoma (inclusive CHIP, OR: 1.31, 95% CI: 1.16–1.49, $p = 2.21 \times 10^{-5}$; exclusive CHIP, OR: 1.27, 95% CI: 1.10–1.47, $p = 9.09 \times 10^{-4}$; DNMT3A CHIP, OR: 1.23, 95% CI: 1.13–1.34, $p = 1.07 \times 10^{-6}$), with limited evidence in papillary renal cell carcinoma (inclusive CHIP, OR: 1.25, 95% CI: 0.98–1.58; exclusive CHIP, OR: 1.18, 95% CI: 0.92–1.51; DNMT3A CHIP, OR: 1.16, 95% CI: 0.96–1.39, Supplementary Table S10).

Basal cell carcinoma

For a 1-unit increase in log-transformed odds of CHIP, the combined OR for basal cell carcinoma estimated from FinnGen and MVP was 1.30 (95% CI: 1.17–1.45, $p = 9.0 \times 10^{-5}$) for overall inclusive CHIP, 1.17 (95% CI: 1.09–1.26, $p = 1.47 \times 10^{-3}$) for overall exclusive CHIP, and 1.15 (95% CI: 1.08–1.22, $p = 1.20 \times 10^{-3}$) for DNMT3A CHIP. When restricting multivariable MR analysis corrected for telomere length, we obtained similar results, with overall exclusive CHIP remaining associated with basal cell carcinoma (Supplementary Table S19).

Malignant melanoma

In the combined datasets, our MR analysis discovered that genetically predicted CHIP or its sub-types could increase the risk of malignant melanoma after Bonferroni adjustment, which was supported by different MR methods (Supplementary Table S7). As estimated by the IVW method, the odds of malignant melanoma was 1.35 (95% CI: 1.23–1.49, $p = 5.41 \times 10^{-8}$) for inclusive CHIP, 1.25 (95% CI: 1.13–1.38, $p = 8.57 \times 10^{-4}$) for exclusive CHIP, 1.18 (95% CI: 1.09–1.27, p = 0.002) for DNMT3A CHIP, and 1.25 (95% CI: 1.09–1.43, p = 0.003) for TET2 CHIP. Multivariable MR adjusting for telomere length provided strong evidence for genetically proxied overall exclusive CHIP on higher malignant melanoma risk (Supplementary Table S19).

Sensitivity analysis

Results for genetic susceptibility to CHIP and risk of cancer outcomes were directionally consistent in alternative MR methods (Supplementary Table S7). The MR pleiotropy residual sum and outlier test identified one to seven outliers, but similar magnitude associations were observed after removal of these variants (Supplementary Table S13). Although some heterogeneity was detected, it did not invalidate the IVW using a random effects model of MR results, which may balance the combined heterogeneity (Supplementary Table S14). No bidirectional effects were identified using the MR-Steiger directionality test (Supplementary Table S15). In reverse MR analyses, genetic susceptibility to cancer was not significantly associated with CHIP or its sub-types (Supplementary Table S16). In addition, no horizontal pleiotropy was observed in MR-Egger intercept analysis (Supplementary Table S17). After examining the Open Targets Platform, we found that several of the CHIP genetic variants were also associated with blood cell-related phenotypes and telomere length, which may result in the presence of horizontal pleiotropy (Supplementary Table S18). We then repeated the primary analyses using a genetic instrument excluding the TERT (rs7705526 and rs2853677) and the TP53 locus (rs78378222), but similar magnitude associations were observed when these variants were excluded from the analyses (Supplementary Table S20). Furthermore, pathway enrichment analysis suggested that that instrument-tagged genes were significantly enriched in drug resistance, DNA damage and hematopoietic regulatory pathways (Supplementary Figure 1). Moreover, the results from the leave-one-out sensitivity analysis did not reveal any influential SNPs driving the associations (Supplementary Figures S2–S19).

Discussion

We systematically assessed the causal association of genetic susceptibility to overall and sub-types of CHIP with the risk of 18 cancer types. Genetic instruments for CHIP were obtained from a large-scale GWAS, which improved the statistic power for the MR analysis. In line with findings from previous studies [19, 20], we found that genetic susceptibility to CHIP was associated with an increased risk of lung cancer, malignant

melanoma, and basal cell carcinoma. We identified several novel associations of genetic susceptibility to CHIP with an increased risk of thyroid cancer, kidney cancer, and brain cancer. We also found significant associations of genetically predicted CHIP with some histological subtypes of cancer (e.g., papillary adenocarcinoma of the thyroid and clear cell renal cell carcinoma).

The clinical relevance of CHIP to thyroid cancer has been reported by several observational studies. Coombs et al. showed that thyroid carcinoma was the most common solid tumor associated with CHIP, with a prevalence of 36% [35]. Similarly, a recent study found that the prevalence of CHIP in patients with thyroid cancer was 37% [36]. However, the causal effect of CHIP on thyroid cancer remains unclear. It has been proposed that radioactive iodine (RAI) exposure may induce the high prevalence of CHIP in patients with thyroid cancer, whereas previous findings exploring the effect of RAI on CHIP among thyroid cancer patients were inconsistent [36, 37]. Although the detailed mechanism by which the hematopoietic system interacts with thyroid cancer cells remains unknown, genetic evidence from our MR study suggested that CHIP might increase the risk of thyroid cancer in the long-term. Since genetic predicted over exclusive CHIP was also found to be associated with thyroid cancer, mechanisms other than RAI may also be at play, such as tumor-associated macrophages found in anaplastic thyroid cancer [38].

We found strong evidence for an association between genetically predicted CHIP and kidney cancer risk. Although prospective studies investigating associations of CHIP with the development of kidney cancer are limited, intriguing findings have been reported. CHIP was significantly associated with various adverse kidney outcomes including acute kidney injury [10], chronic kidney disease [39], and kidney function decline [40]. Subsequent evidence from animal studies also supported the causal effects of CHIP on kidney inflammation and fibrosis [10, 41]. Given the positive feedback loop between CHIP and inflammation, a possible mechanism explaining the relation between kidney cancer and CHIP may be the clonal expansion in both myeloid and lymphoid cell lines. However, the mechanisms driving the association identified in our MR analysis should be further elucidated in future studies.

There was strong evidence to support a positive association of genetically predicted overall and sub-types of CHIP with brain cancer. There is low possibility of false-positive and reverse causation in our analysis because of the strict genetic instruments selection procedure and MR Steiger test, alongside the consistent findings observed from two independent studies, which further improve the robustness of the MR analysis. Although epidemiological evidence for the association of CHIP in brain cancer is scarce, large longitudinal studies may support the benefit of monitoring healthy people with CHIP to optimize disease prediction models [42].

Previous studies suggested that CHIP could contribute to the development of prostate cancer, breast cancer, and ovarian cancer [18, 19]. However, other studies reported null or inverse associations [43, 44]. Our MR results found genetically predicted CHIP was not causally associated with prostate cancer, breast cancer, or ovarian cancer, and we deemed that the previously observed association might be confounded by cancer treatments (e.g., chemotherapy), limited sample sizes, and sampling variability. In addition, the causal effect of CHIP may differ depending on the tissue micro-environment and immune interactions [45, 46]. Indeed, a recent large-scale cohort study found that primary tumor regions from patients with CHIP had a higher representation of myeloid cells compared to tumor regions from patients without CHIP [47]. However, the micro-environment or immune interactions could not be assessed on the basis of the summary-level data. Consequently, the putative influence of CHIP in the development of these cancers remains uncertain and further investigations are needed to confirm our findings.

PheWAS and pathway enrichment analysis suggested that several mechanistically distinct classes of genetic loci were associated with CHIP: loci conferring CHIP-intrinsic, cell-autonomous clonal selection mechanisms, and proxy loci tagging upstream systemic hematopoietic regulatory processes that independently promote both hematopoietic clonal expansion and malignant transformation [1, 2]. Indeed, several enriched pathways directly align with core CHIP pathogenesis, including somatic mutation surveillance, hematopoietic stem cell (HSC) clonal competition, and DNA damage response signaling [48]. These mechanisms act in a CHIP-specific manner, driving the selective outgrowth of somatically mutated HSC clones and defining the initiation and progression of CHIP itself. In contrast, multiple top-enriched pathways represent upstream foundational biological regulators, namely telomere homeostasis, HSC proliferative control, and B-cell developmental biology, which serve as shared predisposing determinants rather than CHIP-exclusive drivers [49]. Genetically regulated telomere length shapes lifelong HSC replicative reserve and genomic stability; shortened telomeres increase replicative stress, facilitate clonal selection, and elevate cancer risk through genome instability, independent of CHIP somatic mutations [50, 51]. Similarly, altered HSC proliferation programs expand the vulnerable HSC pool, increasing the likelihood of somatic mutation accumulation and clonal dominance while promoting oncogenic transformation via cell-cycle dysregulation. Enriched B-cell biology pathways further reflect adaptive immune microenvironment modulation, which indirectly remodels bone marrow niche conditions to favor clonal expansion and subsequent malignancy [52]. It is possible that CHIP-specific loci directly mediate clonal hematopoiesis initiation, whereas telomere, HSC proliferation, and B-cell-related loci represent upstream pleiotropic factors that independently cause both age-related clonal expansion and cancer predisposition through distinct, CHIP-independent biological pathways.

Strengths of this analysis include the systematic evaluation of CHIP, representative of overall and sub-types of CHIP, in the risk of 18 cancer types using large-scale GWAS data from different resources, which ensured adequate statistical power and the robustness of findings. Because of different study designs and powers of different datasets, definitive conclusions are hard to draw. However, there is little possibility of false-positive and reverse causation in our study because of the application of strict instrument selection, validation processes, and the MR Steiger test as well as the consistent results in FinnGen, MVP, and PLCO studies. Large consortia and other larger GWAS meta-analyses also supported these findings. Additional support for the robustness of our findings comes from the directionally

consistent estimates across MR methods (e.g., IVW, weighted median, and MR-RAPS) and the absence of horizontal pleiotropy (MR-Egger intercepts and MR-PRESSO estimations). Results from Open Target Platform searching also confirmed that none of the selected genetic variants were deemed to be at risk of horizontal pleiotropy.

Despite these strengths, potential limitations should be considered. First, our MR analysis estimated the effect of CHIP based on germline predictors of CHIP rather than the direct effects of CHIP. This is based on the assumption that the effect of genetically predicted CHIP is proportional to its overall impact, which may not be in line with its actual mechanism. Second, statistical power can be limited in some specific cancers (e.g., brain cancer) and histological subtypes (e.g., follicular thyroid cancer or clear cell ovarian cancer) due to small sample sizes. It is still essential to confirm our results through larger sample sizes. Third, the gene-gene or gene-environment interactions and nonlinearity effects of CHIP on cancer could not be estimated using summary-level data. Fourth, we cannot definitively rule out the possibility of horizontal pleiotropy, although we performed various sensitivity analyses and showed the validity of these genetic instruments. For example, CHIP with TET2 mutations has been linked to cancer-associated risk factors including obesity [53] and systemic inflammation [5]. Fifth, horizontal pleiotropy cannot be excluded when using SNPs located at TERT and TP53 regions as instruments for CHIP in primary analysis. We conducted additional sensitivity analyses using genetic instruments excluding the TERT and the TP53 locus for CHIP to test for the influence of pleiotropy on our estimates, and our results remain robust. Additionally, our analyses did not adjust for chemotherapeutic treatment or blood sampling time of cancer cases, which may influence causal estimates. Lastly, our study comprised only European cohorts, which limits the generalizability of the findings to other ethnic populations.

In conclusion, our study demonstrates that genetic susceptibility to CHIP is related to an increased risk for thyroid cancer, lung cancer, kidney cancer, brain cancer, basal cell carcinoma, and malignant melanoma. Our findings provide genetic support that CHIP may serve as a novel biomarker for early cancer detection and highlight the importance of timely screening for CHIP in cancer prevention.

Author contributions

All authors listed have made a substantial, direct, and intellectual contribution to the work and approved it for publication.

Data availability

Data are available in a public, open access repository. The summary statistics of FinnGen GWAS data can be accessed at https://www.finngen.fi/en. The PLCO GWAS summary statistics can be accessed at https://exploregwas.cancer.gov/plco-atlas/). The summary level statistics from UKBB GWAS can be accessed via https://www.nealelab.is/uk-biobank. Summary statistics of cancer and CHIP used in this study are publicly available on the GWAS Catalog project (https://www.ebi.ac.uk/gwas/).

Ethics statement

All GWAS studies had been approved by its Ethical Review Committee and permits the use of summary data without restriction. Human subjects were not included in this study and participant consent was not required for this study because all summary-level genetic data were obtained from sources available to the public.

Funding

The author(s) declared that financial support was not received for this work and/or its publication.

Acknowledgements

We are grateful to all participants and investigators from the FinnGen cohort, MVP cohort, UK Biobank, PLCO consortium, BCAC consortium, TRICL consortium, PRACTICAL consortium, OCAC consortium and other larger GWAS meta-analyses for sharing GWAS summary statistics. We would like to thank all the other investigators for making summary statistics openly available.

Conflict of interest

The author(s) declared no potential conflicts of interest with respect to the research, authorship, and/or publication of this article.

Generative AI statement

The author(s) declared that generative AI was not used in the creation of this manuscript.

Any alternative text (alt text) provided alongside figures in this article has been generated by Frontiers with the support of artificial intelligence and reasonable efforts have been made to ensure accuracy, including review by the authors wherever possible. If you identify any issues, please contact us.

Supplementary material

The Supplementary Material for this article can be found online at: https://www.ebm-journal.org/articles/10.3389/ebm.2026.10923/full#supplementary-material

References

1. Jaiswal S, Ebert BL. Clonal hematopoiesis in human aging and disease. *Science* (2019) 366(6465):eaan4673. doi: 10.1126/science.aan4673

2. Genovese G, Kähler AK, Handsaker RE, Lindberg J, Rose SA, Bakhoum SF, et al. Clonal hematopoiesis and blood-cancer risk inferred from blood DNA sequence. *N Engl J Med* (2014) 371(26):2477–87. doi: 10.1056/NEJMoa1409405

3. Jaiswal S, Fontanillas P, Flannick J, Manning A, Grauman PV, Mar BG, et al. Age-related clonal hematopoiesis associated with adverse outcomes. *N Engl J Med* (2014) 371(26):2488–98. doi: 10.1056/NEJMoa1408617

4. Jaiswal S, Natarajan P, Silver AJ, Gibson CJ, Bick AG, Shvartz E, et al. Clonal hematopoiesis and risk of atherosclerotic cardiovascular disease. *N Engl J Med* (2017) 377(2):111–21. doi: 10.1056/NEJMoa1701719

5. Fuster JJ, MacLauchlan S, Zuriaga MA, Polackal MN, Ostriker AC, Chakraborty R, et al. Clonal hematopoiesis associated with TET2 deficiency accelerates atherosclerosis development in mice. *Science* (2017) 355(6327):842–7. doi: 10.1126/science.aag1381

6. Miller PG, Qiao D, Rojas-Quintero J, Honigberg MC, Sperling AS, Gibson CJ, et al. Association of clonal hematopoiesis with chronic obstructive pulmonary disease. *Blood* (2022) 139(3):357–68. doi: 10.1182/blood.2021013531

7. Wong WJ, Emdin C, Bick AG, Zekavat SM, Niroula A, Pirruccello JP, et al. Clonal haematopoiesis and risk of chronic liver disease. *Nature* (2023) 616(7958):747–54. doi: 10.1038/s41586-023-05857-4

8. Bouzid H, Belk JA, Jan M, Qi Y, Sarnowski C, Wirth S, et al. Clonal hematopoiesis is associated with protection from Alzheimer's disease. *Nat Med* (2023) 29(7):1662–70. doi: 10.1038/s41591-023-02397-2

9. Wang H, Divaris K, Pan B, Li X, Lim JH, Saha G, et al. Clonal hematopoiesis driven by mutated DNMT3A promotes inflammatory bone loss. *Cell* (2024) 187(14): 3690–711.e19. doi: 10.1016/j.cell.2024.05.003

10. Vlasschaert C, Robinson-Cohen C, Chen J, Akwo E, Parker AC, Silver SA, et al. Clonal hematopoiesis of indeterminate potential is associated with acute kidney injury. *Nat Med* (2024) 30(3):810–7. doi: 10.1038/s41591-024-02854-6

11. Jaiswal S, Libby P. Clonal haematopoiesis: connecting ageing and inflammation in cardiovascular disease. *Nat Rev Cardiol* (2020) 17(3):137–44. doi: 10.1038/s41569-019-0247-5

12. Severson EA, Riedlinger GM, Connelly CF, Vergilio JA, Goldfinger M, Ramkissoon S, et al. Detection of clonal hematopoiesis of indeterminate potential in clinical sequencing of solid tumor specimens. *Blood* (2018) 131(22):2501–5. doi: 10.1182/blood-2018-03-840629

13. Coombs CC, Gillis NK, Tan X, Berg JS, Ball M, Balasis ME, et al. Identification of clonal hematopoiesis mutations in solid tumor patients undergoing unpaired next-generation sequencing assays. *Clin Cancer Res* (2018) 24(23):5918–24. doi: 10.1158/1078-0432.CCR-18-1201

14. Tian R, Wiley B, Liu J, Zong X, Truong B, Zhao S, et al. Clonal hematopoiesis and risk of incident lung cancer. *J Clin Oncol* (2023) 41(7):1423–33. doi: 10.1200/JCO.22.00857

15. Binnewies M, Roberts EW, Kersten K, Chan V, Fearon DF, Merad M, et al. Understanding the tumor immune microenvironment (TIME) for effective therapy. *Nat Med* (2018) 24(5):541–50. doi: 10.1038/s41591-018-0014-x

16. Hanahan D, Weinberg RA. Hallmarks of cancer: the next generation. *Cell* (2011) 144(5):646–74. doi: 10.1016/j.cell.2011.02.013

17. Ptashkin RN, Mandelker DL, Coombs CC, Bolton K, Yelskaya Z, Hyman DM, et al. Prevalence of clonal hematopoiesis mutations in tumor-only clinical genomic profiling of solid tumors. *JAMA Oncol* (2018) 4(11):1589–93. doi: 10.1001/jamaoncol.2018.2297

18. Bick AG, Weinstock JS, Nandakumar SK, Fulco CP, Bao EL, Zekavat SM, et al. Inherited causes of clonal haematopoiesis in 97,691 whole genomes. *Nature* (2020) 586(7831):763–8. doi: 10.1038/s41586-020-2819-2

19. Kar SP, Quiros PM, Gu M, Jiang T, Mitchell J, Langdon R, et al. Genome-wide analyses of 200,453 individuals yield new insights into the causes and consequences of clonal hematopoiesis. *Nat Genet* (2022) 54(8):1155–66. doi: 10.1038/s41588-022-01121-z

20. Kessler MD, Damask A, O'Keeffe S, Banerjee N, Li D, Watanabe K, et al. Common and rare variant associations with clonal haematopoiesis phenotypes. *Nature* (2022) 612(7939):301–9. doi: 10.1038/s41586-022-05448-9

21. Herbrich S, Chaib M, Anandhan S, Andrewes SW, Nagarajan A, Guan B, et al. TET2-mutant clonal hematopoiesis enhances macrophage antigen presentation and improves immune checkpoint therapy in solid tumors. *Cancer Cell* (2026) 44(1):187–202.e7. doi: 10.1016/j.ccell.2025.09.011

22. Richmond RC, Davey Smith G. Mendelian randomization: concepts and scope. *Cold Spring Harb Perspect Med* (2022) 12(1):a040501. doi: 10.1101/cshperspect.a040501

23. Skrivankova VW, Richmond RC, Woolf BAR, Yarmolinsky J, Davies NM, Swanson SA, et al. Strengthening the reporting of observational studies in epidemiology using mendelian randomization: the STROBE-MR statement. *JAMA* (2021) 326(16):1614–21. doi: 10.1001/jama.2021.18236

24. Burgess S, Thompson SG. Bias in causal estimates from Mendelian randomization studies with weak instruments. *Stat Med* (2011) 30(11):1312–23. doi: 10.1002/sim.4197

25. Kurki MI, Karjalainen J, Palta P, Sipilä TP, Kristiansson K, Donner KM, et al. FinnGen provides genetic insights from a well-phenotyped isolated population. *Nature* (2023) 613(7944):508–18. doi: 10.1038/s41586-022-05473-8

26. Verma A, Huffman JE, Rodriguez A, Conery M, Liu M, Ho YL, et al. Diversity and scale: genetic architecture of 2068 traits in the VA million veteran program. *Science* (2024) 385(6706):eadj1182. doi: 10.1126/science.adj1182

27. Machiela MJ, Huang WY, Wong W, Berndt SI, Sampson J, De Almeida J, et al. GWAS explorer: an open-source tool to explore, visualize, and access GWAS summary statistics in the PLCO Atlas. *Sci Data* (2023) 10(1):25. doi: 10.1038/s41597-022-01921-2

28. Ghoussaini M, Mountjoy E, Carmona M, Peat G, Schmidt EM, Hercules A, et al. Open targets genetics: systematic identification of trait-associated genes using large-scale genetics and functional genomics. *Nucleic Acids Res* (2021) 49(D1):D1311–20. doi: 10.1093/nar/gkaa840

29. Elizarraras JM, Liao Y, Shi Z, Zhu Q, Pico AR, Zhang B. WebGestalt 2024: faster gene set analysis and new support for metabolomics and multi-omics. *Nucleic Acids Res* (2024) 52(W1):W415–W421. doi: 10.1093/nar/gkae456

30. Bowden J, Del Greco MF, Minelli C, Davey Smith G, Sheehan N, Thompson J. A framework for the investigation of pleiotropy in two-sample summary data Mendelian randomization. *Stat Med* (2017) 36(11):1783–802. doi: 10.1002/sim.7221

31. Zhao QY, Wang JS, Bowden J, Small DS. Statistical inference in two-sample summary-data Mendelian randomization using robust adjusted profile score. *Ann Statist* (2020) 48(3):1742–69. doi: 10.1214/19-AOS1866

32. Verbanck M, Chen CY, Neale B Detection of widespread horizontal pleiotropy in causal relationships inferred from mendelian randomization between complex traits and diseases. *Nat Genet* (2018) 50(5):693–8. doi: 10.1038/s41588-018-0099-7

33. Burgess S, Thompson SG. Interpreting findings from mendelian randomization using the MR-Egger method. *Eur J Epidemiol* (2017) 32(5):377–89. doi: 10.1007/s10654-017-0255-x

34. Hemani G, Tilling K, Davey Smith G. Orienting the causal relationship between imprecisely measured traits using GWAS summary data. *PLoS Genet* (2017) 13(11): e1007081. doi: 10.1371/journal.pgen.1007081

35. Coombs CC, Zehir A, Devlin SM, Kishtagari A, Syed A, Jonsson P, et al. Therapy-related clonal hematopoiesis in patients with non-hematologic cancers is common and associated with adverse clinical outcomes. *Cell Stem Cell* (2017) 21(3):374–82.e4. doi: 10.1016/j.stem.2017.07.010

36. Boucai L, Falcone J, Ukena J, Coombs CC, Zehir A, Ptashkin R, et al. Radioactive iodine-related clonal hematopoiesis in thyroid cancer is common and associated with decreased survival. *J Clin Endocrinol Metab* (2018) 103(11):4216–23. doi: 10.1210/jc.2018-00803

37. Boucai L, Ptashkin RN, Levine RL, Fagin JA. Effects of radioactive iodine on clonal hematopoiesis in patients with thyroid cancer: a prospective study. *Clin Endocrinol (Oxf)* (2023) 99(1):122–9. doi: 10.1111/cen.14925

38. Ryder M, Ghossein RA, Ricarte-Filho JCM, Knauf JA, Fagin JA. Increased density of tumor-associated macrophages is associated with decreased survival in advanced thyroid cancer. *Endocr Relat Cancer* (2008) 15(4):1069–74. doi: 10.1677/ERC-08-0036

39. Vlasschaert C, McNaughton AJM, Chong M, Cook EK, Hopman W, Kestenbaum B, et al. Association of clonal hematopoiesis of indeterminate potential with worse kidney function and anemia in two cohorts of patients with advanced chronic kidney disease. *J Am Soc Nephrol* (2022) 33(5):985–95. doi: 10.1681/ASN.2021060774

40. Kestenbaum B, Bick AG, Vlasschaert C, Rauh MJ, Lanktree MB, Franceschini N, et al. Clonal hematopoiesis of indeterminate potential and kidney function decline in the general population. *Am J Kidney Dis* (2023) 81(3):329–35. doi: 10.1053/j.ajkd.2022.08.014

41. Vlasschaert C, Pan Y, Chen J, Akwo E, Rao V, Hixson JE, et al. Clonal hematopoiesis of indeterminate potential and progression of CKD. *J Am Soc Nephrol* (2025) 36(9): 1764–74. doi: 10.1681/ASN.0000000680

42. Okamura R, Piccioni DE, Boichard A, Lee S, Jimenez RE, Sicklick JK, et al. High prevalence of clonal hematopoiesis-type genomic abnormalities in cell-free DNA in invasive gliomas after treatment. *Int J Cancer* (2021) 148(11):2839–47. doi: 10.1002/ijc.33481

43. Wang A, Xu Y, Yu Y, Nead KT, Kim T, Xu K, et al. Clonal hematopoiesis and risk of prostate cancer in large samples of European ancestry men. *Hum Mol Genet* (2022) 32(3):489–95. doi: 10.1093/hmg/ddac214

44. Pich O, Reyes-Salazar I, Gonzalez-Perez A, Lopez-Bigas N. Discovering the drivers of clonal hematopoiesis. *Nat Commun* (2022) 13(1):4267. doi: 10.1038/s41467-022-31878-0

45. Ricciuti B, Scalera S, Wang X, Elkrief A, Tagliamento M, Gariazzo E, et al. DNA methyltransferase 3A (DNMT3A) mutations and PD-(L)1 blockade efficacy in non-small cell lung cancer. *Ann Oncol* (2025) 36(10):1132–41. doi: 10.1016/j.annonc.2025.06.003

46. Buttigieg MM, Vlasschaert C, Bick AG, Vanner RJ, Rauh MJ. Inflammatory reprogramming of the solid tumor microenvironment by infiltrating clonal hematopoiesis is associated with adverse outcomes. *Cell Rep Med* (2025) 6(3):101989. doi: 10.1016/j.xcrm.2025.101989

47. Pich O, Bernard E, Zagorulya M, Rowan A, Pospori C, Slama R, et al. Tumor-infiltrating clonal hematopoiesis. *N Engl J Med* (2025) 392(16):1594–608. doi: 10.1056/NEJMoa2413361

48. Cai X, Bowman RL, Trowbridge JJ. Clonal hematopoiesis in myeloid malignancies and solid tumors. *Nat Cancer* (2025) 6(7):1133–44. doi: 10.1038/s43018-025-01014-0

49. McLoughlin MA, Cheloor Kovilakam S, Dunn WG, Gu M, Tobin J, Pershad Y, et al. Telomere attrition becomes an instrument for clonal selection in aging hematopoiesis and leukemogenesis. *Nat Genet* (2025) 57(9):2215–25. doi: 10.1038/s41588-025-02296-x

50. DeBoy EA, Tassia MG, Schratz KE, Yan SM, Cosner ZL, McNally EJ, et al. Familial clonal hematopoiesis in a long telomere syndrome. *N Engl J Med* (2023) 388(26):2422–33. doi: 10.1056/NEJMoa2300503

51. Prummel KD, Woods K, Kholmatov M, Schmitt EC, Vlachou EP, Labyadh M, et al. Inflammatory stromal and T cells mediate human bone marrow niche remodeling in clonal hematopoiesis and myelodysplasia. *Nat Commun* (2025) 16(1):10042. doi: 10.1038/s41467-025-65803-y

52. Schleicher WE, Hoag B, De Dominici M, DeGregori J, Pietras EM. CHIP: a clonal odyssey of the bone marrow niche. *J Clin Invest* (2024) 134(15):e180068. doi: 10.1172/JCI180068

53. Fuster JJ, Zuriaga MA, Zorita V, MacLauchlan S, Polackal MN, Viana-Huete V, et al. TET2-Loss-of-Function-Driven clonal hematopoiesis exacerbates experimental insulin resistance in aging and obesity. *Cell Rep* (2020) 33(4):108326. doi: 10.1016/j.celrep.2020.108326

EBM Experimental Biology and Medicine

TYPE Original Research
PUBLISHED 13 July 2026
DOI 10.3389/ebm.2026.10948

Check for updates

OPEN ACCESS

*CORRESPONDENCE
Hao Zhang,
zh_hao_neurol@163.com
Zhonghua Liu,
zhonghua_reha@163.com

†These authors have contributed equally to this work

RECEIVED 23 December 2025
REVISED 19 June 2026
ACCEPTED 01 July 2026
PUBLISHED 13 July 2026

CITATION
Cai H, Huang Z, Liang J, Zhang H and Liu Z (2026) Genetic evidence for causal relationships between brain functional networks and domain-specific recovery after nondisabling ischemic stroke. *Exp. Biol. Med.* 251:10948. doi: 10.3389/ebm.2026.10948

COPYRIGHT
© 2026 Cai, Huang, Liang, Zhang and Liu. This is an open-access article distributed under the terms of the Creative Commons Attribution License (CC BY). The use, distribution or reproduction in other forums is permitted, provided the original author(s) and the copyright owner(s) are credited and that the original publication in this journal is cited, in accordance with accepted academic practice. No use, distribution or reproduction is permitted which does not comply with these terms.

Genetic evidence for causal relationships between brain functional networks and domain-specific recovery after nondisabling ischemic stroke

Huan Cai[1†], Zhenchun Huang[2†], Jialin Liang[3], Hao Zhang[4*] and Zhonghua Liu[1*]

[1]Department of Rehabilitation, Zhongshan City People's Hospital, Zhongshan, Guangdong, China, [2]Department of Cardiology, Shantou Central Hospital, Shantou, Guangdong, China, [3]Department of Endocrinology and Metabolism, Zhongshan City People's Hospital, Zhongshan, Guangdong, China, [4]Department of Neurology, Affiliated Hangzhou First People's Hospital, Westlake University School of Medicine, Hangzhou, Zhejiang, China

Abstract

Intrinsic brain networks are crucial for post-stroke recovery, but the causal relationships between specific networks and domain-specific recovery outcomes, as well as the role of lipid metabolism, remain unclear. This study leveraged Mendelian randomization (MR) to evaluate 191 resting-state functional magnetic resonance imaging (rs-fMRI) BOLD-derived phenotypes in relation to post-stroke recovery after nondisabling ischemic stroke. Genetic instruments for rs-fMRI phenotypes were derived from a UK Biobank genome-wide association study (n = 34,691). Outcomes included motor, cognitive, and global recovery after nondisabling ischemic stroke, assessed using longitudinal National Institutes of Health Stroke Scale subscales over 2 years (n = 1,270). Primary analyses used the multiplicative random-effects inverse-variance weighted method. A two-step MR analysis investigated whether brain networks mediate the effects of lipids on post-stroke outcomes. Higher BOLD-derived functional connectivity within the triple network (default mode network, central executive network, and salience network) was associated with better motor and cognitive outcomes. Higher genetically predicted orbitofrontal node amplitude in the limbic network correlated with better motor recovery, while stronger parieto-frontal connectivity was associated with cognitive recovery. Genetically proxied higher low-density lipoprotein cholesterol (LDL-C) was associated with poorer cognitive recovery, with evidence suggesting partial mediation through differences in BOLD-derived triple-network connectivity. This MR study supports a potential causal role of BOLD-derived functional network phenotypes, particularly the triple network, in motor and cognitive recovery, and further suggests that differences in triple-network connectivity act as a partial mediator linking elevated LDL-C liability to impaired cognitive recovery. These findings provide hypothesis-generating evidence for future mechanistic studies and for exploring whether specific brain network-targeted interventions could have a role in stroke recovery.

KEYWORDS
functional connectivity, lipid metabolism, Mendelian randomization, rs-fMRI, stroke recovery

Impact statement

While correlations between functional connectivity and specific aspects of stroke recovery have been reported, the causal nature of these associations warrants clarification. This study provides genetic evidence supporting potential causal contributions of specific intrinsic brain networks in post-stroke recovery, moving beyond prior correlational findings. It identifies genetically predicted higher BOLD-derived functional connectivity within the triple network as relevant to both motor and cognitive recovery and suggests that elevated low-density lipoprotein cholesterol was associated with poorer cognitive outcomes partially through differences in this network. These findings offer a preliminary and hypothesis generating rationale for targeting triple network connectivity as a potential biomarker and candidate intervention-relevant network feature in post-stroke recovery, and for testing whether lipid management is associated with preservation of intrinsic network function and cognitive recovery in prospective clinical studies.

Introduction

Ischemic stroke is a leading cause of death and disability worldwide, highlighting the need to understand its risk factors and post-stroke recovery mechanisms. Despite advances in understanding stroke pathogenesis, the mechanisms driving post-stroke functional recovery remain poorly understood [1].

Functional connectivity (FC) refers to temporal dependencies in neural activity across distinct brain regions and is fundamental to neural plasticity [2]. Resting-state functional magnetic resonance imaging (rs-fMRI) non-invasively maps these connectivity patterns by measuring spontaneous low-frequency blood oxygen level–dependent (BOLD) signal fluctuations, which indirectly index neural activity through the hemodynamic response and are influenced by cerebral blood flow, vascular reactivity, oxygen metabolism, and endothelial function [2]. Given the importance of neural plasticity in post-stroke recovery, FC was prioritized as a key network-level phenotype for investigating the brain's capacity to reorganize and support recovery after stroke-related injury.

Growing evidence links altered intrinsic brain functional networks to post-stroke recovery outcomes. Disrupted FC after a stroke correlates with functional impairment, while its reestablishment facilitates recovery [3–5]. Although FC correlates with specific aspects of stroke recovery [6], such as motor function [7, 8] and cognition [9], causality remains unclear.

Mendelian randomization (MR) infers causality using genetic variants as instrumental variables (IVs). A recent bidirectional MR study did not establish robust causal links between 191 rs-fMRI phenotypes and post-stroke functional recovery [10], potentially attributable to the use of the modified Rankin Scale (mRS), which combines varied neurological impairments into a single measure and may obscure domain-specific recovery. No MR study has yet examined causal relationships between FC and domain-specific stroke recovery.

Furthermore, emerging evidence implicates a complex interplay between lipid profiles and brain networks. Imbalances in lipid metabolism may disrupt FC, especially in regions associated with cognition [11, 12], which are critical for post-stroke recovery. However, whether brain networks can mediate the effect of blood lipids on recovery remains unknown.

Thus, this study employed MR to evaluate relationships between intrinsic rs-fMRI phenotypes and domain-specific stroke recovery, as well as whether these network phenotypes mediate associations between lifelong genetic liability to lipid traits and stroke recovery.

Materials and methods

All summary-level genomic data are publicly available (Supplementary Table 1 in the electronic Supplementary Material). The study design is shown in Figure 1. All data sources were approved by relevant institutional review boards in the original studies, and all participants provided informed consent. This study follows the STROBE-MR statement [13].

Genome-wide association study (GWAS) of 191 rs-fMRI phenotypes

Summary GWAS data for rs-fMRI phenotypes were sourced from the UK Biobank (n = 34,691) [14]. Fluctuation amplitude was defined as the temporal standard deviation of node features within a given component. Pairwise FC was defined as temporal correlation between BOLD signal time series for each pair of nodes. Global connectivity was defined by extracting the top six principal components from the node adjacency matrix. At the genome-wide significance level, 191 phenotypes were linked to genetic variation, comprising 75 regional BOLD fluctuation amplitude traits, 111 pairwise FC traits, and 5 global FC traits (Supplementary Table 2).

GWAS of domain-specific stroke recovery

Genetic associations for post-stroke motor, cognitive, and global recovery were obtained from a GWAS of 1,270 nondisabling ischemic stroke patients, defined as modified Rankin Scale (mRS) ≤ 3, from the Vitamin Intervention for Stroke Prevention (VISP) trial with a National Institutes of Health Stroke Scale (NIHSS) score greater than zero at randomization and no recurrent stroke [15]. All participants were followed up every 3 months for 2 years.

Three recovery phenotypes were defined by changes in motor, cognitive, and global impairments at each time point. Motor impairment was measured as the change in the sum of the NIHSS motor scores for Facial Palsy, Dysarthria, Motor Arm, and Motor Leg, termed NIH Motor-6. Similarly, cognitive impairment was defined as the change in the sum of the NIHSS cognitive scores, termed NIHSS Cog-4, for Level of Consciousness (LOC) Questions, LOC Commands, Aphasia, and Inattention/Neglect. Global impairment was the change in the total NIHSS score. A linear mixed-effects model estimated the changes in NIHSS

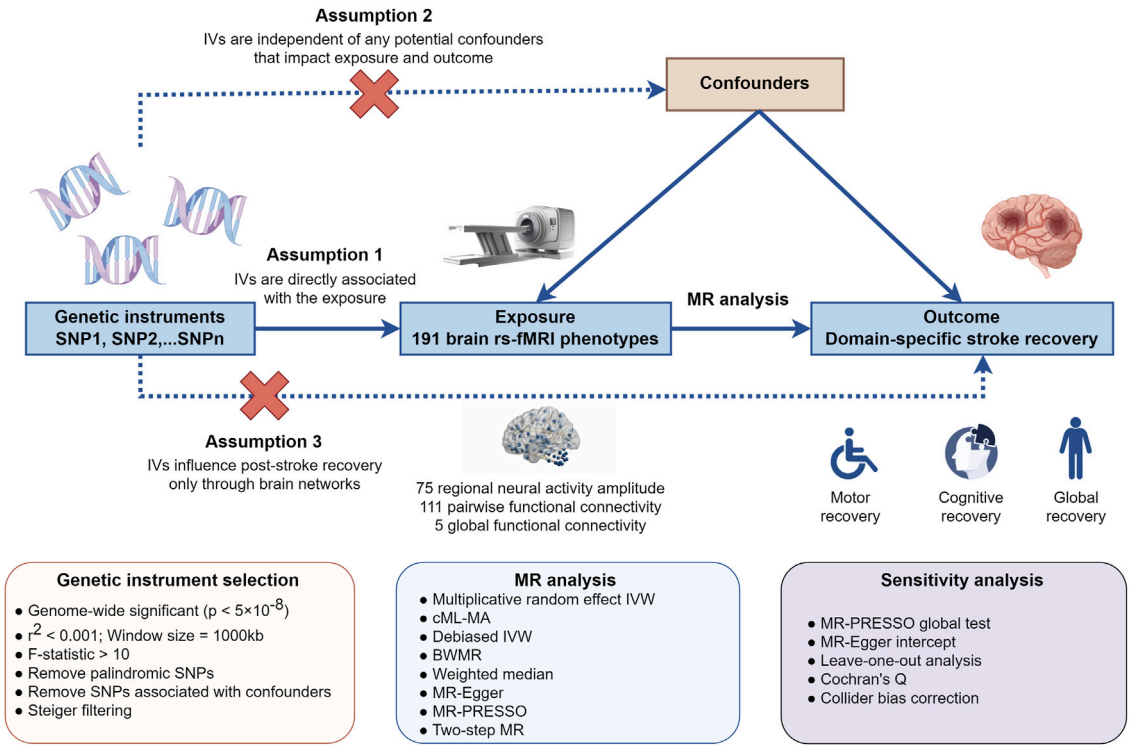


FIGURE 1
Study design and three core assumptions of the MR analysis. IV, instrumental variable; MR, Mendelian randomization; SNP, single-nucleotide polymorphism; rs-fMRI, resting-state functional magnetic resonance imaging; IVW, inverse-variance weighted; cML-MA, Constrained Maximum Likelihood Mixed-Model Association; MR-PRESSO, MR-Pleiotropy Residual Sum and Outlier; BWMR, Bayesian Weighted MR.

scores for each phenotype (delta = initial score − follow-up score) [15].

Genetic instrument selection

We first selected independent single-nucleotide polymorphisms (SNPs) ($r^2 < 0.001$, window size = 1,000 kb) with genome-wide significance ($p < 5 \times 10^{-8}$). SNPs with an *F*-statistic < 10 were excluded. We then excluded SNPs linked to confounders (e.g., depression [16], migraine [17], insomnia [16]) affecting both brain networks and post-stroke functional outcomes [18–20]. We used the GWAS Catalog database to identify and exclude these SNPs (Supplementary Table 3). Third, we applied Steiger filtering to reduce the likelihood of reverse-direction instruments, and removed networks with fewer than three IVs required for some sensitivity analyses.

Negligible sample overlap between exposure and outcome datasets was confirmed. We used proxy SNPs ($r^2 > 0.8$) from 1000 Genomes European reference data if needed, and removed ambiguous palindromic SNPs.

Two-sample MR analyses

Multiplicative random-effects inverse-variance weighted (IVW) MR was the primary method. Supplementary analyses included weighted median [21], MR-Egger [22], Constrained Maximum Likelihood Mixed-Model Association [23], debiased IVW [24], and Bayesian Weighted Mendelian Randomization [25]. MR-Pleiotropy Residual Sum and Outlier (MR-PRESSO) was used to identify potential outliers [26]. These methods collectively enhance robustness to IV assumption violations.

A causal relationship was inferred if all MR methods showed directionally consistent estimates and the IVW $p < 8.73 \times 10^{-5}$ (Bonferroni correction for 191 phenotypes and 3 outcomes).

Sensitivity analyses

We tested SNP heterogeneity with Cochran's *Q* statistic and used leave-one-out plots to check if single SNPs drove the results. In addition, we repeated our analysis using a relaxed IV selection threshold of $p < 1 \times 10^{-6}$ to check for consistency in the direction with those obtained from the genome-wide significant threshold. To assess the possibility of reverse causality, we performed reverse MR analyses in significant rs-fMRI phenotypes from forward MR using IVs with a suggestive significance threshold ($p < 5 \times 10^{-6}$). MR-PRESSO global test and MR-Egger intercept were used to detect horizontal pleiotropy.

To address collider bias risk when analyses are conditioned on ischemic stroke survivors, we repeated MR analyses using genetic effects on recovery outcomes adjusted via corrected weighted least squares (CWLS) [27], based on summary ischemic stroke data from the GIGASTROKE consortium of European ancestry [28].

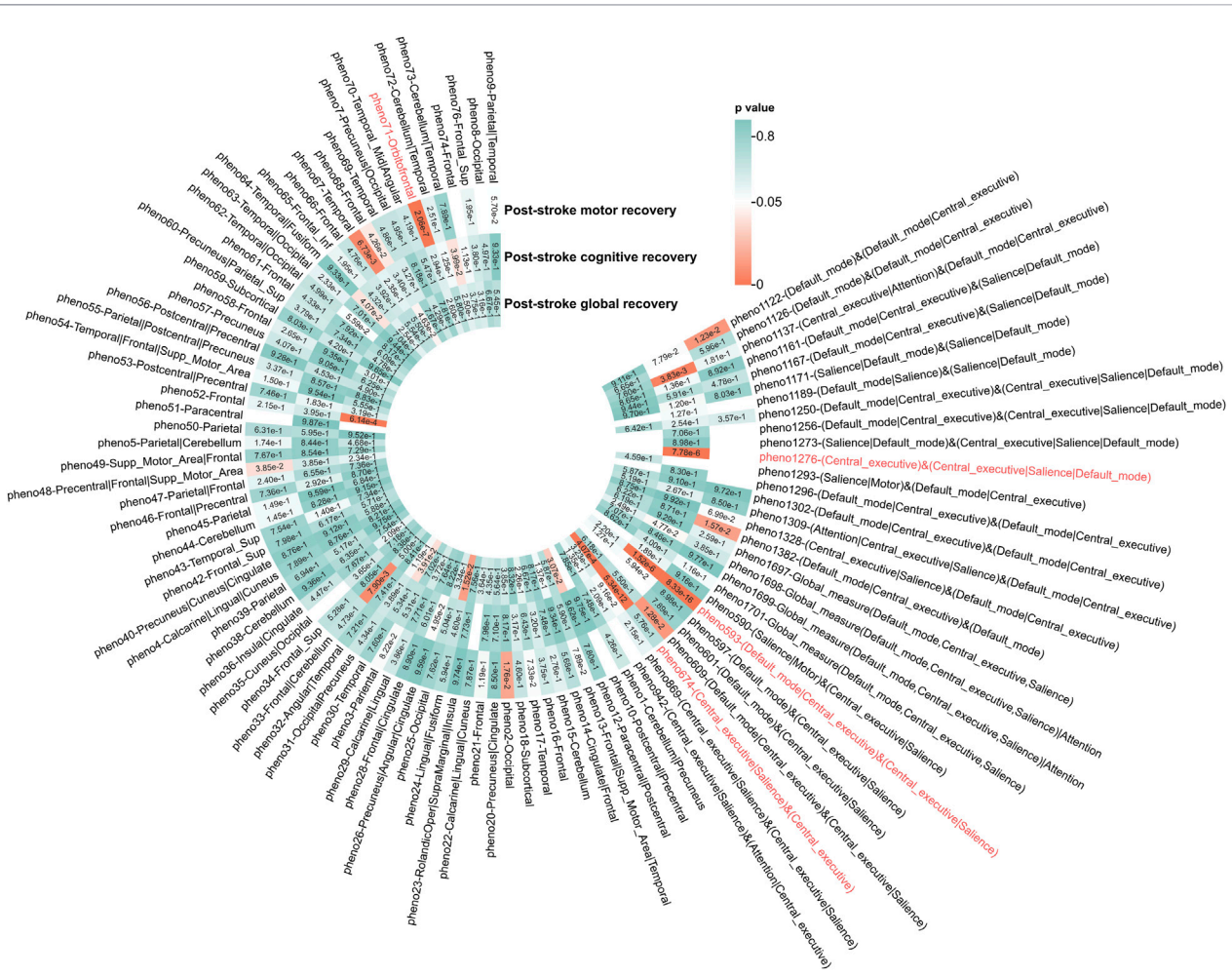


FIGURE 2
Circular heatmap for the IVW MR estimates of associations between rs-fMRI phenotypes and domain-specific stroke recovery.

Mediation MR

We used two-step MR to examine whether genetically proxied lipid traits were linked to post-stroke outcomes through BOLD-derived rs-fMRI network phenotypes. Summary statistics of three blood lipid measures, including triglycerides, low-density lipoprotein cholesterol (LDL-C), and high-density lipoprotein cholesterol (HDL-C), were obtained from the most recent circulating metabolite GWAS analysis of 136,016 participants [29]. We first estimated the causal effect of lipid traits on intrinsic functional networks (coefficient β_{XM}) and on post-stroke recovery patterns (coefficient β_{XY}), then assessed the causal effect of rs-fMRI phenotypes on specific subdomains of post-ischemic stroke recovery (coefficient β_{MY}). We calculated the mediation effect of BOLD-derived network phenotypes using the product of coefficients method [30]. The mediation effect ($\beta_{XM} \times \beta_{MY}$) was then divided by the total effect (β_{XY}) to calculate the proportion of the mediation effect. Standard errors for the mediation effect were calculated with the delta method. Notably, only rs-fMRI phenotypes showing robust evidence in the primary univariable MR were taken forward to mediation analyses.

Lipid and rs-fMRI traits were measured continuously and standardized to standard deviations. Analyses were performed in R (v4.2.1) with TwoSampleMR (v0.6.8) [31], RMediation (v1.2.2) [32], and MRPRESSO (v1.0) [26] packages.

Results

Genetically predicted rs-fMRI phenotypes and specific domains of post-stroke recovery

The full primary MR results are shown in Supplementary Tables 4–6. Twenty-four rs-fMRI phenotypes were nominally associated with domain-specific stroke recovery ($p < 0.05$, Figure 2). We identified four BOLD-derived brain functional network phenotypes showing robust MR evidence of association with two distinct recovery phenotypes (motor and cognitive recovery) after Bonferroni correction in the primary IVW analysis (Figure 3). The genetic variants used as instruments for significant intrinsic brain activity phenotypes are presented in Supplementary Table 7.

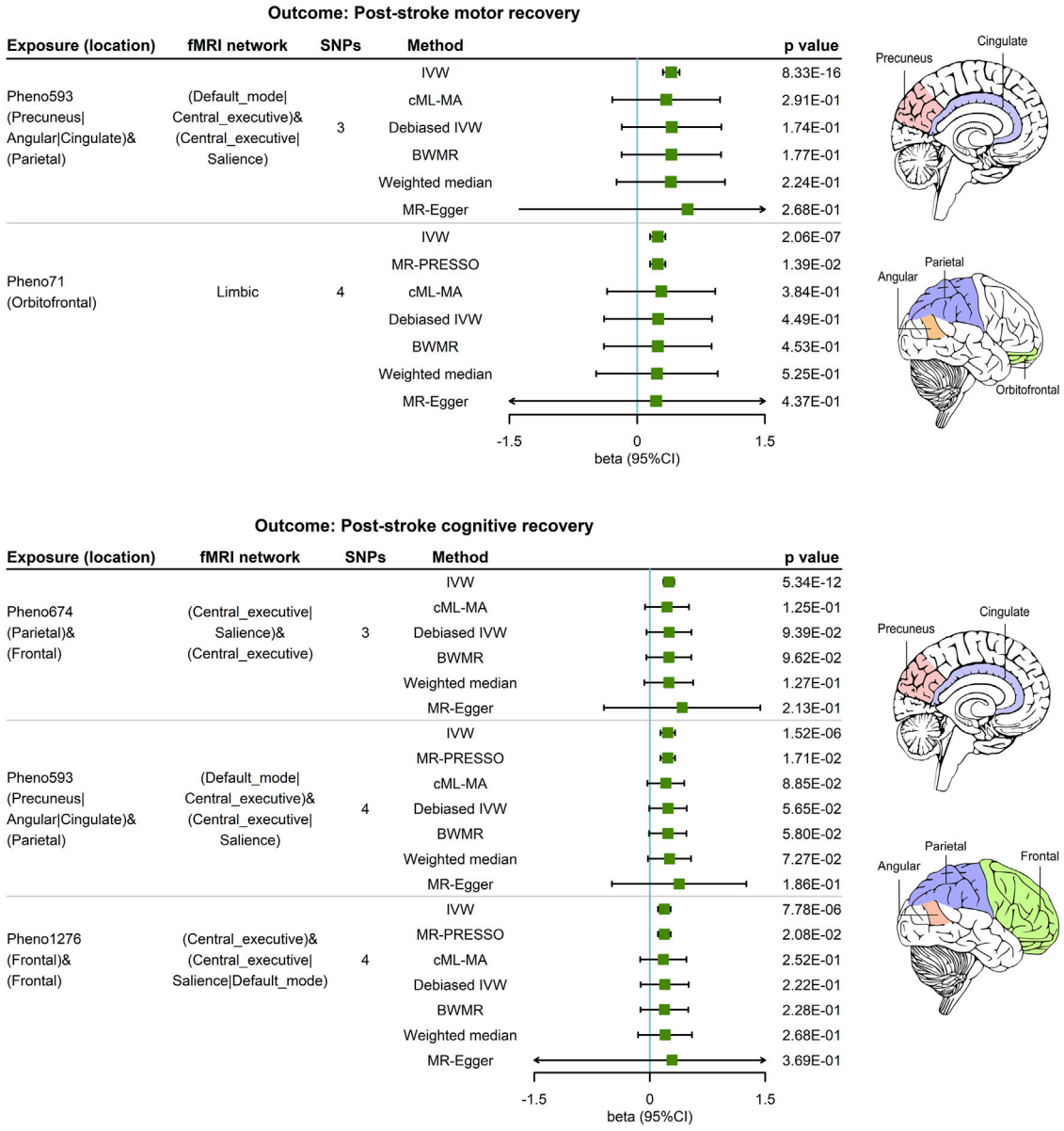


FIGURE 3
Causal relationships that remained significant after Bonferroni correction in MR analysis results. Left: forest plot illustrating the significant causal estimates using six MR methods. Right: pattern diagram showing the brain anatomical regions of the corresponding rs-fMRI phenotypes. CI, confidence interval.

However, no significant association survived multiple testing correction for post-stroke global recovery.

Two rs-fMRI phenotypes showed genetically supported evidence of association with motor improvement (Figure 3). Pheno593 reflects connectivity in the precuneus, angular gyrus, or cingulate, and parietal regions. The BOLD-derived signals of these brain regions involve FC in the triple network (default mode network (DMN)/central executive network (CEN) and CEN/salience network (SN)). Higher genetically predicted FC in these networks was associated with greater motor improvement (IVW $\beta = 0.399$, 95% confidence interval [CI] = 0.302–0.496, $p = 8.33 \times 10^{-16}$). In the limbic network, increased BOLD fluctuation amplitude of the orbitofrontal region was linked to a better motor outcome (IVW $\beta = 0.241$, 95% CI = 0.150–0.331, $p = 7.78 \times 10^{-6}$).

Three rs-fMRI phenotypes showed evidence for a potential causal contribution to post-stroke cognitive recovery (Figure 3). Pheno674 involves FC between parietal and frontal regions. Higher genetically predicted CEN-SN connectivity was associated with a better cognitive outcome (IVW $\beta = 0.245$, 95% CI = 0.176–0.315, $p = 5.34 \times 10^{-12}$). For Pheno593, connectivity in the precuneus, angular gyrus, or cingulate area, and parietal area positively correlated with cognitive recovery (IVW $\beta = 0.232$, 95% CI = 0.138–0.327, $p = 1.52 \times 10^{-6}$). For Pheno1276, resting frontal BOLD-derived signal features were linked to cognitive changes after stroke, with higher FC between CEN and SN or DMN or CEN associated with greater

TABLE 1 Pleiotropy and heterogeneity tests for significant exposure-outcome pairs in forward Mendelian randomization.

Exposure	Outcome	Pleiotropy			Heterogeneity (IVW)	
		MR-PRESSO global *p* value	MR-Egger intercept	*p* value	Cochran's *Q*	*p* value
Pheno593	Post-stroke motor recovery	NA	−0.018	0.851	0.057	0.972
Pheno71	Post-stroke motor recovery	0.994	0.018	0.911	0.064	0.996
Pheno593	Post-stroke cognitive recovery	0.909	−0.009	0.776	0.479	0.923
Pheno1276	Post-stroke cognitive recovery	0.974	−0.008	0.876	0.226	0.973
Pheno674	Post-stroke cognitive recovery	NA	−0.022	0.794	0.120	0.942

Abbreviations: MR-PRESSO, Mendelian randomization-pleiotropy residual sum and outlier; IVW, inverse-variance weighted; NA, not applicable.

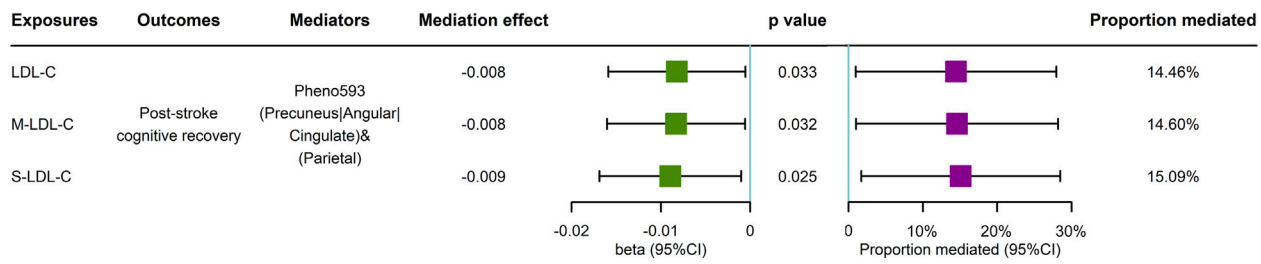


FIGURE 4
Associations between genetically predicted LDL-C, M-LDL-C, S-LDL-C and post-stroke cognitive recovery mediated by brain networks. LDL-C: low-density lipoprotein cholesterol; M-LDL-C, total cholesterol in medium LDL; S-LDL-C, total cholesterol in small LDL.

cognitive improvement (IVW β = 0.188, 95% CI = 0.106–0.270, $p = 7.78 \times 10^{-6}$).

These findings were supported by other MR analyses (Figure 3; Supplementary Tables 8,9). MR-PRESSO detected no significant outliers in exposure-outcome pairs for which the test was applicable.

Sensitivity analysis

Cochran's *Q* test showed no statistical evidence of heterogeneity among individual SNPs (Table 1). The scatterplots, forest plots, and leave-one-out plots suggested that no single SNP drove the associations (Supplementary Figures 1–6 in the electronic Supplementary Material). No statistical evidence of horizontal pleiotropy was detected by MR-PRESSO global test and MR-Egger intercept (all $p > 0.05$, Table 1). Results using the relaxed threshold were still statistically significant and directionally consistent with the primary analysis (Supplementary Table 10). Reverse MR analyses (Supplementary Tables 11, 12) showed no evidence of reverse causality. Associations remained stable after adjusting for collider bias (Supplementary Tables 8,9).

Mediation analysis

We found that genetically predicted higher LDL-C levels, but not triglycerides or HDL-C, were associated with poorer cognitive recovery (IVW β = −0.057; 95% CI = −0.105, −0.008; $p = 0.022$, Supplementary Figures 7,8). We found no MR evidence supporting associations between lipid traits and motor recovery. We then conducted MR analysis of LDL-C and its subfractions, including total cholesterol in large LDL, total cholesterol in medium LDL (M-LDL-C), and total cholesterol in small LDL (S-LDL-C), to examine whether they were associated with three imaging phenotypes that showed a potential causal contribution to post-stroke cognitive recovery. We found that LDL-C and its subfractions were associated with Pheno593, but not Pheno674 or Pheno1276 (Supplementary Figures 8,9). Finally, for Pheno593, our exploratory mediation analysis suggested that BOLD-derived connectivity in the precuneus, angular gyrus, or cingulate, and parietal regions, as well as the triple network (DMN/CEN and CEN/SN), may partially mediate the associations between genetic liability to LDL-C, M-LDL-C, and S-LDL-C and cognitive recovery (Figure 4). Specifically, the mediation effects were estimated to be −0.008 (95% CI -0.016, −0.001; $p = 0.033$) for LDL-C, −0.008 (95% CI -0.016, −0.001; $p = 0.032$) for M-LDL-C, and −0.009 (95% CI -0.017, −0.001; $p = 0.025$) for S-LDL-C, with mediation proportions of 14.46% (95% CI 0.96%–27.96%), 14.60% (95% CI 1.01%–28.18%), and 15.09% (95% CI 1.70%–28.48%), respectively. No statistical evidence of horizontal pleiotropy or heterogeneity was detected, and the Steiger directionality tests supported the inferred causal direction (Supplementary Table 13).

Discussion

Using MR, we found that specific rs-fMRI phenotypes were associated with motor and cognitive recovery, and that

BOLD-derived connectivity may partly mediate associations between genetic liability to lipid traits and cognitive recovery. These findings may help inform future research on connectivity profiles related to poor recovery.

Our results support a genetically informed association between triple-network (DMN-CEN-SN) connectivity and both motor and cognitive recovery after stroke. Higher genetically predicted BOLD-derived connectivity within this large-scale network system was associated with better recovery outcomes (Pheno593), suggesting that post-stroke recovery may depend not only on restoration of domain-specific circuits, but also on the integrity of domain-general networks that coordinate attention, executive control, self-monitoring, and adaptive learning [33, 34]. Within the triple-network framework, the SN, anchored in the anterior insula and dorsal anterior cingulate cortex, detects behaviorally relevant stimuli and facilitates dynamic switching between the DMN and the CEN. The CEN supports goal-directed control, working memory, performance monitoring, and error correction, whereas the DMN contributes to memory-based prediction, self-referential processing, and internally guided cognition [33]. These processes are directly relevant to cognitive recovery after stroke, as impairments in attention allocation, executive control, memory retrieval, and self-monitoring are common contributors to post-stroke cognitive dysfunction [33]. Consistent with this view, previous studies have shown that alterations in triple-network organization are associated with cognitive impairment [35], and that preservation or restoration of FC within and between regions of the DMN is related to better cognitive outcomes after stroke [6]. Importantly, the same network architecture may also support motor recovery. Although motor restoration is strongly influenced by the integrity of sensorimotor pathways and interhemispheric motor connectivity [6], successful motor rehabilitation also requires attention to task-relevant cues, selection of compensatory strategies, feedback-based error correction, and motor relearning [36]. These functions depend heavily on interactions between the SN and CEN and may interact with DMN-related memory and self-monitoring processes [37]. Thus, more favorable triple-network connectivity may provide a domain-general network-level scaffold through which cognitive-control systems support adaptive motor performance, particularly when primary sensorimotor pathways are disrupted [37], although the rs-fMRI phenotype may also partly index vascular support for network function.

This concurrent association with motor and cognitive recovery may reflect large-scale network integration, shared plasticity mechanisms, and vascular support for metabolically demanding recovery processes. Stroke recovery is thought to rely on experience-dependent plasticity, including unmasking of latent synaptic connections, long-term potentiation-like mechanisms, and functional reorganization of spared cortical and subcortical circuits [1]. The hubs of the SN and CEN are anatomically and functionally connected with association cortices and secondary motor regions, including the premotor cortex and supplementary motor area, through cortico-cortical and cortico-striatal-thalamic pathways [38, 39]. These pathways may serve as convergence zones where salience detection, executive control, memory-based prediction, and motor planning are integrated during rehabilitation-related learning. Therefore, stronger genetically predicted triple-network connectivity may reflect an inherited propensity for more efficient large-scale network communication or more favorable neurovascular coupling and vascular reactivity, which could facilitate plastic reorganization and coordinated recovery across both cognitive and motor domains.

Within the limbic network, we found that genetically predicted higher node amplitude in the orbitofrontal region was linked to better motor outcomes (Pheno71). The limbic network's involvement in motor recovery may suggest an interplay between emotional/motivational factors and physical rehabilitation, expanding traditional models focused solely on sensorimotor pathways.

The parieto-frontal network is integral to various cognitive processes, including attention, working memory, and executive functions [40]. Our MR analysis showed that the parieto-frontal network (Pheno674) exhibited a positive association with better cognitive outcomes, consistent with the previous findings of reduced global and local efficiency in the parieto-frontal network in subjects with cognitive impairment [41].

In conjunction with a prior study [12], our results provide genetic evidence consistent with the possibility that FC mediates the relationship between atherogenic lipid profiles and cognition, and extend this hypothesis to stroke recovery. While LDL-C is a well-established risk factor for ischemic stroke, its role in recovery is less understood, particularly because post-stroke LDL-C levels are influenced by treatment and clinical factors. Prior research indicated that higher LDL-C levels correlated with greater cognitive impairment in patients with cerebral small vessel disease, suggesting that LDL-C may contribute to cognitive decline through vascular mechanisms [42]. Our findings suggest that genetic liability to atherogenic lipid (LDL-C, M-LDL-C, S-LDL-C) traits may be associated with poorer cognitive recovery after stroke partly through genetically proxied differences in BOLD-derived triple-network connectivity, possibly through effects on neuroinflammation [43, 44], vascular integrity, endothelial function, cerebral perfusion, neurovascular coupling, amyloidogenic factors [45], neural repair mechanisms, or shared genetic influences. Future studies should test whether optimized lipid management can preserve brain networks or mitigate cognitive deficits after stroke.

Several limitations should be considered. First, because the VISP outcome cohort consisted predominantly of patients with nondisabling ischemic stroke of European ancestry, the modest sample limits generalizability to more clinically heterogeneous populations and to other ancestry groups. Second, resting-state BOLD response reflects spontaneous low-frequency neural activity but is also influenced by neurovascular coupling, vascular reactivity, and metabolic integrity. Therefore, this phenotype may capture variation in both functional network organization and the vascular–metabolic support systems. In the context of lipid metabolism, this is particularly important because atherogenic lipid profiles may affect endothelial function, cerebral perfusion, and vascular integrity, which could in turn alter rs-fMRI connectivity estimates independently of, or in combination with, neural communication. Thus, mediation by rs-fMRI phenotypes should be interpreted as reflecting BOLD-derived neurovascular or hemodynamic pathways, not purely neural connectivity. Third, recovery phenotypes based on NIHSS subscales are relatively coarse compared to detailed assessments. Fourth, MR estimates reflect the

lifelong genetic liability to BOLD-derived brain functional phenotypes, with genetic instruments for the 191 rs-fMRI traits derived from healthy UK Biobank participants. Therefore, these findings do not prove that modifying FC after stroke would improve recovery, especially given lesion-related reorganization and disconnection. Fifth, our summary-level MR design could not account for lesion localization. Lesions situated within or adjacent to the key networks examined here may themselves alter the measured FC and could modulate the observed network–recovery relationships. Because the outcome GWAS did not provide lesion-location information, we were unable to stratify or adjust for this anatomical confounder. Finally, limited sample size of the outcome GWAS and instrument availability may reduce power and precision of MR estimates, and increase susceptibility to winner's curse or overestimation. Although Steiger directionality tests and pleiotropy sensitivity analyses supported the robustness of the mediation-related associations, shared genetic architecture and unmeasured pleiotropic pathways cannot be ruled out. The reported effect sizes for the detected associations should be interpreted as preliminary rather than definitive estimates of magnitude, especially for the mediation analysis, because the lipid instruments represent lifelong genetic predisposition rather than longitudinally measured or treated LDL-C levels. Despite these limitations, our findings suggest a biologically plausible and testable pathway linking lipid genetic liability, brain network organization, and recovery.

Conclusion

This MR study provides preliminary genetic evidence supporting potential causal contributions of four BOLD-derived rs-fMRI phenotypes to motor and cognitive recovery after nondisabling ischemic stroke, highlighting the possible relevance of the triple network (DMN, CEN, SN). Additionally, BOLD-derived connectivity features involving DMN, CEN, and SN networks may in part mediate the association between genetically proxied lipid traits and cognitive outcomes. However, this potential pathway should be interpreted cautiously and requires validation in additional cohorts and larger GWAS datasets with more available instruments, ideally including detailed lesion localization, serial post-stroke lipid measurements, medication data, and post-stroke rs-fMRI measures. Future research could use these hypothesis-generating findings to identify candidate network targets for mechanistic studies and to evaluate whether interventions such as noninvasive brain stimulation can modulate relevant connectivity patterns and improve stroke recovery.

Author contributions

HC: Writing – original draft, Supervision, Conceptualization. ZH: Supervision, Writing – review and editing, Software. JL: Methodology, Formal Analysis, Data curation. HZ: Writing – review and editing, Validation, Supervision. ZL: Writing – review and editing, Supervision, Methodology, Investigation, Data curation. All authors contributed to the article and approved the submitted version.

Data availability

Publicly available datasets were analyzed in this study. The summary level data for rs-fMRI phenotypes are available at https://doi.org/10.5281/zenodo.5775047. The summary level data for post-stroke recovery phenotypes and GIGASTROKE data are available at the Cerebrovascular Disease Knowledge Portal. The summary level data for blood lipid measures are available through the NHGRI-EBI GWAS Catalogue.

Ethics statement

The studies involving humans were approved by relevant institutional review boards in the original studies. The studies were conducted in accordance with the local legislation and institutional requirements. The participants provided their written informed consent to participate in this study.

Funding

The author(s) declared that financial support was received for this work and/or its publication. This study was supported by the Social Public Welfare and Basic Research Project of Zhongshan City (No. 2023B3025) and the Research Project of the Traditional Chinese Medicine Bureau of Guangdong Province (No. 20251440).

Acknowledgements

We gratefully thank the UK Biobank, International Stroke Genetics Consortium (ISGC) Cerebrovascular Disease Knowledge Portal, and GIGASTROKE consortium for providing summary statistics data.

Conflict of interest

The author(s) declared no potential conflicts of interest with respect to the research, authorship, and/or publication of this article.

Generative AI statement

The author(s) declared that generative AI was not used in the creation of this manuscript.

Any alternative text (alt text) provided alongside figures in this article has been generated by Frontiers with the support of artificial intelligence and reasonable efforts have been made to ensure accuracy, including review by the authors wherever possible. If you identify any issues, please contact us.

Supplementary material

The Supplementary Material for this article can be found online at: https://www.ebm-journal.org/articles/10.3389/ebm.2026.10948/full#supplementary-material

References

1. Grefkes C, Fink GR. Recovery from stroke: current concepts and future perspectives. *Neurol Res Pract* (2020) 2:17. doi:10.1186/s42466-020-00060-6

2. van den Heuvel MP, Hulshoff Pol HE. Exploring the brain network: a review on resting-state fMRI functional connectivity. *Eur Neuropsychopharmacol* (2010) 20: 519–34. doi:10.1016/j.euroneuro.2010.03.008

3. van Meer MP, van der Marel K, Wang K, Otte WM, El Bouazati S, Roeling TA, et al. Recovery of sensorimotor function after experimental stroke correlates with restoration of resting-state interhemispheric functional connectivity. *J Neurosci* (2010) 30:3964–72. doi:10.1523/JNEUROSCI.5709-09.2010

4. Arun KM, Smitha KA, Sylaja PN, Kesavadas C. Identifying resting-state functional connectivity changes in the motor cortex using fNIRS during recovery from stroke. *Brain Topogr* (2020) 33:710–9. doi:10.1007/s10548-020-00785-2

5. Golestani AM, Tymchuk S, Demchuk A, Goodyear BG, Group V-S. Longitudinal evaluation of resting-state FMRI after acute stroke with hemiparesis. *Neurorehabil Neural Repair* (2013) 27:153–63. doi:10.1177/1545968312457827

6. Ismail UN, Yahya N, Manan HA. Investigating functional connectivity related to stroke recovery: a systematic review. *Brain Res* (2024) 1840:149023. doi:10.1016/j.brainres.2024.149023

7. Park CH, Chang WH, Ohn SH, Kim ST, Bang OY, Pascual-Leone A, et al. Longitudinal changes of resting-state functional connectivity during motor recovery after stroke. *Stroke* (2011) 42:1357–62. doi:10.1161/STROKEAHA.110.596155

8. Wu CW, Lin SN, Hsu LM, Yeh SC, Guu SF, Lee SH, et al. Synchrony between default-mode and sensorimotor networks facilitates motor function in stroke rehabilitation: a pilot fMRI study. *Front Neurosci* (2020) 14:548. doi:10.3389/fnins.2020.00548

9. Vicentini JE, Weiler M, Casseb RF, Almeida SR, Valler L, de Campos BM, et al. Subacute functional connectivity correlates with cognitive recovery six months after stroke. *Neuroimage Clin* (2021) 29:102538. doi:10.1016/j.nicl.2020.102538

10. Li MZ, Shi YL, He XJ, Wang SC, Liu J, Wang Z, et al. Resting-state fMRI and post-ischemic stroke functional recovery: unraveling causality and predicting therapeutic targets. *Int J Mol Sci* (2025) 26:3608. doi:10.3390/ijms26083608

11. Xia W, Zhang B, Yang Y, Wang P, Yang Y, Wang S. Poorly controlled cholesterol is associated with cognitive impairment in T2DM: a resting-state fMRI study. *Lipids Health Dis* (2015) 14:47. doi:10.1186/s12944-015-0046-x

12. Zhang W, Fu L, Bi Y, Liu J, Li X, Zhang X, et al. Large-scale functional network connectivity mediates the associations between lipids metabolism and cognition in type 2 diabetes. *J Cereb Blood Flow Metab* (2024) 44:384–96. doi:10.1177/0271678X231204426

13. Skrivankova VW, Richmond RC, Woolf BAR, Yarmolinsky J, Davies NM, Swanson SA, et al. Strengthening the reporting of observational studies in epidemiology using mendelian randomization: the STROBE-MR statement. *JAMA* (2021) 326:1614–21. doi:10.1001/jama.2021.18236

14. Zhao B, Li T, Smith SM, Xiong D, Wang X, Yang Y, et al. Common variants contribute to intrinsic human brain functional networks. *Nat Genet* (2022) 54:508–17. doi:10.1038/s41588-022-01039-6

15. Aldridge CM, Braun R, Lohse K, de Havenon A, Cole JW, Cramer SC, et al. Genome-wide association studies of 3 distinct recovery phenotypes in mild ischemic stroke. *Neurology* (2024) 102:e208011. doi:10.1212/WNL.0000000000208011

16. Mu C, Dang X, Luo XJ. Mendelian randomization analyses reveal causal relationships between brain functional networks and risk of psychiatric disorders. *Nat Hum Behav* (2024) 8:1417–28. doi:10.1038/s41562-024-01879-8

17. Lu Q, Jia Z, Gu H. Association between brain resting-state functional activities and migraine: a bidirectional mendelian randomization study. *Sci Rep* (2024) 14:23901. doi:10.1038/s41598-024-74745-2

18. Zhang Z, Wang M, Gill D, Liu X, Zhu W. Association of genetically predicted anxiety and depression with functional outcome after ischemic stroke: a mendelian randomization study. *Neurology* (2024) 103:e209776. doi:10.1212/WNL.0000000000209776

19. Zhang Z, Wang M, Gill D, Zhu W, Liu X. Genetically predicted sleep traits and functional outcome after ischemic stroke: a mendelian randomization study. *Neurology* (2023) 100:e1159–e65. doi:10.1212/WNL.0000000000206745

20. Wang M, Daghlas I, Zhang Z, Ye D, Li S, Liu D. Genetic liability to migraine and functional outcome after ischemic stroke. *Eur Stroke J* (2023) 8:517–21. doi:10.1177/23969873231164728

21. Bowden J, Davey Smith G, Haycock PC, Burgess S. Consistent estimation in Mendelian randomization with some invalid instruments using a weighted median estimator. *Genet Epidemiol* (2016) 40:304–14. doi:10.1002/gepi.21965

22. Bowden J, Davey Smith G, Burgess S. Mendelian randomization with invalid instruments: effect estimation and bias detection through egger regression. *Int J Epidemiol* (2015) 44:512–25. doi:10.1093/ije/dyv080

23. Xue H, Shen X, Pan W. Constrained maximum likelihood-based mendelian randomization robust to both correlated and uncorrelated pleiotropic effects. *Am J Hum Genet* (2021) 108:1251–69. doi:10.1016/j.ajhg.2021.05.014

24. Su Y, Xu S, Ma Y, Yin P, Hao X, Zhou J, et al. A modified debiased inverse-variance weighted estimator in two-sample summary-data Mendelian randomization. *Stat Med* (2024) 43:5484–96. doi:10.1002/sim.10245

25. Zhao J, Ming J, Hu X, Chen G, Liu J, Yang C. Bayesian weighted Mendelian randomization for causal inference based on summary statistics. *Bioinformatics* (2020) 36:1501–8. doi:10.1093/bioinformatics/btz749

26. Verbanck M, Chen CY, Neale B, Do R. Detection of widespread horizontal pleiotropy in causal relationships inferred from Mendelian randomization between complex traits and diseases. *Nat Genet* (2018) 50:693–8. doi:10.1038/s41588-018-0099-7

27. Cai S, Hartley A, Mahmoud O, Tilling K, Dudbridge F. Adjusting for collider bias in genetic association studies using instrumental variable methods. *Genet Epidemiol* (2022) 46:303–16. doi:10.1002/gepi.22455

28. Mishra A, Malik R, Hachiya T, Jurgenson T, Namba S, Posner DC, et al. Stroke genetics informs drug discovery and risk prediction across ancestries. *Nature* (2022) 611: 115–23. doi:10.1038/s41586-022-05165-3

29. Karjalainen MK, Karthikeyan S, Oliver-Williams C, Sliz E, Allara E, Fung WT, et al. Genome-wide characterization of circulating metabolic biomarkers. *Nature* (2024) 628: 130–8. doi:10.1038/s41586-024-07148-y

30. Carter AR, Sanderson E, Hammerton G, Richmond RC, Davey Smith G, Heron J, et al. Mendelian randomisation for mediation analysis: current methods and challenges for implementation. *Eur J Epidemiol* (2021) 36:465–78. doi:10.1007/s10654-021-00757-1

31. Hemani G, Zheng J, Elsworth B, Wade KH, Haberland V, Baird D, et al. The MR-Base platform supports systematic causal inference across the human phenome. *Elife* (2018) 7:e34408. doi:10.7554/eLife.34408

32. Tofighi D, MacKinnon DP. RMediation: an R package for mediation analysis confidence intervals. *Behav Res Methods* (2011) 43:692–700. doi:10.3758/s13428-011-0076-x

33. Menon V. Large-scale brain networks and psychopathology: a unifying triple network model. *Trends Cogn Sci* (2011) 15:483–506. doi:10.1016/j.tics.2011.08.003

34. Siegel JS, Ramsey LE, Snyder AZ, Metcalf NV, Chacko RV, Weinberger K, et al. Disruptions of network connectivity predict impairment in multiple behavioral domains after stroke. *Proc Natl Acad Sci U S A* (2016) 113:E4367–76. doi:10.1073/pnas.1521083113

35. Wei HL, Wei C, Yu YS, Yu X, Chen Y, Li J, et al. Dysfunction of the triple-network model is associated with cognitive impairment in patients with cerebral small vessel disease. *Heliyon* (2024) 10:e24701. doi:10.1016/j.heliyon.2024.e24701

36. Kwakkel G, Stinear C, Essers B, Munoz-Novoa M, Branscheidt M, Cabanas-Valdes R, et al. Motor rehabilitation after stroke: European stroke organisation (ESO) consensus-based definition and guiding framework. *Eur Stroke J* (2023) 8:880–94. doi:10.1177/23969873231191304

37. Lee J, Kim YH. Does a cognitive network contribute to motor recovery after ischemic stroke? *Neurorehabil Neural Repair* (2023) 37:458–65. doi:10.1177/15459683231177604

38. Menon V, Uddin LQ. Saliency, switching, attention and control: a network model of insula function. *Brain Struct Funct* (2010) 214:655–67. doi:10.1007/s00429-010-0262-0

39. Peters SK, Dunlop K, Downar J. Cortico-striatal-thalamic loop circuits of the salience network: a central pathway in psychiatric disease and treatment. *Front Syst Neurosci* (2016) 10:104. doi:10.3389/fnsys.2016.00104

40. Frontzkowski L, Fehring F, Frey BM, Wrobel PP, Reibelt A, Higgen F, et al. Frontoparietal structural network disconnections correlate with outcome after a severe stroke. *Hum Brain Mapp* (2024) 45:e70060. doi:10.1002/hbm.70060

41. Chen H, Huang L, Yang D, Ye Q, Guo M, Qin R, et al. Nodal global efficiency in front-parietal lobe mediated periventricular white matter hyperintensity (PWMH)-related cognitive impairment. *Front Aging Neurosci* (2019) 11:347. doi:10.3389/fnagi.2019.00347

42. Cheng Y, Li L, Lv Y, Zhang L, Chen W, Xu G. Association between cerebral small vessel disease and plasma levels of LDL cholesterol and homocysteine: implications for cognitive function. *J Med Biochem* (2024) 43:696–703. doi:10.5937/jomb0-50100

43. Sohrabi Y, Schwarz D, Reinecke H. LDL-C augments whereas HDL-C prevents inflammatory innate immune memory. *Trends Mol Med* (2022) 28:1–4. doi:10.1016/j.molmed.2021.11.003

44. Izumida T, Nakamura Y, Hino Y, Ishikawa S. Combined effect of small dense low-density lipoprotein cholesterol (sdLDL-C) and remnant-like particle cholesterol (RLP-C) on low-grade inflammation. *J Atheroscler Thromb* (2020) 27:319–30. doi:10.5551/jat.49528

45. Wingo AP, Vattathil SM, Liu J, Fan W, Cutler DJ, Levey AI, et al. LDL cholesterol is associated with higher AD neuropathology burden independent of APOE. *J Neurol Neurosurg Psychiatry* (2022) 93:930–8. doi:10.1136/jnnp-2021-328164

EBM Experimental Biology and Medicine

TYPE Review
PUBLISHED 06 August 2026
DOI 10.3389/ebm.2026.11192

Check for updates

OPEN ACCESS

*CORRESPONDENCE
Ruixue Wang,
wangruixue39854@126.com
Chaochao Zhao,
zhaochaochao@fosu.edu.cn

‡These authors have contributed equally to this work

RECEIVED 13 May 2026
REVISED 08 June 2026
ACCEPTED 16 June 2026
PUBLISHED 06 August 2026

CITATION
Huang B, Yang Q, Wang R and Zhao C (2026) The role and mechanism of neutrophils in oncolytic virus therapy. *Exp. Biol. Med.* 251:11192. doi: 10.3389/ebm.2026.11192

COPYRIGHT
© 2026 Huang, Yang, Wang and Zhao. This is an open-access article distributed under the terms of the Creative Commons Attribution License (CC BY). The use, distribution or reproduction in other forums is permitted, provided the original author(s) and the copyright owner(s) are credited and that the original publication in this journal is cited, in accordance with accepted academic practice. No use, distribution or reproduction is permitted which does not comply with these terms.

The role and mechanism of neutrophils in oncolytic virus therapy

Baixian Huang‡, Qixin Yang‡, Ruixue Wang* and Chaochao Zhao *

School of Medicine, Foshan University, Foshan, Guangdong, China

Abstract

Oncolytic viruses (OVs) are a class of viruses capable of specifically infecting and killing tumor cells. They exert antitumor effects through direct lysis of tumor cells, activation of the immune system, and disruption of tumor vasculature. Neutrophils, which originate from the bone marrow, are the most abundant leukocytes in peripheral blood and the immune system and play a dual regulatory role in oncolytic virotherapy. In different TME, neutrophils can polarize into two phenotypes: N1 and N2. N1 neutrophils, owing to their chemotaxis and tumor-homing capabilities, can serve as delivery vehicles for OVs, enhance the therapeutic efficacy of oncolytic virotherapy, and activate host immune responses. In contrast, N2 neutrophils impair the efficacy of OVs through their antiviral activity and immunosuppressive functions. Therefore, an in-depth understanding of the mechanisms underlying the role of neutrophils in oncolytic virotherapy is of great significance for optimizing OV-based therapies and improving their clinical application outcomes.

KEYWORDS
immune response, N1/N2 phenotypes, neutrophils, oncolytic viruses, tumor microenvironment

Impact statement

Neutrophils exert a dual regulatory role in oncolytic virotherapy but remain poorly understood, limiting clinical translation. This review systematically clarifies N1/N2 phenotypic polarization, pro-tumor/anti-tumor mechanisms, and interactions with the TME. It integrates key molecular pathways and emerging intervention strategies to guide rational optimization of OV regimens. This work advances targeted immunovirotherapy, supports precise neutrophil modulation, and promotes safer, more effective clinical application of OV therapy.

Introduction

The earliest reports of oncolytic viruses (OVs) date back to 1904, when scientists observed an unexpected remission of leukemia symptoms in a female chronic leukemia patient following infection with the influenza virus [1]. Subsequently, in 1912, Italian physician Depace reported spontaneous regression and shrinkage of cervical cancer in a patient after administration of an attenuated rabies vaccine [2]. These observations spurred interest in the potential oncolytic properties of viruses. The evolution of OV

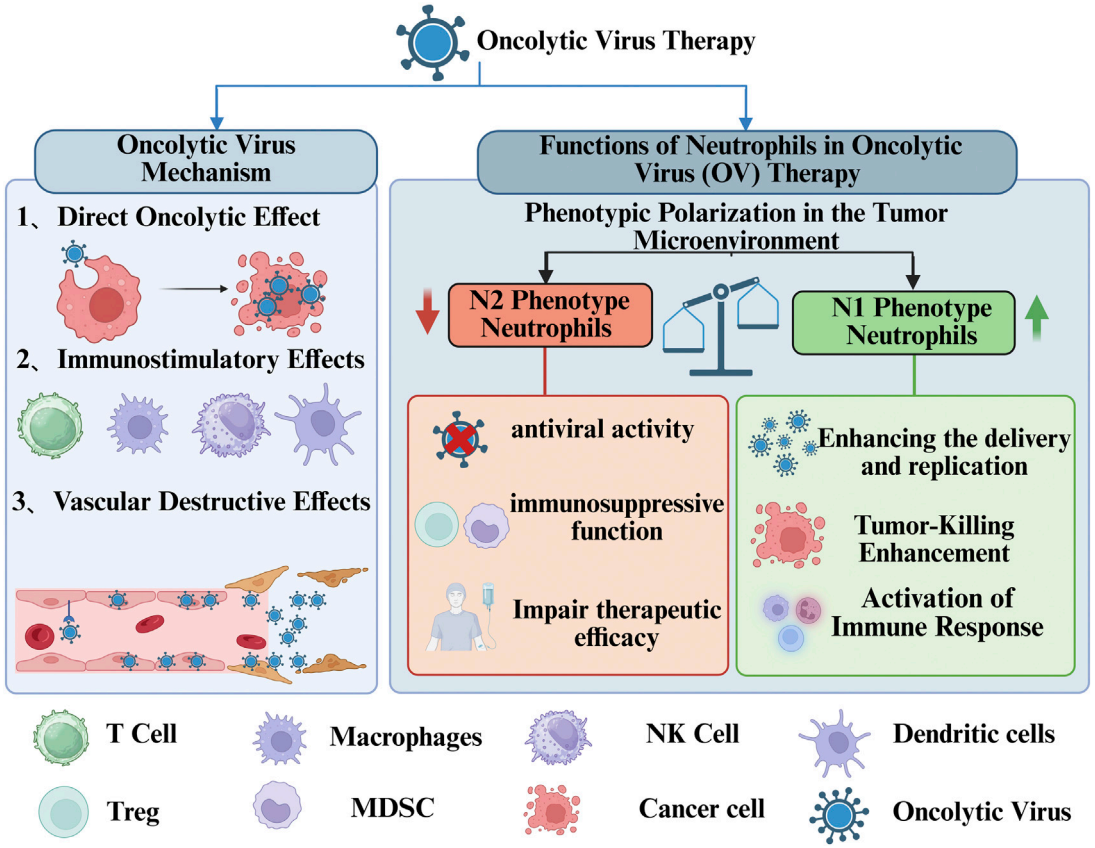


FIGURE 1
Oncolytic virus therapy and neutrophil. Created with BioGDP.com [8].

research can be broadly divided into three stages. The first stage primarily involved the direct use of wild-type viruses. As early as a century ago, physicians attempted to inject live viruses into cancer patients, aiming to combat tumors through a "poison against poison" strategy. Although these early efforts yielded transient oncolytic effects, they often resulted in significant toxicities due to wild-type virus infection [3]. In the 1990s, advances in gene editing enabled targeted modification of wild-type viral genomes, allowing for tumor-specific replication. While most of these modified OVs exhibited limited efficacy, their toxicity profiles were markedly reduced, thereby establishing a safety foundation for subsequent development. The third stage, initiated in the current century, is characterized by the insertion of exogenous genes into OV to enhance their therapeutic effects. In 2015, Talimogene laherparepvec became the first OV therapy to receive regulatory approval worldwide [4], and since then, an increasing number of OV candidates have entered clinical trials.

Overview of oncolytic viruses

OVs are defined as viruses capable of specifically infecting and replicating within tumor cells, ultimately inducing tumor cell lysis and death. The fundamental principle of this therapeutic approach lies in the selective infection of tumor cells by OVs. Beyond their direct cytolytic effect on tumor cells [5], these viruses can further potentiate antitumor immunity by activating the host immune system [6]. Compared with conventional treatment modalities, OVs therapy offers precise targeting of tumor tissues while causing minimal damage to adjacent healthy tissues. Additionally, OVs can remodel the tumor immune microenvironment and enhance the host's immune response [7] as shown as Figure 1. Collectively, these properties position OV therapy as a promising strategy capable of achieving more durable and broad-spectrum efficacy in cancer treatment. Currently, a variety of OVs have entered clinical trials, as summarized in Supplementary Table 1.

OVs can be categorized based on their nucleic acid composition into double-stranded DNA viruses, double-stranded RNA viruses, positive-sense single-stranded RNA viruses, and negative-sense single-stranded RNA viruses [9]. According to their origin, they are primarily divided into two classes: naturally occurring viruses and genetically engineered viruses [10]. Although naturally occurring viruses are capable of selectively infecting and killing tumor cells, they are often limited by low therapeutic efficacy and insufficient safety. In contrast, genetically engineered viruses, through the insertion or deletion of specific genes, exhibit enhanced selectivity and replication capacity within tumor cells while reducing damage to normal tissues. Moreover, these modifications enable OVs to evade recognition and clearance by

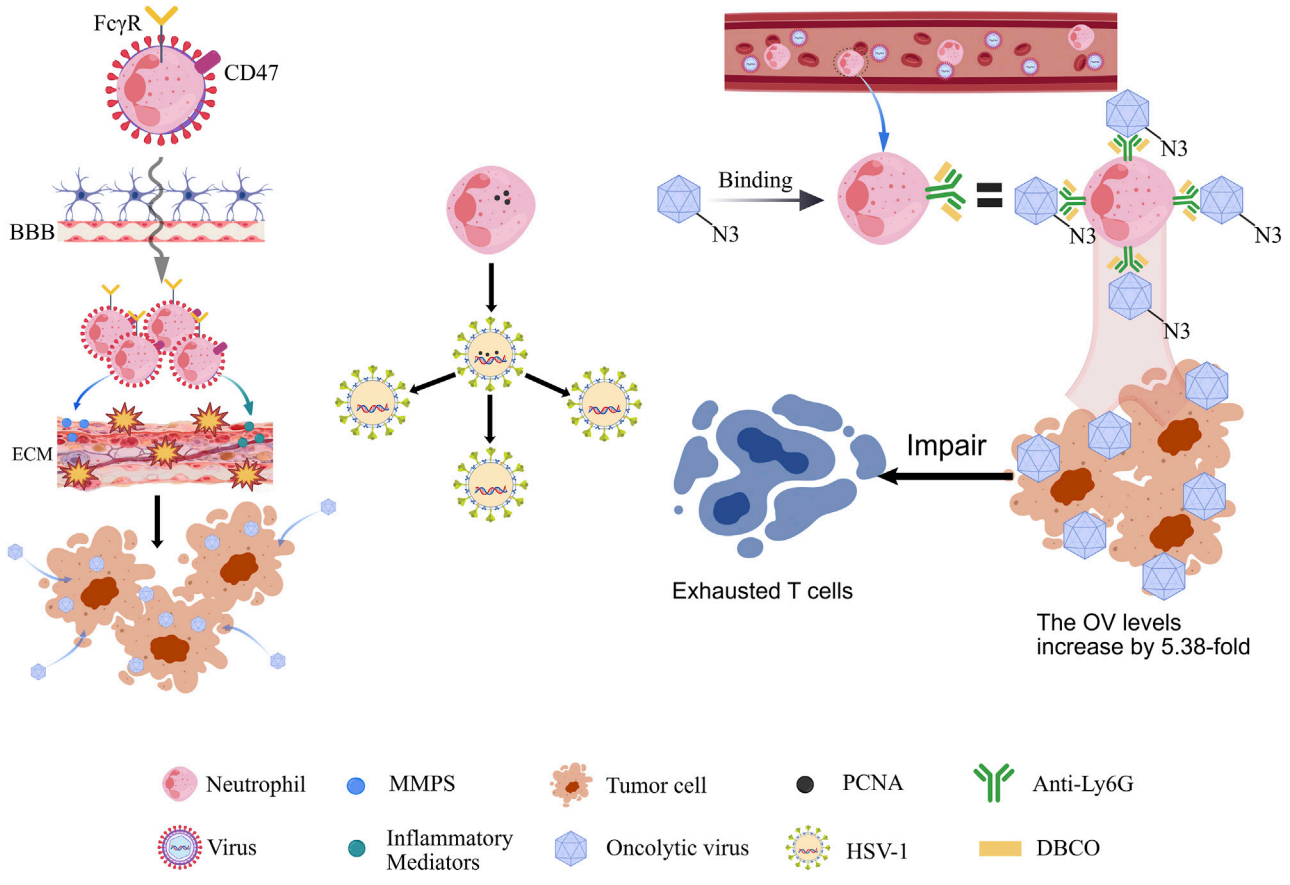


FIGURE 2
Enhancing the delivery and *in vivo* replication of oncolytic viruses. Created with BioGDP.com [8].

the host immune system, thereby prolonging their persistence in the body and improving therapeutic outcomes [11].

Overview of neutrophils

Neutrophils (also known as neutrophil granulocytes or neutrophilic leukocytes) originate from the bone marrow [12] and represent the most abundant type of white blood cells in peripheral blood and the immune system, accounting for approximately 50%–70% of total leukocytes in mammalian blood [13]. With the development of the tumor microenvironment (TME) concept, studies have revealed the infiltration of various immune cell types within the TME, among which T lymphocytes and macrophages have been extensively investigated. In recent years, neutrophils have also garnered considerable attention. Research indicates that neutrophils can polarize into distinct phenotypes depending on the TME context. Neutrophil phenotype 1 (N1) typically appears during the early stages of tumor development and primarily functions to inhibit tumor growth. In contrast, neutrophil phenotype 2 (N2) is more prevalent in later stages and predominantly promotes tumor progression [14] (Figure 1). Therefore, inhibiting the polarization of neutrophils toward the N2 phenotype while promoting their conversion to the N1 phenotype represents a key strategy in tumor therapy. For instance, Yasufumi Kaneda and colleagues demonstrated that inactivated Sendai virus envelopes can polarize neutrophils toward the N1 phenotype. N1 neutrophils exhibit antitumor properties and enhance cytotoxic T lymphocyte activity, thereby suppressing tumor growth [15]. Under specific conditions, N1 and N2 phenotypes can interconvert. For example, transforming growth factor-beta (TGF-β) regulates the transition of neutrophils to the N2 phenotype [14]. In a pancreatic cancer liver metastasis model, TGF-β secreted by tumors activates SMAD3 signaling pathway in neutrophils, induces the expression of nuclear factor erythroid 2, and subsequently activates peptidyl-arginine deiminase 4, driving neutrophil polarization toward the N2 phenotype and promoting tumor metastasis [16]. Furthermore, neutrophils can interact with cancer cells to facilitate tumor growth. In lung cancer, tumor cells secrete factors that increase the number of osteocalcin-positive osteoblasts, which in turn activate SiglecF-expressing neutrophils, thereby promoting lung cancer progression [17]. Beyond the N1/N2 polarization model mentioned above, a growing number of studies have revealed the high heterogeneity of neutrophils within the TME. Multiple neutrophil subsets with distinct functions have now been identified, including low-density neutrophils [18], antigen-presenting neutrophils [19], aged neutrophils [20], single-cell transcriptome-defined subsets [21], and they play

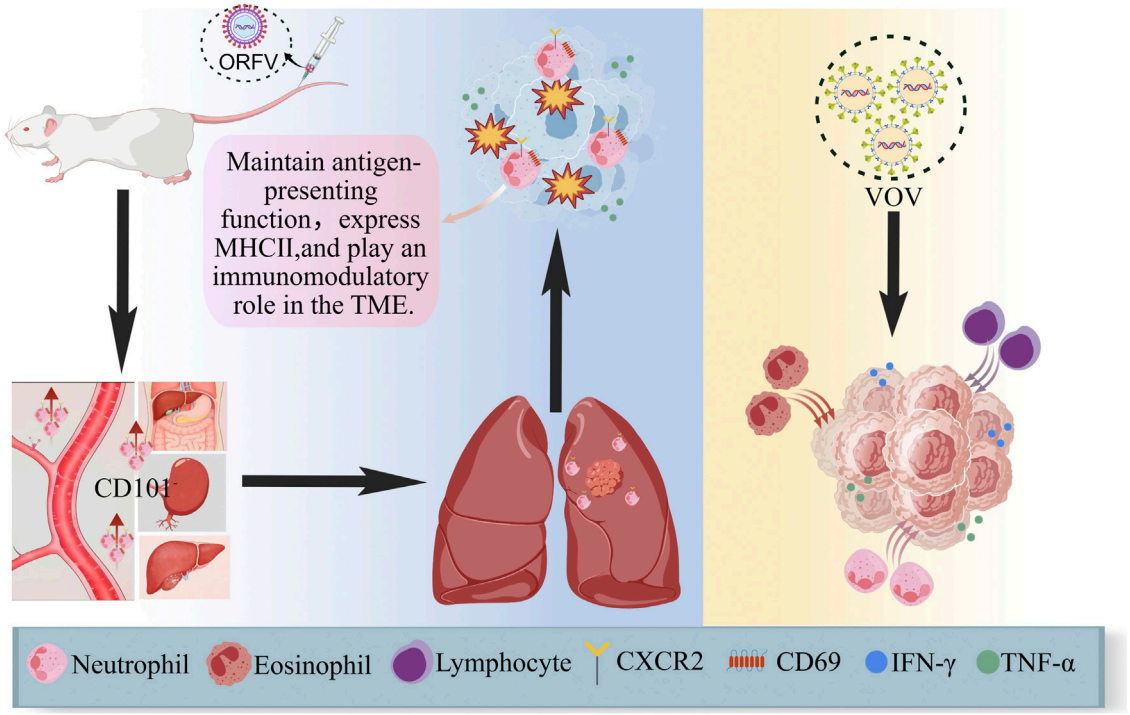


FIGURE 3
Mechanisms of neutrophil-enhanced tumor killing. Created with BioGDP.com [8].

very different, sometimes even opposite roles in cancer therapy. A detailed summary is provided in Supplementary Table 2.

Oncolytic virus mechanism

Direct oncolytic effect

Genetically engineered OVs are capable of specifically targeting tumor cells and selectively replicating within them, ultimately inducing tumor cell lysis. For instance, Teserpaturev (G47Δ), an OV approved for clinical use in Japan, exerts its direct oncolytic effect by targeting aberrant signaling pathways in gliomas [22]. In the early stages of glioma cell infection, herpes simplex virus type 1 (HSV-1) enhances the antitumor efficacy of oncolytic HSV-1 (oHSV-1) in glioma-bearing xenograft mouse models by selectively reducing the expression of the METTL14 protein [23].

Immunostimulatory effects

As pathogen-associated molecular patterns, OVs can activate innate immune cells, including macrophages and natural killer cells, thereby stimulating a non-specific immune response in the host [24]. OVs engineered to express immunomodulatory genes—such as interleukin-21 and granulocyte-macrophage colony-stimulating factor (GM-CSF)—can promote T cell activation and subsequently trigger an adaptive immune response. For example, Talimogene laherparepvec, which carries the GM-CSF gene, enhances T cell-mediated immunity by recruiting and activating dendritic cells, thereby inducing antitumor responses both at the injection site and systemically [25]. Studies have shown that oncolytic herpes simplex viruses potentiate antitumor immunity by increasing the expression of interferon-stimulated genes, promoting the accumulation of endogenous Z-RNA, and activating Z-DNA binding protein 1, which in turn triggers Z-DNA binding protein 1-mediated PANoptosis, a distinct form of innate immune inflammatory cell death [26]. Newcastle disease virus (NDV) has been developed as an effective OV agent, capable of selective replication in tumor cells, inducing costimulatory activity in T cells, activating macrophages, and exhibiting multiple immunostimulatory functions [27]. In a mouse model of transplanted digestive system tumors, esophageal and colorectal cancer cells demonstrated a robust cytotoxic response to the attenuated NDV strain AMHA1, and this response was positively correlated with the multiplicity of infection [28]. Additionally, OV-mOX40L—constructed by inserting mouse OX40L into HSV-1—has been shown to increase the proportion of N1 neutrophils while decreasing that of N2 neutrophils, thereby inhibiting tumor activity in the treatment of pancreatic ductal adenocarcinoma [29].

Vascular destructive effects

OV can directly infect and lyse tumor vascular endothelial cells by recognizing specific surface receptors, such as CD46 and CD155, thereby inducing the collapse of vascular structures. For example, the EV-A71-miR124T nanocapsules developed by the team at the

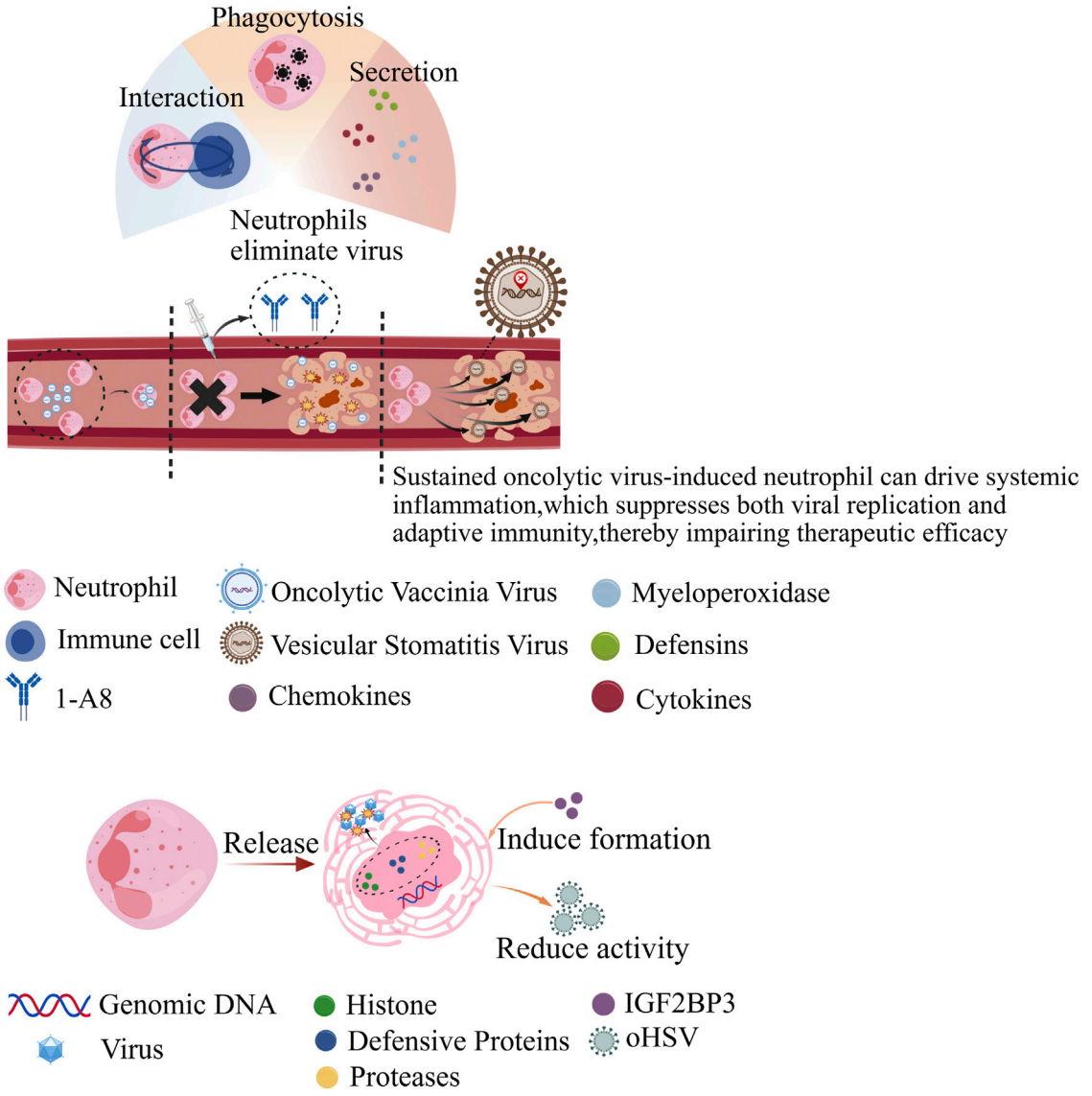


FIGURE 4
Mechanisms of neutrophil antiviral activity. Created with BioGDP.com [8].

Wuhan Institute of Virology are capable of crossing the blood–brain barrier and selectively releasing OVs at the tumor site. This strategy enables precise delivery of OVs to the vascular endothelial cells of gliomas, disrupting tumor blood vessels while preserving the integrity of vessels in normal brain tissue, thus achieving targeted killing of glioma cells [30]. Additionally, the NDV-GT OV developed by the team at Guangxi Medical University induces the expression of the porcine α1,3GT gene on the surface of tumor cells, leading to the generation of α-Gal antigens. In clinical trials, this mechanism results in tumor vascular embolism and necrosis, with a disease control rate of 90%. Concurrently, NDV-GT activates the immune system, inducing substantial infiltration of macrophages and neutrophils around tumor blood vessels, which subsequently secrete pro-inflammatory factors such as tumor necrosis factor-alpha (TNF-α), interleukin-1β, and matrix metalloproteinases, further damaging the vascular basement membrane [31]. Moreover, certain OVs can infect tumor vascular endothelial cells and inhibit the expression of angiogenic factors, including vascular endothelial growth factor [32] and fibroblast growth factor, thereby blocking new blood vessel formation.

The core regulatory role of neutrophils

Positive regulation mechanism

Enhancing the delivery and replication of oncolytic viruses *in vivo*

Neutrophils, with their inherent chemotactic and tumor-homing abilities [33], can carry OVs across physiological barriers (such as the blood-brain barrier) or immunosuppressive microenvironments, achieving targeted delivery. After

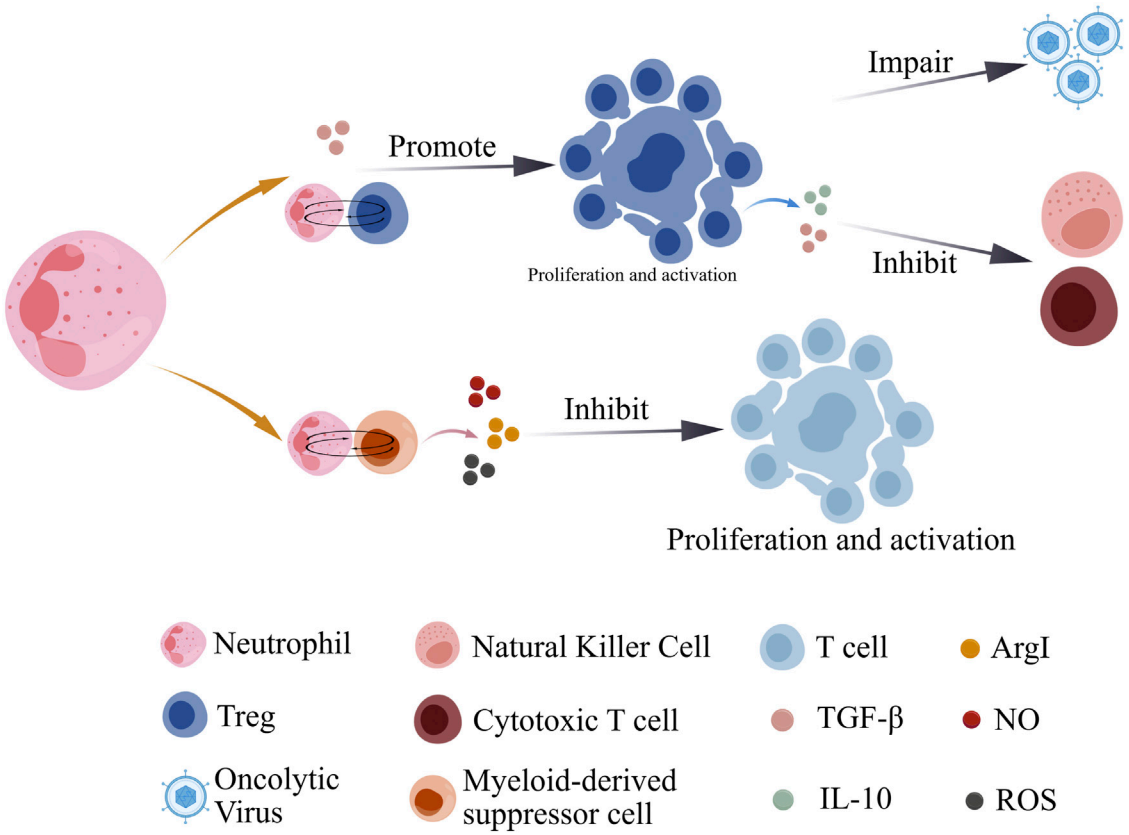


FIGURE 5
Mechanisms of neutrophil-mediated immunosuppressive microenvironment. Created with BioGDP.com [8].

intravenous injection, OVs can be captured by receptors on the surface of neutrophils (such as FcγR), forming a "virus-neutrophil complex". For example, researchers observed in a clinical trial (ChiCTR2300069323) that increased intratumoral neutrophil infiltration in gastric cancer patients with OV therapy was associated with exacerbated $CD8^+$ T cell exhaustion, suggesting that neutrophils may compromise viral efficacy. Inspired by this observation, the investigators designed a bifunctional bioorthogonal delivery system, by using an anti-Ly6G antibody modified with DBCO to tag circulating neutrophils. This approach significantly boosted the virus load inside the tumor. Once the virus reached the tumor site, the neutrophils underwent apoptosis, which relieved immunosuppression and reduced T cell exhaustion, turning neutrophils from a therapeutic obstacle into an effective delivery vehicle [34]. After genetic engineering modification (such as insertion of the CD47 domain), OVs can inhibit the phagocytosis of neutrophils [35], prolong virus survival time, and ensure their effective release at the tumor site. In addition, neutrophils can also destroy tumor vascular basement membranes and extracellular matrix by secreting matrix metalloproteinases and inflammatory factors, further enhancing the penetration ability of OVs into tumors. Recent studies have also found the presence of proliferating cell nuclear antigen in the cytoplasm of neutrophils [36], which plays a key role in the replication process of HSV-1 [37]. In conclusion, Figure 2 illustrates the mechanisms of enhancing the delivery and in vivo replication of oncolytic viruses.

Tumor-killing enhancement

In a mouse model of lung melanoma metastasis, treatment with orf virus (ORFV) significantly increased the number of white blood cells, predominantly neutrophils, in the peripheral blood, peritoneal cavity, spleen, liver, and TME. These systemic neutrophils were capable of migrating into the TME and exhibited predominantly an immature phenotype ($CD101^-$), with high expression of the chemokine receptor CXCR2 and the activation marker CD69. ORFV-activated neutrophils directly killed tumor cells through the secretion of TNF-α. *In vitro* experiments demonstrated that ORFV-treated neutrophils displayed markedly enhanced cytotoxicity against B16F10 melanoma cells. Moreover, in addition to retaining their intrinsic antigen-presenting capacity, these neutrophils expressed major histocompatibility complex class II(MHC-II), thereby contributing to immunomodulatory functions within the TME [38].

Similarly, vaccinia virus-based oncolytic therapy enhances the secretion of TNF-α and interferon-gamma at the tumor site, inducing the activation and recruitment of neutrophils, eosinophils, and lymphocytes into tumor tissues, thereby potentiating the immune response to eliminate tumor cells [39]. Other studies have shown that following infection with vesicular stomatitis virus (VSV), the number of neutrophils in the bone marrow of mice decreases markedly within 24 h, accompanied by their rapid release and migration to other tissues. At 3 hours

post-infection, the proportion of neutrophils in the peripheral blood increases significantly, and over time, neutrophils gradually transition from a mature ($CD101^+$) to an immature ($CD101^-$) phenotype. At 24 h post-infection, the proportion of neutrophils in the spleen increases significantly. These splenic neutrophils exhibit enhanced antigen-presenting capacity (indicated by increased expression of MHC-II) and elevated secretion of inflammatory cytokines, such as interleukin-20, thereby playing an immune-activating role in oncolytic virotherapy and promoting T cell-mediated antitumor immune responses [40]. The mechanisms of neutrophil-enhanced tumor killing enhancement were illustrated in Figure 3.

Activation of immune response

In a study on the treatment of pancreatic ductal adenocarcinoma using VSV, researchers found that VSV-S, constructed by inserting a Smac expression cassette into the VSV genome, could induce remodeling of the TME. This remodeling was primarily characterized by a marked increase in neutrophil infiltration, alongside significant reductions in myeloid-derived suppressor cells (MDSCs) and macrophages. Furthermore, the levels of immunosuppressive factors such as arginase I, TGF-β, and interleukin-10 were substantially decreased. Collectively, these changes shifted the TME from an immunosuppressive to an immunostimulatory state, thereby enhancing the antitumor immune response [41]. Another study demonstrated that a novel oncolytic adenovirus (ADV) could trigger effector mechanisms of immunoglobulin G1 (IgG1) and immunoglobulin A1 (IgA1) by secreting a cross-hybridizing Fc fusion peptide targeting programmed death-ligand 1. This approach activated neutrophils and integrated multiple effector mechanisms, significantly improving tumor cell killing efficiency [42]. In the Raji (Burkitt lymphoma) model, neutrophil depletion markedly diminished the therapeutic efficacy of oncolytic measles virus (MV) [43]. Moreover, neutrophils were found to further enhance the antitumor effects induced by MV through GM-CSF [44]. MV-s-NAP, a recombinant virus constructed using MV and *Helicobacter pylori* neutrophil-activating protein (NAP), exhibited antitumor activity in both subcutaneous and pleural effusion mouse models of metastatic breast cancer. The primary mechanism involves NAP recruiting innate immune cells, including neutrophils and macrophages, to the infection site, promoting the production of reactive oxygen species (ROS) and pro-inflammatory mediators, and thereby inducing a Th1-polarized immune response [45]. The novel oncolytic ADV Adf35 (Uppsala University) expresses NAP and reverses the immunosuppressive TME [46]. Effector memory/effector $CD8^+$ T cells (TEM/TE) are key antitumor effectors with strong cytolytic activity and high interferon-gamma secretion [47], but ADV therapy often reduces their TME infiltration. To address this, Gu constructed ADV^{NE}, a recombinant oncolytic ADV expressing neutrophil elastase (NE), a serine protease with antitumor activity [48]. ADV^{NE} induces pyroptosis in colorectal cancer cells, releasing HMGB1, which binds to macrophage TLR4 and activates the MyD88-NFκB-NLRP3 pathway, promoting M1 polarization of tumor-associated macrophages [49, 50]. M1 macrophages then enhance TEM/TE infiltration, overcoming the limitation of ADV monotherapy and improving anti-colorectal cancer efficacy [51]. Furthermore, neutrophils within the TME can differentiate into antigen-presenting cells, presenting virus-released tumor antigens to T cells and thereby amplifying the antitumor immune response [52]. Additional studies have demonstrated that modified vaccinia virus induces neutrophil migration primarily via the chemokine receptors CCR1 and CXCR2, promoting neutrophil infiltration and inflammatory responses, and enhancing the vaccinia virus-elicited adaptive immunity [53]. In another study, researchers administered the low-dose oncolytic poxvirus JX-594 via intratumoral injection to patients with advanced metastatic melanoma, then the release of GM-CSF led to a marked elevation in peripheral blood neutrophil levels in a subset of patients, and induced local lymphocyte infiltration and tumor necrosis at the injection site [54]. Table 1 is a summary of the above examples.

Negative regulation mechanism

Antiviral activity

As the first line of defense in the immune system [55], neutrophils secrete various antimicrobial and antiviral substances, including myeloperoxidase, defensins, and antimicrobial peptides. Additionally, neutrophils can clear viruses through direct phagocytosis, interaction with other immune cells, or release of cytokines and chemokines [56]. For instance, most oncolytic vaccinia viruses are phagocytosed and degraded by neutrophils in the bloodstream. Depletion of neutrophils using anti-Ly6G antibodies leads to increased accumulation of circulating oncolytic vaccinia viruses in peripheral blood and enhanced viral deposition at tumor sites, thereby potentiating antitumor efficacy [57]. Other studies have shown that following initial administration of VSV, the virus binds to endothelial cells, triggering tumor infection and activating a pro-inflammatory response; however, this initial OV dose also induces neutrophil migration to the tumor and limits viral replication [58]. Persistently elevated neutrophil levels induced by OVs may also cause systemic inflammation, which can inhibit both OV replication and adaptive immune responses, thereby attenuating the antitumor effects of oncolytic virotherapy [39].

Neutrophils can also suppress the activity of OVs through the release of neutrophil extracellular traps (NET) [59], while simultaneously promoting tumor cell proliferation and invasion. The research team led by Minfeng Shu at Fudan University demonstrated that in oHSV therapy, upregulation of insulin-like growth factor 2 mRNA-binding protein induces NET formation, thereby reducing the oncolytic activity of oHSV [60]. NETosis is a form of inflammatory cell death in neutrophils, characterized by the release of extracellular structures composed of genomic DNA, histones, defense proteins, and proteases [61]. These structures not only trap viruses but also contribute to viral inactivation through their associated granular proteins [62]. The mechanisms of neutrophil antiviral activity were illustrated in Figure 4.

TABLE 1 Mechanisms of immune response activation by neutrophils.

Oncolytic virus	Mechanisms of neutrophil-mediated anti-tumor effects	References
VSV	Increasing tumor infiltration of neutrophils TME shifted toward immune activation	[41]
Ad-cab	Enhances tumor cell killing by activating neutrophils through IgG1/IgA1 engagement	[42]
MV	Raji model: neutrophils releasing TRAIL and multiple antitumor cytokines to induce tumor cell apoptosis	[43]
	Breast cancer: Recruits and activates neutrophils and other immune cells, induces Th1 polarization and pro-inflammatory cytokine release	[45]
Adf35	Recruits and activates neutrophils and other immune cells to reverse the immunosuppressive tumor microenvironment	[46]
ADV^{NE}	Differentiate into antigen-presenting cells within the tumor microenvironment to present tumor antigens to T cells	[47–52]
MVA	CCR1 and CXCR2 induce neutrophil migration and enhance adaptive immunity	[53]
JX-594	Elevated neutrophil levels recruit immune cells	[54]

Mediating immunosuppressive microenvironment

Neutrophils in the TME induce the expansion of regulatory T cells (Tregs), thereby inhibiting the anti-tumor immune response [63] and attenuating the efficacy of OVs. Tregs are a subset of cells with immunosuppressive functions that suppress the activity of cytotoxic T cells and natural killer cells by secreting inhibitory cytokines such as interleukin-10 and TGF-β. Neutrophils also promote the proliferation and activation of Tregs through the secretion of cytokines or direct interaction with Tregs [14]. Furthermore, neutrophils can interact with MDSCs, facilitating their maturation and functional competence. MDSCs [64] accumulate extensively in the TME [65] and subsequently inhibit T cell proliferation and activation by secreting substances such as arginase I, nitric oxide, and reactive oxygen species [66], which represents one of the core mechanisms by which they mediate tumor immune escape. The mechanisms of neutrophil-mediated immunosuppressive microenvironment were illustrated in Figure 5.

Discussion

Neutrophils serve as the first line of defense in the immune system. The recently proposed consensus roadmap for neutrophil classification indicates that these cells are not a homogeneous population, but can depart from their intrinsic developmental trajectories and undergo deterministic reprogramming within specific local microenvironments. During the TME remodeling induced by OV therapy, tumor-infiltrating neutrophils not only shift from their original antiviral state but can also be polarized into antitumor effector cells capable of directly killing tumor cells or highly expressing MHC-II molecules and co-stimulatory markers. The mechanistic role of neutrophils in OV therapy is dual-edged. On one hand, neutrophils can ferry OVs across physiological barriers and activate anti-tumor immune responses. On the other hand, they can inactivate OVs through the release of NETs and collaborate with Tregs and MDSCs to establish an immunosuppressive network that undermines OV therapeutic efficacy. A study reported that neutrophil depletion using anti-Ly6G antibodies significantly prolongs the half-life of OVs in the peripheral blood and substantially enhances their targeted delivery to tumor sites [57]. However, depleting neutrophils or artificially blocking their recruitment to sites of pathology would clinically recapitulate the fatal condition of leukocyte adhesion deficiency, then lead to a complete breakdown of host defense against bacterial and fungal pathogens and predispos patients to acute, uncontrollable, and life-threatening infections. Therefore, the future optimization strategy should not be the blunt depletion of the entire neutrophil compartment, but rather a shift toward more refined and precise immunomodulatory approaches. For example, targeting specific chemokine receptors such as CXCR2 or selectively interfering with particular immunosuppressive subsets can block their recruitment while preserving normal immune surveillance in the periphery. Multiple preclinical and clinical studies are progressively validating the feasibility of this strategy. In a phase II clinical trial, the CXCR2 antagonist navarixin in combination with pembrolizumab for the treatment of advanced solid tumors induced neutropenia without associated fever or infection [67]. Although the combination regimen was prematurely terminated due to insufficient efficacy, the favorable safety profile and neutrophil-modulating capacity of navarixin provide an important foundation for future combination with OV therapy. Similarly, the selective PAD4 inhibitor JBI-589 transcriptionally downregulates CXCR2 expression, thereby precisely blocking neutrophil migration into the TME, suppressing tumor progression, and enhancing the efficacy of immune checkpoint inhibitors [68]. Another CXCR2 antagonist, SB225002, blocks radiotherapy-induced activation of the CXCR2-CXCL signaling axis, inhibits neutrophil recruitment, and reduces TGF-β expression, thereby reversing the

polarization of neutrophils toward a pro-tumor N2 phenotype and alleviating the immunosuppressive microenvironment [69]. These drugs that precisely control neutrophil migration and polarization offer powerful tools for combining with OV therapy. This conceptual shift from "global depletion" to "precision modulation" may represent the key to advancing OV-based combination immunotherapy toward safe and effective clinical application. Moreover, the complexity and heterogeneity of the TME can significantly influence the efficacy of OV therapy. Neutrophil responses vary from patient to patient, and such individual differences make it very difficult to predict treatment outcomes. Therefore, personalized treatment strategies are needed.

Future translational research should focus on potential regulatory directions, including temporally dynamic regulation of neutrophil functions, spatial blockade of their pathological recruitment to tumor sites, synergistic combination with immune checkpoint inhibitors, and clinically precise patient stratification based on neutrophil-related biomarkers. A thorough mechanistic understanding of neutrophil behavior in the context of OV therapy is importance for optimizing this therapeutic modality and advancing its clinical applicability.

Author contributions

BH prepared the draft manuscript. RW, CZ, BH, and QY revised and edited the manuscript. All authors contributed to the article and approved the submitted version.

Funding

The author(s) declared that financial support was received for this work and/or its publication. This study was supported by grants from the National Natural Science Foundation of China (No. 32202770), Foshan Science and Technology Innovation Project (2320001007516). The funding sources had no role in the study design, data collection, data analysis, interpretation or writing of the report.

Acknowledgements

We are grateful to Shuai Jiang for providing Generic Diagramming Platform. We declare that we have not used AI-generated work in this manuscript.

Conflict of interest

The author(s) declared no potential conflicts of interest with respect to the research, authorship, and/or publication of this article.

Generative AI statement

The author(s) declared that generative AI was not used in the creation of this manuscript.

Any alternative text (alt text) provided alongside figures in this article has been generated by Frontiers with the support of artificial intelligence and reasonable efforts have been made to ensure accuracy, including review by the authors wherever possible. If you identify any issues, please contact us.

Supplementary material

The Supplementary Material for this article can be found online at: https://www.ebm-journal.org/articles/10.3389/ebm.2026.11192/full#supplementary-material

References

1. Kelly E, Russell SJ. History of oncolytic viruses: genesis to genetic engineering. *Mol Ther* (2007) 15:651–9. doi:10.1038/sj.mt.6300108

2. Das R, Langou S, Le TT, Prasad P, Lin F, Nguyen TD. Electrical stimulation for immune modulation in cancer treatments. *Front Bioeng Biotechnol* (2021) 9:795300. doi:10.3389/fbioe.2021.795300

3. Alemany R. Viruses in cancer treatment. *Clin & Translational Oncol* (2013) 15:182–8. doi:10.1007/s12094-012-0951-7

4. Watanabe D, Goshima F. Oncolytic virotherapy by HSV. *Adv Exp Med Biol* (2018) 1045:63–84. doi:10.1007/978-981-10-7230-7_4

5. Abd-Aziz N, Poh CL. Development of oncolytic viruses for cancer therapy. *Transl Res* (2021) 237:98–123. doi:10.1016/j.trsl.2021.04.008

6. Volovat SR, Scripcariu DV, Vasilache IA, Stolniceanu CR, Volovat C, Augustin IG, et al. Oncolytic virotherapy: a new paradigm in cancer immunotherapy. *Int J Mol Sci* (2024) 25:1180. doi:10.3390/ijms25021180

7. Chen Y, Chen X, Bao W, Liu G, Wei W, Ping Y. An oncolytic virus-T cell chimera for cancer immunotherapy. *Nat Biotechnol* (2024) 42:1876–87. doi:10.1038/s41587-023-02118-7

8. Jiang S, Li H, Zhang L, Mu W, Zhang Y, Chen T, et al. Generic diagramming platform (GDP): a comprehensive database of high-quality biomedical graphics. *Nucleic Acids Res* (2025) 53(D1):D1670–D1676. doi:10.1093/nar/gkae973

9. Sm OB, Mathis JM. Oncolytic virotherapy for breast cancer treatment. *Curr Gene Ther* (2018) 18:192–205. doi:10.2174/1566523218666180910163805

10. Zhu X, Fan C, Xiong Z, Chen M, Li Z, Tao T, et al. Development and application of oncolytic viruses as the nemesis of tumor cells. *Front Microbiol* (2023) 14:1188526. doi:10.3389/fmicb.2023.1188526

11. Ma R, Li Z, Chiocca EA, Caligiuri MA, Yu J. The emerging field of oncolytic virus-based cancer immunotherapy. *Trends Cancer* (2023) 9:122–39. doi:10.1016/j.trecan.2022.10.003

12. Borregaard N. Neutrophils, from marrow to microbes. *Immunity* (2010) 33:657–70. doi:10.1016/j.immuni.2010.11.011

13. Lehrer RI, Ganz T, Selsted ME, Babior BM, Curnutte JT. Neutrophils and host defense. *Ann Intern Med* (1988) 109:127–42. doi:10.7326/0003-4819-109-2-127

14. Fridlender ZG, Sun J, Kim S, Kapoor V, Cheng G, Ling L, et al. Polarization of tumor-associated neutrophil phenotype by TGF-beta: "N1" *versus* "N2" TAN. *Cancer Cell* (2009) 16:183–94. doi:10.1016/j.ccr.2009.06.017

15. Pan YC, Nishikawa T, Chang CY, Tai JA, Kaneda Y. CXCL2 combined with HVJ-E suppresses tumor growth and lung metastasis in breast cancer and enhances anti-PD-1 antibody therapy. *Mol Ther Oncolytics* (2021) 20:175–86. doi:10.1016/j.omto.2020.12.011

16. Xu W, Liu J, Liu Q, Xu J, Zhou L, Liang Z, et al. NFE2-driven neutrophil polarization promotes pancreatic cancer liver metastasis progression. *Cell Rep* (2025) 44:115226. doi:10.1016/j.celrep.2024.115226

17. Azevedo PO, Paiva AE, Santos GSP, Lousado L, Andreotti JP, Sena IFG, et al. Cross-talk between lung cancer and bones results in neutrophils that promote tumor progression. *Cancer Metastasis Rev* (2018) 37:779–90. doi:10.1007/s10555-018-9759-4

18. Correia BF, Grosa D, Salvador R, Brites I, Martins T, Vitorino M, et al. Neutrophils matter: new clinical insights on their role in the progression of metastatic breast cancer. *Breast Cancer Res* (2025) 27:223. doi:10.1186/s13058-025-02201-8

19. Tang Z, Hu J, Li XC, Wang W, Zhang HY, Guo YY, et al. A subset of neutrophils activates anti-tumor immunity and inhibits non-small-cell lung cancer progression. *Dev Cell* (2025) 60:379–95.e8. doi:10.1016/j.devcel.2024.10.010

20. Zhu Q, Zhang G, Cao M, Huang H, He D, Zang Z, et al. Microbiota-shaped neutrophil senescence regulates sexual dimorphism in bladder cancer. *Nat Immunol* (2025) 26:722–36. doi:10.1038/s41590-025-02126-6

21. Lyu A, Fan Z, Clark M, Lea A, Wolters R, Qiu L, et al. 463 dissecting myeloid-driven mechanisms of immunotherapy resistance in prostate cancer bone metastases. *J ImmunoTherapy Cancer* (2025) 13:A528. doi:10.1136/jitc-2025-SITC2025.0463

22. Frampton JE. Teserpaturev/G47Δ: first approval. *BioDrugs* (2022) 36:667–72. doi:10.1007/s40259-022-00553-7

23. Chen Y, Bian S, Zhang J, Luan Y, Yin B, Dai W, et al. HSV-1-induced N6-methyladenosine reprogramming via ICP0-mediated suppression of METTL14 potentiates oncolytic activity in glioma. *Cell Rep* (2024) 43:114756. doi:10.1016/j.celrep.2024.114756

24. Peng Y, Yin S, Wang M. Extracellular vesicles of bacteria as potential targets for immune interventions. *Hum Vaccin Immunother* (2021) 17:897–903. doi:10.1080/21645515.2020.1799667

25. MacArthur TA, Fahy AS, Jakub JW. Surgical resection after talimogene laherparepvec for melanoma: persistent fuorodeoxyglucose avidity on positron emission tomography despite no viable disease. *Am Surg* (2021) 87:849–54. doi:10.1177/00031348211023434

26. Wang S, Song A, Xie J, Wang YY, Wang WD, Zhang MJ, et al. Fn-OMV potentiates ZBP1-mediated PANoptosis triggered by oncolytic HSV-1 to fuel antitumor immunity. *Nat Commun* (2024) 15:3669. doi:10.1038/s41467-024-48032-7

27. Miyahira Y, García-Sastre A, Rodriguez D, Rodriguez JR, Murata K, Tsuji M, et al. Recombinant viruses expressing a human malaria antigen can elicit potentially protective immune CD8+ responses in mice. *Proc Natl Acad Sci U S A* (1998) 95:3954–9. doi:10.1073/pnas.95.7.3954

28. Hamad MA, Almzaien AK, Jameel FR, Mohammad MH, Al-Shammari AM. The oncolytic effect of Newcastle disease virus attenuated AMHA1 strain against digestive system tumors. *Vet World* (2024) 17:2688–93. doi:10.14202/vetworld.2024.2688-2693

29. Liu S, Li F, Ma Q, Du M, Wang H, Zhu Y, et al. OX40L-Armed oncolytic virus boosts T-cell response and remodels tumor microenvironment for pancreatic cancer treatment. *Theranostics* (2023) 13:4016–29. doi:10.7150/thno.83495

30. He Y, Li W, Zhang X, Cui Z. Oncolytic virus targeted therapy for glioma *via* intravenous delivery. *Adv Healthc Mater* (2025) 14:e2404965. doi:10.1002/adhm.202404965

31. Zhong L, Gan L, Wang B, Wu T, Yao F, Gong W, et al. Hyperacute rejection-engineered oncolytic virus for interventional clinical trial in refractory cancer patients. *Cell* (2025) 188:1119–36.e23. doi:10.1016/j.cell.2024.12.010

32. Sánchez-Martínez C, Grueso E, Calvo-López T, Martinez-Ortega J, Ruiz A, Almendral JM. VEGF-virus interactions: pathogenic mechanisms and therapeutic applications. *Cells* (2024) 13:1815. doi:10.3390/cells13211815

33. Jaillon S, Ponzetta A, Di Mitri D, Santoni A, Bonecchi R, Mantovani A. Neutrophil diversity and plasticity in tumour progression and therapy. *Nat Rev Cancer* (2020) 20:485–503. doi:10.1038/s41568-020-0281-y

34. Zhao X, Huang H, Liu M, Wang P, Song S, Cheng Z, et al. *In vivo* neutrophils hitchhiking for tumor targeting and microenvironment regulation boosts oncolytic virus therapy. *Cell Rep Med* (2025) 6:102314. doi:10.1016/j.xcrm.2025.102314

35. Yang H, Shao R, Huang H, Wang X, Rong Z, Lin Y. Engineering macrophages to phagocytose cancer cells by blocking the CD47/SIRPα axis. *Cancer Med* (2019) 8:4245–53. doi:10.1002/cam4.2332

36. Park SY, Jeong MS, Han CW, Yu HS, Jang SB. Structural and functional insight into proliferating cell nuclear antigen. *J Microbiol Biotechnol* (2016) 26:637–47. doi:10.4014/jmb.1509.09051

37. Kwan A, McDermott-Brown I, Muthana M. Proliferating cell nuclear antigen in the era of oncolytic virotherapy. *Viruses* (2024) 16:1264. doi:10.3390/v16081264

38. Minott JA, van Vloten JP, Chan L, Mehrani Y, Bridle BW, Karimi K. The role of neutrophils in oncolytic orf virus-mediated cancer immunotherapy. *Cells* (2022) 11:2858. doi:10.3390/cells11182858

39. Cyrelle Ornella MS, Kim JJ, Cho E, Cho M, Hwang TH. Dose considerations for vaccinia Oncolytic virus based on retrospective reanalysis of early and late clinical trials. *Vaccines (Basel)* (2024) 12:1010. doi:10.3390/vaccines12091010

40. Stegelmeier AA, Chan L, Mehrani Y, Petrik JJ, Wootton SK, Bridle B, et al. Characterization of the impact of oncolytic vesicular stomatitis virus on the trafficking, phenotype, and antigen presentation potential of neutrophils and their ability to acquire a non-structural viral protein. *Int J Mol Sci* (2020) 21:6347. doi:10.3390/ijms21176347

41. Tang S, Shi L, Luker BT, Mickler C, Suresh B, Lesinski GB, et al. Modulation of the tumor microenvironment by armed vesicular stomatitis virus in a syngeneic pancreatic cancer model. *Virol J* (2022) 19:32. doi:10.1186/s12985-022-01757-7

42. Correction: novel oncolytic adenovirus expressing enhanced cross-hybrid IgGA Fc PD-L1 inhibitor activates multiple immune effector populations leading to enhanced tumor killing *in vitro*, *in vivo* and with patient-derived tumor organoids. *J Immunother Cancer* (2021) 9:1. doi:10.1136/jitc-2021-003000corr1

43. Dey A, Zhang Y, Castleton AZ, Bailey K, Beaton B, Patel B, et al. The role of neutrophils in measles virus-mediated oncolysis differs between B-cell malignancies and is not always enhanced by GCSF. *Mol Ther* (2016) 24:184–92. doi:10.1038/mt.2015.149

44. Grote D, Cattaneo R, Fielding AK. Neutrophils contribute to the measles virus-induced antitumor effect: enhancement by granulocyte macrophage colony-stimulating factor expression. *Cancer Res* (2003) 63:6463–8.

45. Viker KB, Steele MB, Iankov ID, Concilio SC, Ammayappan A, Bolon B, et al. Preclinical safety assessment of MV-s-NAP, a novel oncolytic measles virus strain armed with an H. Pylori immunostimulatory bacterial transgene. *Mol Ther Methods Clin Dev* (2022) 26:532–46. doi:10.1016/j.omtm.2022.07.014

46. Yngve E, Eriksson M, Hedin A, Ali A, Jin C, Korsgren O, et al. Biodistribution and toxicity evaluation of oncolytic adenovirus Adf35(OGN) in Syrian hamster and mouse. *Cancer Gene Ther* (2025) 32:297–305. doi:10.1038/s41417-025-00875-y

47. Tang X, Mao X, Ling P, Yu M, Pan H, Wang J, et al. Glycolysis inhibition induces anti-tumor central memory CD8+T cell differentiation upon combination with microwave ablation therapy. *Nat Commun* (2024) 15:4665. doi:10.1038/s41467-024-49059-6

48. Cui C, Chakraborty K, Tang XA, Zhou G, Schoenfelt KQ, Becker KM, et al. Neutrophil elastase selectively kills cancer cells and attenuates tumorigenesis. *Cell* (2021) 184:3163–77.e21. doi:10.1016/j.cell.2021.04.016

49. Yang H, Hreggvidsdottir HS, Palmblad K, Wang H, Ochani M, Li J, et al. A critical cysteine is required for HMGB1 binding to toll-like receptor 4 and activation of macrophage cytokine release. *Proc Natl Acad Sci* (2010) 107:11942–7. doi:10.1073/pnas.1003893107

50. Qian W, Huang L, Xu Y, Lu W, Wen W, Guo Z, et al. Hypoxic ASCs-derived exosomes attenuate colitis by regulating macrophage polarization *via* miR-216a-5p/HMGB1 axis. *Inflamm Bowel Dis* (2022) 29:602–19. doi:10.1093/ibd/izac225

51. Wang S, Kong L, Wang L, Zhuang Y, Guo C, Zhang Y, et al. Viral expression of NE/PPE enhances anti-colorectal cancer efficacy of oncolytic adenovirus by promoting TAM M1 polarization to reverse insufficient effector memory/effector CD8(+) T cell infiltration. *J Exp Clin Cancer Res* (2025) 44:97. doi:10.1186/s13046-025-03358-y

52. Singhal S, Bhojnagarwala PS, O'Brien S, Moon EK, Garfall AL, Rao AS, et al. Origin and role of a subset of tumor-associated neutrophils with antigen-presenting cell features in early-stage human lung cancer. *Cancer Cell* (2016) 30:120–35. doi:10.1016/j.ccell.2016.06.001

53. Price PJ, Luckow B, Torres-Domínguez LE, Brandmüller C, Zorn J, Kirschning CJ, et al. Chemokine (C-C motif) receptor 1 is required for efficient recruitment of neutrophils during respiratory infection with modified vaccinia virus Ankara. *J Virol* (2014) 88:10840–50. doi:10.1128/jvi.01524-14

54. Hwang TH, Moon A, Burke J, Ribas A, Stephenson J, Breitbach CJ, et al. A mechanistic proof-of-concept clinical trial with JX-594, a targeted multi-mechanistic oncolytic poxvirus, in patients with metastatic melanoma. *Mol Ther* (2011) 19:1913–22. doi:10.1038/mt.2011.132

55. Burn GL, Foti A, Marsman G, Patel DF, Zychlinsky A. The neutrophil. *Immunity* (2021) 54:1377–91. doi:10.1016/j.immuni.2021.06.006

56. Herro R, Grimes HL. The diverse roles of neutrophils from protection to pathogenesis. *Nat Immunol* (2024) 25:2209–19. doi:10.1038/s41590-024-02006-5

57. Zhou D, Xu W, Ding X, Guo H, Wang J, Zhao G, et al. Transient inhibition of neutrophil functions enhances the antitumor effect of intravenously delivered oncolytic vaccinia virus. *Cancer Sci* (2024) 115:1129–40. doi:10.1111/cas.16105

58. Naumenko V, Rajwani J, Turk M, Zhang C, Tse M, Davis RP, et al. Repeated dosing improves oncolytic rhabdovirus therapy in mice *via* interactions with intravascular monocytes. *Commun Biol* (2022) 5:1385. doi:10.1038/s42003-022-04254-3

59. Brinkmann V, Reichard U, Goosmann C, Fauler B, Uhlemann Y, Weiss DS, et al. Neutrophil extracellular traps kill bacteria. *Science* (2004) 303:1532–5. doi:10.1126/science.1092385

60. Vorobjeva NV, Pinegin BV. Neutrophil extracellular traps: mechanisms of formation and role in health and disease. *Biochemistry (Mosc)* (2014) 79:1286–96. doi:10.1134/s0006297914120025

61. Agraz-Cibrian JM, Giraldo DM, Mary FM, Urcuqui-Inchima S. Understanding the molecular mechanisms of NETs and their role in antiviral innate immunity. *Virus Res* (2017) 228:124–33. doi:10.1016/j.virusres.2016.11.033

62. Dai W, Tian R, Yu L, Bian S, Chen Y, Yin B, et al. Overcoming therapeutic resistance in oncolytic herpes virotherapy by targeting IGF2BP3-induced NETosis in malignant glioma. *Nat Commun* (2024) 15:131. doi:10.1038/s41467-023-44576-2

63. Mishalian I, Bayuh R, Eruslanov E, Michaeli J, Levy L, Zolotarov L, et al. Neutrophils recruit regulatory T-cells into tumors *via* secretion of CCL17--a new mechanism of impaired antitumor immunity. *Int J Cancer* (2014) 135:1178–86. doi:10.1002/ijc.28770

64. Akkari L, Amit I, Bronte V, Fridlender ZG, Gabrilovich DI, Ginhoux F, et al. Defining myeloid-derived suppressor cells. *Nat Rev Immunol* (2024) 24:850–7. doi:10.1038/s41577-024-01062-0

65. Oo MW, Kawai H, Takabatake K, Tomida S, Eguchi T, Ono K, et al. Resident stroma-secreted chemokine CCL2 governs myeloid-derived suppressor cells in the tumor microenvironment. *JCI Insight* (2022) 7:e148960. doi:10.1172/jci.insight.148960

66. Li C, Xue Y, Yinwang E, Ye Z. The recruitment and immune suppression mechanisms of myeloid-derived suppressor cells and their impact on bone metastatic cancer. *Cancer Rep (Hoboken)* (2025) 8:e70044. doi:10.1002/cnr2.70044

67. Armstrong AJ, Geva R, Chung HC, Lemech C, Miller WH, Hansen AR, et al. CXCR2 antagonist navarixin in combination with pembrolizumab in select advanced solid tumors: a phase 2 randomized trial. *Invest New Drugs* (2024) 42:145–59. doi:10.1007/s10637-023-01410-2

68. Deng H, Lin C, Garcia-Gerique L, Fu S, Cruz Z, Bonner EE, et al. A novel selective inhibitor JBI-589 targets PAD4-Mediated neutrophil migration to suppress tumor progression. *Cancer Res* (2022) 82:3561–72. doi:10.1158/0008-5472.Can-21-4045

69. Ni Y, Zhou X, Tang Y, Ren W, Liang X, Lin Y, et al. SB225002 enhances radiosensitivity in cervical cancer *via* direct neutrophil inhibition and tumor cell suppression. *Cancer Lett* (2026) 638:218153. doi:10.1016/j.canlet.2025.218153

EBM Experimental Biology and Medicine

TYPE Review
PUBLISHED 19 March 2026
DOI 10.3389/ebm.2026.10933

Check for updates

OPEN ACCESS

*CORRESPONDENCE
Kynen Piacentini,
kynen.piacentini@murdoch.edu.au

RECEIVED 15 December 2025
REVISED 14 February 2026
ACCEPTED 04 March 2026
PUBLISHED 19 March 2026
CORRECTED 30 March 2026

CITATION
Piacentini K, Gaitatzis A and Kõks S (2026) Genetics of epilepsy. *Exp. Biol. Med.* 251:10933. doi: 10.3389/ebm.2026.10933

COPYRIGHT
© 2026 Piacentini, Gaitatzis and Kõks. This is an open-access article distributed under the terms of the Creative Commons Attribution License (CC BY). The use, distribution or reproduction in other forums is permitted, provided the original author(s) and the copyright owner(s) are credited and that the original publication in this journal is cited, in accordance with accepted academic practice. No use, distribution or reproduction is permitted which does not comply with these terms.

Genetics of epilepsy

Kynen Piacentini[1,2]*, Athanasios Gaitatzis[1,3] and Sulev Kõks[1,2]

[1]Perron Institute for Neurological and Translational Science, Perth, WA, Australia, [2]Centre for Molecular Medicine and Innovative Therapeutics, Murdoch University, Perth, WA, Australia, [3]Neurology Department, Sir Charles Gairdner Hospital, Nedlands, WA, Australia

Abstract

Epilepsy is one of the most common neurological diseases in the world, but it is also complex and difficult to study. There is a significant genetic component to epilepsy and more information is being published frequently. It is difficult to group and summarise all of this information in a way that is beneficial for both researchers and clinicians. The aim of this paper is to create a summary of all currently known epilepsy associated genes in order to aid epilepsy research to better understand the aetiology of the disease. This was achieved through gathering genetic data from three databases: Online Mendelian Inheritance in Man (OMIM), Clincal Genome (ClinGen), and PubMed. Genes were filtered based on specific criteria and were summarised into three tables: Epilepsy genes, Epilepsy associated genes and Predicted epilepsy associated genes. A fourth table was produced to showcase all epilepsy genes that were identified in all three databases. A total of 2,536 genes were identified to have some level of association with epilepsy. A total of 238 genes were classified as Epilepsy genes, 1,317 genes were classified as Epilepsy associated genes and 981 genes were classified as Predicted epilepsy genes. Finally, 86 genes were identified to be epilepsy genes that were found in all three genetic databases and represent the highest confidence in association with epilepsy. The significance of this study involves the ability to give researchers an up-to-date list of genes that have an association to epilepsy and a summary of information about said genes.

KEYWORDS

disease phenotype, epilepsy, epilepsy associated genes, inheritance pattern, predicted epilepsy associated genes

Impact statement

Epilepsy is a complex neurological disease that involves a huge genetic component that is not fully understood. This study provides a current list of all genes that have some association with epilepsy by grouping each gene on their specific association level. This study identified a total of 2,536 genes that have some level of association with epilepsy compared to a study by Zheng MW, et al. [1] who identified a total of 1506 genes to be associated with epilepsy back in 2023 (published in 2024). This study provides mode/s of inheritance details for each gene, phenotypic details of each gene (Supplementary Table S1) and an overall classification. With this information, researchers are able to gain an insight on an up-to-date catalogue of epilepsy associated genes in which to base their future studies on. Recognition of the genes associated with epilepsy will benefit future

screening strategies and aid in the discovery of the precise clinical molecular diagnosis and how we manage epilepsy.

Introduction

Neurological diseases are inherently complex due to the intricate anatomy and function of the nervous system, the presence of multiple causal and contributing factors, diverse symptoms and diagnostic challenges. Many of these diseases are heritable, meaning that genetic factors play a large role in their development, expression and progression. Epilepsy is the second most prevalent chronic neurological disease with thousands of associated genes contributing to its diverse clinical manifestations, with new genetic links to different types of epilepsy uncovered every year [2]. Advances in next-generation sequencing technologies and bioinformatics have accelerated the discovery of new epilepsy associated genes and our understanding of the disease. Many papers have previously analysed the total number of genes that are associated with epilepsy. In 2017, Wang et al. [3] identified 977 genes that were associated with epilepsy based on clinical-genetic evidence. In 2024, Zhang MW, et al. [1] almost doubled this number identifying 1506 genes that were associated with epilepsy based on the same clinical-genetic evidence. Over the past several years a significant number of epilepsy associated genes has been identified. Many novel genes have been introduced and many are no longer considered to be associated with epilepsy. With an ever changing and evolving list of epilepsy associated genes, studies need to be continuously updated to aid epilepsy research. Many previous papers have focussed on providing a list of genes that can be potentially useful in clinical genetic diagnosis and precise treatment of epilepsy. To update the current list of epilepsy associated genes we utilised three major databases, this includes the Online Mendelian Inheritance in Man (OMIM) database, PubMed and ClinGen. The purpose of this study is to group together all genes potentially associated with epilepsy to specifically aid genetics research in the field of epilepsy.

Methods

To update the list of genes associated with epilepsy, a systematic study was conducted based on data from several online databases until November 2025. After obtaining and filtering through the list of genes identified from the OMIM, ClinGen and PubMed database, genes were grouped into three categories: "Epilepsy genes" (Table 1), "Epilepsy associated genes" (Table 2) or "Predicted epilepsy associated genes" (Table 3) based on independent criteria for each database. Requirements for each category can be found in Supplementary Table S1. A table was produced for each category showcasing the current list of genes associated with epilepsy as well as the mode of inheritance and phenotype. Another table (Table 4) was created to summarise all epilepsy genes that were identified in all databases that includes each genes phenotype/s and mode/s of inheritance. The phenotypes found in Table 4 were database derived and formatted and confirmed manually.

Genes were first searched in the OMIM database[1] using the following terms: epilepsy, epilepsies, epileptic, convulsion, convulsions, seizure, seizures. The OMIM database utilises a phenotype map key to further characterise each gene. We took advantage of this key to categorise genes into their respective categories. The phenotype map key is comprised of four types, this includes [2] there is a gene-disease relationship, however the underlying genetic defect is unknown according to the University of California Santa Cruz (UCSC) genome browser [3]; the gene has been included through linkage analysis (mapping studies), however a specific gene mutation has yet to be identified [1]; the molecular basis of the disorder is known and a mutation has been identified [4]; the disorder is a contiguous gene deletion or duplication syndrome (multiple genes are deleted or duplicated) according to the UCSC genome browser. Genes from the OMIM database were categorised as "Epilepsy genes" if they had a phenotype map key of 1 and the phenotype included at least one of the key words that was originally searched. Genes were categorised as "Epilepsy associated genes" if the phenotype map key was 1,3 and/or 4 and the phenotype did not include one of the epilepsy key words. Finally, genes were grouped into the "Predicted epilepsy associated genes" category if the phenotype map key was 2 or blank and the phenotype did not include one of the epilepsy key words.

ClinGen[2] was the second database utilised where we included all genes in the gene-disease validity section. Genes were grouped into the three categories based on their classification and phenotype. Classifications included disputed, limited, moderate and definitive. Genes were immediately excluded if their classification was disputed. Only genes with one of the epilepsy key words as previously mentioned were included. Genes were added to the current "Epilepsy genes" list if they were classified as definitive, genes were added to "Epilepsy associated genes" if they were classified as moderate and genes were added to "Predicted epilepsy associated genes if they were classified as limited.

The final database utilised was PubMed[3] where we followed a similar procedure as the OMIM database. Genes were added to the list based on if the key words were included in its respective phenotype. Only genes found in *homo sapiens* were recorded for this study. Genes that did not included one or more of the epilepsy key words were assigned to the Epilepsy associated genes

1 https://www.omim.org/

2 https://clinicalgenome.org/

3 https://pubmed.ncbi.nlm.nih.gov/

group. We understand that the PubMed database is a literature database rather than a curated gene-disease resource. To resolve this, genes found only within the PubMed database, the highest level of classification they received was "Epilepsy associated genes." Priority was given to the other databases OMIM and ClinGen as they are curated gene-disease resources. To resolve conflicting classifications across the three databases, a predefined hierarchical evidence framework was applied. Gene categories were ranking according to confidence level where the highest confidence classification was "Epilepsy genes" and the lowest was "Predicted epilepsy associated genes". When a gene was assigned to multiple categories across different databases, the highest confidence classification was retained as the final group. This approach ensured consistent prioritisation based on evidence strength rather than source frequency.

Results

The present study filtered through a list of 3686 epilepsy-associated genes from OMIM, 1977 epilepsy-associated genes from PubMed and 3334 genes from ClinGen and grouped the genes according to their potential associated with epilepsy and the mode of inheritance. These genes included 238 epilepsy genes, 1317 epilepsy associated genes, and 981 predicted epilepsy associated genes, which were recruited from OMIM, and genes were added from ClinGen and PubMed accordingly. The distribution of these genes between the databases is illustrated in Figure 1A and the distribution of the modes of inheritance is illustrated in Figure 1B. Therefore, based on the criteria of this study, a total of 2536 genes currently have some association with epilepsy.

Epilepsy genes

Overall, 238 genes were classified as epilepsy genes compared to that of 168 epilepsy genes found by Zhang MW, et al. [1]. These 238 genes were listed according to their mode of inheritance as stated within each genetic database, many of which have multiple modes of inheritance. Most epilepsy genes (58.0%) were of autosomal recessive inheritance; 48.7% genes were of autosomal dominant inheritance; and 4.2% genes were of X-linked inheritance. Notable phenotypes for epilepsy genes include encephalopathy (43.7%), neurodevelopmental disorder (23.5%), microcephaly (8.4%), myoclonic (8.0%), and hypotonia (7.1%). All genes found in this category suggested a mode of inheritance that was either autosomal or X-linked, except for PIGT. This gene included the mode of inheritance, somatic mutation.

Epilepsy associated genes

A total of 1317 genes were categorised as epilepsy associated genes in this study compared with the study by Zhang MW, et al. [1] who identified 974 epilepsy-related genes. These 1317 genes were listed according to their mode of inheritance as stated within each genetic database with many having multiple modes of inheritance. Most epilepsy genes were of autosomal recessive inheritance (65.1%); 34.1% genes were of autosomal dominant inheritance; and 8.2% genes were of X-linked inheritance. Notable phenotypes for epilepsy genes include mitochondrial

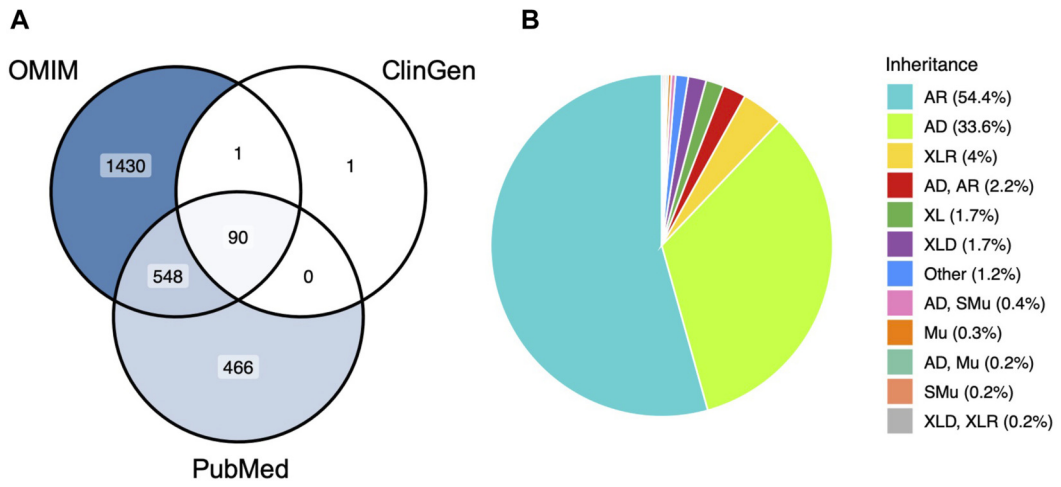


FIGURE 1
The overall organisation of epilepsy associated genes. **(A)** Distribution of epilepsy associated genes between databases after filtering. **(B)** Distribution of the 11 most common modes of inheritance from the 2536 epilepsy associated genes. AR: autosomal recessive; AD: autosomal dominant; XL: X-linked; XLR: X-linked recessive; XLD: X-linked dominant; SMu: somatic mutation; Mu: multifactorial.

TABLE 1 Epilepsy genes.

Inheritance	Genes
AD	*AGO1, AP2M1, ARFGEF1, ATN1, ATP1A1, ATP1A3, ATP6V0C, CACNA1A, CACNA1C, CACNA1E, CACNA1I, CDK19, CELF2, CHD2, CHRNA2, CHRNA4, CHRNB2, CUL3, CUX2, CYFIP2, DHX16, DLL1, EEF1A2, FBXO28, FGF12, FZR1, GABRA1, GABRA5, GABRB1, GABRB2, GABRB3, GABRG2, GNAO1, GRIA4, GRIN2A, GRIN2B, GRIN2D, HCN1, HECW2, HNRNPU, IRF2BPL, KCNA2, KCNB1, KCNC1, KCNC2, KCNH5, KCNK4, KCNQ2, KCNT1, KCNT2, LGI1,* ***MARCHF6****, MAST3, NACC1, NBEA, NCDN, NEUROD2, NPRL2, NPRL3, NSF, NTRK2, PACS2, PAK1, PHACTR1, PHF21A, PPP3CA, PRRT2, RHOBTB2, RNF13, RORA, SAMD12, SCN1A, SCN2A, SCN3A, SEMA6B, SERPINI1, SETD1A, SETD1B, SIK1, SLC1A2, SLC32A1, SLC6A1, SNAP25, SPTAN1, STARD7, STX1B, TANC2,* ***TCP1****, WASF1, YWHAG*
AD | AR	*ATP6V0A1, CACNA1D, CLCN3, EXT2,* ***EIF4A2****, GLS, KCNQ3, TBC1D24, ATP1A2, GLUL, KCNMA1, DIAPH1, DNM1, SCN1B, STXBP1, CPA6, ACTL6B, ATP6V1A, DEAF1, GRIK2, GRIN1, DEPDC5, NARS1, NUS1*
AD | AR | SMu	*PIGT*
AR	*ABCA2, ADAM22, ADARB1, ADPRS,* ***AFG2A****, ALDH7A1, AP3B2, ARV1, ASAH1, BRAT1, CACNA1B, CACNA2D1, CACNA2D2, CAD, CERS1, CHKA, CLN8, CNPY3, CNTN2, CPLX1, CPSF3, CSTB, DENND5A, DHPS, DOCK7, EMC10, EPM2A, ESAM, EXOC7, FRRS1L, GAD1, GOSR2, GOT2, GRM7, GTF3C3, HACE1, HECTD4, HID1, IER3IP1, ITPA, KCTD7, LIAS, LNPK, MDH2, MED11, MED17, MED23, MTHFS, NAPB, NECAP1, NHLRC1, NRROS, NSRP1, OTUD6B, OTUD7A, OXR1, P4HTM, PARS2, PDE2A, PI4K2A, PIGB, PIGF, PIGK, PIGN, PIGP, PIGQ, PIGS, PIGU, PLCB1, PLPBP, PNKP, PNPO, PPFIBP1, PRICKLE1, PRMT7, PTPN23, QARS1, RTN4IP1, RTTN, SARS1, SCARB2, SLC13A5, SLC25A12, SLC25A22, SLC31A1, SLC35A3, SLC38A3, SLC7A6OS,* ***SNF8****, SNIP1,* ***SPOUT1****, ST3GAL3, STRADA, SV2A, SYNJ1, SZT2, TBC1D2B, TIAM1, TRAK1, TRAPPC4, TRAPPC6B, TUBGCP2, UBA5, UGDH, UGP2, VARS1, VPS50, WARS2, WDR4, WDR45B, WWOX, YIPF5*
XL	*ALG13, ARHGEF9, GABRA3, PCDH19, SYN1*
XLD	*CDKL5, SMC1A*
XLR	*PIGA, ARX*
XLD | XLR	*FGF13*

AD, autosomal dominant; AR, autosomal recessive; XL, X-linked; XLD, X-linked dominant; XLR, X-linked recessive; DR, digenic recessive; Mu, multifactorial inheritance; SMu, somatic mutation; SMo, somatic mosaicism; DD, digenic dominant; PR, psuedoautosomal recessive; UN, unknown. Genes that have been identified in this study that were not present within the Zhang MW, et al. [1] have been highlighted in bold.

dysfunction (8.9%), neurodevelopmental disorder (6.8%), microcephaly (3.6%), encephalopathy (2.5%) and hypotonia (2.5%). The gene DHRSX was the only gene in the entire study to have a suggested mode of psudoautosomal recessive.

Predicted epilepsy associated genes

A total of 981 genes were categorised as predicted epilepsy associated genes in this study compared with the study by Zhang MW, et al. [1] who identified 364 neurodevelopment-related genes. These 981 genes were listed according to their mode of inheritance as stated within each genetic database with the majority having multiple modes of inheritance. Common modes of inheritance include autosomal recessive inheritance (20.9%), autosomal dominant inheritance (18.7%), and unknown mode of inheritance (68.2%). Notable phenotypes for epilepsy genes include unknown phenotype (16.6%), mitochondrial dysfunction (4.5%), encephalopathy (3.2%), neurodevelopmental disorder (1.1%) and immunodeficiency (1.1%).

Frequently reported/identified epilepsy genes

A total of 86 epilepsy genes have been reported/identified in all three databases analysed in this study and have been classified as epilepsy genes. Along with each associated phenotypes and mode of inheritance. Figure 1A states that there are 90 genes that have been identified and filtered from all three databases. The genes ABAT and DPM2 were excluded due to their placement in the category epilepsy associated genes and the genes GABRD and SLC12A5 were excluded due to their placement in the category predicted epilepsy associated genes.

Notable phenotypes for the common epilepsy genes (Table 4) include encephalopathy (48.8%), neurodevelopmental disorder (12.8%), myoclonic (10.5%), microcephaly (8.1%) and hypotonia (3.5%). When comparing the phenotype distribution of the frequently reported/identified epilepsy genes (Table 4) to the phenotype distribution of epilepsy genes (Table 1) there is some variation. There is a 5.1% increase with the encephalopathy phenotype compared to the epilepsy genes found in Table 1. There is a 10.7% decrease with the neurodevelopmental disorder phenotype, a 2.5% increase with the progressive myoclonic phenotype, a 0.3% decrease with the microcephaly phenotype

TABLE 2 Epilepsy associated genes.

Inheritance	Genes
AD	*ACTA2, ACTB, ACTG1, ACVR1, **ACVRL1**, ADGRL1, ADNP, AFF3, AGO2, AHDC1, AKT2, AKT3, ANK2, ANKH, ANKRD11, ANKRD17, APP, ARCN1, ARF1, **ARHGAP31**, ARID1A, ARID1B, ARID2, ASH1L, ASXL1, ASXL2, ASXL3, ATP2B1, ATP6V1B2, ATXN10, AUTS2, BCL11B, BICD2, BICRA, BMP4, BRAF, BRPF1, CACNA1G, **CALM1**, CALM2, CAMK2B, CAMK2G, CAMTA1, **CAPRIN1**, CCM2, **CCT3**, **CD96**, CDC42, CDC42BPB, CDK13, CDK8, CEP85L, CERT1, CHAMP1, **CHASERR**, CHD1, CHD3, CHD5, CHD8, CHN1, CIC, CLCN6, CLDN11, CLTC, CNOT1, CNOT3, CREBBP, CSNK2A1, CSNK2B, CTNNB1, CUX1, **CYP2C9**, DAGLA, **DDX6**, DHX30, **DHX9**, DIP2B, DLG4, **DMPK**, DNAJC5, DNMT1, DNMT3A, DPYSL5, **DUSP6**, DYNC1H1, DYRK1A, EBF3, EED, EFTUD2, EHMT1, ELN, ENG, EZH2, FAM111A, FBXO11, **FBXW11**, FBXW7, **FGF14**, FGF8, FGFR1, **FOSL2**, FOXG1, FOXP1, **FOXP2**, FRMD5, **FRYL**, FXYD2, GABBR1, GARS1, GATA3, GATA6, GATAD2B, GFAP, GLI2, GLI3, GLUD1, GNA11, GNAI1, **GNAS**, GNB1, **GPRC5B**, GRIA2, H3-3A, H3-3B, H4C3, H4C5, HDAC4, HIVEP2, **HNRNPC**, **HNRNPH1**, **HNRNPR**, **HRAS**, **JPH3**, KANSL1, KAT5, KAT6A, KAT8, KCNA1, KCND3, KCNE2, KCNH1, KCNH2, KCNJ2, KCNJ5, KCNJ6, KCNQ5, KDM3B, KDM4B, KDM6B, KIF11, KIF2A, KIF5C, KMT2A, KMT2C, KMT2D, KMT2E, KMT5B, KRAS, KRIT1, LMBRD2, LMNB1, LMX1B, LRP12, **LRRC8C**, MACF1, MAF, MAGEL2, MAP2K1, MAPK1, MAPK8IP3, MAPRE2, MAST1, MATR3, MBD5, MED12L, MED13, MED13L, MEF2C, MEN1, **MIB1**, MN1, **MSL2**, MSX2, MTOR, MTSS2, **MYCN**, MYOCD, MYRF, MYT1L, NAA15, NEDD4L, NFE2L2, NFIA, NFIB, NIPA1, NIPBL, **NLRP3**, NOTCH1, NOTCH2, NOTCH2NLC, NOVA2, NPTX1, NR2F1, NR4A2, NSD1, NSD2, OTX2, PACS1, PAFAH1B1, **PANX1**, PAX2, **PDCD10**, **PDGFB**, PDYN, PIK3R2, **PNKD**, POGZ, POLR2A, POU3F3, PPFIA3, PPP1R12A, PPP2CA, PPP2R1A, **PPP2R5C**, PPP2R5D, PRKAG2, PRKAR1B, PROK2, PROKR2, **PRPF6**, **PRR12**, PSEN2, PSMD12, PTCH1, PTPN11, PUF60, PUM1, PURA, RAB11B, RAC1, RAC3, RALA, **RAP1B**, RFX7, RNF125, RNF2, **RNU4-2**, RRAGD, RYR2, SATB1, SATB2, SCAF4, **SCN2B**, SET, SETBP1, SETD2, SETD5, **SF3B2**, SGCE, SIAH1, SIN3A, SIX3, **SLC17A8**, SLC1A3, SLC20A2, SMAD2, **SMAD4**, SMARCA2, SMARCC2, **SMARCD1**, **SNRPE**, SNTA1, SON, SOX2, SOX4, SOX5, **SOX6**, SPAST, SPEN, SPOP, SPTBN1, SPTLC2, SRCAP, SRP54, **SRSF1**, STAG1, **STOX1**, SUPT16H, SYNGAP1, **SYT1**, **TAF4**, TBL1XR1, TBX1, TCF20, TCF4, **TEK**, TLK2, TMEM106B, **TMEM151A**, TMEM163, TMEM63A, TNPO2, TOP2B, TRAF3, TRAF7, TRIM71, TRIM8, TRIO, TRIP12, TSC1, TUBA1A, **TUBB**, TUBB2A, TUBB2B, TUBB3, TUBB4A, TUBG1, U2AF2, **UBAP2L**, UBE3A, UBTF, USP7, VAMP2, VPS4A, WAC, WDR26, WDR37, XPR1, ZBTB18, ZEB2, ZMIZ1, ZMYM2, ZMYND11, ZNF292, ZSWIM6*
AD | AR	*ABCC8, FGFR3, FTL, GCM2, KCNJ11, SLC16A1, CRYAB, ACOX1, AFG3L2, ALDH18A1, AP1G1, **CFAP43**, CLCN1, CLPB, COL18A1, COL3A1, DCHS1, DHX37, DSTYK, ERLIN2, FAR1, GCK, GRM1, HPD, HTT, IFIH1, KIF1A, MFN2, **MYH3**, NALCN, **PLG**, POLR1A, POLR3B, PPOX, PROC, PROS1, RBP4, **SAMD9**, SCN9A, **SCNN1G**, SLC12A2, SLC25A4, SQSTM1, STAT1, STT3A, STUB1, THRB, YARS1, **AQP2**, **DISP1**, GLRA1, HESX1, OPLAH, POLRMT, PTH, **SPG7**, TET3, ZFP57, DNM1L, EIF2AK2, ITPR1, ALPL, ATAD3A, GCH1, GRN, ALG8, AP4E1, BSCL2, COG4, CSF1R, ELOVL4, **EVC2**, FH, **GH1**, GJA1, **GNE**, HEPACAM, **HK1**, HMBS, HSPD1, INSR, KCNE1, **KLHL24**, KLHL7, OPA3, ORAI1, PARN, PDE10A, PNPT1, POLG, POMP, PPP2R3C, **RHAG**, RRM2B, RTN2, RYR3, SCN4A, SCO2, SDHA, SDHD, SLC12A6, SLC33A1, TWNK, WARS1, **CHRNA1**, ACO2, PEX6*
AD | AR | DD	*ADGRV1*
AD | AR | IC	*SDHB*
AD | DD	*CAV3*
AD | IC	*RAI1*
AD | SMo	*PRKACB*
AD | SMu	*NF1*
AR	*AASS, ABAT, ABHD12, ABHD16A, **ACACA**, **ACAD8**, ACADM, ACADS, ACADSB, **ACBD6**, ACSF3, ACY1, ADA2, ADAMTSL2, **ADAT3**, ADD3, ADGRG1, ADK, ADSL, **AFG2B**, AGA, AGL, AGPS, **AHCY**, AHI1, AIMP1, AIMP2, ALDH3A2, ALDH4A1, ALDH5A1, ALDOB, ALG1, ALG11, ALG12, ALG2, ALG3, ALG6, ALG9, ALKBH8, AMACR, AMFR, AMT, ANK3, ANKLE2, ANO10, AP4B1, AP4M1, AP4S1, APC2, ARFGEF2, ARG1, ARHGDIA, ARL6IP1, ARMC9, ARSA, ASL, ASNS, ASPA, ASPM, ASS1, ATAD1, ATG7, ATIC, ATP13A2, ATP5F1D, ATP5F1E, ATP5PO, ATP6V0A2, ATP9A, AUH, B3GALNT2, **B3GAT3**, **B4GALT1**, B4GAT1, BCAS3, BCKDHA, **BCKDHB**, BCKDK, BCS1L, **BET1**, **BIN1**, BLOC1S6, **BLTP1**, BOLA3, **BORCS8**, BTD, C12orf57, C2orf69, **CA8**, CAMSAP1, CAPN15, **CAPNS1**, CARD9, **CARS1**, CARS2, **CASP2**, CASQ2, **CBS**, CC2D1A, CC2D2A, CCBE1, CCDC88A, CD59, CDK10, **CDK5RAP2**, **CEP135**, **CEP152**, CEP164, CHKB, CIT, CKAP2L, CLDN16, CLN3, CLN5, CLN6, CLP1, CLPP, CNTNAP1, **COA8**, COASY, **COG3**, COG5, COG6, COG7, COLGALT1, COPB1, COQ4, COQ6, COQ8A, COQ9, CORO1A, COX10, COX11, COX15, COX4I1, COX6B1, CPT1A, CRADD, CRB2, CRBN, CRIPT, CRLF1, CRLS1, CSPP1, CTC1, CTH, CTNNA2, CTSA, CTSD, CTSF, **CTU2**, CYB5R3, CYP27A1, CYP27B1, D2HGDH, DAP3, DARS2, DBH, DBT, DCAF17, DDHD2, DDX59, DEGS1, **DGUOK**, DHCR24, **DHCR7**, DHFR, **DIS3L2**, DLD, DNAJC12, DNAJC21, DNAJC6, **DOCK3**, DOCK6, DOCK8, DOHH, DOLK, DPAGT1, DPH1, DPH5, DPM1, DPM2, DPP9, DPYD, DPYS, **DRG1**, **DST**, DTYMK, DYNC1I2, EARS2, ECHS1, ECM1, **EDEM3**, **EEF1D**, **EEFSEC**, EIF2B1, EIF2B2, EIF2B3, EIF2B4, EIF2B5, EIF3F, ELP2, EMC1, **EMG1**, EML1, ENTPD1, EPG5, **EPRS1**, **ERCC8**, ESCO2, **ETFA**, **ETFB**, ETFDH, ETHE1, EXOC2, EXOSC3, EXOSC5, EXOSC9, EXTL3, FA2H, FADD, **FAM177A1**, FANCA, FARS2, FARSB, FASTKD2, FAT4, FBP1, FBXL4, FBXO22, FCHO1, FCSK, FDFT1, **FDXR**, **FILIP1**, **FITM2**, FKTN, **FLVCR1**, FLVCR2, FMN2, FOLR1, FOXRED1, FRA10AC1, **FUCA1**, FUT8, **FXN**, GALC, GALNT2, GAMT, GCDH, GCSH, GEMIN4, GFER, GFM1, GFM2, **GIPC3**, GLB1, GLDC, GLE1, GLRB, **GLRX5**, GLYCTK, GM2A, GMPPB, GNB5, GNPAT, **GNS**, GOLGA2, GPAA1, GPHN, GPSM2, GPT2, GPX4, **GRID2**, GSS, **GSX2**, **GTPBP1**, GTPBP2, GTPBP3, **GUCY1A1**, GYS1, GYS2, **HADH**, HADHA, HADHB, HAX1, HERC1, HEXB, HGSNAT, HHAT, HIBCH, HINT1, HLCS, HMGCL, HMGCS2, **HOXA1**, HPDL, HSD17B4, HYCC1, IARS1, IARS2, IDH3A, IFNAR1, **IL7**, **IMPA1**, INPP5K, INTS1, INTS11, IQSEC1, IREB2, ISCA1, ISCA2, ISG15, **IVD**, JAM2, JAM3, KATNB1, **KCNJ1**, KCNJ10, **KCNJ16**, KDM5A, KDM5B, **KICS2**, **KIF26A**, KLC2, KNL1, KPNA7, KPTN, L2HGDH, LAMA2, LAMB1, LAMC3, LARS2, LCP2, **LDHD**, LETM1, LGI3, LGI4, LIG3, LINGO1, LINS1, LIPT2, LMBRD1, LONP1, LRP2, LRPPRC, **LRRK1**, LSS, **LYST**, MAD1L1, MADD, MAGI2, MAN1B1, **MAN2B2**, MANBA, MAPKAPK5, MBOAT7, **MC2R**, MCCC1, MCCC2, MCM3AP, **MCPH1**, **MECR**, **MED16**, MED25, MED27, MEGF10, METTL23, METTL5, MFF, MFSD2A, MFSD8, MGAT2, MGP, MICOS13, MICU1, MIPEP, MKS1, MLC1, MLYCD, MMAA, MMACHC, MMADHC, MOCS1, MOCS2, MOGS, MPC1, MPDU1, MPDZ, MPI, MPV17, MRAP, MRM2, **MRPL39**, **MRPL49**, MRPS22, MTFMT, MTO1, MTX2, MYMK, MYO5A, MYORG, **NAA20**, **NAA60**, NADK2, NAE1, NAGA, **NAGS**, NANS, **NAV3**, NAXD, NAXE, NBAS, NCAPD3, NDE1, NDST1, **NDUFA11**, NDUFA2, NDUFA6, NDUFA8, NDUFAF2, NDUFAF3, NDUFAF4, NDUFAF5, NDUFAF6, NDUFAF8, NDUFB8, NDUFC2, **NDUFS1**, NDUFS3, NDUFS4, **NDUFS6**, NDUFS7, NDUFS8, NDUFV1, NDUFV2, NEU1, **NEUROG1**, NFASC, NFS1, NFU1, NGLY1, **NHLRC2**, NNT, NPC1, NPC2, NRCAM, NSUN2, NSUN3, **NSUN6**, **NT5E**, NTNG2, NTRK1, NUBPL, **NUP188**, **NUP62**, OCLN, OGDH, OSGEP, OSTM1, PANK2, PC, PCCA, PCCB, PCDH12, PCDHGC4, PCK1, PCLO, PCNT, PCYT2, PDHB, PDHX, PDP1, **PDSS1**, PDSS2, **PDXK**, PDZD8, PET100, PEX1, PEX10, PEX12, PEX13, PEX14, **PEX16**, PEX19, PEX2, PEX26, PEX5, PEX7, **PFKM**, PGAP1, PGAP2, PGAP3, PGM1, PGM2L1, PGM3, PHGDH, PHKG2, PI4KA, PIBF1, PIDD1, PIGC, PIGH, PIGL, PIGM, PIGO, PIGV, PIGW, PIGY, **PINK1**, **PISD**, PITRM1, PKHD1L1, PLA2G6, PLAA, PLCH1, PLEKHG2, **PLK4**, **PLOD3**, PLVAP, PLXNA1, PMM2, PMPCB, POLR3A, POLR3K, POMGNT1, POMT1, POMT2, PPCS, PPIL1, PPP1R15B, **PPP1R21**, PPT1, PRDM13, PRDX1, PRF1, PRKDC, PRKN, **PROP1**, PRORP, PRUNE1, PSAT1, PSMB8, PSPH, **PTCD3**, **PTF1A**, **PTPMT1**, PTRH2, **PTRHD1**, PTS, **PUS1**, PUS3, PYCR2, QDPR, RAB18, RAB27A, RAB3GAP1, RAB3GAP2, RALGAPA1, **RAP1GDS1**, RAPSN, RARS1, RARS2, RBCK1, RBL2, RBM8A, RBSN, **RECQL4**, RFT1, RMND1, RNASEH2A, RNASET2, **RNU4ATAC**, RNU7-1, ROGDI, RPIA, RSRC1, RUBCN, RUSC2, SACS, SASS6, SCYL1, SCYL2, SELENOI, SEPSECS, SERAC1, SGPL1, SGSH, **SIL1**, SLC12A1, SLC12A3, SLC17A5, SLC18A2, SLC19A2, SLC19A3, SLC1A4, SLC25A1, SLC25A13, SLC25A15, SLC25A19, SLC25A20, SLC25A3, SLC25A36, SLC25A42, SLC25A46, SLC26A4, SLC35A1, SLC35C1, SLC39A8, SLC44A1, SLC45A1, SLC46A1, SLC4A10, SLC5A6, SLC6A19, SLC6A9, SLC9A1, SMARCAL1, SMC5, SMG9, SMO, SMPD4, SNAP29, **SNAPC4**, SNORD118, SNX14, SPTBN4, SQOR, SRD5A3, ST3GAL5, STAMBP, STAR, STAT2, STIL, STT3B, STX11, STXBP2, SUCLA2, SUCLG1, SUMF1, SUOX, SURF1, SVBP, TAF13, TAF2, TAF8, TANGO2, TARS2, TASP1, TBC1D20, TBC1D23, **TBC1D7**, TBCD, TBCE, TBCK, TBX19, TCIRG1, TDP2, TECPR2, **TEFM**, TELO2, **TGDS**, THG1L, THOC6, THUMPD1, TIMM50, TIMMDC1, TMCO1, TMEM147, TMEM165, TMEM222, TMEM70, TMEM94, TMTC3, TMX2, TOE1, **TOP6BL**, TP53RK, **TP73**, TPK1, TPP1, TRAPPC10, TRAPPC11, TRAPPC12, TRAPPC2L, TRAPPC9, **TRIM2**, TRIP13, TRIT1, TRMT1, TRMT10A, TRMT5, TRNT1, TRPM6, TSEN15, TSEN2, TSFM, TSPYL1, TTC5, TTI1, **TTI2**, TUBGCP6, TYROBP, **UBE3B**, UBE3C, UBE4A, UBR7, UFC1, UFM1, UNC13D, UNC80, UPB1, UQCC2, USP18, USP53, VARS2, **VDR**, VLDLR, **VMA22**, VPS13A, VPS13B, VPS13D, VPS35L, VPS41, VPS51, VPS53, WASHC4, **WBP4**, WDR62, WDR73, **WDR81**, **WDR83OS**, **WLS**, XPNPEP3, YIF1B, YRDC, ZBTB11, ZFYVE26, ZMPSTE24, ZNF142, ZNF335, ZNF526, ZNF668, ZNFX1, ZNHIT3*

(*Continued*)

TABLE 2 Continued

Inheritance	Genes
AR | SMu	*PAX7*
PR	***DHRSX***
SMu	***MAP3K3***
SMu | XLD	*SLC35A2*
XL	***ABCB7***, *CNKSR2, DCX, FRMPD4, GLA, GLRA2, HUWE1, NONO, OTC,* ***RLIM***, *RNF113A, SLITRK2, TFE3, THOC2, XK, ZDHHC9*
XLD	***ACSL4***, *AMER1, BCOR,* ***CCNQ***, *CLCN4, GDI1, HCCS, HNRNPH2, HSD17B10, IQSEC2, KDM6A, MSL3, NEXMIF, PDHA1,* ***RPS6KA3***, *TCEAL1, WDR45, NHS, SLC9A6, FMR1,* ***PLS3***
XLR	*ABCD1, AIFM1, ANOS1, AP1S2,* ***ARSL***, *ATP6AP1, ATP7A, AVPR2, BCAP31, BCORL1,* ***C1GALT1C1***, ***CD40LG***, *CHRDL1, CUL4B, DLG3, EIF2S3, FAM50A, FGD1, FTSJ1, GK,* ***GPC3***, *GRIA3, HCFC1, HPRT1, IDS, IL1RAPL1, KDM5C, KIF4A, KLHL15, LAGE3,* ***LAS1L***, ***MAGT1***, *MAOA, NDUFA1, OCRL, OGT, OPHN1, OTUD5, PAK3, PGK1, PHF6, PLP1,* ***POLA1***, *PQBP1, RAB39B, RBM10,* ***SH2D1A***, *SLC6A8,* ***SLC9A7***, *SMS, SSR4, STS, SYP, TAF1, UBE2A, USP27X,* ***WNK3***, ***ZRSR2***, *CASK,* ***PRPS1***
XLD | XLR	*NAA10, IKBKG, ATRX, EBP, MED12, NSDHL, DDX3X, NDP, USP9X, ZC4H2*
UN	***CD2AP***, *COG8, EMX2, GNAQ, IDH2,* ***IKZF2***, *KCNK9,* ***NR4A3***, *PIK3CA, SEZ6,* ***SEZ6L***, ***SEZ6L2***, *SPR*

AD, autosomal dominant; AR, autosomal recessive; XL, X-linked; XLD, X-linked dominant; XLR, X-linked recessive; DR, digenic recessive; Mu, multifactorial inheritance; SMu, somatic mutation; SMo, somatic mosaicism; DD, digenic dominant; PR, psuedoautosomal recessive; UN, unknown. Genes that have been identified in this study that were not present within the Zhang MW, et al. [1] have been highlighted in bold.

and a 3.6% decrease with the hypotonia phenotype compared to the epilepsy genes phenotype distribution.

Discussion

The aim of the present study was to provide a list of the current genes that are or have a predicted association with epilepsy. Previously, a study by Zhang MW, et al. [1] identified 1440 epilepsy associated genes based on OMIM, PubMed and the human genome mutation database (HGMD). The epilepsy keywords that were searched within each database remain the same between this study and the one performed by Zhang MW, et al. The current study identified a list of 2,536 epilepsy associated genes based on experimental and clinical evidence as provided by the three databases: OMIM, ClinGen and PubMed. This was done by evaluating gene-disease associations that involved multiple aspects of evidence and characteristics. The wide acceptance of genes from these three databases allowed for the incorporation of more potentially disease-associated genes, giving researchers a broader catalogue of genes to study. To aid in this endeavour, genes were categorised into three categories based on the level of currently known association to epilepsy.

This study identified 238 genes (Table 1) that are classified as epilepsy genes, which is more than that of Zhang MW, et al. [1] who classified 168 genes as epilepsy genes. It is important to note that the comparison of results made between this study and the study by Zhang MW, et al. [1] used different parameters and databases. Most of the epilepsy genes identified in this study had a phenotype of encephalopathy (43.7%) which is to be expected when looking at a list of genes with the strongest link to epilepsy.

This study identified 1317 genes (Table 2) that are classified as epilepsy associated genes, which is more than that of Zhang MW, et al. [1] who classified 364 neurodevelopment-associated epilepsy genes. Most of these genes had a phenotype of mitochondrial dysfunction (8.9%) and neurodevelopmental dysfunction (6.8%). This category produced the largest list of genes which also produced the largest variation in phenotypes. This explains the lower distribution percentages of each phenotype listed.

This study identified 981 genes (Table 3) that are classified as predicted epilepsy associated genes, which is more than that of Zhang MW, et al. [1] who classified 974 genes as epilepsy-related genes. Most of these genes had an unknown phenotype (16.6%) but were still classified into potential epilepsy associated genes by the databases looked at in this study.

Finally, we provided a list of 86 genes (Table 4) that are categorised as epilepsy genes and were identified in all databases. Summarised phenotypes have been included for each of these genes. Some of the least published genes from this list include *FRRS1L, NECAP1, NSRP1, QARS1* and *VARS1*. The ferric chelate reductase 1 like protein (*FRRS1L*) is a protein coding gene that encodes an important receptor protein in the brain and modulates glutamate signalling. Loss of the *FRRS1L* gene has shown to disrupt synaptic AMPA receptor function resulting in neurodevelopmental, motor and cognitive abnormalities [5]. Variants in this gene have caused epileptic encephalopathy with hyperkinetic movements [6] and epileptic-dyskinetic encephalopathy [7]. NECAP endocytosis associated 1 (*NECAP1*) is a coding gene that produces a protein that localises to clathrin-coated vesicles, where it binds components of the adapter protein complexes and aids in endocytosis. This gene has been linked to early onset epileptic encephalopathy through next-generation sequencing [8]. However, the genetic aetiology of *NECAP1* remains to be fully understood. *NSRP1* is involved in developmental process and regulation of alternative mRNA splicing, via spliceosome. This gene has been associated with breast cancer [9], spastic cerebral palsy and epilepsy [10]. These papers are both recent and introductory into the investigation of connecting this gene to an association with a disease phenotype. *QARS1* is involved with dendritic and axonal development. This gene has been associated

TABLE 3 Predicted epilepsy associated genes.

Inheritance	Genes
AD	***ABCC11***, AKAP9, ALG10B, ***APOL2***, ***APOL4***, ***APOLD1***, ATP11A, ATP2A2, BAP1, BPTF, CACNA1H, CACNB4, CACNG2, CALM3, ***CHI3L1***, COL4A1, COL4A2, ***CST3***, CTLA4, ***DAOA***, ***DISC2***, ***DNASE1***, DRD3, ***EDNRA***, EFHC1, ***EIF2AK1***, ***ELP4***, ***EPB41L1***, ERMARD, FBP2, ***FCGR2B***, FGFR2, ***FTH1***, GABBR2, GABRD, GAL, GNB2, HCN2, HCN4, HNF1B, HTR2A, IRF3, KCNN2, KDM1A, KIF5A, LRRK2, MAP1B, ***NEUROD1***, NOL3, NOTCH3, NRAS, PAK2, ***PDGFRB***, PHOX2B, ***PLAU***, PRNP, PSEN1, PTEN, RANBP2, RAPGEF2, ***REST***, ***RET***, RORB, RTN4R, ***SAMD9L***, SCN8A, SHANK3, SMARCA4, SMARCB1, SMARCC1, SMARCE1, SNORA31, SPECC1L, SPTSSA, SYN2, ***TNFRSF1A***, TNRC6A, TRPM3, TRRAP, TSC2, TTR, ***USP25***, WDFY3, YEATS2, ZIC1
AD | AR	CASR, SLC2A1, TREX1, AARS1, ANTXR1, APOE, ***ATR***, BUB1B, CCDC88C, ***CILK1***, CLCN2, ***CRELD1***, DHTKD1, DMXL2, ***ESR1***, ***EVC***, ***FCGR2A***, ***HBB***, IFT140, IL6ST, KCNQ1, ***LBR***, LMAN2L, ***MPO***, NAGLU, ***PIEZO2***, POLE, PRODH, PSAP, RELN, RYR1, ***SLC4A1***, TBK1, ***TNFRSF11A***, UCHL1, UFSP2, WFS1, SLC12A5, ***CD46***, RNF213, TICAM1, TLR3, CFH, ***CFHR1***, ***CFHR3***, ***ACKR1***, COQ2, CPT2, ATP5F1A, CAMK2A, CDH2, DHDDS, ***EPO***, ***ERBB3***, FIG4, GJC2, GRIA1, ***HNF1A***, HTRA1, ***IFNG***, LMNB2, ***LRP1***, MDM2, MTHFR, ***PIEZO1***, POLG2, ***PTPN22***, RAD21, ROBO1, SCN5A, TGFB1, THAP11, ***TNF***, ***NEK1***, UGT1A1
AD | AR | Mu	***GBA1***, F2, POMC, ***HLA-DQB1***
AD | AR | DR	***SLC36A2***, PIK3CD
AD | AR | SMu	***SUFU***, ***ELP1***, BRCA2, ATM, MINPP1, ERCC6
AD | AR | SMu | Mu	IL6
AD | SMu	TP53, CBL
AD | Mu	NOS3, TBP, MAPT, GABRA2, NOD2
AR	ABCA5, ABCB1, ***ACE***, ***ACER3***, ***ACP2***, ***AHSG***, ALG14, AMPD2, AP3D1, ***AQP4***, ARNT2, ATPAF2, B9D2, BCL10, CAMLG, ***CCT5***, ***CD36***, CDC40, CDK5, ***CDK6***, CENPE, CEP290, ***CEP63***, ***CHP1***, CHRNA3, CNP, CNTNAP2, COG2, COQ5, COX8A, ***CPAP***, CPS1, DALRD3, ***DBR1***, DPM3, EGF, EN1, EXOC8, ***FBXO31***, FTO, GET4, GGT1, GUF1, HERC2, HEXA, HMOX1, HTRA2, IBA57, IFNAR2, INTS8, KARS1, KIAA0753, KIF7, LAMA5, LARS1, LSM11, ***MAL***, MCM8, MDH1, MRPL12, MTHFD1, MTR, ***MTRR***, MYO1H, NARS2, NAT8L, NDUFA13, ***NDUFA4***, NIN, NRXN1, NUP133, NUP214, PAH, PCSK1, PDCD6IP, PEX3, ***PHYKPL***, PIGG, PNPLA8, POMK, PPA2, PRDM8, PRIMA1, ***PSMB1***, ***RFX5***, ***RNH1***, RNU12, ***RRP7A***, SARDH, SEC31A, ***SEL1L***, SHQ1, ***SIK3***, ***SLC19A1***, SLC24A4, ***SLC24A5***, SLC25A10, SLC28A1, SOBP, SYT14, TDP1, TMEM67, ***TREM2***, ***TSEN34***, TSEN54, ***TSPEAR***, ***TSPOAP1***, TXN2, ***UQCC3***, VPS11, WIPI2, ***ZPR1***
AR | Mu	***HLA-DQA1***
DR	KNSTRN
XL	***G6PD***, NLGN3
XLD	NDUFB11
XLR	ATP6AP2, HS6ST2, L1CAM, MBTPS2, MID2, PTCHD1, ***RBMX***, RPL10, TMLHE
XLD | XLR	DKC1, FLNA, MECP2, OFD1
UN	***ABCC1***, ABCC12, ABCC2, ***ABCC5***, ***ABCG2***, ***ACHE***, ACMSD, ***ACOD1***, ACOT7, ADA, ***ADAM23***, ***ADCY9***, ***ADGRB3***, ***ADGRL3***, ***ADIPOQ***, ***ADORA1***, ADORA2A, ADRA2B, ***AGAP2***, ***AGER***, ***AGMO***, ***AGTR1***, AGTR2, ***AHR***, ***AJAP1***, ***AK5***, AKAP5, ***ALB***, ***ALDH2***, ***AMPH***, ***ANKK1***, ANO3, ***ANO4***, ***ANXA7***, ***APLN***, ***APTX***, ***AQP1***, ***AQP9***, ***ARF6***, ***ARHGAP44***, ARHGEF15, ***ARHGEF5***, ***ARL6IP6***, ***ARPC2***, ***ASIC2***, ***ASIC3***, ***ASNSD1***, ***ATF2***, ***ATF3***, ***ATF5***, ***ATG5***, ***ATL1***, ***ATOX1***, ***ATP10A***, ***ATP2B2***, ***AVP***, ***AZGP1***, ***BACE1***, ***BAK1***, ***BCHE***, BCL11A, ***BCL2A1***, BDNF, ***BMAL1***, ***BORCS5***, BRD2, BRWD3, BSN, ***C1orf94***, C3, C9orf72, ***CACNG4***, ***CALB1***, ***CALB2***, ***CALHM1***, ***CAMK4***, CAPN1, ***CAPN2***, CAPZA2, ***CASP1***, ***CASP3***, ***CAT***, ***CBLN1***, ***CBX1***, CCDC186, ***CCDC82***, ***CCL2***, ***CCL4***, CCN3, ***CCR5***, ***CCS***, ***CCT4***, ***CCT6A***, ***CCT7***, ***CCT8***, ***CD34***, ***CD40***, ***CD44***, ***CDIP1***, ***CDK5R1***, ***CDK5RAP3***, ***CDKN2B-AS1***, ***CDYL***, CELF4, CELSR1, CELSR3, ***CFL1***, CHD4, CHL1, CHRFAM7A, CHRM1, ***CHRM3***, ***CHRNA5***, CHRNA7, ***CISH***, CLCN7, ***CLDN5***, ***CLDND1***, ***CLEC16A***, CLIP1, CLOCK, ***CLPTM1***, CLTCL1, ***CLU***, CNOT2, ***CNOT9***, ***CNR1***, ***CNRIP1***, ***COL1A1***, COL6A2, ***COPZ2***, ***COX20***, CP, ***CPEB4***, ***CPLX2***, ***CR1***, ***CREB1***, ***CREM***, CRH, ***CRMP1***, ***CRP***, CSMD1, CSMD3, CSNK1E, CSNK1G1, ***CSNK1G2***, CTNND2, ***CXCL13***, ***CXCL8***, ***CXCR2***, ***CXCR5***, CYFIP1, ***CYP19A1***, ***CYP1A1***, ***CYP1A2***, ***CYP24A1***, ***CYP2C19***, ***CYP2D6***, ***CYP3A4***, ***CYP3A5***, ***DAPK1***, ***DBN1***, ***DBP***, DCAF13, DCLK2, ***DDX54***, DENND2B, ***DFFB***, DGKD, DHRS9, ***DIPK2A***, ***DIRAS1***, ***DISC1***, DLG2, DLGAP2, ***DLGAP3***, ***DLX1***, DMD, ***DNAJA3***, ***DOC2A***, ***DPYSL2***, ***DRD1***, DSCAM, ***DTNBP1***, ***DUSP4***, ***EDN1***, ***EFHC2***, ***EGFR***, ***EGR1***, ***EIF2S1***, ELFN1, ***ENO2***, ***EPHX1***, ***EPM2AIP1***, ERBB4, ***ERMN***, ***ERN1***, ***ESM1***, ***EZR***, ***FAAH***, FAAH2, ***FAM3C***, ***FANCL***, FAT1, ***FGA***, FGB, ***FGF2***, ***FGF22***, ***FGF7***, ***FGG***, ***FKBP5***, ***FLT1***, FN1, ***FNDC5***, ***FOS***, ***FOXO3***, ***FOXO4***, FURIN, ***FYN***, FZD9, ***GABARAP***, GABRA4, GABRA6, GABRE, ***GABRR1***, GABRR2, ***GAD2***, ***GAPDH***, ***GAS1***, ***GC***, ***GDNF***, ***GEMIN5***, ***GHRH***, GHRL, ***GJB1***, GJD2, ***GLO1***, GLP1R, ***GNB3***, ***GNG3***, ***GOLIM4***, ***GPC4***, GPR37L1, ***GPX1***, GRIK1, ***GRIK5***, GRINA, ***GRM2***, GRM3, GRM4, ***GRM5***, ***GRPR***, ***GSK3A***, ***GSK3B***, GSN, ***GSTA1***, ***GSTA4***, GSTM1, ***GSTP1***, ***GSTT1***, ***GYG2***, ***GYPA***, ***GYPB***, ***GYPC***, ***HCN3***, ***HCRT***, ***HDAC2***, ***HIF1A***, HIP1, ***HLA-B***, ***HLA-DRB1***, ***HLF***, ***HMGB1***, ***HOMER1***, ***HP***, ***HRH3***, ***HSPA8***, ***HSPB1***, ***HSPBAP1***, HSPE1, HTR1A, ***HTR1B***, HTR2C, ***HTR3A***, HTR6, ***HTR7***, ***HULC***, ***ICAM1***, ***ICAM5***, IDH1, ***IDO1***, ***IFI44L***, ***IFNA1***, ***IGF1***, ***IGF1R***, IL10, ***IL17A***, ***IL17RA***, ***IL18***, ***IL1A***, IL1B, ***IL1R1***, ***IL1RN***, ***IL2***, ***IL33***, ***IL4***, ***IL7R***, ***IMMT***, ***IMPA2***, INPP4A, ***IRAK1***, ***IRS1***, ***IRS2***, ***ITGA2***, ***ITSN1***, JMJD1C, JRK, ***JUN***, ***KCNA3***, ***KCNA4***, ***KCNA6***, KCNAB1, KCNAB2, ***KCNAB3***, KCND2, ***KCNH3***, ***KCNH7***, ***KCNIP3***, ***KCNJ3***, ***KCNJ8***, ***KCNK18***, ***KCNK2***, ***KCNK3***, KCNMB1, ***KCNMB4***, ***KCNN4***, ***KCNV1***, KCNV2, ***KDM2B***, ***KEAP1***, ***KIF16B***, ***KL***, KLHL20, ***KLRC1***, ***KLRK1***, ***LEP***, LEPR, ***LGI2***, ***LGMN***, ***LINC01621***, ***LOC101927235***, ***LOC102724058***, ***LOC108228197***, ***LOC108228198***, ***LOC108228208***, ***LOC108228209***, ***MAOB***, MAP2, MAPK10, ***MARK2***, MAST4, ***MBP***, MC3R, ME2, ***MED1***, ***MGMT***, MICAL1, ***MICU2***, ***MIR124-1***, MIR128-1, ***MIR128-2***, ***MIR129-1***, ***MIR129-2***, ***MIR132***, ***MIR134***, ***MIR135B***, ***MIR139***, ***MIR145***, ***MIR146A***, ***MIR148A***, ***MIR153-1***, ***MIR153-2***, ***MIR155***, ***MIR15A***, ***MIR181A1***, ***MIR196B***, ***MIR199A1***, ***MIR199A2***, ***MIR204***, ***MIR211***, ***MIR212***, ***MIR217***, ***MIR218-1***, ***MIR219A1***, ***MIR29A***, ***MIR335***, ***MIR372***, MLLT3, ***MMP2***, ***MMP3***, ***MMP8***, ***MMP9***, ***MT-ATP6***, ***MT-ATP8***, ***MT-CO2***, ***MT-ND1***, ***MT-ND4***, ***MT-ND5***, ***MT-ND6***, ***MT-RNR1***, ***MT-RNR2***, ***MT-TF***, ***MT-TL1***, ***MT-TS1***, ***MT2A***, MUSK, ***MVP***, ***MYH10***, ***NAPA***, ***NAT2***, ***NAV1***, ***NCAM1***, NCOR2, ***NEAT1***, ***NES***, ***NFE2L1***, ***NFIX***, ***NFKB1***, NIPA2, ***NKAIN1***, ***NKAIN2***, ***NKAIN4***, NLGN1, ***NLRP1***, ***NNMT***, ***NOS1***, ***NOS2***, ***NOTCH4***, ***NPAP1***, ***NPPB***, ***NPPC***, ***NPY***, ***NPY1R***, ***NPY2R***, ***NR1I2***, ***NR1I3***, ***NR3C1***, ***NRDC***, ***NREP***, ***NRG1***, NRXN2, NTF3, NTNG1, ***NUCB2***, ***NUSAP1***, ***NWD1***, OGDHL, ***OLIG2***, ***OMA1***, ***OPALIN***, OPRM1, ***OPTN***, ***OSBPL11***, ***OTX1***, ***OXT***, ***P2RX3***, ***P2RX7***, ***P2RY1***, ***P2RY12***, ***P2RY2***, ***PADI4***, ***PADI6***, ***PAQR8***, ***PARP6***, PAX6, PCDH7, ***PCMT1***, ***PER2***, ***PEX5L***, ***PGF***, ***PHF24***, ***PHLDA1***, ***PHOX2A***, ***PIK3C2B***, PIK3R4, ***PIN1***, ***PJA1***, PLA2G4A, ***PLAT***, ***PLAUR***, PLCB4, ***PLCG1***, ***PNOC***, ***POU2AF1***, ***PPARG***, ***PPFIA1***, ***PPP2R2C***, PPP5C, ***PPT2***, PRICKLE2, PRKD1, PRL, PROM1, ***PRR15L***, PTGS2, PTPRD, ***PVALB***, ***PWP2***, ***QKI***, ***RAB40AL***, ***RACK1***, ***RALBP1***, ***RAP1A***, ***RARRES2***, ***RASGRF1***, RBFOX1, RBFOX3, RFX3, RFX4, ***RHOA***, ***RINT1***, ***RNU2-2***, ***RNU5B-1***, ***RPS6KA2***, ***RTN4***, ***S100B***, ***SAA1***, SCAMP5, ***SCN1A-AS1***, ***SCN3B***, ***SEMA7A***, ***SERINC1***, ***SERINC2***, ***SERINC5***, ***SERPINE1***, ***SGK1***, ***SH3BGRL2***, ***SH3GL2***, SHANK2, ***SHH***, SHROOM4, ***SIRT1***, ***SKAP1***, ***SLC13A1***, SLC16A4, SLC16A7, SLC1A1, SLC22A1, SLC29A1, ***SLC39A7***, ***SLC4A5***, ***SLC5A11***, SLC6A3, SLC6A4, ***SLC7A10***, SLC7A11, SLC9A9, ***SLIT2***, ***SLITRK3***, ***SLITRK5***, ***SMAD3***, SMG6, ***SNHG1***, ***SNN***, ***SNRPD1***, ***SNX11***, ***SNX25***, ***SOCS1***, ***SOD1***, ***SOD2***, ***SORBS2***, ***SORCS2***, SORCS3, SOX11, ***SOX7***, ***SP1***, SRGAP2, SRPX2, ***SRR***, ***SSTR2***, ***ST8SIA1***, ***STAT3***, ***STIM1***, ***STIM2***, ***STK24***, ***STMN1***, ***STX1A***, STXBP5L, STYXL1, SUCO, ***SV2B***, ***SYNRG***, ***SYT11***, ***SYVN1***, ***TAC1***, ***TACR1***, TAP1, ***TBC1D32***, ***TEF***, ***TERT***, ***TET1***, ***TET2***, TFAM, ***TGFBR2***, ***THBS1***, ***THBS2***, ***TIMP1***, ***TIMP2***, ***TIMP4***, ***TIRAP***, ***TLE1***, ***TLN2***, ***TLR4***, ***TLR7***, ***TMEFF1***, ***TMEM25***, TMEM63B, ***TNFRSF13C***, ***TNFRSF1B***, ***TNFSF13B***, TNK2, ***TOMM40***, ***TOP2A***, TOP3B, ***TPH2***, ***TRIM3***, TRMT44, ***TRPC3***, ***TRPC4***, TRPC6, ***TRPM2***, ***TRPM7***, ***TRPV1***, ***TRPV4***, ***TSPO***, ***TUBG2***, ***TUG1***, TXNRD1, ***U2AF1***, UBA1, ***UBC***, ***UBQLN1***, UBR4, UBR5, ***UCP2***, ***UGT1A4***, ***UGT1A6***, UGT1A9, ***UGT2B7***, UNC13B, UPF1, ***USF1***, ***VEGFA***, ***VEZT***, VRK2, ***VWF***, ***WHCR***, ***WNT8B***, YWHAE, ***YWHAQ***, ***YWHAZ***, ZDHHC15, ***ZFAS1***, ZFHX3, ***ZFYVE27***, ***ZNF143***, ***ZNF385D***, ***ZSCAN25***, COMT

AD, autosomal dominant; AR, autosomal recessive; XL, X-linked; XLD, X-linked dominant; XLR, X-linked recessive; DR, digenic recessive; Mu, multifactorial inheritance; SMu, somatic mutation; SMo, somatic mosaicism; DD, digenic dominant; PR, psuedoautosomal recessive; UN, unknown. Genes underlined did not have a phenotype registered within any database. Genes that have been identified in this study that were not present within the Zhang MW, et al. [1] have been highlighted in bold.

10.3389/ebm.2026.10933

TABLE 4 Epilepsy genes found in all databases.

Gene	Inheritance	Phenotype/s
ALDH7A1	AR	• Epilepsy, early-onset, vitamin B6-dependent
ALG13	XL	• Developmental and epileptic encephalopathy
ARX	XLR | XL	• Developmental and epileptic encephalopathy • Hydranencephaly with abnormal genitalia • Intellectual developmental disorder • Lissencephaly • Partington syndrome • Proud syndrome
ATP1A2	AD | AR	• Alternating hemiplegia of childhood • Developmental and epileptic encephalopathy • Fetal akinesia, respiratory insufficiency, microcephaly, polymicrogyria, and dysmorphic facies
BRAT1	AR	• Neurodevelopmental disorder with cerebellar atrophy and with or without seizures • Rigidity and multifocal seizure syndrome, lethal neonatal
CACNA1E	AD	• Developmental and epileptic encephalopathy
CAD	AR	• Developmental and epileptic encephalopathy
CERS1	AR	• Epilepsy, progressive myoclonic
CHRNA2	AD	• Epilepsy, nocturnal frontal lobe
CHRNA4	AD	• Epilepsy, nocturnal frontal lobe
CHRNB2	AD	• Epilepsy, nocturnal frontal lobe
CNNM2	AD | AR	• Hypomagnesemia, renal • Hypomagnesemia, seizures, and impaired intellectual development
CSTB	AR	• Epilepsy, progressive myoclonic
CUX2	AD	• Developmental and epileptic encephalopathy
DEPDC5	AR | AD	• Developmental and epileptic encephalopathy • Epilepsy, familial focal
DIAPH1	AD | AR	• Deafness, with or without thrombocytopenia • Seizures, cortical blindness, microcephaly syndrome
DLL1	AD	• Neurodevelopmental disorder with nonspecific brain abnormalities and with or without seizures
DNM1	AD | AR	• Developmental and epileptic encephalopathy
DOCK7	AR	• Developmental and epileptic encephalopathy
FGF12	AD	• Developmental and epileptic encephalopathy
FRRS1L	AR	• Developmental and epileptic encephalopathy
GABRA1	AD	• Developmental and epileptic encephalopathy
GABRB1	AD	• Developmental and epileptic encephalopathy
GABRB3	AD	• Developmental and epileptic encephalopathy
GABRG2	AD	• Developmental and epileptic encephalopathy • Febrile seizures • Generalized epilepsy with febrile seizures
GAD1	AR	• Developmental and epileptic encephalopathy
GLUL	AD | AR	• Glutamine deficiency

(*Continued*)

TABLE 4 Continued

Gene	Inheritance	Phenotype/s
GNAO1	AD	• Developmental and epileptic encephalopathy • Neurodevelopmental disorder with involuntary movements
GOSR2	AR	• Epilepsy, progressive myoclonic • Muscular dystrophy, congenital, with or without seizures
GRIA4	AD	• Neurodevelopmental disorder with or without seizures and gait abnormalities
HCN1	AD	• Developmental and epileptic encephalopathy • Generalized epilepsy with febrile seizures
ITPA	AR	• Inosine triphosphatase deficiency • Developmental and epileptic encephalopathy
KCNA2	AD	• Developmental and epileptic encephalopathy
KCNC1	AD	• Epilepsy, progressive myoclonic
KCNC2	AD	• Developmental and epileptic encephalopathy
KCNH5	AD	• Developmental and epileptic encephalopathy
KCNK4	AD	• Facial dysmorphism, hypertrichosis, epilepsy, intellectual/developmental delay, and gingival overgrowth syndrome
KCNMA1	AD | AR	• Epilepsy, idiopathic generalized • Cerebellar atrophy, developmental delay, and seizures • Liang-Wang syndrome • Paroxysmal nonkinesigenic dyskinesia, with or without generalized epilepsy
KCNQ2	AD	• Developmental and epileptic encephalopathy • Myokymia • Seizures, benign neonatal
KCNQ3	AD | AR	• Seizures, benign neonatal
KCNT1	AD	• Developmental and epileptic encephalopathy • Epilepsy nocturnal frontal lobe
KCTD7	AR	• Epilepsy, progressive myoclonic, with or without intracellular inclusions
LGI1	AD	• Epilepsy, familial temporal lobe
NACC1	AD	• Neurodevelopmental disorder with epilepsy, cataracts, feeding difficulties, and delayed brain myelination
NARS1	AR | AD	• Neurodevelopmental disorder with microcephaly, impaired language, and gait abnormalities • Neurodevelopmental disorder with microcephaly, impaired language, epilepsy, and gait abnormalities
NECAP1	AR	• Developmental and epileptic encephalopathy
NPRL2	AD	• Epilepsy, familial focal
NPRL3	AD	• Epilepsy, familial focal
NRROS	AR	• Seizures, early-onset, with neurodegeneration and brain calcification
NSRP1	AR	• Neurodevelopmental disorder with spasticity, seizures, and brain abnormalities
NUS1	AR | AD	• Congenital disorder of glycosylation, type 1aa • Intellectual developmental disorder, autosomal dominant 55, with seizures
PACS2	AD	• Developmental and epileptic encephalopathy
PIGB	AR	• Developmental and epileptic encephalopathy
PIGF	AR	• Onychodystrophy, osteodystrophy, impaired intellectual development, and seizures syndrome

(*Continued*)

TABLE 4 Continued

Gene	Inheritance	Phenotype/s
PIGN	AR	• Multiple congenital anomalies-hypotonia-seizures syndrome
PIGP	AR	• Developmental and epileptic encephalopathy
PIGQ	AR	• Multiple congenital anomalies-hypotonia-seizures syndrome
PIGT	AD | SMu | AR	• Paroxysmal nocturnal hemoglobinuria • Multiple congenital anomalies-hypotonia-seizures syndrome
PLCB1	AR	• Developmental and epileptic encephalopathy
PNKP	AR	• Charcot-Marie-Tooth disease, type 2B2 • Ataxia-oculomotor apraxia • Microcephaly, seizures, and developmental delay
PNPO	AR	• Pyridoxamine 5′-phosphate oxidase deficiency
PRICKLE1	AR	• Epilepsy, progressive myoclonic
PRRT2	AD	• Convulsions, familial infantile, with paroxysmal choreoathetosis • Episodic kinesigenic dyskinesia • Seizures, benign familial infantile
QARS1	AR	• Microcephaly, progressive, seizures, and cerebral and cerebellar atrophy
SARS1	AR	• Neurodevelopmental disorder with microcephaly, ataxia, and seizures
SCARB2	AR	• Epilepsy, progressive myoclonic, with or without renal failure
SCN1A	AD	• Developmental and epileptic encephalopathy • Dravet syndrome • Febrile seizures • Generalized epilepsy with febrile seizures plus • Migraine, familial hemiplegic
SCN1B	AD | AR	• Atrial fibrillation • Brugada syndrome • Cardiac conduction defect, nonspecific • Developmental and epileptic encephalopathy • Generalized epilepsy with febrile seizures plus
SCN3A	AD	• Developmental and epileptic encephalopathy • Epilepsy, familial focal
SEMA6B	AD	• Epilepsy, progressive myoclonic
SERPINI1	AD	• Encephalopathy, with neuroserpin inclusion bodies
SIK1	AD	• Developmental and epileptic encephalopathy
SLC1A2	AD	• Developmental and epileptic encephalopathy
SLC25A22	AR	• Developmental and epileptic encephalopathy
SNAP25	AD	• Developmental and epileptic encephalopathy
SPTAN1	AD	• Developmental and epileptic encephalopathy • Developmental delay with or without epilepsy • Neuronopathy, distal hereditary motor • Spastic paraplegia, with or without cerebellar ataxia
STX1B	AD	• Generalized epilepsy with febrile seizures plus
STXBP1	AD | AR	• Developmental and epileptic encephalopathy
SYNJ1	AR	• Developmental and epileptic encephalopathy • Parkinson disease, early-onset
SZT2	AR	• Developmental and epileptic encephalopathy

(*Continued*)

TABLE 4 Continued

Gene	Inheritance	Phenotype/s
TANC2	AD	• Intellectual developmental disorder with autistic features and language delay, with or without seizures
TRAPPC4	AR	• Neurodevelopmental disorder with epilepsy, spasticity, and brain atrophy
TRAPPC6B	AR	• Neurodevelopmental disorder with microcephaly, epilepsy, and brain atrophy
UBA5	AR	• Spinocerebellar ataxia • Developmental and epileptic encephalopathy
VARS1	AR	• Neurodevelopmental disorder with microcephaly, seizures, and cortical atrophy
WWOX	AR	• Developmental and epileptic encephalopathy • Esophageal squamous cell carcinoma • Spinocerebellar ataxia

AD, autosomal dominant; AR, autosomal recessive; XL, X-linked; XLD, X-linked dominant; XLR, X-linked recessive; DR, digenic recessive; Mu, multifactorial inheritance; SMu, somatic mutation; SMo, somatic mosaicism; DD, digenic dominant; PR, psuedoautosomal recessive; UN, unknown.

with epileptic encephalopathy [11, 12] and breast cancer [13]. Finally, *VARS1* shares similar functions with *QARS1* in which they both encode tRNA synthetases but effect different tRNA functions. *VARS1* has been associated with improving melanoma immunotherapy efficacy [14], hepatocellular carcinoma [15] and neurodevelopment disorder [16].

This study has several limitations that should be taken into consideration. To generate this list, all genes were included from all three databases whether they showed a direct link to epilepsy or not. Such genes, for example, that did not have an established phenotype were grouped into the predicted epilepsy associated genes category. These genes have been underlined within Table 3 and makeup approximately 16% of the genes in the Predicted associated epilepsy gene category. Comparisons were made throughout the paper with a previous paper by Zheng MW, et al. [1] and it should be noted that our paper used different parameters and databases to this paper. This comparison is to show a general trend of how our understanding of epilepsy associated genes are progressing. Finally, it should be noted that there may be potential biases in such data produced from all three databases.

In conclusion, the present study updates the list of epilepsy associated genes based on currently available genetic databases, to provide a catalogue of genetic information in the hopes to better understand the aetiology of epilepsy and possibly other neurodevelopmental diseases. This list showcases a range of inheritance modes and phenotypes of the most common genes to aid in this endeavour.

Author contributions

KP wrote the amanuscript, performed experiments, and conducted data reconstruction/evaluation. SK conceived of the study, and provided thorough technical support. AG provided technical support. All authors contributed to the article and approved the submitted version.

Funding

The author(s) declared that financial support was not received for this work and/or its publication.

Conflict of interest

The author(s) declared no potential conflicts of interest with respect to the research, authorship, and/or publication of this article.

Correction note

This article has been corrected with minor changes. These changes do not impact the scientific content of the article.

Generative AI statement

The author(s) declared that generative AI was not used in the creation of this manuscript.

Any alternative text (alt text) provided alongside figures in this article has been generated by Frontiers with the support of artificial intelligence and reasonable efforts have been made to ensure accuracy, including review by the authors wherever possible. If you identify any issues, please contact us.

Supplementary material

The Supplementary Material for this article can be found online at: https://www.ebm-journal.org/articles/10.3389/ebm.2026.10933/full#supplementary-material

References

1. Zhang MW, Liang XY, Wang J, Gao LD, Liao HJ, He YH, et al. Epilepsy-associated genes: an update. *Seizure* (2024) **116**:4–13. doi:10.1016/j.seizure.2023.09.021

2. Kotloski RJ, Dowding J, Hermann BP, Sutula TP. Epilepsy and aging. *Handb Clin Neurol* (2019) **167**:455–75. doi:10.1016/B978-0-12-804766-8.00025-X

3. Wang J, Lin ZJ, Liu L, Xu HQ, Shi YW, Yi YH, et al. Epilepsy-associated genes. *Seizure* (2017) **44**:11–20. doi:10.1016/j.seizure.2016.11.030

4. Amberger JS, Bocchini CA, Schiettecatte F, Scott AF, Hamosh A. OMIM.org: Online mendelian inheritance in Man (OMIM®), an online catalog of human genes and genetic disorders. *Nucleic Acids Res* (2015) **43**:D789–D798. doi:10.1093/nar/gku1205

5. Stewart M, Lau P, Banks G, Bains RS, Castroflorio E, Oliver PL, et al. Loss of *Frrs1l* disrupts synaptic AMPA receptor function, and results in neurodevelopmental, motor, cognitive and electrographical abnormalities. *Dis Model Mech* (2019) **12**(2). doi:10.1242/dmm.036806

6. Abdelmoumen I, Jimenez S, Valencia I, Melvin J, Legido A, Diaz-Diaz MM, et al. Boricua founder variant in *FRRS1L* causes epileptic encephalopathy With hyperkinetic movements. *J Child Neurol* (2021) **36**(2):93–8. doi:10.1177/0883073820953001

7. Madeo M, Stewart M, Sun Y, Sahir N, Wiethoff S, Chandrasekar I, et al. Loss-of-Function mutations in FRRS1L lead to an epileptic-dyskinetic encephalopathy. *Am J Hum Genet* (2016) **98**(6):1249–55. doi:10.1016/j.ajhg.2016.04.008

8. Bariş S, Kırık S, Balasar Ö. Importance of targeted next-generation sequencing in pediatric patients with developmental epileptic encephalopathy. *Rev Assoc Med Bras* (2023) **69**(10):e20230547. doi:10.1590/1806-9282.20230547

9. Yu S, Si Y, Xu M, Wang Y, Liu C, Bi C, et al. Downregulation of the splicing regulator NSRP1 confers resistance to CDK4/6 inhibitors via activation of interferon signaling in breast cancer. *J Biol Chem* (2025) **301**(1):108070. doi:10.1016/j.jbc.2024.108070

10. Calame DG, Bakhtiari S, Logan R, Coban-Akdemir Z, Du H, Mitani T, et al. Biallelic loss-of-function variants in the splicing regulator NSRP1 cause a severe neurodevelopmental disorder with spastic cerebral palsy and epilepsy. *Genet Med* (2021) **23**(12):2455–60. doi:10.1038/s41436-021-01291-x

11. Ahmad R, Naeem M, Houlden H. QARS1 associated developmental epileptic encephalopathy: first report of a rare homozygous missense variant from Pakistan causing nonepileptic phenotype in a family of seven patients and a comprehensive review of the literature. *Mol Biol Rep* (2025) **52**(1):528. doi:10.1007/s11033-025-10574-4

12. Srivastava P, Uddin MW, Diwakar K, Biswal S, Senapati A. Homozygous mutation in the QARS1 gene causing developmental epileptic encephalopathy in siblings in the Southeast Asian region: an interesting case report and discussion. *Cureus* (2025) **17**(2):e78333. doi:10.7759/cureus.78333

13. Zhou Y, Yu S, Zhu L, Wang Y, Duan C, Li D, et al. Molecular biomarkers for the prognosis of breast cancer: role of amino acid metabolism genes. *J Physiol Biochem* (2025) **81**(2):441–57. doi:10.1007/s13105-025-01088-5

14. Wu Z, Lei K, Li H, He J, Shi E. Transcriptome-based network analysis related to M2-like tumor-associated macrophage infiltration identified VARS1 as a potential target for improving melanoma immunotherapy efficacy. *J Transl Med* (2022) **20**(1):489. doi:10.1186/s12967-022-03686-z

15. Hermán-Sánchez N, Del Rio-Moreno M, Ciria R, Sánchez-Frias ME, Fernández-Barrena MG, Uriarte I, et al. Quantitative proteomic analysis unveils a critical role of VARS1 in hepatocellular carcinoma aggressiveness through the modulation of MAGI1 expression. *Mol Cancer* (2025) **24**(1):15. doi:10.1186/s12943-024-02206-5

16. Hiz S, Kiliç S, Bademci G, Karakulak T, Erdoğan A, Özden B, et al. *VARS1* mutations associated with neurodevelopmental disorder are located on a short amino acid stretch of the anticodon-binding domain. *Turk J Biol* (2022) **46**(6):458–64. doi:10.55730/1300-0152.2631

EBM Experimental Biology and Medicine

TYPE Mini Review
PUBLISHED 30 June 2026
DOI 10.3389/ebm.2026.11128

Check for updates

OPEN ACCESS

*CORRESPONDENCE
Zhuoshi Wang,
hsyk2017@163.com

RECEIVED 03 April 2026
REVISED 03 June 2026
ACCEPTED 11 June 2026
PUBLISHED 30 June 2026

CITATION
Liu X, Zhang M and Wang Z (2026) Mitochondrial transfer and mesenchymal stem cells in ophthalmology: current evidence and therapeutic implications. *Exp. Biol. Med.* 251:11128. doi: 10.3389/ebm.2026.11128

COPYRIGHT
© 2026 Liu, Zhang and Wang. This is an open-access article distributed under the terms of the Creative Commons Attribution License (CC BY). The use, distribution or reproduction in other forums is permitted, provided the original author(s) and the copyright owner(s) are credited and that the original publication in this journal is cited, in accordance with accepted academic practice. No use, distribution or reproduction is permitted which does not comply with these terms.

Mitochondrial transfer and mesenchymal stem cells in ophthalmology: current evidence and therapeutic implications

Xiaoli Liu[1,2], Mingqi Zhang[1,2] and Zhuoshi Wang[1,3]*

[1]Liaoning Key Lab of Ophthalmic Stem Cells, He University, Shenyang, China, [2]School of Pharmacy, He University, Shenyang, China, [3]Science and Education Department, He Eye Specialist Hospital, Shenyang, China

Abstract

Mitochondrial dysfunction, driven by genetic mutations or oxidative stress, is a central contributor to the onset and progression of ophthalmic diseases. In recent years, intercellular mitochondrial transfer (MT) has emerged as a novel mechanism of cellular communication and repair in ocular tissues. MT occurs through tunneling nanotubes, extracellular vesicles (EVs), cell fusion, or transmitophagy, and has been shown to support photoreceptor survival, maintain retinal homeostasis, and protect against oxidative injury. Mesenchymal stem cells (MSCs), owing to their remarkable reparative and immunomodulatory properties, have attracted particular attention as efficient mitochondrial donors. Evidence from experimental models demonstrates that MSC-mediated MT can restore bioenergetics, mitigate oxidative stress, and rescue cellular function in inherited optic neuropathies, corneal injuries, retinal degenerative diseases, and ischemic retinopathies. This review summarizes current evidence of MT in ophthalmology, highlights the therapeutic contributions of MSCs, discusses the molecular and microenvironmental factors regulating MT efficiency, and outlines unresolved challenges. We further provide perspectives on how mitochondrial transfer may be translated into innovative therapies for ocular disorders.

KEYWORDS
clinical translation, mesenchymal stem cells, mitochondrial transfer, ophthalmic diseases, retinal degeneration

Impact statement

To our knowledge, this review is one of the first comprehensive summaries focusing on mitochondrial application of mesenchymal stem cells in ophthalmology. As a novel emerging field, mitochondrial transplantation opens up a new direction for stem cell therapy, addressing the urgent need for innovative therapeutic strategies in ophthalmic diseases. It advances the field by systematically organizing the latest research findings, clarifying the potential of mesenchymal stem cell mitochondria in treating ocular disorders. The review imparts new perspectives on the clinical transformation value of this novel technology, guiding subsequent basic and clinical research, and promoting the development of innovative stem cell-based therapeutic approaches for refractory ophthalmic diseases.

Background

Mitochondria, the "powerhouses of the cell," generate ATP through oxidative phosphorylation and are essential for calcium signaling, reactive oxygen species (ROS) regulation, apoptosis, and inflammation [1, 2]. Balanced mitochondrial fusion, fission, biogenesis, and mitophagy preserve mitochondrial integrity and function [2]. Mutations in mitochondrial or nuclear DNA disrupt these processes, leading to structural and functional abnormalities collectively termed mitochondrial diseases [3].

The first inherited mitochondrial optic neuropathy described was Leber hereditary optic neuropathy (LHON), caused by three primary mtDNA mutations (ND1 G3460A, ND4 G11778A, and ND6 T14484C). These mutations impair complex I, reduce ATP production, elevate ROS, and selectively damage retinal ganglion cells (RGCs) and the optic nerve [4]. Mitochondrial dysfunction is also a key pathogenic driver in secondary ophthalmic disorders, such as glaucoma, diabetic retinopathy (DR), and age-related macular degeneration (AMD) [5–8].

Conventional therapies—including pharmacological agents, laser treatments, and surgery—slow progression but fail to restore function in severely damaged corneal, retinal, or optic nerve tissues [9]. Mesenchymal stem cells (MSCs) have thus gained attention for their regenerative potential in ocular diseases [10]. While MSCs exert effects through differentiation, paracrine signaling, and immune regulation, growing evidence highlights mitochondrial transfer (MT) as an additional mechanism of repair [11].

This review provides a systematic overview of MT in ocular cells, with emphasis on MSC-mediated MT (Table 1). We discuss its therapeutic applications across diverse ophthalmic diseases, analyze key regulatory factors, and propose perspectives for clinical translation.

Inherited mitochondrial diseases

Leber hereditary optic neuropathy (LHON)

LHON is the most common inherited mitochondrial optic neuropathy, with ND4 mutations accounting for most cases. Gene therapy using recombinant adeno-associated virus (AAV) vectors encoding wild-type ND4 has demonstrated significant bilateral visual improvement in clinical trials [25–30]. Interestingly, contralateral effects suggest intercellular mitochondrial or vector transfer along optic pathways (Figure 1A) [31].

Beyond gene therapy, MSC-mediated MT has emerged as a complementary strategy. Studies using induced pluripotent stem cell (iPSC)-derived models showed that MSCs could restore mitochondrial DNA ratios, improve mitochondrial function, and enhance electrophysiological activity in LHON-derived neurons [12]. In mouse models of mitochondrial complex I deficiency, intravitreal MSCs transplantation protected RGCs and preserved retinal function by delivering functional mitochondria across the inner limiting membrane (ILM) [14]. The release of mitochondria-containing EVs from MSCs also effectively delivered functional mitochondria to damaged cells, restoring mitochondrial functions in both LHON cell models and LHON-like male mice [13].

These findings indicate that MSC-mediated MT provides a promising therapeutic approach for LHON and other inherited mitochondrial disorders such as mitochondrial encephalomyopathy, lactic acidosis, and stroke-like episodes (MELAS), myoclonic epilepsy with ragged red fibers (MERRF) [32, 33].

Although gene therapy and MSC-mediated MT show promise in inherited mitochondrial optic neuropathies, several challenges remain. The mechanisms underlying the contralateral effect of lenadogene nolparvovec are still debated, and the efficiency and long-term stability of MSC-derived mitochondrial integration in human retinas are unknown. Most findings come from rodent models, raising concerns about translational relevance, while evidence from other mitochondrial diseases (e.g., MELAS, MERRF) remains preliminary.

Future studies should clarify the mechanistic basis of contralateral effects, optimize MSCs delivery to overcome retinal barriers, and establish quantitative *in vivo* tracking methods. Large-animal studies and long-term safety evaluations will be critical, and combining gene therapy with MT may ultimately offer synergistic benefits for inherited mitochondrial eye diseases.

Corneal diseases

Corneal epithelial cells (CECs) are highly susceptible to oxidative stress and mitochondrial dysfunction, contributing to conditions such as dry eye disease and corneal chemical burns [15, 34–37]. It has been observed that intercellular MT occurs among CECs and corneal endothelial cells. Stress conditions further facilitate this process (Figure 1B), implying a damage-induced "SOS" signaling mechanism [21, 38, 39].

In alkali-burned corneal models, MSCs transplantation supported wound healing and mitochondrial repair (Figure 1B). Notably, when tunneling nanotubes (TNTs)-mediated contact was blocked, MSCs lost much of their reparative effect, confirming the essential role of MT [15]. Thus, MT complements paracrine signaling to protect corneal cells from mitochondrial dysfunction. Interestingly, human corneal epithelial cells could internalize exogenous mitochondria isolated from MSCs (Figure 1B). A single subconjunctival injection of isolated mitochondria reduced inflammatory cell infiltration induced by acid burn and accelerated the corneal repair process [16].

Most studies focus on acute injury models, and the long-term stability of transferred mitochondria in chronic corneal diseases remains unclear. Future work should evaluate chronic models,

Abbreviations: MSCs, mesenchymal stem cells; ROS, reactive oxygen species; BMSCs, bone marrow mesenchymal stem cells; ASCs, adipose-derived stem cells; RCS, Royal College of Surgeons; NPCs, neural progenitor cells; ILM, inner limiting membrane; MT, mitochondrial transfer; EV, extracellular vesicle; LHON, Leber hereditary optic neuropathy; RGCs, retinal ganglion cells; DR, diabetic retinopathy; AMD, age-related macular degeneration; AAV, adeno-associated virus; iPSCs, induced pluripotent stem cells; CECs, corneal epithelial cells; TNTs, tunneling nanotubes; MG, Müller glia; RPE, retinal pigment epithelium; oAβ, oligomeric amyloid beta; UC, umbilical cord; WJ, Wharton's Jelly; hE-MSCs, human endometrium-derived MSCs.

TABLE 1 Application of MSCs derived mitochondria in various ophthalmic diseases.

Disease	Source	Model	Methods	Route	Action	References
LHON	Human UC-MSCs	LHON iPSC derived NPCs	Mitochondria reporter systems; Quantifying mitochondrial DNA	Not verified	Improve mitochondrial function and increase the proportion of normal mitochondrial DNA in LHON, as well as ameliorate the electrophysiological function of neurons differentiated from LHON patient-derived neural progenitor cells	[12]
LHON	Rat ASCs	LHON model cells (GM10742 cells); mtND4R340H mtTg LHON male mice; rot-induced LHON male mouse model	Mitochondria reporter systems; mitochondrial dyes	Extracellular vesicles	Restore mitochondrial function and alleviate LHON-associated symptoms in LHON male mice, as well as promote mitochondrial function in the rot-induced pan-mitochondrial disease model	[13]
Leigh syndrome	Human iPSC- MSCs	Ndufs4 gene knockout mice*; primary mouse RGCs	Mitochondria reporter systems; Quantifying mitochondrial DNA; mitochondrial dyes	Not verified	Reduce the loss of RGCs, promote mitochondrial transfer to RGCs across the ILM to protect retinal function, and inhibited abnormal activation of MG as well as the inflammatory state of the degenerated retina	[14]
Corneal injury (alkaline burns)	Human iPSC- MSCs	Primary hCECs; alkali-injured rabbit model	Mitochondria reporter systems; mitochondrial dyes	TNTs	Reduce oxidative stress-induced mitochondrial damage and rapid repair of alkaline burn induced corneal mitochondrial dysfunction	[15]
Corneal injury (acid burn)	Human UC-MSCs derived mitochondria	Primary human corneal epithelial cells; mice with acid-induced corneal burns	Mitochondria reporter systems; mitochondrial dyes	Co-culture; subconjunctival injection	Reduce apoptosis and oxidative stress levels, inhibite acid burn–induced inflammatory cell infiltration, and accelerate the repair process in a mouse model of corneal acid burn	[16]
AMD	BMMCs derived mitochondria	oAβ treated ARPE-19 cells; oAβ treated mice	Mitochondria reporter systems; mitochondrial dyes	Co-culture; intravitreal injection are transferred to the RPE layer	Enhance Aβ clearance, and prevent disruption of tight junctions	[17]
AMD	UC-MSCs derived mitochondria	Replicative senescence-induced ARPE-19 cells; Oxidative stress induced senescence in ARPE-19 cells	Mitochondria reporter systems	Co-culture	Improve mitochondrial dysfunction and alleviate cellular senescence hallmarks	[18]
AMD	Human WJ-MSCs derived mitochondria; human E-MSCs derived mitochondria	Oxidative damage (H_2O_2)-induced ARPE-19 cells	Mitochondrial dyes (TMRM staining)	Co-culture	WJ MSCs: Enhance cell survival and activate autophagy pathways E-MSCs: Repair retinal damage and enhance RPE function	[19]

(*Continued*)

TABLE 1 Continued

Disease	Source	Model	Methods	Route	Action	References
RD	BMSCs; BMSCs derived mitochondria	Rotenone treated primary MG; RCS rats	Mitochondria reporter systems	TNTs and cell fusion	Integrated into the mitochondrial network of MG; restore mitochondrial structural and functional damage, reduce oxidative stress and gliosis, and partially protecte the visual function of degenerative rat retina	[20]
Ocular tissue regeneration	UC-MSCs	Corneal endothelial cells; 661W cells; ARPE-19 cells; rotenone treated corneal endothelial cells; C57BL/6J mice	Mitochondria reporter systems	TNTs	Increase aerobic capacity and upregulation of mitochondrial genes	[21]
Retinal degenerative diseases	Human ASCs	RPE-1 cells with hypoxia treatment or serum starvation	Mitochondrial dyes	TNTs	Support cellular stability under stress	[22]
Ischemic retinopathies	Human iPSC-MSCs; ASCs	THP-1 cells, primary mouse splenocyte; ocular hypertension-induced ischemia-reperfusion injured mice	Mitochondria reporter systems	TNTs	Reprogram mouse $CD4^+$T cells into $CD4^+CD25^+Foxp3^+$Tregs and enable Foxp3+Tregs to be recruited to counteract inflammation and retinal degeneration Induced by ischemia-reperfusion injury *in vivo*	[23]
Retinal ischemia	Rat primary BMSCs	MCAO sprague-dawley rat model and an OGD RPE cell model	Mitochondrial dyes	Not verified	Restore mitochondrial function, mitochondrial network morphology, and mitochondrial dynamics in OGD cell models, while reducing RGC loss and optic nerve damage in MCAO rats	[24]

*The NADH: ubiquinone oxidoreductase iron-sulfur protein 4 (Ndufs4) gene knockout (KO) mice, initially used as a model for Leigh syndrome, were characterized by mitochondrial complex I dysfunction.

clarify the relative role of MT versus paracrine signaling, and optimize safe delivery methods for clinical translation.

Retinal degenerative diseases

Photoreceptor degeneration and AMD

Retinal degenerative diseases such as AMD and retinitis pigmentosa feature irreversible loss of photoreceptors and RPE cells [40]; these metabolically active, mitochondria-rich cells develop progressive mitochondrial dysfunction with reduced membrane potential, accumulated DNA mutations, increased oxidative stress and impaired quality control, which leads to energy deficiency, oxidative damage, cell death and subsequent retinal neuronal impairment [41, 42]. Photoreceptor transplantation is a potential therapy for retinal diseases, acting mainly through cell replacement and intercellular component transfer [43]. Donor photoreceptors delivered proteins, RNA and functional mitochondria to recipient cells via photoreceptor nanotubes (^{Ph}NTs) [44, 45], and mitochondria derived from MSCs or donor photoreceptors can improve the metabolism of host cells (Figure 1C) [21, 44, 45]. It remains unclear how cell replacement and material transfer respectively contribute to therapeutic outcomes. Moreover, MSCs-derived mitochondria and lysosomes can also be exchanged between photoreceptors through TNTs (Figure 1D) [21].

Exogenous mitochondrial delivery from MSCs also mitigates AMD-related mitochondrial dysfunction (Figure 1E). For example, bone marrow mononuclear cells (BMMCs)–derived mitochondria improved RPE function in oligomeric amyloid beta (oAβ)–treated models [17], while umbilical cord mesenchymal stem cells (UC-MSCs) -derived mitochondria alleviated senescence-associated mitochondrial defects [18]. Tissue source influences outcomes: human Wharton's Jelly MSCs (hWJ-MSCs) promoted autophagy, whereas human endometrium-derived MSCs(hE-MSCs) enhanced RPE

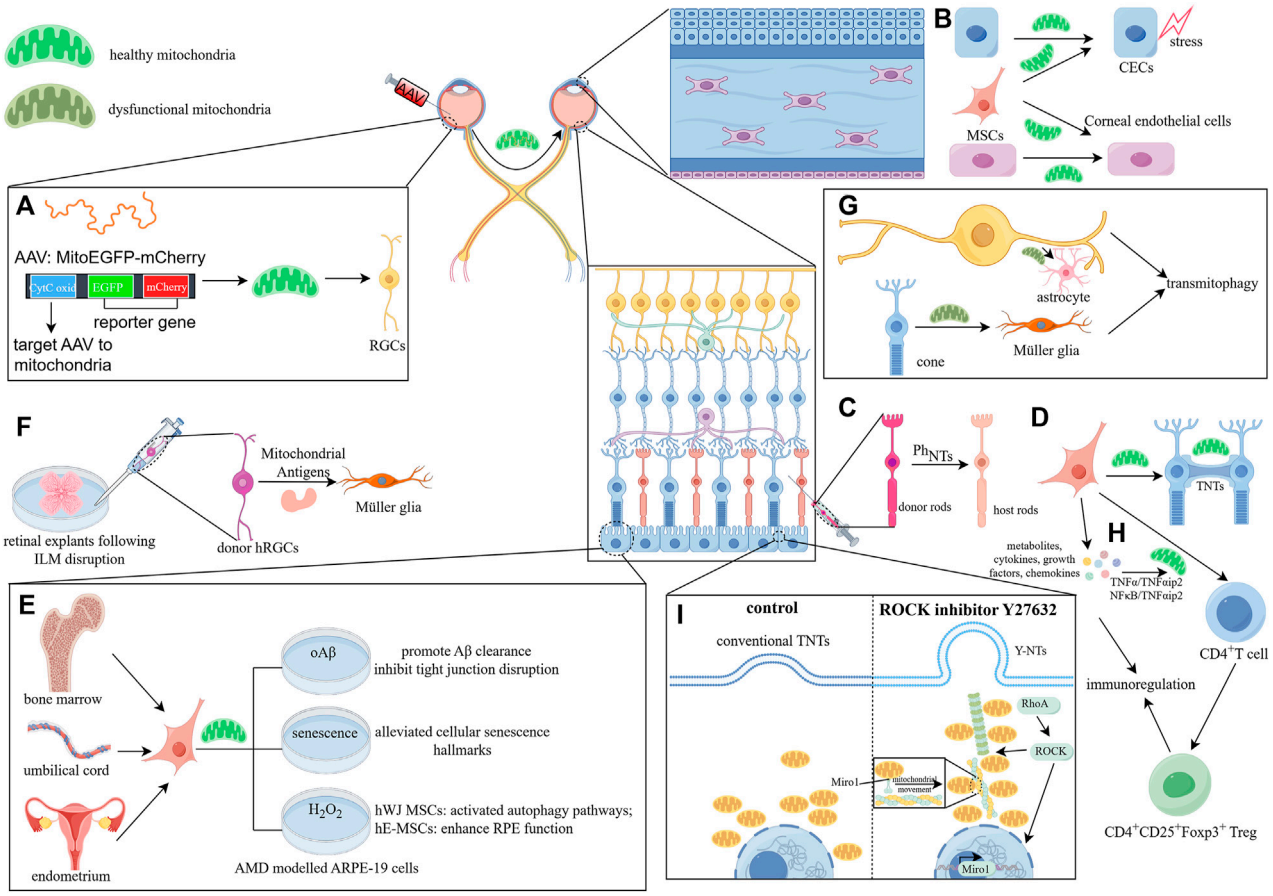


FIGURE 1
The development of mitochondrial transfer in the field of ophthalmology. **(A)** In Leber hereditary optic neuropathy (LHON) mouse models, adeno-associated virus (AAV)-loaded mitochondria travel along the visual system to the contralateral optic nerve and retina; the underlying mechanism remains unclear. **(B)** Intercellular mitochondrial transfer occurs in corneal epithelial cells (CECs) as well as between corneal endothelial cells in stress environments. Mesenchymal stem cells (MSCs), serving as efficient mitochondrial donors, participate in corneal injury repair. **(C)** Donor photoreceptors deliver proteins, RNA and functional mitochondria to host cells through photoreceptor nanotubes (^{Ph}NTs). **(D)** MSCs-derived mitochondria transfer between 661W cells (a cone photoreceptor cell line) through tunneling nanotubes (TNTs). **(E)** MSCs from different sources exert mitochondrial repair effects on ARPE-19 (human RPE cell line)-based age-related macular degeneration (AMD) models. **(F)** After inner limiting membrane (ILM) disruption, transplanted human embryonic stem cell derived retinal ganglion cells (RGCs) transfer mitochondrial antigens to Müller Glia (MG), enabling MG reprogramming to supplement RGCs for cell replacement therapy. **(G)** In neurons, transmitophagy was first reported between RGC axon mitochondria and astrocytes; damaged cone mitochondria are delivered to MG for degradation under mitochondrial stress. **(H)** MSCs transfer mitochondria to T cells to suppress effector T cells and induce Treg migration and anti-inflammation. MSCs also exert immunomodulation through paracrine factors (cytokines, growth factors, EVs) and control mitochondrial transfer via the TNFα/TNFαip2 and NFκB/TNFαip2 pathway. **(I)** Proper-dose Y27632 induces longer nanotubes in ARPE-19 cells, enhancing NTs-mediated mitochondrial transport via cytoskeletal remodeling. It upregulates Miro1 to modulate mitochondrial dynamics and movement. This image is drawn by Figdraw.

function, highlighting source-dependent therapeutic mechanisms [19].

Muller glia and transmitophagy

Müller glia (MG) play a central role in retinal homeostasis. Studies in degenerative models show that MG internalize MSCs-derived mitochondria, restoring mitochondrial structure and suppressing gliosis [20]. After ILM disruption, transplanting human embryonic stem cell derived RGCs into the mouse retina resulted in the transfer of donor RGCs substances, including mitochondrial antigens, to recipient MG (Figure 1F) [46]. Moreover, RGCs and cones can donate damaged mitochondria to glial cells for degradation, a process termed transmitophagy (Figure 1G) [47, 48]. This highlights glial cells participation in mitochondrial quality control and neuroprotection.

Although mitochondrial transfer has been implicated in photoreceptor rescue, RPE repair, and Müller glia support, several important questions remain unanswered. The relative contribution of MT versus other forms of material exchange—such as cytoplasmic or nuclear transfer—remains controversial, particularly in photoreceptor transplantation studies. Moreover, while MSCs-derived mitochondria have shown benefits in AMD and retinitis pigmentosa models, differences in therapeutic outcomes between tissue sources (e.g., Wharton's Jelly vs. endometrium MSCs) highlight the need for systematic comparative studies. The persistence of

transferred mitochondria and their functional integration into highly specialized retinal cells also remain poorly defined. Furthermore, transmitophagy appears to play a role in Müller glia support and neuroprotection, but its regulation and therapeutic implications in human disease are not well understood. Future directions should include longitudinal *in vivo* imaging, single-cell transcriptomic approaches to map donor–recipient interactions, and controlled studies comparing MT to direct mitochondrial transplantation. Ultimately, clarifying these mechanisms will be essential to translate MT into durable therapies for retinal degenerative diseases.

Ischemic retinopathy and glaucoma

Neurovascular coupling in the retina depends on pericyte communication through interpericyte TNTs (IP-TNTs) [49]. In diabetic retinopathy, pericyte loss and disrupted TNTs contribute to vascular dysfunction [50, 51]. Similarly, glaucoma is associated with impaired IP-TNTs, leading to reduced capillary diameter and blood flow [52, 53]. Whether mitochondrial transfer through IP-TNTs contributes to neurovascular regulation remains an open question.

Previous studies have shown that MSCs exert their immunomodulatory effects by releasing various mediators, including immunosuppressive molecules, growth factors, EVs, chemokines, cytokines, complement components, and various metabolites [54, 55]. MSCs-mediated MT also modulates immune responses (Figure 1H). By transferring mitochondria to T cells, MSCs promote regulatory T cell differentiation and suppress retinal inflammation in ischemia-reperfusion models (Figure 1H) [23, 56–61]. In stroke models, MSCs restored mitochondrial morphology and reduced RGCs loss [24]. These findings suggest MT as a dual mechanism: supporting vascular integrity and regulating retinal immune homeostasis.

The exact role of MT in neurovascular coupling and visual restoration is still uncertain, and current evidence is mainly from rodent models. Future efforts should employ large-animal models and real-time tracking to clarify mechanisms and assess long-term safety.

Factors influencing mitochondrial transfer

Under physiological conditions, MT occurs occasionally at a low frequency among ocular cells. Live-cell imaging of ^{Ph}NT-connected photoreceptors revealed merely two definitive MT events across 50 cell pairs during a 60-min observation period [45]. Fluorescence assays performed after 24 h of co-culture showed that the basal transfer rate was below 5% in untreated ARPE19 cells and 4% in CECs, with an even lower rate observed in corneal endothelial cells [21, 39]. The efficiency of MT is shaped by a combination of donor cell characteristics, transfer routes, recipient cell conditions, and the surrounding microenvironment. Among donor-related factors, the source of MSCs, the functional integrity of their mitochondria, and the expression of trafficking proteins such as Miro1 play decisive roles in determining transfer capacity [14, 15, 23, 62, 63]. As superior mitochondrial donors, MSCs achieve much higher transfer efficiency than native ocular cells. In co-culture, the MT rate from MSCs to corneal endothelial cells was approximately 29.42%, greatly surpassing the low spontaneous transfer level among common ocular cells [21]. With respect to transfer routes, TNTs represent the predominant mechanism, and their formation is tightly regulated by cytoskeletal remodeling and Rho GTPase signaling [64]. Pharmacological modulation, such as the use of ROCK inhibitors (e.g., Y-27632), has been shown to enhance TNTs formation and consequently increase MT efficiency (Figure 1I) [39, 65, 66]. At optimal concentrations, Y-27632 raised MT efficiency above 20% in ARPE-19 cells and increased the rate from approximately 4% to 7%–10% in CECs [39, 66]. Besides conventional TNTs, Y-27632 induced Y-NTs, an elongated subtype of intercellular nanotubes, in ARPE-19 cells and facilitated nanotube-dependent mitochondrial transport via cytoskeletal remodeling [66]. Mechanistically, it upregulated Miro1 to regulate mitochondrial dynamics; Miro1 controls mitochondrial movement by interacting with actin filaments and microtubules, thereby boosting intercellular mitochondrial transfer [2]. In addition, alternative pathways—including EVs, gap junctions, and transient cell fusion—also contribute under specific conditions [20, 67–72]. Wang, Y., et al discovered that the release of mitochondria-containing EVs from MSCs is regulated by the CD38/IP3R/Ca^{2+} pathway. Using a non-viral gene delivery vector to overexpress CD38 in MSCs, they generated “super donor” cells that produce “Super-EV-Mitochondria” with three times the mitochondrial yield and improved quality compared to normal MSC-derived EVs [13]. Recipient cell status is another critical determinant; cells experiencing mitochondrial dysfunction or oxidative stress tend to emit “rescue” signals that increase their susceptibility to accepting functional mitochondria [21, 73]. However, this improvement is limited and cannot substantially elevate the overall transfer efficiency. After hyperosmotic injury to CECs, MT increased slightly but remained markedly lower than in the Y27632 group, rendering large-scale cell repair unfeasible [39]. Additionally, recipient ocular cell type affected mitochondrial uptake efficiency; the photoreceptor cell line 661W exhibited a greater capacity to accept mitochondria from co-cultured MSCs than ARPE-19 cells [21]. Finally, the microenvironment exerts a substantial influence, as oxidative stress, hypoxia, and inflammatory signaling pathways, such as TNFα/TNFαip2, NFκB/TNFαip2, promote TNTs formation and intercellular transfer (Figure 1H) [15, 22, 63, 74, 75]. Collectively, these regulatory factors highlight potential intervention points to optimize MSC-mediated MT for therapeutic application in ophthalmic diseases.

Discussion

Mitochondrial transfer represents a paradigm shift in the understanding of intercellular communication and tissue repair within ophthalmology. Accumulating preclinical evidence demonstrates that MSC-mediated MT can restore cellular bioenergetics, enhance resistance to oxidative stress, and protect both retinal and corneal cells from degeneration. Despite this promise, several critical challenges must be overcome before clinical application can be realized.

Unlike systemic mitochondrial therapy, intraocular mitochondrial transplantation is restricted by the blood-ocular barrier, vitreoretinal

barrier and the eye's immune-privileged microenvironment, which greatly hinder the delivery, survival and functional integration of donor mitochondria. Common routes including intravitreal, subretinal and intravenous injection also have technical defects and potential complications. In addition, non-standard isolation and storage methods reduce mitochondrial activity [41]. The long-term efficacy, biosafety and molecular mechanisms of mitochondrial transplantation in retinal repair remain unclear.

The MitoCatch system, a cell-specific mitochondrial delivery platform, effectively addressed the inadequate targeting capability and low delivery efficiency of conventional mitochondrial transplantation. Its reliability was validated in cellular models, *ex vivo* human tissues and *in vivo* animal models. Relevant studies on LHON neurons and mouse optic nerve injury models further confirmed that targeted mitochondrial transplantation reversed mitochondrial dysfunction and prevented cellular degeneration [76]. This technology provided a new direction for the treatment of neurodegenerative diseases, optic atrophy and other intractable mitochondrial disorders.

Current researches mainly verify the short-term protective effects of MSC-mediated MT via *in vitro* cell models and animal models. These simplified models cannot fully simulate the complex *in vivo* ocular microenvironment. Moreover, there is a lack of mature quantitative methods to assess MT efficiency and functional recovery *in vivo*. Existing studies have only observed phenotypic improvements such as improved energy metabolism and relieved oxidative stress, while the regulatory roles of MT in ROS signaling, mitochondrial quality control and cell apoptosis remain poorly understood.

MSCs have been proven superior to ocular cells as mitochondrial donors. Nevertheless, the field still lacks unified criteria for donor screening and tissue-specific delivery schemes. Inconsistent donor sources and immature delivery systems may trigger abnormal cell proliferation and oncogenic risks. Comparative studies between MSC-mediated indirect mitochondrial transplantation and direct mitochondrial transplantation are required to evaluate their operability, efficacy and safety. Systematic assessments of long-term mitochondrial stability, immune responses and therapeutic outcomes in classic models such as AMD and LHON are also urgently needed.

Future studies should first establish standardized quantitative assays to dynamically monitor the *in vivo* behavior of mitochondria and evaluate therapeutic outcomes. Second, in-depth investigations are required to clarify the regulatory mechanisms of core signaling pathways including PTEN/PI3K/AKT during treatment [77]. Furthermore, given the substantial pathological heterogeneity among various retinal degenerative diseases, individualized transplantation protocols should be formulated according to disease categories and patient-specific conditions.

In summary, MT is a promising therapeutic strategy for retinal degenerative diseases. By correcting mitochondrial dysfunction, it restores cellular energy balance and mitigates oxidative damage. With continuous technological optimization, mechanistic research and safety verification, MT is expected to evolve into a mature clinical therapy for irreversible visual impairment.

Author contributions

Conceptualization, XL; writing—original draft preparation, MZ; writing—review and editing, ZW; supervision. All authors contributed to the article and approved the submitted version.

Funding

The author(s) declared that financial support was received for this work and/or its publication. This work was supported by Liaoning Provincial Science and Technology Program (grant number 2023-MSLH-074) and the project of Education Department of Liaoning Province (grant number LJ232413610015 and LJ212513610007).

Conflict of interest

The author(s) declared no potential conflicts of interest with respect to the research, authorship, and/or publication of this article.

Generative AI statement

The author(s) declared that generative AI was used in the creation of this manuscript. The authors acknowledge the use of Doubao in the preparation of this manuscript. Doubao was utilized for language polishing, grammatical revision, and formatting assistance. All content generated by AI has been rigorously checked for accuracy, and the authors take full responsibility for the final version of the manuscript.

Any alternative text (alt text) provided alongside figures in this article has been generated by Frontiers with the support of artificial intelligence and reasonable efforts have been made to ensure accuracy, including review by the authors wherever possible. If you identify any issues, please contact us.

References

1. Abu-Amero KK, Almadani B, Abualkhair S, Hameed S, Kondkar AA, Sollazzo A, et al. Mitochondrial DNA pathogenic variants in ophthalmic diseases: a review. *Genes* (2025) 16(3):347. doi:10.3390/genes16030347

2. Iorio R, Petricca S, Mattei V, Delle Monache S. Horizontal mitochondrial transfer as a novel bioenergetic tool for mesenchymal stromal/stem cells: molecular mechanisms and therapeutic potential in a variety of diseases. *J Translational Medicine* (2024) 22(1):491. doi:10.1186/s12967-024-05047-4

3. Zeviani M, Carelli V. Mitochondrial retinopathies. *Int Journal Molecular Sciences* (2021) 23(1):210. doi:10.3390/ijms23010210

4. Protasoni M, Zeviani M. Mitochondrial structure and bioenergetics in normal and disease conditions. *Int Journal Molecular Sciences* (2021) 22(2):586. doi:10.3390/ijms22020586

5. Brooks CD, Kodati B, Stankowska DL, Krishnamoorthy RR. Role of mitophagy in ocular neurodegeneration. *Front Neuroscience* (2023) 17:1299552. doi:10.3389/fnins.2023.1299552

6. Canter JA, Olson LM, Spencer K, Schnetz-Boutaud N, Anderson B, Hauser MA, et al. Mitochondrial DNA polymorphism A4917G is independently associated with age-related macular degeneration. *PloS One* (2008) 3(5):e2091. doi:10.1371/journal.pone.0002091

7. Sarhangi N, Khatami F, Keshtkar A, Heshmat R, Atlasi R, Mohammadamoli M. The role of mitochondrial DNA (mtDNA) in the development of diabetic retinopathy (DR): a systematic review. Medical hypothesis. *Discovery & Innovation Ophthalmology Journal* (2017) 6(2):30–8.

8. Collins DW, Gudiseva HV, Chavali VRM, Trachtman B, Ramakrishnan M, Merritt WT, III, et al. The MT-CO1 V83I polymorphism is a risk factor for primary open-angle glaucoma in African American men. *Invest Ophthalmology & Visual Science* (2018) 59(5):1751–9. doi:10.1167/iovs.17-23277

9. Hermankova B, Javorkova E, Palacka K, Holan V. Perspectives and limitations of mesenchymal stem cell-based therapy for corneal injuries and retinal diseases. *Cell Transplantation* (2025) 34:9636897241312798. doi:10.1177/09636897241312798

10. Adak S, Magdalene D, Deshmukh S, Das D, Jaganathan BG. A review on mesenchymal stem cells for treatment of retinal diseases. *Stem Cell Reviews Reports* (2021) 17(4):1154–73. doi:10.1007/s12015-020-10090-x

11. Velarde F, Ezquerra S, Delbruyere X, Caicedo A, Hidalgo Y, Khoury M. Mesenchymal stem cell-mediated transfer of mitochondria: mechanisms and functional impact. *Cell Molecular Life Sciences : CMLS* (2022) 79(3):177. doi:10.1007/s00018-022-04207-3

12. Wang R, Bao F, Lu M, Jia X, Xiao J, Wu Y, et al. MSC-mediated mitochondrial transfer restores mitochondrial DNA and function in neural progenitor cells of Leber's hereditary optic neuropathy. *Sci China Life Sciences* (2024) 67(11):2511–9. doi:10.1007/s11427-024-2647-8

13. Wang Y, Yu HY, Yi ZJ, Qi LY, Yang JS, Xie HX, et al. Super mitochondria-enriched extracellular vesicles enable enhanced mitochondria transfer. *Nat Communications* (2025) 16(1):9448. doi:10.1038/s41467-025-64486-9

14. Jiang D, Xiong G, Feng H, Zhang Z, Chen P, Yan B, et al. Donation of mitochondria by iPSC-derived mesenchymal stem cells protects retinal ganglion cells against mitochondrial complex I defect-induced degeneration. *Theranostics* (2019) 9(8):2395–410. doi:10.7150/thno.29422

15. Jiang D, Gao F, Zhang Y, Wong DS, Li Q, Tse HF, et al. Mitochondrial transfer of mesenchymal stem cells effectively protects corneal epithelial cells from mitochondrial damage. *Cell Death & Disease* (2016) 7(11):e2467. doi:10.1038/cddis.2016.358

16. Jiang D, Yu J, Wu X, Yu X, Jin P, Zheng H, et al. Isolated mitochondrial transplantation as a novel treatment for corneal chemical burns. *Invest Ophthalmology & Visual Science* (2025) 66(3):14. doi:10.1167/iovs.66.3.14

17. Noh SE, Lee SJ, Cho CS, Jo DH, Park KS, Kim JH. Mitochondrial transplantation attenuates oligomeric amyloid-beta-induced mitochondrial dysfunction and tight junction protein destruction in retinal pigment epithelium. *Free Radical Biology & Medicine* (2024) 212:10–21. doi:10.1016/j.freeradbiomed.2023.12.012

18. Noh SE, Lee SJ, Lee TG, Park KS, Kim JH. Inhibition of cellular senescence hallmarks by mitochondrial transplantation in senescence-induced ARPE-19 cells. *Neurobiol Aging* (2023) 121:157–65. doi:10.1016/j.neurobiolaging.2022.11.003

19. Kılıç KC, Duruksu G, Öztürk A, Rençber SF, Kılıç B, Yazır Y. Therapeutic potential of adult stem cells-derived mitochondria transfer combined with curcumin administration into ARPE-19 cells in age-related macular degeneration model. *Tissue & Cell* (2025) 93:102687. doi:10.1016/j.tice.2024.102687

20. Huang X, Luodan A, Gao H, He J, Ge L, Cha Z, et al. Mitochondrial transfer between BMSCs and Müller promotes mitochondrial fusion and suppresses gliosis in degenerative retina. *iScience* (2024) 27(7):110309. doi:10.1016/j.isci.2024.110309

21. Jiang D, Chen FX, Zhou H, Lu YY, Tan H, Yu SJ, et al. Bioenergetic Crosstalk between mesenchymal stem cells and various ocular cells through the intercellular trafficking of mitochondria. *Theranostics* (2020) 10(16):7260–72. doi:10.7150/thno.46332

22. Gozel M, Senkoylu K, Kesim C, Hasanreisoglu M. Adipose-derived mesenchymal stem cells and retinal pigment epithelial cells interactions in a stress environment *via* tunneling nanotubes. *PloS One* (2025) 20(8):e0329672. doi:10.1371/journal.pone.0329672

23. Agrawal M, Rasiah PK, Bajwa A, Rajasingh J, Gangaraju R. Mesenchymal stem cell induced Foxp3(+) tregs suppress effector T cells and protect against retinal ischemic injury. *Cells* (2021) 10(11):3006. doi:10.3390/cells10113006

24. Nguyen H, Lee JY, Sanberg PR, Napoli E, Borlongan CV. Eye opener in stroke. *Stroke* (2019) 50(8):2197–206. doi:10.1161/strokeaha.119.025249

25. Hellström M, Ruitenberg MJ, Pollett MA, Ehlert EM, Twisk J, Verhaagen J, et al. Cellular tropism and transduction properties of seven adeno-associated viral vector serotypes in adult retina after intravitreal injection. *Gene Therapy* (2009) 16(4):521–32. doi:10.1038/gt.2008.178

26. Newman NJ, Yu-Wai-Man P, Subramanian PS, Moster ML, Wang AG, Donahue SP, et al. Randomized trial of bilateral gene therapy injection for m.11778G>A MT-ND4 leber optic neuropathy. *Brain* (2023) 146(4):1328–41. doi:10.1093/brain/awac421

27. Biousse V, Newman NJ, Yu-Wai-Man P, Carelli V, Moster ML, Vignal-Clermont C, et al. Long-term Follow-Up after unilateral intravitreal gene therapy for Leber Hereditary optic neuropathy: the RESTORE study. *J Neuro-Ophthalmology : The Official Journal North Am Neuro-Ophthalmology Soc* (2021) 41(3):309–15. doi:10.1097/wno.0000000000001367

28. Newman NJ, Yu-Wai-Man P, Carelli V, Biousse V, Moster ML, Vignal-Clermont C, et al. Intravitreal gene therapy vs. natural history in patients with Leber Hereditary optic neuropathy carrying the m.11778G>A ND4 mutation: systematic review and indirect comparison. *Front Neurology* (2021) 12:662838. doi:10.3389/fneur.2021.662838

29. Yang S, Ma SQ, Wan X, He H, Pei H, Zhao MJ, et al. Long-term outcomes of gene therapy for the treatment of Leber's hereditary optic neuropathy. *EBioMedicine* (2016) 10:258–68. doi:10.1016/j.ebiom.2016.07.002

30. Yu-Wai-Man P, Newman NJ, Carelli V, Moster ML, Biousse V, Sadun AA, et al. Bilateral visual improvement with unilateral gene therapy injection for Leber hereditary optic neuropathy. *Sci Translational Medicine* (2020) 12(573). doi:10.1126/scitranslmed.aaz7423

31. Ezan P, Hardy E, Bemelmans A, Taiel M, Dossi E, Rouach N. Retinal damage promotes mitochondrial transfer in the visual system of a mouse model of Leber hereditary optic neuropathy. *Neurobiol Disease* (2024) 201:106681. doi:10.1016/j.nbd.2024.106681

32. Lin TK, Chen SD, Chuang YC, Lan MY, Chuang JH, Wang PW, et al. Mitochondrial transfer of wharton's jelly mesenchymal stem cells eliminates mutation burden and rescues mitochondrial bioenergetics in rotenone-stressed MELAS fibroblasts. *Oxidative Medicine Cellular Longevity* (2019) 2019:9537504. doi:10.1155/2019/9537504

33. Chuang YC, Liou CW, Chen SD, Wang PW, Chuang JH, Tiao MM, et al. Mitochondrial transfer from wharton's Jelly mesenchymal stem cell to MERRF cybrid reduces oxidative stress and improves mitochondrial bioenergetics. *Oxidative Medicine Cellular Longevity* (2017) 2017:5691215. doi:10.1155/2017/5691215

34. Zheng Q, Ren Y, Reinach PS, Xiao B, Lu H, Zhu Y, et al. Reactive oxygen species activated NLRP3 inflammasomes initiate inflammation in hyperosmolarity stressed human corneal epithelial cells and environment-induced dry eye patients. *Exp Eye Research* (2015) 134:133–40. doi:10.1016/j.exer.2015.02.013

35. Bron AJ, de Paiva CS, Chauhan SK, Bonini S, Gabison EE, Jain S, et al. TFOS DEWS II pathophysiology report. *The Ocular Surface* (2017) 15(3):438–510. doi:10.1016/j.jtos.2017.05.011

36. Ouyang W, Yan D, Hu J, Liu Z. Multifaceted mitochondrial as a novel therapeutic target in dry eye: insights and interventions. *Cell Death Discovery* (2024) 10(1):398. doi:10.1038/s41420-024-02159-0

37. Mao K, Huang Y, Liu Z, Sui W, Liu C, Li Y, et al. Oxidative stress mediates retinal damage after corneal alkali burn through the activation of the cGAS/STING pathway. *Exp Eye Research* (2025) 251:110228. doi:10.1016/j.exer.2024.110228

38. Chinnery HR, Keller KE. Tunneling nanotubes and the eye: intercellular communication and implications for ocular health and disease. *Biomed Research International* (2020) 2020:7246785. doi:10.1155/2020/7246785

39. Jiang D, Xu W, Peng F, Sun Y, Pan C, Yu J, et al. Tunneling nanotubes-based intercellular mitochondrial trafficking as a novel therapeutic target in dry eye. *Exp Eye Research* (2023) 232:109497. doi:10.1016/j.exer.2023.109497

40. Holan V, Palacka K, Hermankova B. Mesenchymal stem cell-based therapy for retinal degenerative diseases: experimental models and clinical trials. *Cells* (2021) 10(3):588. doi:10.3390/cells10030588

41. Chi J, Fan B, Li Y, Jiao Q, Li GY. Mitochondrial transplantation: a promising strategy for the treatment of retinal degenerative diseases. *Neural Regeneration Research* (2025) 20(12):3370–87. doi:10.4103/nrr.Nrr-d-24-00851

42. Barot M, Gokulgandhi MR, Mitra AK. Mitochondrial dysfunction in retinal diseases. *Curr Eye Research* (2011) 36(12):1069–77. doi:10.3109/02713683.2011.607536

43. Wang J, Nnoromele PO, Liu YV, Johnston RJ, Jr, Singh MS. Cellular component transfer between photoreceptor cells of the retina. *Prog Retinal Eye Research* (2025) 104:101317. doi:10.1016/j.preteyeres.2024.101317

44. Ortin-Martinez A, Yan NE, Tsai ELS, Comanita L, Gurdita A, Tachibana N, et al. Photoreceptor nanotubes mediate the *in vivo* exchange of intracellular material. *The EMBO Journal* (2021) 40(22):e107264. doi:10.15252/embj.2020107264

45. Kalargyrou AA, Basche M, Hare A, West EL, Smith AJ, Ali RR, et al. Nanotube-like processes facilitate material transfer between photoreceptors. *EMBO Reports* (2021) 22(11):e53732. doi:10.15252/embr.202153732

46. Zhang KY, Nagalingam A, Mary S, Aguzzi EA, Li W, Chetla N, et al. Rare intercellular material transfer as a confound to interpreting inner retinal neuronal transplantation following internal limiting membrane disruption. *Stem Cell Reports* (2023) 18(11):2203–21. doi:10.1016/j.stemcr.2023.09.005

47. Davis CH, Kim KY, Bushong EA, Mills EA, Boassa D, Shih T, et al. Transcellular degradation of axonal mitochondria. *Proc Natl Acad Sci USA* (2014) 111(26):9633–8. doi:10.1073/pnas.1404651111

48. Hutto RA, Rutter KM, Giarmarco MM, Parker ED, Chambers ZS, Brockerhoff SE. Cone photoreceptors transfer damaged mitochondria to Müller glia. *Cell Reports* (2023) 42(2):112115. doi:10.1016/j.celrep.2023.112115

49. Alarcon-Martinez L, Villafranca-Baughman D, Quintero H, Kacerovsky JB, Dotigny F, Murai KK, et al. Interpericyte tunnelling nanotubes regulate neurovascular coupling. *Nature* (2020) 585(7823):91–5. doi:10.1038/s41586-020-2589-x

50. Hammes HP, Lin J, Renner O, Shani M, Lundqvist A, Betsholtz C, et al. Pericytes and the pathogenesis of diabetic retinopathy. *Diabetes* (2002) 51(10):3107–12. doi:10.2337/diabetes.51.10.3107

51. Kempf S, Popp R, Naeem Z, Frömel T, Wittig I, Klatt S, et al. Pericyte-to-Endothelial cell communication *via* tunneling nanotubes is disrupted by a diol of docosahexaenoic acid. *Cells* (2024) 13(17):1429. doi:10.3390/cells13171429

52. McDonald H, Gardner-Russell J, Alarcon-Martinez L. Orchestrating blood flow in the retina: Interpericyte tunnelling nanotube communication. *Results Problems Cell Differentiation* (2024) 73:229–47. doi:10.1007/978-3-031-62036-2_11

53. Alarcon-Martinez L, Shiga Y, Villafranca-Baughman D, Belforte N, Quintero H, Dotigny F, et al. Pericyte dysfunction and loss of interpericyte tunneling nanotubes promote neurovascular deficits in glaucoma. *Proc Natl Acad Sci USA* (2022) 119(7): e2110329119. doi:10.1073/pnas.2110329119

54. Huang Y, Wu Q, Tam PKH. Immunomodulatory mechanisms of mesenchymal stem cells and their potential clinical applications. *Int Journal Molecular Sciences* (2022) 23(17):10023. doi:10.3390/ijms231710023

55. Li P, Ou Q, Shi S, Shao C. Immunomodulatory properties of mesenchymal stem cells/dental stem cells and their therapeutic applications. *Cell & Molecular Immunology* (2023) 20(6):558–69. doi:10.1038/s41423-023-00998-y

56. Court AC, Le-Gatt A, Luz-Crawford P, Parra E, Aliaga-Tobar V, Bátiz LF, et al. Mitochondrial transfer from MSCs to T cells induces Treg differentiation and restricts inflammatory response. *EMBO Reports* (2020) 21(2):e48052. doi:10.15252/embr.201948052

57. Do JS, Zwick D, Kenyon JD, Zhong F, Askew D, Huang AY, et al. Mesenchymal stromal cell mitochondrial transfer to human induced T-regulatory cells mediates FOXP3 stability. *Scientific Reports* (2021) 11(1):10676. doi:10.1038/s41598-021-90115-8

58. Khanh VTH, Chen H, Pan L, Cho KS, Doesburg D, Thee EF, et al. CD4(+) T-Cell responses mediate progressive neurodegeneration in experimental ischemic retinopathy. *The Am Journal Pathology* (2020) 190(8):1723–34. doi:10.1016/j.ajpath.2020.04.011

59. Maloy KJ, Salaun L, Cahill R, Dougan G, Saunders NJ, Powrie F. CD4+CD25+ T(R) cells suppress innate immune pathology through cytokine-dependent mechanisms. *The J Experimental Medicine* (2003) 197(1):111–9. doi:10.1084/jem.20021345

60. André S, Tough DF, Lacroix-Desmazes S, Kaveri SV, Bayry J. Surveillance of antigen-presenting cells by CD4+ CD25+ regulatory T cells in autoimmunity: immunopathogenesis and therapeutic implications. *The Am Journal Pathology* (2009) 174(5):1575–87. doi:10.2353/ajpath.2009.080987

61. Taams LS, van Amelsfort JM, Tiemessen MM, Jacobs KM, de Jong EC, Akbar AN, et al. Modulation of monocyte/macrophage function by human CD4+CD25+ regulatory T cells. *Hum Immunology* (2005) 66(3):222–30. doi:10.1016/j.humimm.2004.12.006

62. Ahmad T, Mukherjee S, Pattnaik B, Kumar M, Singh S, Kumar M, et al. Miro1 regulates intercellular mitochondrial transport & enhances mesenchymal stem cell rescue efficacy. *The EMBO Journal* (2014) 33(9):994–1010. doi:10.1002/embj.201386030

63. Zhang Y, Yu Z, Jiang D, Liang X, Liao S, Zhang Z, et al. iPSC-MSCs with high intrinsic MIRO1 and sensitivity to TNF-α yield efficacious mitochondrial transfer to rescue anthracycline-induced cardiomyopathy. *Stem Cell Reports* (2016) 7(4):749–63. doi:10.1016/j.stemcr.2016.08.009

64. Feng T, Xu Q, Wang S, Hou D, Wu X. Interplay between tunneling nanotubes and Wnt signaling: insights into cytoskeletal regulation and therapeutic potential. *Biochem Biophysics Reports* (2025) 43:102065. doi:10.1016/j.bbrep.2025.102065

65. Keller KE, Bradley JM, Sun YY, Yang YF, Acott TS. Tunneling nanotubes are novel cellular structures that communicate signals between trabecular meshwork cells. *Invest Ophthalmology & Visual Science* (2017) 58(12):5298–307. doi:10.1167/iovs.17-22732

66. Yuan J, Chen F, Jiang D, Xu Z, Zhang H, Jin ZB. ROCK inhibitor enhances mitochondrial transfer *via* tunneling nanotubes in retinal pigment epithelium. *Theranostics* (2024) 14(15):5762–77. doi:10.7150/thno.96508

67. Morrison TJ, Jackson MV, Cunningham EK, Kissenpfennig A, McAuley DF, O'Kane CM, et al. Mesenchymal stromal cells modulate macrophages in clinically relevant lung injury models by extracellular vesicle mitochondrial transfer. *Am Journal Respiratory Critical Care Medicine* (2017) 196(10):1275–86. doi:10.1164/rccm.201701-0170OC

68. Souidi N, Stolk M, Seifert M. Ischemia-reperfusion injury: beneficial effects of mesenchymal stromal cells. *Curr Opinion Organ Transplantation* (2013) 18(1):34–43. doi:10.1097/MOT.0b013e32835c2a05

69. Wittig D, Wang X, Walter C, Gerdes HH, Funk RH, Roehlecke C. Multi-level communication of human retinal pigment epithelial cells *via* tunneling nanotubes. *PloS One* (2012) 7(3):e33195. doi:10.1371/journal.pone.0033195

70. Li X. Gap junction protein connexin43 and tunneling nanotubes in human trabecular meshwork cells. *Int Journal Physiology, Pathophysiology Pharmacology* (2019) 11(5):212–9.

71. Pesaresi M, Sebastian-Perez R, Cosma MP. Dedifferentiation, transdifferentiation and cell fusion: *in vivo* reprogramming strategies for regenerative medicine. *The FEBS Journal* (2019) 286(6):1074–93. doi:10.1111/febs.14633

72. Acquistapace A, Bru T, Lesault PF, Figeac F, Coudert AE, le Coz O, et al. Human mesenchymal stem cells reprogram adult cardiomyocytes toward a progenitor-like state through partial cell fusion and mitochondria transfer. *Stem Cells (Dayton, Ohio)* (2011) 29(5):812–24. doi:10.1002/stem.632

73. Mahrouf-Yorgov M, Augeul L, Da Silva CC, Jourdan M, Rigolet M, Manin S, et al. Mesenchymal stem cells sense mitochondria released from damaged cells as danger signals to activate their rescue properties. *Cell Death Differentiation* (2017) 24(7): 1224–38. doi:10.1038/cdd.2017.51

74. Liu Q, Zhang X, Zhu T, Xu Z, Dong Y, Chen B. Mitochondrial transfer from mesenchymal stem cells: mechanisms and functions. *Mitochondrion* (2024) 79:101950. doi:10.1016/j.mito.2024.101950

75. Jing M, Xiong X, Mao X, Song Q, Zhang L, Ouyang Y, et al. HMGB1 promotes mitochondrial transfer between hepatocellular carcinoma cells through RHOT1 and RAC1 under hypoxia. *Cell Death & Disease* (2024) 15(2):155. doi:10.1038/s41419-024-06536-6

76. Ayupov T, Moreno-Juan V, Curtoni S, Fratzl A, Sharma U, Posada-Céspedes S, et al. Cell-type-targeted mitochondrial transplantation rescues cell degeneration. *Nature* (2026) 653(8113):221–31. doi:10.1038/s41586-026-10391-0

77. Liu X, Zhang Y, Yang X, Zhang Y, Liu Y, Wang L, et al. Mitochondrial transplantation inhibits cholangiocarcinoma cells growth by balancing oxidative stress tolerance through PTEN/PI3K/AKT signaling pathway. *Tissue & Cell* (2023) 85:102243. doi:10.1016/j.tice.2023.102243

EBM Experimental Biology and Medicine

TYPE Original Research
PUBLISHED 11 August 2026
DOI 10.3389/ebm.2026.10915

Check for updates

OPEN ACCESS

*CORRESPONDENCE
Huisheng Wu,
01020026@gzpt.edu.cn

RECEIVED 22 December 2025
REVISED 23 April 2026
ACCEPTED 07 July 2026
PUBLISHED 11 August 2026

CITATION
Gu H and Wu H (2026) The value of serum exosomal miRNA signature profiles for the early diagnosis of feline infectious peritonitis.
Exp. Biol. Med. 251:10915.
doi: 10.3389/ebm.2026.10915

COPYRIGHT
© 2026 Gu and Wu. This is an open-access article distributed under the terms of the Creative Commons Attribution License (CC BY). The use, distribution or reproduction in other forums is permitted, provided the original author(s) and the copyright owner(s) are credited and that the original publication in this journal is cited, in accordance with accepted academic practice. No use, distribution or reproduction is permitted which does not comply with these terms.

The value of serum exosomal miRNA signature profiles for the early diagnosis of feline infectious peritonitis

Hongxia Gu[1,2] and Huisheng Wu[1,2]*

[1]Ganzhou Vocational and Technical College, Gan Zhou, China, [2]Key Laboratory of Animal Pathogens and Biosecurity Prevention and Control in Ganzhou, Gan Zhou, China

Abstract

Feline Infectious Peritonitis (FIP) is a highly lethal disease in cats, and early differential diagnosis remains a significant clinical challenge. In this study, we analyzed differences in serum exosomal miRNA expression between FIP-affected cats and healthy control cats via high-throughput sequencing and identified five significantly differentially expressed miRNAs (miR-21-5p, miR-155-5p, miR-200c-3p, miR-486-5p, and miR-423-5p). A combined diagnostic model was constructed based on three key miRNAs (miR-21-5p, miR-155-5p, and miR-423-5p). ROC curve analysis showed that a combined model of these three key miRNAs had an area under the curve (AUC) of 0.93, with a sensitivity and specificity of 88.6% and 91.2%, respectively. These results indicate that the serum exosomal miRNA signature could be used as a novel biomarker for the early diagnosis of FIP, providing a non-invasive diagnostic tool in clinical practice.

KEYWORDS
biomarkers, early diagnosis, exosomes, feline infectious peritonitis, miRNA

Impact statement

This manuscript significantly advances the field of feline infectious peritonitis (FIP) diagnosis by identifying a novel biomarker for early detection.Unlike traditional methods that are invasive or lack sensitivity, our study reveals that specific serum exosomal miRNAs can accurately distinguish FIP-affected cats from healthy ones. This non-invasive approach offers high sensitivity and specificity, providing a valuable tool for early intervention and treatment. Our findings fill a critical gap in FIP diagnostics, offering hope for improved management and outcomes in affected felines.

Introduction

Feline infectious peritonitis (FIP) is caused by virulent mutants of feline coronavirus (FCoV), with diverse clinical symptoms and non-characteristic manifestations, making early diagnosis extremely difficult. Traditional diagnostic methods rely primarily on histopathology or immunohistochemistry; however, these methods are invasive, and their sensitivity and accuracy are insufficient for early clinical diagnosis. Exosomes, as important mediators of intercellular communication, play a critical role in the physiological and pathological processes

of various diseases, and the miRNAs encapsulated in exosomes can regulate the pathogenesis of multiple diseases [1–4].

Traditional diagnostic methods have significant clinical limitations: serological testing is susceptible to viral variation and cross-reactivity interference [5, 6]; molecular methods, such as PCR, have high sensitivity but cannot distinguish pathogenic feline infectious peritonitis virus (FIPV) from non-pathogenic feline enteric coronavirus (FECV) [7, 8]; imaging and pathological examinations depend on symptoms of the middle and late stages of the disease, making early intervention almost impossible [9, 10].

The potential of exosomal miRNAs as novel biomarkers is supported by their unique biological properties: ① Stability: exosomes encapsulate miRNAs to protect them from degradation by RNases, making them stably detectable in body fluids such as serum [11]; ② Specificity: miRNA expression can accurately distinguish different pathological states, such as inflammation, infection, or tumorigenesis. Previous studies have found that FIP-associated uveitis is closely related to peripheral immune status, suggesting that miRNAs may be involved in the immune regulation of FIP progression [12, 13].

In recent years, numerous studies have confirmed that circulating miRNAs can be used for the diagnosis of various malignant tumors and infectious diseases. However, the clinical utility of exosomal miRNAs in FIP diagnosis has not been fully explored. The aim of this study is to investigate the value of serum exosomal miRNAs in the early differential diagnosis of FIP to provide a new strategy for optimizing the clinical diagnosis and treatment of FIP [14–16].

Materials and methods

Sample collection

All animal experiments in this study were conducted in strict accordance with relevant national laws and regulations on animal welfare and were approved by the Animal Ethics Committee (Approval No. 2025-0617-0036). All samples were collected from cats diagnosed with FIP from January 2023 to December 2023, and age- and breed-matched healthy cats were enrolled during the same period as the control group. The diagnosis of FIP was confirmed in accordance with the Expert Consensus for Diagnosis of Feline Infectious Peritonitis formulated by the Chinese Veterinary Medical Association in 2021.

The inclusion criteria for FIP cases were as follows: cats had to meet any of the following conditions, and other differential diseases had to be excluded: (1) histopathological confirmation of typical granulomatous lesions [10, 11]; (2) positive immunohistochemical staining for FCoV antigen in infected cells, combined with positive FCoV nucleic acid test results; (3) typical clinical symptoms (e.g., persistent high fever, abdominal distension with massive effusion, and uveitis), combined with positive ultrasound signs of ascites and diffuse nodular shadows in both lungs on chest radiographs [11–15].

A total of 32 cats with FIP were finally included in this study, including 16 cats with exudative FIP and 16 cats with non-exudative FIP. For the 16 exudative FIP cats, body weights ranged from 2.6 kg to 4.8 kg, with an average weight of 3.7 kg and a median weight of 3.5 kg. For the 16 non-exudative FIP cats, body weight ranged from 2.4 kg to 4.5 kg, with an average weight of 3.4 kg and a median weight of 3.3 kg. The sex distribution among the 32 FIP cats was 18 males and 14 females. All cats underwent a detailed clinical examination to ensure that they had no history of other underlying diseases or infectious diseases. To control for confounding factors, consistency in sex, age, and breed was ensured as much as possible during case enrollment.

The healthy control group consisted of 20 age- and breed-matched cats without any clinical symptoms. All control cats tested negative for FCoV infection via routine blood tests, serum biochemical tests, and FCoV PCR tests. The basic information of all included cats is shown in Table 1.

All cats were fasted for 12 h prior to sample collection to reduce the interference of lipemia on serum exosome isolation. A total of 5 mL of whole blood was collected via jugular vein puncture, injected into anticoagulant-free vacuum blood collection tubes (BD, USA), and centrifuged at 3,000× g for 15 min (centrifuge model: Eppendorf 5810R, Germany) after standing for 30 min at room temperature to isolate the upper serum layer. To prevent the effect of repeated freezing and thawing on miRNA stability, the serum was dispensed into 1.5 mL RNase-free EP tubes (Axygen, USA) at a volume of 200 μL per tube and immediately stored in an ultra-low-temperature refrigerator (Thermo Fisher Scientific, USA) at −80 °C. All operations were performed in a biological safety cabinet (ESCO, Singapore), and operators wore sterile gloves and masks to prevent sample contamination.

Exosome isolation and characterization

Serum exosomes were isolated by ultracentrifugation according to the guidelines of the International Society for the Study of Extracellular Vesicles (ISEV). Briefly, the frozen serum was thawed at 4 °C and centrifuged at 2,000× g for 10 min to remove residual cellular debris. The supernatant was transferred to a new tube and centrifuged at 100,00× g for 30 min to remove apoptotic microsomes and macrovesicles (centrifuge: Optima XPN-100, Beckman Coulter, USA). Next, particles larger than >200 nm were removed by filtration using a 0.22-μm pore size PVDF filter membrane (Millipore, USA). The filtrate was transferred to an ultracentrifuge tube (Beckman Coulter, USA) and centrifuged at 1,100,00× g at 4 °C for 70 min (rotor model: Type 70 Ti). The supernatant was discarded, and the precipitate was resuspended in pre-cooled PBS, and the ultracentrifugation step was repeated once to improve exosome purity. The final precipitate was resuspended in 100 μL of PBS, and the exosome protein concentration was then quantified using the BCA method (Pierce™ BCA Protein Assay Kit, Thermo Fisher, USA).

Exosome identification was performed via morphology, particle size, and analysis of marker proteins: (1) Transmission electron microscopy (TEM): 10 μL of the exosome suspension was dropped onto a copper mesh (carbon support film, Beijing Zhongmiao Science and Technology Instrument, Beijing, China), negatively stained with 2% phosphotungstic acid for 1 min, dried, and observed under a JEM-1400 Flash electron microscope (JEOL, Japan) at an accelerating voltage of 80 kV; (2) Nanoparticle tracking Analysis (NTA): A NanoSight NS300 system (Malvern Panalytical, UK) was used to dilute the exosome suspension to 10^7-10^8 particles/mL with PBS, the injection flow rate was set to 25 μL/

TABLE 1 Basic information and clinical symptoms of cats in each group.

Group	Quantity	Age range (months)	Sex ratio (male: female)	Breed distribution	Clinical symptoms
FIP group (exudative)	16	6–36	9:7	Various breeds (British shorthair, American shorthair, Persian, etc.)	Persistent high fever, abdominal distension with large fluid accumulation, uveitis, etc.
FIP group (non-exudative)	16	8–42	9:7	Various breeds (British shorthair, American shorthair, Persian, etc.)	Persistent high fever, weight loss, loss of appetite, etc.
Healthy control group	20	6–48	11:9	Various breeds (British shorthair, American shorthair, Persian, etc.)	No clinical symptoms

min, and each sample was tested in triplicate. The particle size distribution and particle concentration were analyzed using NTA 3.4 software; (3) Western blot analysis of marker proteins: 20 μg of exosomal proteins were separated using 10% SDS-PAGE electrophoresis and transferred to a PVDF membrane (Millipore, USA). The membrane was blocked with 5% skim milk for 1 h, and incubated sequentially with primary antibodies (CD63, Abcam ab68418, 1:1000; TSG101, Abcam ab125011, 1:800) and HRP-labeled goat anti-rabbit IgG secondary antibody (Abcam ab6721, 1:5000). Protein bands were visualized via an ECL chemiluminescence kit (ImageQuant LAS 4000, GE Healthcare, USA).

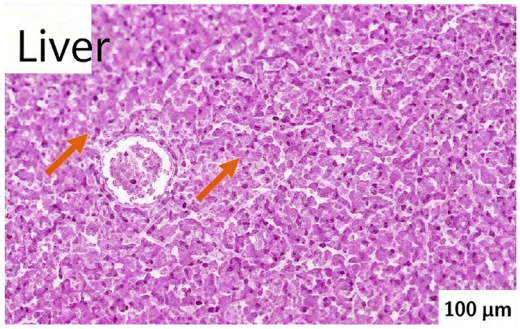


FIGURE 1
Typical cup-shaped morphology of exosomes observed by transmission electron microscopy.

miRNA sequencing and validation

Exosomal total RNA was extracted using the miRNeasy Serum/Plasma Kit (Qiagen, Germany), and 5 μL of synthetic cel-miR-39-3p (final concentration 1.6×10^8 copies/μL) was added as an external reference to correct for extraction efficiency. The RNA concentration was measured using a Qubit 4.0 fluorometer (Thermo Fisher, USA), and the RNA integrity was assessed using an Agilent 2100 Bioanalyzer (Agilent, USA), with all RIN values > 7.0.

High-throughput sequencing was performed on the Illumina HiSeq 4000 platform. Briefly, small RNA libraries were constructed using the NEBNext Multiplex Small RNA Library Prep Kit (NEB, USA), including 3′ adapter ligation, 5′ adapter ligation, reverse transcription, and PCR amplification (12 cycles). Library fragments of 140–160 bp were selected for sequencing.

Sequencing data quality was assessed using FastQC, adapter sequences were trimmed using Cutadapt, and clean reads were aligned to the cat genome (Felis_catus_9.0) and the miRBase 22 database. Gene expression was normalized using the TPM (Transcripts Per Million) method. The screening criteria for differentially expressed miRNAs were $|\log2(\text{fold change})| \geq 2$ and $P < 0.05$ after Benjamini-Hochberg correction.

Candidate miRNAs were validated by qRT-PCR. cDNA was synthesized by reverse transcription using the TaqMan Advanced miRNA cDNA Synthesis Kit (Thermo Fisher, USA), with U6 snRNA and cel-miR-39-3p as internal references. The primer and probe sequences were designed with reference to miRBase, with detailed information as follows: miR-21-5p: TM-002112; miR-155-5p: TM-002571; miR-423-5p: TM-002340; U6 snRNA: TM-001973; cel-miR-39-3p: TM-000200. The qRT-PCR reaction system consisted of 20 μL, including 10 μL of TaqMan Fast Advanced Master Mix, 1 μL of probe, 2 μL of cDNA, and 7 μL of RNase-free water. The reaction was performed on a QuantStudio 6 Flex system (Thermo Fisher, USA), with the procedure set to 95 °C for 20 s, followed by 40 cycles of 95 °C for 3 s and 60 °C for 30 s. Relative expression was calculated using the $2^{(-\Delta\Delta Ct)}$ method, with three technical replicates for each sample.

Statistical analyses

Data are presented as the mean ± standard deviation or the median (interquartile range). Normally distributed data were analyzed using an independent samples t-test (SPSS 26.0, IBM, USA), and non-normally distributed data were analyzed using a Mann-Whitney U test. Differences in miRNA expression among multiple groups were analyzed using the Kruskal-Wallis test, with Dunn's method for multiple comparison correction. Diagnostic performance was assessed using receiver operating characteristic (ROC) curves, and the area under the curve (AUC), sensitivity, and specificity were also calculated. A combined diagnostic model was constructed using logistic regression analysis, and model comparisons were performed using the DeLong test. $P < 0.05$ was considered statistically significant.

To ensure the reliability of the findings, strict sample collection criteria, standardized exosome isolation protocols, and comprehensive miRNA sequencing and validation techniques were employed. These methods were designed to minimize experimental variability and ensure that the observed

TABLE 2 Exosome particle size and concentration.

Groups	Particle concentration ($\times 10^{10}$ particles/mL)	Main peak particle size (nm)	Particle size range (nm)
Healthy control	2.8 ± 0.6	128	90–160
Group FIP group	3.1 ± 0.7	128	95–158

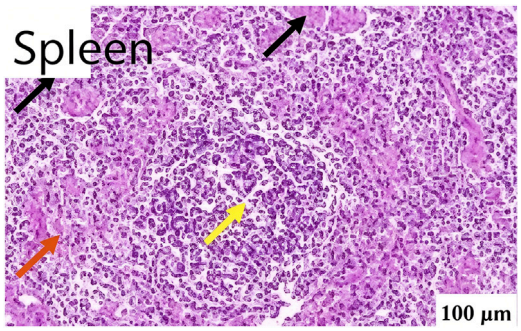


FIGURE 2
Particle size distribution of exosomes determined by nanoparticle tracking analysis.

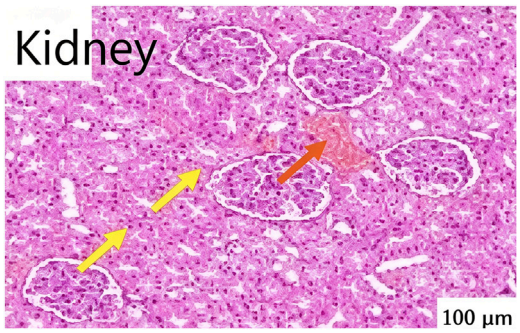


FIGURE 3
Western blot analysis of CD63 and TSG101 protein expression.

differences in miRNA expression truly reflect the FIP disease state.

Results

Exosome characterization

Serum-derived exosomes obtained by ultracentrifugation were validated via multiple methods, including analysis of morphology, particle size, and marker proteins. There was no significant difference in the particle size or concentration of exosomes between the healthy control group and the FIP group (P = 0.15), which suggests that the pathological process of FIP does not significantly alter the total number of circulating exosomes but may specifically change the composition of miRNA cargo within exosomes.

A typical "cup-shaped" exosome morphology was observed through TEM (Figure 1), with an average diameter of 80–150 nm, which was consistent with the vesicle characteristics reported in previous literature. NTA results showed that the exosome particle concentration in the FIP group was (3.1 ± 0.7)$\times 10^{10}$ particles/mL, and that in the healthy control group was (2.8 ± 0.6)$\times 10^{10}$ particles/mL, with no statistically significant difference between the two groups (P > 0.05). The particle size distribution of exosomes in both groups was mainly clustered at 128 nm (95% CI: 112–145 nm) (Table 2; Figure 2). Western blot results showed that the two exosome marker proteins, CD63 and TSG101, were highly expressed in the exosome samples from both the FIP group and the control group but were not detected in the whole serum samples (Table 3; Figure 3), indicating that the isolation method used could effectively minimize interference from non-exosomal proteins. Meanwhile, correlation analysis of exosome protein concentration and total serum protein concentration showed a Pearson correlation coefficient of r = 0.15 (P = 0.32), confirming that exosomes were successfully isolated from serum samples and could be used for subsequent miRNA analysis.

Identification of differentially expressed miRNAs

A total of 489 miRNAs were detected by high-throughput sequencing. Among these, 23 miRNAs showed statistically significant differential expression between the FIP group and the healthy control group (|log2 FC|≥2, P < 0.05). Five miRNAs with the most significant differences were selected for further analysis: among the upregulated miRNAs, miR-21-5p (log2 FC = 3.82, P = 1.2 × 10^{-5}), miR-155-5p (log2 FC = 2.95, P = 3.8 × 10^{-4}), and miR-486-5p (log2 FC = 2.13, P = 0.002) showed the greatest upregulation; among the downregulated miRNAs, miR-423-5p (log2 FC = −2.67, P = 6.5 × 10^{-4}) and miR-200c-3p (log2 FC = −1.98, P = 0.008) showed the greatest downregulation (Table 4; Figure 4).

Stratified analysis of exudative and non-exudative FIP subgroups revealed that the expression trends for the five miRNAs were consistent in both subgroups, with all coefficients of variation (CV) values < 15%, and no significant difference observed in the expression levels between the two subgroups (all P > 0.05) (Table 5; Figure 5), suggesting that the expression of these five miRNAs is not affected by the clinical phenotype of FIP.

TABLE 3 Exosome marker protein expression (Western blot gray scale values).

Groups	CD63 (relative expression)	TSG101 (relative expression)	Whole serum (CD63)
Healthy control	1.32 ± 0.21	1.15 ± 0.18	Not detected
Group FIP group	1.45 ± 0.24	1.27 ± 0.22	Not detected

TABLE 4 Analysis of the top five differential miRNA expression.

miRNA name	log2FC	P-value	Expression regulation	Functional annotation (KEGG pathway)
miR-21-5p	3.82	1.2×10^{-5}	Upregulated	NF-κB signaling pathway, apoptosis
miR-155-5p	2.95	3.8×10^{-4}	Upregulated	Inflammatory response, toll-like receptor signaling
miR-423-5p	−2.67	6.5×10^{-4}	Downregulated	Immunomodulation, PI3K-Akt pathway
miR-486-5p	2.13	0.002	Upregulated	Angiogenesis, hypoxic stress response
miR-200c-3p	−1.98	0.008	Downregulated	Epithelial-mesenchymal transition, tumor metastasis

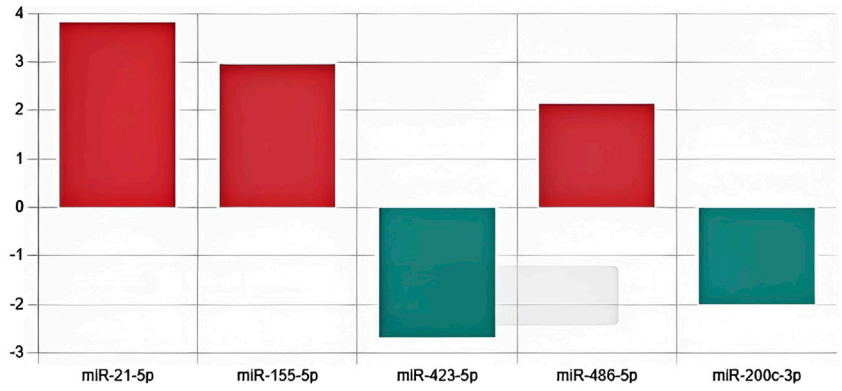


FIGURE 4
Top five differentially expressed miRNAs.

TABLE 5 Expression stability of five miRNAs in FIP subgroups.

miRNA name	Exudative (CV%)	Non-exudative (CV%)	P-value between groups (mann-Whitney U test)
miR-21-5p	12.3	13.8	0.45
miR-155-5p	11.7	14.1	0.38
miR-423-5p	9.8	10.5	0.67
miR-486-5p	13.5	14.9	0.52
miR-200c-3p	14.2	15.3	0.71

qRT-PCR validation results showed a high correlation between high-throughput sequencing data and qRT-PCR data ($r = 0.92$, $P < 0.001$). Compared with the control group, the expression of miR-21-5p in the FIP group was upregulated by 14.3-fold (95% CI: 10.6–19.2), and the expression of miR-423-5p was downregulated by 0.22-fold (95% CI: 0.15–0.31), which were consistent with the sequencing analysis results.

Among the 23 differentially expressed miRNAs identified by high-throughput sequencing, miR-21-5p, miR-155-5p, and miR-423-5p showed particular diagnostic value in FIP diagnosis. A total

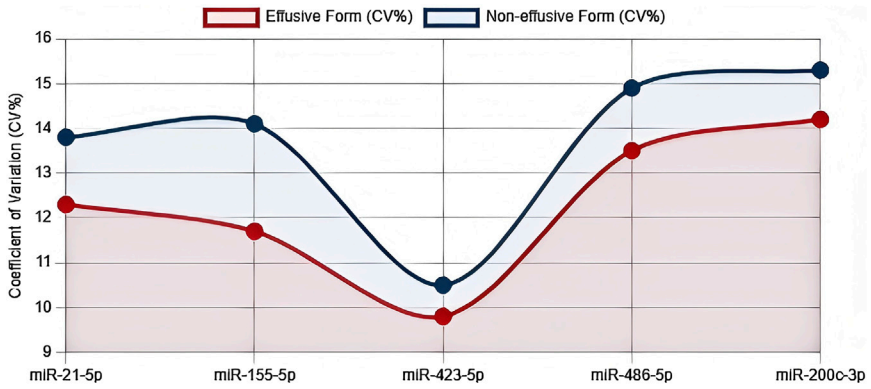


FIGURE 5
miRNA expression stability in FIP Subgroups.



FIGURE 6
Enlarged, hyperemic lymph nodes, with many grayish-white, punctate nodules the size of millet grains diffusely distributed throughout the mesentery.

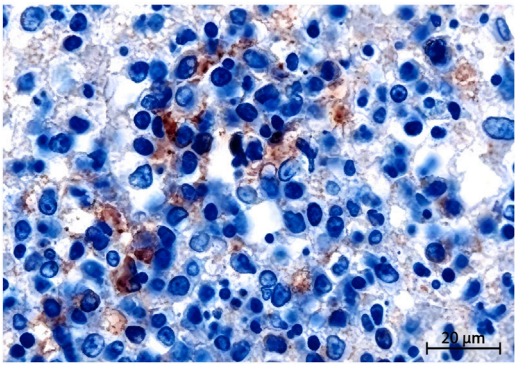


FIGURE 7
Positive immunohistochemical staining in macrophages and lymphocytes of intestinal lymph nodes.

of 489 miRNAs were detected by high-throughput sequencing, among which 23 miRNAs were statistically significant (|log2 FC|≥ 2, P < 0.05) between the FIP group and the normal control group (see Table 3), including the following: among the up-regulated miRNAs,mir-21 -5p (log2 FC = 3.82,P = 1.2 × 10 -5), mir-155 - 5p (log2 FC = 2.95, P = 3.8 × 10 -4), and mir-486 -5p (log2 FC = 2.13, P = 0.002); whereas among the downregulated miRNAs, mir-423 -5p (log2 FC = −2.67, P = 6.5 × 10 -4), and mir-200c -3p (log2 FC = −1.98, P = 0.008) were the most important were the two most variable miRNAs; Stratification of the exudative (FIP-purulent) and non-exudative (FIP-nonpurulent) types revealed consistent expression trends for these five miRNAs, and the CVs were all less than 15% (see Table 4), suggesting that they were not affected by the clinical manifestations. qRT-PCR validation showed that the correlation between the high-throughput sequencing data and the qRT-PCR data was very high (r = 0.92, P < 0.001), and the expression of mir-21-5p and mir-423-5p in the FIP group increased by approximately 14.3-fold (95% CI: 10.6–19.2) and decreased by approximately 0.22-fold (95% CI: 0.15–19.2), respectively, compared with the control group. 95%CI: 0.15 ~ 0.31).

Histopathological validation

To further confirm the FIP diagnosis of the enrolled cases, histopathological and immunohistochemical examinations were performed on 10 FIP cats randomly selected from the experimental group. Typical granulomatous lesions were detected in the histopathological examination of all 10 cases, and immunohistochemical analysis confirmed FCoV antigen expression in coronavirus-infected cells, with positive FCoV nucleic acid test results in all cases (Figures 6, 7). The miRNA expression profiles of these 10 cases were consistent with the overall expression trends of the FIP group, confirming that changes in serum exosomal miRNA expression are closely related to the histopathological features of FIP.

Diagnostic performance

A diagnostic model was constructed based on logistic regression analysis using a combination of three key miRNAs (miR-21-5p, miR-155-5p and miR-423-5p), with the formula:

TABLE 6 Comparison of diagnostic performance parameters.

Diagnostic parameters	AUC (95% CI)	Sensitivity (%)	Specificity (%)	PPV (%)	NPV (%)
miR-21-5p	0.82 (0.72–0.89)	76.5	83.2	80.1	79.8
miR-155-5p	0.79 (0.68–0.87)	71.8	85.6	78.9	79.3
miR-423-5p	0.75 (0.64–0.84)	68.2	81.4	75.6	74.7
Combined model	0.93 (0.86–0.98)	88.6	91.2	89.4	90.7
α 1-acid glycoprotein	0.75 (0.65–0.83)	65.3	79.8	70.2	75.1

TABLE 7 Key parameters for exosome isolation and characterization.

Parametric	Healthy control group (n = 20)	FIP group (n = 32)	Statistical difference (p-value)
Particle			
Concentration (× 1010/mL)	2.8 ± 0.6	3.1 ± 0.7	0.15
Main peak particle size (nm)	128 (112–145)	128 (95–158)	0.87
Relative expression of CD63 Relative	1.32 ± 0.21	1.45 ± 0.24	0.08
Expression of TSG101	1.15 ± 0.18	1.27 ± 0.22	0.12

TABLE 8 Molecular mechanisms of key differentially expressed miRNAs with cross-species comparisons.

miRNA name	Expression trends	Target gene pathway	Known disease associations	Cross-species consistency
miR-21-5p	Upregulated	PTEN/NF-κB	Inflammatory bowel disease, lung cancer	Canine coronavirus infection (upregulated 2.1 times)
miR-155-5p	Upregulated	SOCS1/TLR4	Sepsis, rheumatoid arthritis	Feline leukemia virus infection (upregulated 3.5 times)
miR-423-5p	Downregulated	PI3K-Akt/PDCD4	Chronic hepatitis, immunodeficiency	Canine parvovirus infection (downregulated 1.8 times)
miR-486-5p	Upregulated	FOXO1/hypoxic stress	Cardiovascular diseases, viral infections	Canine parvovirus infection (upregulated 2.3 times)

$$\text{Logit}(P) = 1.32 \times \text{miR}-21-5p + 0.89 \times \text{miR}-155-5p - 2.15 \times \text{miR}-423-5p - 4.76$$

Diagnostic performance was evaluated using ROC curve analysis. The AUC of the combined diagnostic model was 0.93 (95% CI: 0.86–0.98), which was significantly better than individual miRNA models (all $P < 0.01$). The sensitivity, specificity, positive predictive value (PPV), and negative predictive value (NPV) of the combined model were 88.6% (95% CI: 78.4%–94.2%), 91.2% (95% CI: 82.5%–95.8%), 89.4% and 90.7%, respectively, all of which were significantly higher than those of the conventional biomarker, α1-Acid glycoprotein (α1-AG; AUC = 0.75, $P = 0.003$). The combined model improved the overall diagnostic accuracy of FIP by approximately 24% compared with α1-AG measurement.

Subgroup analysis showed that the AUCs for exudative and non-exudative FIP were 0.91 (95% CI: 0.83–0.97) and 0.89 (95% CI: 0.80–0.95), respectively, with no statistically significant difference between the two subgroups ($P = 0.26$), suggesting that this method can be used for the early differential diagnosis of different clinical types of FIP (Table 6).

Conclusions, limitations and future directions

Characteristics of serum exosomes and miRNA enrichment in FIP

In this study, high-quality serum exosomes were successfully isolated by ultracentrifugation, with a typical cup-shaped structure, an average particle size of 128 nm, and positive expression of the specific marker proteins CD63 and TSG101, which fully met the ISEV criteria for exosome identification. Key parameters of exosome

isolation and characterization, including particle concentration, particle size and relative expression of marker proteins, are summarized in Table 7. The expression levels of exosome marker proteins and exosome particle concentrations showed no significant difference between the FIP group and the healthy control group ($P > 0.05$), indicating that the pathological process of FIP does not affect total exosome secretion but specifically alters the miRNA cargo encapsulated in exosomes.

In addition, there was no significant correlation between serum exosome concentration and total serum protein content ($r = -0.15$, $P = 0.32$), confirming that exosomes can be used as stable molecular diagnostic carriers, effectively minimizing interference from free RNA in serum. The abnormal expression of exosomal miRNAs in FIP cats in this study presumably derives from the overactivation of immune cells such as macrophages and lymphocytes induced by FCoV infection, which is consistent with the key pathological mechanism of FIP characterized by an abnormal immune inflammatory response.

Pathological significance of differentially expressed miRNAs in FIP progression

The five significantly differentially expressed miRNAs identified in this study are primarily associated with inflammatory and immune-related signaling pathways. The target gene pathways, known disease associations and cross-species expression consistency of these key miRNAs are detailed in Table 8. Among them, the upregulated miR-21-5p and miR-155-5p are involved in the regulation of NF-κB pathway activation, which may negatively regulate PTEN protein expression, induce the release of pro-inflammatory factors, such as IL-6 and TNF-α, and aggravate granulomatous inflammation in FIP. The downregulated miR-423-5p may regulate the PI3K-Akt signaling pathway, which is closely related to the immunosuppressive state in the late stage of FIP. These miRNA expression patterns are conserved in other viral infectious diseases, suggesting that RNA viruses may interfere with the host miRNA regulatory network in a conserved manner.

Notably, the above regulatory mechanisms are inferred based on KEGG pathway enrichment analysis and cross-species comparison, and no *in vivo* or *in vitro* functional experiments have been performed to verify the direct regulatory effect of these miRNAs on FIP progression. Further functional validation experiments, such as luciferase reporter gene assays or gene knockouts, are needed to confirm specific mechanisms of these miRNAs in FIP pathogenesis.

Diagnostic value of the exosomal miRNA panel and comparison with existing FIP diagnostic methods

The three-miRNA combined diagnostic model constructed in this study achieved an AUC of 0.93, with a sensitivity of 88.6% and a specificity of 91.2%. This result was significantly better than analyses based on individual miRNAs or traditional α1-AG measurements. Compared with existing methods for diagnosing FIP, the serum exosomal miRNA panel has distinct clinical advantages:

Compared with serological antibody testing: Serological tests cannot distinguish between FECV and FIPV infections, and they are susceptible to interference from maternal antibodies in young cats; in contrast, the exosomal miRNA panel can reflect the pathological state of FIP and has higher specificity for differential diagnosis [17].

Compared with RT-PCR-based molecular testing: RT-PCR has high sensitivity but cannot distinguish pathogenic FIPV from non-pathogenic FECV and has a low positive rate in non-exudative FIP without effusion; in contrast, the exosomal miRNA panel uses peripheral blood samples and provides consistent diagnostic performance for both exudative and non-exudative FIP without being limited by clinical phenotype [18].

Compared with histopathology and immunohistochemistry: These methods are invasive, require a tissue biopsy, and are only applicable to post-mortem diagnosis or advanced cases [19,20]; in contrast, exosomal miRNA analysis is non-invasive, only requires 5 mL of peripheral blood, and can facilitate an early diagnosis before the appearance of typical clinical symptoms.

In summary, the serum exosomal miRNA panel constructed in this study can be used as a non-invasive, highly sensitive, and highly specific biomarker for the early diagnosis of FIP, which effectively addresses key limitations of existing diagnostic methods.

Research limitations and future directions

This study confirmed the potential of serum exosomal miRNAs in the early diagnosis of FIP; however, there are still some limitations that need to be addressed in future studies:

Sample size and control group limitations: This study included 32 FIP cats and 20 healthy controls, with a relatively small sample size, which may reduce the statistical power of subgroup analysis. In addition, the study did not include FECV-positive but FIP-negative cats in the disease control group, so the specificity of the diagnostic model for distinguishing FIP from asymptomatic FECV infection needs to be further verified in an expanded multi-center sample cohort.

Insufficient mechanism validation: No *in vivo* or *in vitro* functional experiments were performed to verify the regulatory mechanism of differentially expressed miRNAs in FIP progression, and the current mechanistic inferences are only based on bioinformatics analysis.

Lack of multi-center clinical validation: This study is a single-center study, and multi-center clinical validation is needed to evaluate the universal applicability of this diagnostic method to different cat breeds, age groups, and regions of cats.

Future studies will focus on expanding the sample size and adding an FECV-positive/FIP-negative control group to further optimize the diagnostic model; performing *in vitro* and *in vivo* functional experiments to clarify the specific mechanism of differentially expressed miRNAs in FIP pathogenesis; and constructing a high-throughput rapid detection platform based on this miRNA panel. This will promote the method's clinical transformation and application.

Author contributions

HXG: Conceptualization, Data curation, Formal analysis, Investigation, Writing – original draft. HSW: Conceptualization, Supervision, Project administration, Funding acquisition,

Writing – review and editing. All authors have read and approved the final version of the manuscript.

Data availability

The datasets presented in this study can be found in online repositories. The names of the repository/repositories and accession number(s) can be found in the article/Supplementary Material.

Ethics statement

The animal study was reviewed and approved by the Laboratory Animal Management and Ethics Review Executive Committee of Ganzhou Vocational and Technical College (Approval No. 2025-0617-0036). All animal handling, blood collection and clinical sample use were performed in accordance with relevant national animal welfare regulations and institutional guidelines. Written informed consent for use of clinical samples and anonymized clinical information was obtained from the owners or legal guardians of the cats.

Funding

The author(s) declared that financial support was received for this work and/or its publication. This study was supported by the Construction Project of Key Laboratory of Animal Pathogens and Biosecurity Prevention and Control in Ganzhou (2024YSPT0019).

Conflict of interest

The author(s) declared no potential conflicts of interest with respect to the research, authorship, and/or publication of this article.

Generative AI statement

The author(s) declared that generative AI was not used in the creation of this manuscript.

Any alternative text (alt text) provided alongside figures in this article has been generated by Frontiers with the support of artificial intelligence and reasonable efforts have been made to ensure accuracy, including review by the authors wherever possible. If you identify any issues, please contact us.

References

1. Jin M, Cho JH, Na GY, Yun TS, Song B, Lee SR, et al. Practical approach to development of GS-445124-loaded PLGA nanoparticles for the long-term treatment of feline infectious peritonitis caused by feline coronavirus infection. *Int J Pharmaceutics* (2025) 674:125468. doi: 10.1016/j.ijpharm.2025.125468

2. Kida I, Tamura T, Kuroda Y, Fukuhara T, Maeda K, Matsuno K. Application of versatile reverse genetics system for feline coronavirus. *Microbiol Spectr* (2025) 13(4): e0269224. doi: 10.1128/spectrum.02692-24

3. Ferrero I, Dewilde S, Poletti P, Canepa B, Giachino E, Dall'Ara P, et al. Development of a new indirect ELISA test for the detection of anti-feline coronavirus antibodies in cats. *Vet Sci* (2025) 12(3):245. doi: 10.3390/vetsci12030245

4. Burgener JC, Barker NE, Soare T, Soare DG, Spiri AM, Malbon AJ, et al. Deciphering viral replication dynamics in feline infectious peritonitis: a quantitative approach. *Viruses* (2025) 17(2):279. doi: 10.3390/v17020279

5. Yao Y, Jing R, Liu X, Kang L, Liu P. Cepharanthine: a promising natural compound against feline infectious peritonitis virus infection and associated inflammation. *Virology* (2025) 604:110422. doi: 10.1016/j.virol.2025.110422

6. Repyak K, Atiee G, Cook A, Bryan L, Gremillion C. Thoracic radiographic findings in cats with feline infectious peritonitis. *J Feline Med Surg* (2025) 27(2): 1098612X241309823. doi: 10.1177/1098612X241309823

7. Shah UA, Esparza B, Illanes O, Hemida MG. Comparative genome sequencing analysis of some novel feline infectious peritonitis viruses isolated from some feral cats in Long Island. *Viruses* (2025) 17(2):209. doi: 10.3390/v17020209

8. Jiang Z, Piao L, Ren C, Zhang W, Zhu Y, Kong R. Identifying natural products as feline coronavirus mpro inhibitors by structural-based virtual screening and enzyme-based assays. *ACS Omega* (2025) 10(2):2092–101. doi: 10.1021/acsomega.4c08601

9. Martinez A, Lavergne E, Brauge C, Laveran E, Bertagnoli S, Boucraut-Baralon C, et al. Feline coronavirus-associated uveitis: the eye as a gateway to systemic spread and feline infectious peritonitis? *Vet Microbiol* (2025) 301:110355. doi: 10.1016/j.vetmic.2024.110355

10. Abdu A, Henry EM, André MN, Miller AD, Lejeune M, Berliner EA, et al. Toxoplasmal meningoencephalitis in a 14 week-old shelter cat with presumed feline infectious peritonitis. *Vet Parasitol Reg Stud Rep* (2025) 57:101173. doi: 10.1016/j.vprsr.2024.101173

11. Ševčíková Z, Márková K, Mandelík R, Zákutná Ľ, Hudec E, Karaffová V. Feline infectious peritonitis, two different manifestations of the effusive form. Case report. *Folia Veterinaria* (2024) 68(4):1–7. doi: 10.2478/fv-2024-0031

12. Goto S, Kamiyoshi T, Iwasaki R. Predictive factors associated with short-term mortality in cats with feline infectious peritonitis treated with remdesivir or GS-441524 or both. *J Vet Intern Med* (2025) 39(1):e17249. doi: 10.1111/jvim.17249

13. Lopes R, Sampaio F, Carvalho DLH, Garcês A, Fernandes C, Neves CV, et al. Feline infectious peritonitis effusion index: a novel diagnostic method and validation of flow cytometry-based Delta total nucleated cells analysis on the sysmex XN-1000V. *Vet Sci* (2024) 11(11):563. doi: 10.3390/vetsci11110563

14. Zwicklbauer K, Bergmann M, Alberer M, Both UV, Hartmann K. Feline infectious peritonitis - a current overview. Tierarztliche praxis. *Kleintiere/Heimtiere* (2025) 53(2): 96–102. doi: 10.1055/a-2524-3760

15. Coggins JS, Govendir M, Norris MJ, Malik R, Hall EJ, Thompson MF, et al. Pharmacokinetics of GS-441524 following intravenous remdesivir in six cats and results of therapeutic drug monitoring during treatment of feline infectious peritonitis: 22 cases (2021-2024). *J Small Anim Pract* (2025) 66(7):495–506. doi: 10.1111/jsap.13849

16. Kamiyoshi T, Kamiyoshi N, Jintake C. High-dose induction therapy and treatment termination criteria for feline infectious peritonitis with remdesivir, GS-441524 and adjunctive mefloquine: 46 cases (2023). *J Small Anim Pract* (2025) 66(9):617–26. doi: 10.1111/jsap.13869

17. Long J, Du JG, Liu Y, et al. Establishment of a competitive ELISA antibody detection method based on monoclonal antibody to feline infectious peritonitis virus N protein. *Chin Vet Sci* (2025) 55(02):210–8.

18. Li XY, Xie ZM, Huan YX, et al. Establishment and clinical application of SYBR green real-time fluorescence quantitative PCR method for feline infectious peritonitis virus. *Chin J Vet Med* (2025) 61(03):44–9. doi: 10.20157/j.cnki.zgsyzz.2025.03.006

19. Madeleine IG, Carolyn L, Dayna AG, Maria Bravo A, Jennifer LD. Perirenal hemorrhage associated with feline infectious peritonitis: a novel presentation of a classic disease. *J Vet Diagn Invest* (2025) 37(3):412–417. doi: 10.1177/10406387251341239

20. Sandra F, Katrin H. Diagnosis of feline infectious peritonitis: a review of the current literature. *Viruses* (2019) 11(11):1068. doi: 10.3390/v11111068

EBM Experimental Biology and Medicine

TYPE Correction
PUBLISHED 03 August 2026
DOI 10.3389/ebm.2026.10958

Check for updates

OPEN ACCESS

*CORRESPONDENCE
EBM Production Office,
production@ebm-journal.org,

RECEIVED 26 December 2025
REVISED 26 December 2025
ACCEPTED 13 February 2026
PUBLISHED 03 August 2026

CITATION
EBM Production Office (2026) Correction: Protective effects of berberine-loaded chitosan/solid lipid nanoparticles in streptozotocin-induced gestational diabetes mellitus rats.
Exp. Biol. Med. 251:10958.
doi: 10.3389/ebm.2026.10958

COPYRIGHT
© 2026 EBM Production Office. This is an open-access article distributed under the terms of the Creative Commons Attribution License (CC BY). The use, distribution or reproduction in other forums is permitted, provided the original author(s) and the copyright owner(s) are credited and that the original publication in this journal is cited, in accordance with accepted academic practice. No use, distribution or reproduction is permitted which does not comply with these terms.

Correction: Protective effects of berberine-loaded chitosan/solid lipid nanoparticles in streptozotocin-induced gestational diabetes mellitus rats

EBM Production Office*

Frontiers Media SA, Lausanne, Switzerland

KEYWORDS

berberine, chitosan, gestational diabetes mellitus, rat, solid lipid nanoparticle

A Correction on
Protective effects of berberine-loaded chitosan/solid lipid nanoparticles in streptozotocin-induced gestational diabetes mellitus rats

by Liu Y, Hussain SA and Yue H (2025). Exp. Biol. Med. 250:10749. doi: 10.3389/ebm.2025.10749

In the main article, the name of the ethics committee was erroneously given as "the Institutional Ethics Committee and Research Advisory Committee of the King Saud University, Saudi Arabia" and the location that the rats were obtained from was erroneously given as "the laboratory animal research center of the College of Science, King Saud University, Saudi Arabia".

A correction has been made to the **Material and Methods section,** subsection 'Gestational rats'. The correct paragraph appears below:

"Forty-nine female (180 ± 10 g) and seven male (230 ± 10 g) Wistar-Albino rats (8–10 weeks old) were obtained from Takassusi BioMedical, Riyadh, Saudi Arabia. All animal experiments were performed in full accordance with the Animal Welfare instructions and approved by Zhinanzhen Biology Ethics Committee, [No.: A2025000127.]"

The original version of this article has been updated.

Experimental Biology & Medicine Conference

Orlando, FL - October 13 -16, 2024

Please visit **exbiomedcon.org** or scan the QR code for more info.

Keynote Lecturers



Namandjè Bumpus, Ph.D.
Chief Scientist - US Food and Drug Administration

Advancing Emerging Technologies in Regulatory Science



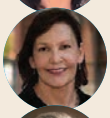
Michael Friedlander, Ph.D.
Vice President - Health Sciences and Technology at Virginia Tech

All events will take place at the Embassy Suites by Hilton, Orlando Lake Buena Vista South

Cardiovascular



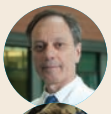
Delphine Gomez, Ph.D.
University of Pittsburgh



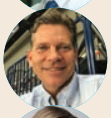
Karen Hirschi, Ph.D.
University of Virginia



Jay Humphrey, Ph.D.
Yale University



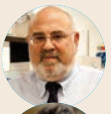
Ali J. Marian, M.D.
The University of Texas Health Science Center at Houston



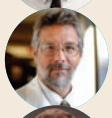
Joseph Miano, Ph.D.
Medical College of Georgia



Dianna Milewicz, M.D., Ph.D.
University of Texas Heath Science Center Houston



Robert Schwartz, Ph.D.
University of Houston



George Taffet, M.D.
Baylor College of Medicine



David Zawieja, Ph.D.
Texas A&M University Health Science Center

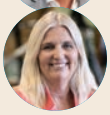
Neuroscience



Lique Coolen, Ph.D.
Kent State university



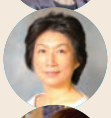
Michael Fehlings, M.D.
University of Toronto



Susan Harkema, Ph.D.
University of Louisville



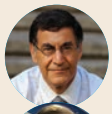
Maria Lehtinen, Ph.D.
Harvard University



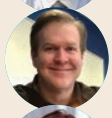
Fang Liu, Ph.D.
NCTR/US Food and Drug Administration



Agnes Luo, Ph.D.
University Cincinnati



Mervyn Maze, MBChB
University of California San Francisco

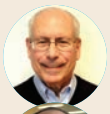


Dorian McGavern, Ph.D.
National Institute of Neurological Diorders and Stroke



Vesna Jevtovic-Todorovic, M.D., Ph.D.
University of Colorado School of Medicine

Regenerative Medicine



Arnold I. Caplan, Ph.D.
Case Western Reserve



Jian Feng, Ph.D.
State University of New York at Buffalo



Joshua Hare, M.D.
University of Miami



Karen Hasty, Ph.D.
University of Tennessee Health Science Center



Rajasingh Johnson, Ph.D.
University of Tennessee Health Science Center



Y. James Kang, DVM, Ph.D.
Sichuan University



Kwang-Soo Kim,Ph.D.
Harvard University



Joanne Kurtzberg, M.D.
Duke University



Jun Wu, Ph.D.
UT Southwestern

Trainees



Justin Boyd, Ph.D.
Vaxxinity



Udayan Apte, Ph.D.
U of Kansas Medical Center



Ram Kumar, Ph.D.
U of Kansas Medical Center

And More

Career Development
Short Talks
Poster Sessions
Member Blitz

SEBM SOCIETY FOR EXPERIMENTAL BIOLOGY AND MEDICINE

EBM Experimental Biology and Medicine

Scope

Experimental Biology and Medicine (EBM) is a global, peer-reviewed journal dedicated to the publication of multidisciplinary and interdisciplinary research in the biomedical sciences. The journal covers the spectrum of translational research from T0, basic research, to T4, population health. Articles in EBM represent cutting edge research at the overlapping junctions of the biological, physical and engineering sciences that impact upon the health and welfare of the world's population. EBM is particularly appropriate for publication of papers that are multidisciplinary in nature, are of potential interest to a wide audience, and represent experimental medicine in the broadest sense of the term. However, manuscripts reporting novel findings on any topic in the realm of experimental biology and medicine are most welcome.

EBM publishes Research, Reviews, Mini Reviews, and Brief Communications in the following categories.

- Anatomy/Pathology
- Artificial Intelligence/ Machine Learning Applications to Biomedical Research
- Biochemistry and Molecular Biology
- Bioimaging
- Biomedical Engineering
- Bionanoscience
- Cell and Developmental Biology
- Clinical Trials
- Endocrinology and Nutrition
- Environmental Health/Biomarkers/ Precision Medicine
- Genomics, Proteomics, and Bioinformatics
- Immunology/Microbiology/Virology
- Mechanisms of Aging
- Neuroscience
- Pharmacology and Toxicology
- Physiology and Pathophysiology
- Population Health
- Stem Cell Biology
- Structural Biology
- Synthetic Biology
- Systems Biology and Microphysiological Systems
- Translational Research

Submit your work to Experimental Biology and Medicine at
ebm-journal.org/submission

More information
ebm-journal.org/journals/experimental-biology-and-medicine

EBM Experimental Biology and Medicine

EBM is the official journal of the Society for Experimental Biology and Medicine

Experimental Biology and Medicine (EBM) is a global, peer-reviewed journal dedicated to the publication of multidisciplinary and interdisciplinary research in the biomedical sciences.

Discover more of our Special Issues

See more →



Contact

development@ebm-journal.org

See more

ebm-journal.org

publishingpartnerships.frontiersin.org/our-partners